



AMERICAN UNIVERSITY OF BEIRUT

New Analysis of the Primordial Nucleosynthesis
in Light of the Lithium Problem

by

Tahani Ramez Makki

A doctoral dissertation
submitted in partial fulfillment of the requirements
for the degree of Doctor of Philosophy in Physics
to the Department of Physics
of the Faculty of Arts and Sciences
at the American University of Beirut

Beirut, Lebanon
September 5, 2019

AMERICAN UNIVERSITY OF BEIRUT

New Analysis of the Primordial Nucleosynthesis
in Light of the Lithium Problem

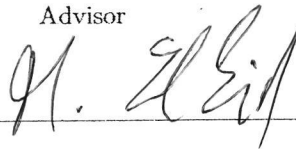
by

Tahani Ramez Makki

Approved by:

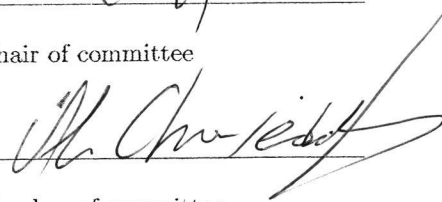
Dr. Mounib El Eid, Professor
(Physics Department)

Advisor



Dr. Ali Chamseddine, Professor
(Physics Department)

Chair of committee



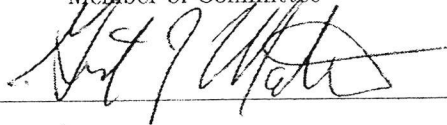
Dr. Leonid Klushin, Professor
(Physics Department)

Member of committee



Dr. Grant Mathews, Professor
(University of Notre Dame, USA)

Member of Committee



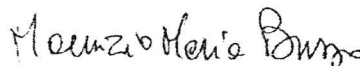
Dr. Carlos Bertulani, Professor
(Texas A&M University-Commerce)

Member of Committee



Dr. Maurizio Busso, Professor
(Istituto Nazionale di Fisica Nucleare, Italy)

Member of Committee



Date of doctoral dissertation defense: September 5, 2019

AMERICAN UNIVERSITY OF BEIRUT

THESIS, DISSERTATION, PROJECT RELEASE FORM

Student Name: Makki Tahani Ramez
Last First Middle

Master's Thesis Master's Project Doctoral Dissertation

I authorize the American University of Beirut to: (a) reproduce hard or electronic copies of my thesis, dissertation, or project; (b) include such copies in the archives and digital repositories of the University; and (c) make freely available such copies to third parties for research or educational purposes.

I authorize the American University of Beirut, to: (a) reproduce hard or electronic copies of it; (b) include such copies in the archives and digital repositories of the University; and (c) make freely available such copies to third parties for research or educational purposes after: **One ___ year from the date of submission of my thesis, dissertation or project.**
Two ___ years from the date of submission of my thesis , dissertation or project.
Three ___ years from the date of submission of my thesis , dissertation or project.



Signature

September 18, 2019

Date

Acknowledgements

Firstly, I would like to express my sincere gratitude to my advisor Prof. Mounib El Eid for the continuous support of my Ph.D study and related research, for his motivation, patience and immense knowledge. His guidance helped me in all the time of research and writing of this thesis. I could not have imagined having a better advisor and mentor for my Ph.D study.

Besides my advisor, I would like to thank the rest of my thesis committee: Prof. Grant Mathews, Prof. Carlos Bertulani, Prof. Maurizio Busso, Prof. Leonid Klushin and the chair of the committee Prof. Ali Chamseddine, for their insightful comments and encouragement which inspired me to widen my research from various perspectives.

I would thank the dean's office of the faculty of arts and sciences at the American University of Beirut(AUB)for supporting travel to international meetings which allowed me to present my work, to improve my skills and meet people in my field of research. I would also thank the National council for scientific research (CNRS) for their partial support of this research. In addition, I would thank the graduate council at AUB for their tremendous help, guidance, and facilities throughout my Ph.D thesis.

Last but not least, I would like to thank my parents and my friends for supporting me spiritually all the time.

An Abstract of the Dissertation of

Tahani Ramez Makki for Doctor of Philosophy
Major: Theoretical Physics

Title: New Analysis of the Primordial Nucleosynthesis in Light of the Lithium Problem.

We are lucky to live in what eventually may be viewed as the best time during which we could explore the mysteries of the universe. One mystery was that the mass fraction of helium was always observed higher than about 0.23 since this is not produced in stars at this level. Another question was where the deuterium has been produced since it is destroyed in stars. The standard big bang nucleosynthesis (SBBN), which is a well-established theory responsible for the production of light elements during the first few minutes after big bang, has answered many of these questions and some still to be answered. It is clear that all abundances agree with observations except for lithium (${}^7\text{Li}$) which is higher by a factor of 3 than observations of the atmospheres of low metal halo stars. This discrepancy constitutes now one of the most intriguing problems in cosmology. In addition, lithium was shown to have a constant behavior as a function of metallicity, the so-called "Spite Plateau". Such behavior is now in conflict with recent observations at very low metallicity which makes the lithium problem more complicated. In the present thesis, we will argue that nuclear physics or astrophysical solutions do not seem to resolve the lithium problem so that non-standard big bang nucleosynthesis should be considered. Therefore, we will give a new analysis of the SBBN in order to see the possibilities to resolve the so-called cosmological lithium problem while taking into account constraints from cosmology, astrophysics and particle physics.

Contents

| | |
|--|-----------|
| Acknowledgements | v |
| Abstract | vi |
| 1 Introduction | 1 |
| 1.1 The stages of our universe | 1 |
| 1.2 How do we know that big bang happened? | 3 |
| 2 Observational constraints on light elements | 11 |
| 2.1 Observational constraints | 11 |
| 2.1.1 Helium-4 | 11 |
| 2.1.2 Deuterium | 12 |
| 2.1.3 Helium-3 (${}^3\text{He}$) | 14 |
| 2.1.4 Lithium (${}^7\text{Li}$) | 15 |
| 3 The Standard Big Bang Nucleosynthesis | 17 |
| 3.1 Standard big bang nucleosynthesis | 17 |
| 3.1.1 Method of calculation | 17 |
| 3.1.2 How to produce light elements? | 18 |
| 4 The present status of the lithium problem | 25 |
| 4.1 Astrophysical Aspects | 26 |
| 4.2 Nuclear Physics Aspects | 27 |
| 4.2.1 The ${}^7\text{Be}(n, \alpha){}^4\text{He}$ rate | 28 |
| 4.2.2 $d + {}^7\text{Be}$ rate | 29 |
| 4.2.3 Electron capture of ${}^7\text{Be}$ | 29 |
| 4.3 Non-standard Physics | 31 |
| 4.3.1 Inhomogeneous nucleosynthesis | 31 |
| 4.3.2 Decay of Massive particles during BBN | 32 |
| 4.4 Other non-standard BBN modifications | 33 |
| 5 The role of neutrinos chemical potential in SBBN | 34 |
| 5.1 Role of neutrinos in SBBN | 34 |
| 5.2 Neutrino degeneracy and oscillations | 36 |

| | | |
|----------|--|-----------|
| 5.3 | Numerical Results | 38 |
| 5.4 | Analytical calculations | 40 |
| 5.4.1 | Stages of big bang nucleosynthesis | 40 |
| 5.4.2 | Deuterium formation epoch | 42 |
| 5.4.3 | Helium-4 | 44 |
| 5.4.4 | Final deuterium abundance | 45 |
| 5.4.5 | Helium-3 and tritium | 47 |
| 5.4.6 | Beryllium and lithium | 48 |
| 6 | Effect of Neutrino temperature and dark components on SBBN | 51 |
| 6.1 | Neutrinos and the effective degrees of freedom | 51 |
| 6.2 | Are neutrinos a candidate for dark matter | 51 |
| 6.3 | Effect of varying neutrino temperature and chemical potential on the lithium production | 52 |
| 6.4 | Axion as dark matter | 57 |
| 6.5 | Effect of photon cooling along with non-standard neutrino properties | 58 |
| 6.6 | The effect of a unified dark fluid | 60 |
| 7 | Constraining the neutron lifetime by SBBN | 66 |
| 8 | Summary and conclusions | 71 |
| A | Freeze-out of neutrons | 74 |
| B | Deuterium bottleneck | 75 |
| C | Final deuterium abundance | 76 |
| D | Entropy conservation | 79 |
| E | Used nuclear rates | 80 |
| F | Abbreviations | 82 |

List of Figures

| | | |
|-----|---|----|
| 1.1 | The universe since the big bang (This data is from U. of Arizona Lectures). | 4 |
| 1.2 | The Hubble law, recessional velocities of sample of galaxies versus distance. The straight line is the best fit to the data and called Hubble law $v = H_0 d$, where H_0 is the present Hubble constant as a slope of the straight line. Note that for each million parsec, the galaxy's speed increases by 73 km/s away from us (Taken from the text "Universe tenth edition" by A. R. Freedman et al., W. H. Freeman and Company). | 5 |
| 1.3 | Apparent magnitude versus redshift. The greater the magnitudes the dimmer the supernova and the larger the distance to the host galaxy. A greater redshift implies a greater recessional velocity (This is data from the supernovae cosmology project/S. Perlmutter; Taken from the text "Universe tenth edition" by A. R. Freedman et al., W. H. Freeman and Company). | 6 |
| 1.4 | The CMB radiation distribution a perfect blackbody of the indicated temperature (a: Courtesy of J. Mather/NASA; b: Courtesy of E. Cheng/NASA COBE Science Team. Taken from "Universe tenth edition" by A. R. Freedman et al., W. H. Freeman and Company). | 9 |
| 2.1 | The evolution of primordial helium-4 observations from 1990 till 2018. The horizontal line represent the SBBN predictions. | 13 |
| 2.2 | Primordial deuterium observations as function of the redshifts of the absorption system. Horizontal lines represent SBBN predictions. | 15 |
| 3.1 | Network of the most important nuclear reactions intervening during BBN. | 22 |
| 3.2 | Light element abundances as a function of temperature/time and the main reactions leading to these abundances. | 23 |

| | | |
|-----|---|----|
| 3.3 | Light element abundances as a function of baryon density calculated by taking the relativistic degrees of freedom intervening during BBN to be $N_{eff} = 3$ and the neutron lifetime $\tau_n = 880.2$. The vertical gray band is the Planck determination of baryon density while the orange band represents the critical density of the universe. Horizontal lines represent observations of light elements. | 24 |
| 4.1 | Primordial lithium observations as a function of metallicity. | 26 |
| 4.2 | Comparison between different calculated rates of ${}^7Be(n, \alpha){}^4He$. The vertical yellow bands indicate the BBN temperature range. Note the significant difference between the new rates and that used by Wagoner especially in the BBN range. | 29 |
| 4.3 | Comparison between the new ${}^7Be+d$ rate and the one by Caughlan-Fowler in the BBN temperature ranges to see the effect on the final abundance of 7Be | 30 |
| 4.4 | 7Be abundance when using the rate by Caughlan-Fowler 1988 (red dashed line) and the new ${}^7Be+d$ rate multiplied by a factor of 25 (blue solid line). | 31 |
| 5.1 | Photon number density as function of temperature during BBN. | 36 |
| 5.2 | Deuterium abundance at the bottleneck temperature as function of the neutrino chemical potentials. The curves with stars are obtained from our analytical calculations while the curves without stars are obtained from numerical ones. | 44 |
| 5.3 | Lithium abundance as function of the deuterium abundance for different values of β_{ν_e} as labeled on the curves with the range of $0 \leq \beta_{\nu_{\mu, \tau}} \leq 5$. The vertical lines in the left panel indicate the range of investigation in this work. | 49 |
| 6.1 | Comparison between the SBBN abundances of light elements as function of temperature (red dashed lines) and those obtained when multiplying neutrino temperature by a factor $\alpha = 1.5$ (blue solid lines) | 56 |
| 6.2 | Effect of adding dark energy density ρ_D on the abundances of helium (blue dotted line, left axis), deuterium (orange solid line, right axis) and lithium (orange dashed line, right axis). | 62 |
| 6.3 | Effect of adding dark entropy S_D (see Eq.(6.21)) on the abundances of helium (blue dotted line, left axis), deuterium (orange solid line, right axis) and lithium (orange dashed line, right axis). | 63 |
| 6.4 | Deuterium abundance as function of temperature when adding dark entropy ($k_s = 0.007, n_s = 5$) compared to SBBN | 65 |

| | | |
|-----|--|----|
| 7.1 | Improvement of the measured neutron lifetime along with the error bars from 1972 till 2018. In order to distinguish two measured values in the same year, we used different colors (red and blue). | 67 |
| 7.2 | light element abundances as function of neutron lifetime for different values of N_{eff} . | 70 |

List of Tables

| | | |
|-----|--|----|
| 2.1 | Primordial helium-4 Observations. | 12 |
| 2.2 | Primordial deuterium observations. | 14 |
| 2.3 | Primordial lithium observations. | 16 |
| 3.1 | Different SBBN predictions compared to observations. | 23 |
| 4.1 | Resultant abundances when reaction rates are multiplied by some factors. | 28 |
| 4.2 | Effect of the new ${}^7\text{Be} + d$ rate on the final lithium abundance. . . | 30 |
| 5.1 | Effect of neutrino chemical potentials ($\beta_{\nu_e} = \beta_{\nu_\mu} = \beta_{\nu_\tau}$) along with varying N_ν on SBBN. | 38 |
| 5.2 | The ranges of $\beta_{\nu_{e,\mu,\tau}}$ and N_ν that lead to a significant decrease of lithium. | 39 |
| 5.3 | The effect of different neutrino chemical potentials showing how ${}^7\text{Li}$ abundance is reduced | 39 |
| 5.4 | Comparison of light elements abundances for $\beta_{\nu_e} = 0.1$, $\beta_{\nu_{\mu,\tau}} = 1$ between fits presented by (Kneller & Steigman, 2004) and the present work based on our analytical and numerical calculations. . | 46 |
| 6.1 | Light elements abundances with varying neutrino number, chemical potential and temperature. | 54 |
| 6.2 | Effect of varying neutrino number, chemical potential and temperature on lithium. | 55 |
| 6.3 | Light elements abundances calculated by adopting the model of photon cooling with axion dark matter after BBN [51]. | 58 |
| 6.4 | Effect of adding photon cooling on lithium along with non-standard neutrino properties. | 59 |
| 6.5 | Effect of adding photon cooling on lithium along with non-standard neutrino properties for $N_\nu = 3$ | 60 |
| 6.6 | Effect of unified dark fluid on lithium along with non-standard neutrino properties. | 64 |
| 6.7 | Effect of unified dark fluid on lithium along with non-standard neutrino properties with $N_\nu = 3$ | 64 |

| | | |
|-----|--|----|
| 7.1 | light element abundances for $N_{\text{eff}} = 2.48$ and $815 < \tau_n < 1123$. . . | 69 |
| 7.2 | light element abundances for $N_{\text{eff}} = 3$ and $783 < \tau_n < 1079$. . . | 69 |
| 7.3 | Light element abundances for $N_{\text{eff}} = 3.5$ and $755 < \tau_n < 1041$. . . | 69 |
| E.1 | Nuclear rates | 80 |

Chapter 1

Introduction

1.1 The stages of our universe

A fascinating feature of cosmology and astrophysics is the understanding of the early evolution of the universe. Since about 13.7 billion years ago, big bang took place and then the universe passes through different epochs. The approximate timeline of the evolution of the universe could be as follows:

- Planck epoch (from zero to 10^{-43} s): we don't know so much about this period, but what we believe characterizes this epoch is that the four fundamental forces (electromagnetic, weak nuclear, strong nuclear and gravitational force) were unified in one fundamental force or have the same strength. At this time the temperature of the universe was too hot around $T = 10^{32}$ K so that subatomic particles could not be created and the horizontal universe was spanning over a region not more than 10^{-35} meters.
- Epoch of Grand Unification (from 10^{-43} to 10^{-36} s): during this period the forces start to separate from each other, especially in the first phase transition, gravity is no longer unified with the other fundamental forces that remain unified. As the universe cools and according to quantum field theory, it is possible to create elementary particles and antiparticles. At the end of this period, the three other fundamental forces separate into two: strong and electroweak interactions.
- Inflationary epoch: it is not known exactly when the inflationary epoch ended but it is thought that it took place between 10^{-36} and 10^{-32} s where the universe undergoes a cosmic inflation that manifested by a rapid exponential expansion. Then, during this small period the volume of the universe increases by a factor at least of 10^{78} . The inflaton, which is a scalar field, was one of the drivers of this phase transition. However, at the

end of this epoch, the decay of the inflaton generates an enormous "reheating" of the universe. This could lead to a homogenous universe populated with hot and dense mixture of gluons, quarks, anti-quarks, leptons etc..

- The Electroweak epoch: in some models, this epoch is considered to be a part of the inflationary epoch. However, in other models, this epoch is considered to be independant and took place after 10^{-32} seconds after big bang. Since the strong nuclear force is now separated from the electroweak one, particles like bosons and Higgs bosons were created during this phase.
- The electroweak symmetry breaking epoch: around 10^{-12} seconds, and as the universe continues to cool down, electroweak symmetry breaking occurs where all particle interacting with the Higgs field become massive. Consequently, the weak and electromagnetic force along with their respective bosons become independent from each other. Then, we will have four different interactions in their present form as: gravitation, electromagnetism, strong and weak interactions. Note that during this epoch the temperature of the universe is still high so that it is impossible to form neutrons and protons.
- Quark and hadron epochs (from 10^{-12} till 1 second): the universe was filled with a quark-gluon plasma, electrons and neutrinos so that the energetic collisions between these particles allowed quarks-anti quarks to annihilate. However, in a process called baryogenesis, one quark for every billion pairs survives leading to excess of quarks over anti-quarks. Afterwards, the universe was cool enough which allows quark to combine to form hadrons (protons and neutrons).
- Lepton epoch (from 1 second to three minutes): After the annihilation of hadrons and anti-hadrons at the end of this epoch, leptons and anti-leptons dominate the universe.
- Nucleosynthesis (from 1s to 20 minutes): during this phase, the universe cooled enough at a point where light nuclei as helium, deuterium and lithium could form by fusion of protons and neutrons. This epoch is the focus of the present work and it is described in details in Chap. 3.
- Photon epoch (from 3 minutes to 377000 years): at the beginning of this epoch, the universe was filled with a plasma of atomic nuclei and electrons. After the annihilation of leptons and anti-leptons, many high-energy gamma photons were created. These photons continue their interaction with the charged nuclei, protons and electrons for 377000 years. Note that during this epoch, there is an important timestamp (47000 years after big bang) where the density of radiation drops below the density of matter, so that the matter dominated era started and lasted for billions of years.

- Recombination, photon decoupling and cosmic microwave background (CMB): around 377000 after big bang, the temperature falls approximately to 3000 degrees. This allowed electrons to combine with hydrogen and helium to form neutral atoms, this process is known as recombination. Consequently, as they make transition to a lower energy state, the electrons release photons and this is known as photon decoupling. Then, any decoupled photons that have not been captured by any other hydrogen atoms can travel freely so that the universe becomes transparent to light for the first time. These photons constitute now what is called cosmic microwave background (CMB) which provides an important evidence of the big bang.
- Dark age: the period after recombination till 150 million years constitutes the dark age. At this time, the universe was dark although photons were present. We do not know much about this period, but the universe was dominated by a mysterious form of matter.
- Reionization (from 150 million to 1 billion years): due to gravitational collapse, the first quasars form causing the emission of intense radiation which reionizes the universe and brings it back from its neutral status to an ionized plasma.
- Stars and Galaxies, solar system and today's universe: matter continues to combine together under the effect of gravity to form stars and galaxies. It is important to mention our star the "Sun" which is a late generation star that has formed along with the solar system roughly 8.5 to 9 billion years after big bang. The age of our universe now is 13.7 billion years, it stops decelerating and begins to accelerate from about 9 billion years after big bang. The precise reason is not known but the most acceptable argument is that the universe is dominated by an unknown form of energy that is called "dark energy" which constitutes 68.3% of the present universe.

1.2 How do we know that big bang happened?

The epoch till the recombination time at about 377000 years after big bang is termed high redshift (z) universe, that is for $z > 1100$. Before the emerging of the microwave background radiation, our knowledge relies on the physical-mathematical modeling of the high redshift universe. On the other hand, the theoretical description has to be tested by observations whenever possible. Fortunately, we have three observational tools that can be related to the big bang creation of the universe which will be described in the following:

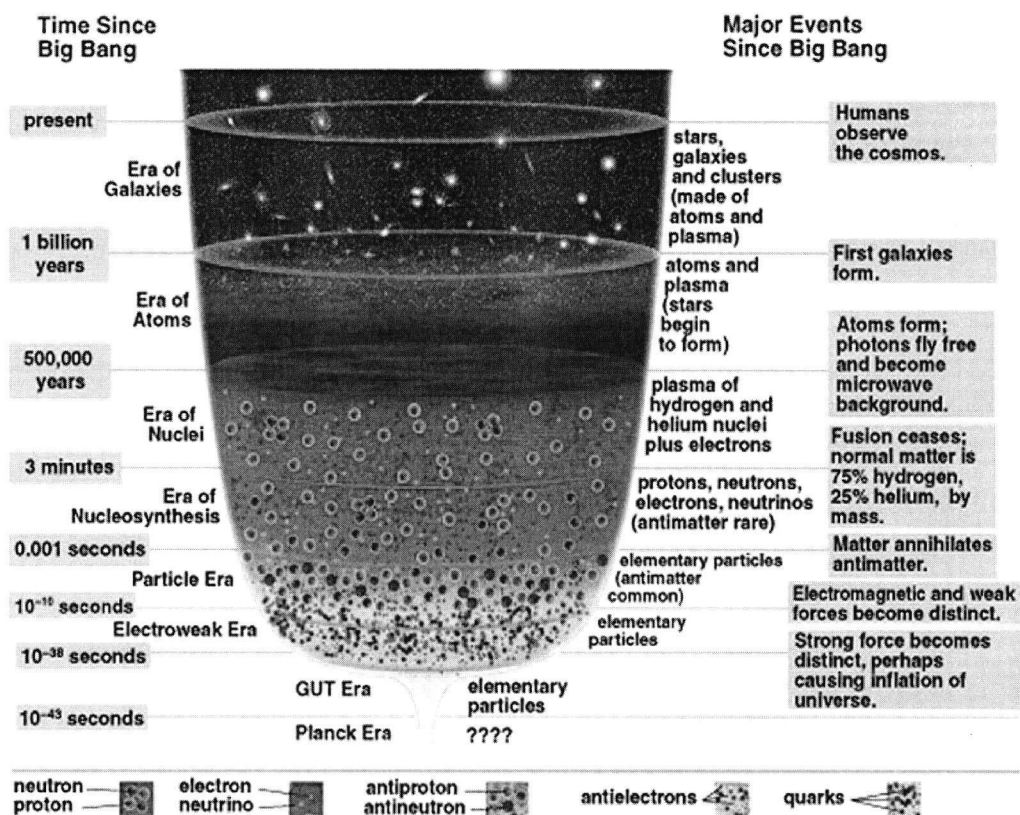


Figure 1.1: The universe since the big bang (This data is from U. of Arizona Lectures).

(a) The expanding universe and the Hubble law:

During the 1920s, Edwin Hubble and Milton Humason photographed spectra of many galaxies with a 2.5m telescope on Mount Wilson, California, USA. They observed the apparent brightness and pulsation periods of Cepheid variables in these galaxies and were able to measure the distance to each galaxy. The result was spectra that were Doppler red-shifted. The striking result was that the more distant the galaxy the greater the redshift and the faster it is receding from us. The redshift is given by $z = (\lambda - \lambda_0)/\lambda_0$ for not too large velocity (non-relativistic), where λ is the shifted wavelength and λ_0 is the unshifted wavelength. From this redshift and the Doppler formula $z=v/c$, Hubble estimated the speed at which the galaxies were receding. The result is shown in Fig. 1.2, which clearly indicates the expansion of the universe.

An important question was whether the expansion rate remains the same. Because there is matter in the universe, gravity pulls the bits of matter toward each other, so that the expansion would slow down with time. However, a surprising

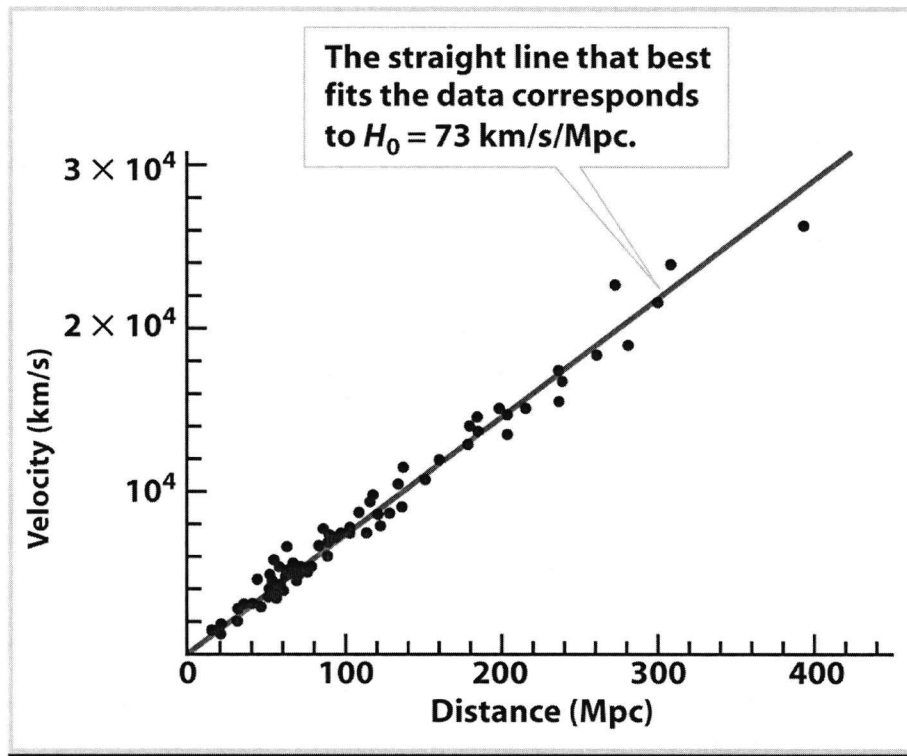


Figure 1.2: The Hubble law, recessional velocities of sample of galaxies versus distance. The straight line is the best fit to the data and called Hubble law $v = H_0 d$, where H_0 is the present Hubble constant as a slope of the straight line. Note that for each million parsec, the galaxy's speed increases by 73 km/s away from us (Taken from the text "Universe tenth edition" by A. R. Freedman et al., W. H. Freeman and Company).

aspect of the universe is that most of the matter does not obey Newton's law of gravity. It is called "dark energy" which could be described by a cosmological constant Λ . It is antigravity matter which remains the greatest mystery in astrophysics. To determine whether the expansion is slowing down or accelerating, a relationship between redshift and distance for extremely remote galaxies may give the answer. If the rate of the expansion in the distant past was the same as it is now, then the same Hubble law should apply to the distant galaxies as to nearby ones. In other words, the deviation from the Hubble law should give the answer. Back to Fig. 1.2 showing distances up to 400 Mpc (about 1.3 billion ly) only. This means, the expansion was constant if we look back 1.3 billion years, which is only 10% of the age of the universe. How to extend our view further back in time? The answer was possible through the observations of type Ia supernova. These events, originating from explosions of white dwarfs in binary

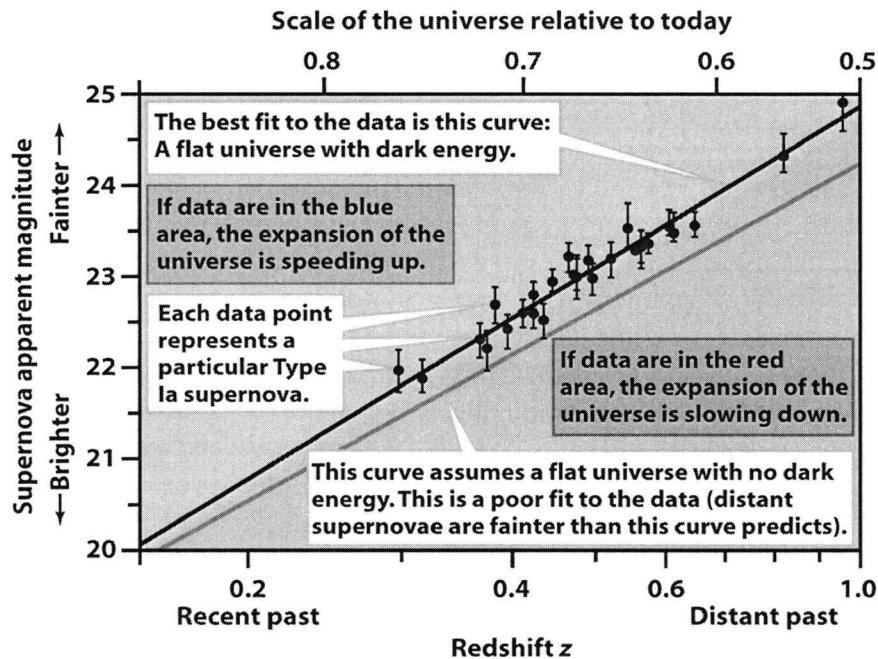


Figure 1.3: Apparent magnitude versus redshift. The greater the magnitudes the dimmer the supernova and the larger the distance to the host galaxy. A greater redshift implies a greater recessional velocity (This is data from the supernovae cosmology project/S. Perlmutter; Taken from the text "Universe tenth edition" by A. R. Freedman et al., W. H. Freeman and Company).

systems, are among the most luminous objects in the universe after big bang and can be observed in the most remote galaxies. Observing the maximum brightness of these supernovae reveals their distances through the inverse square law of radiation and the redshift of the supernovae spectrum determines its recessional velocity. In 1998, two groups-the supernova cosmological project at Lawrence Berkeley National Lab [122]; and the high Z-Supernova Search Team at Mount Stromlo observatory in Australia [133] reported their results from a survey of type Ia supernovae in galaxies at $z=0.2$ corresponding to 750 Mpc (2.4 billion ly). They declared that the expansion of the universe is accelerating-a Nobel Prize-winning discovery tantamount to the discovery of dark energy. Both teams measured how fast the universe was expanding at different times in its history by comparing the brightness and redshifts of Type Ia supernovae. Their results and those from more recent observations are shown in Fig. 1.3. The data in Fig. 1.3 are explained on the basis of relativistic cosmology, which provides a description of the expansion of the universe based on Einstein's general theory of relativity as developed by A. Friedmann, G. Lemaitre and W. De Sitter (We will make use

of the Friedmann's equations in this thesis). The interpretation of the results in Fig. 1.3 is that given the mass density parameter Ω_m (the ratio of the density to the critical one) and the dark energy density parameter Ω_Λ the change with time of the expansion rate can be predicted. In Fig. 1.3, the lower curve is expected assuming a flat present matter dominated universe without dark energy component, or $\Omega_0 = \Omega_m$, that is the density parameter is due to radiation and matter only. In this case, the absence of dark energy means that the gravitational attraction between galaxies would cause the universe to slow down. Thus, the expansion rate would have been greater in the past. The data in Fig. 1.3 agree with the upper curve, which assumes flat universe but with an amount of dark energy consistent with results from the cosmic microwave background, so that: ($\Omega_m = 0.24, \Omega_\Lambda = 0.76, \Omega_0 = \Omega_m + \Omega_\Lambda = 1.00$). This agreement means that the dark energy has made the universe speed up with time so that the expansion rate was slower in the distant past.

Conclusion: as seen in Fig. 1.3, the observed data indicate that a supernova with a certain brightness (distance) has a smaller redshift and hence smaller recessional velocity than would be the case if the expansion rate would have been the same. The data provide compelling evidence for the existence of dark energy in the universe.

(b) Cosmic Microwave Background (CMB):

Big bang nucleosynthesis (BBN) tells us that the universe was very hot and underwent a rapid expansion. This means that the universe should be filled with radiation that is called the "Cosmic Microwave Background Radiation" (CMB). About 377,000 years after BBN, the universe was cool enough so that hydrogen could form. However, CMB photons interact very weakly with hydrogen so they continue traveling in a straight line. The CMB radiation distribution resembles a perfect blackbody (see Fig. 1.4). In addition, the remarkable feature of the CMB is that its intensity is extremely isotropic except for small fluctuations of about 10^{-5} and this is a striking confirmation of Einstein's assumption that the universe is isotropic. This radiation appears to come from a spherical surface around the observer such that the radius of the shell is the distance each photon has travelled since it was last scattered at the epoch of recombination. This surface is what is called the last scattering surface. Although the surface of last scattering has a temperature of 3000 K, the cosmic microwave background photons now have a temperature of about 2.7 K. This factor of 1000 reduction in temperature is the result of the factor of 1000 expansion between the time the photons were emitted and now. The photons have cooled and become redshifted as a result of the expansion of the universe. For example, when the universe is three times bigger than it is now, the CMB will have a temperature of about 1 K. The last scattering surface is sometimes called the cosmic photosphere, by analogy with the visible 'surface' of the Sun where radiation produced by nuclear reactions is last scattered by the solar material. The energy source for the Sun's photons is

not in the photosphere: it comes from nuclear fusion at the centre of the Sun. Similarly, the CMB photons were not created at the surface of last scattering: they were produced at a much earlier epoch in the evolution of the universe. A tiny fraction (about one in a billion) of these photons, however, were created by recombination transitions at the last scattering surface. There should therefore be very weak emission lines in the black-body spectrum of the CMB radiation, but none has yet been detected.

Then, the big bang is the same everywhere wherever you look, otherwise one cannot speak of a common temperature of the CMB of about 2.75 Kelvin. We cannot see the CMB with the naked eye because it is in the microwave portion of the electromagnetic spectrum, but it exists everywhere in the universe. Indeed if we could see the CMB radiation, the sky would shine in all directions.

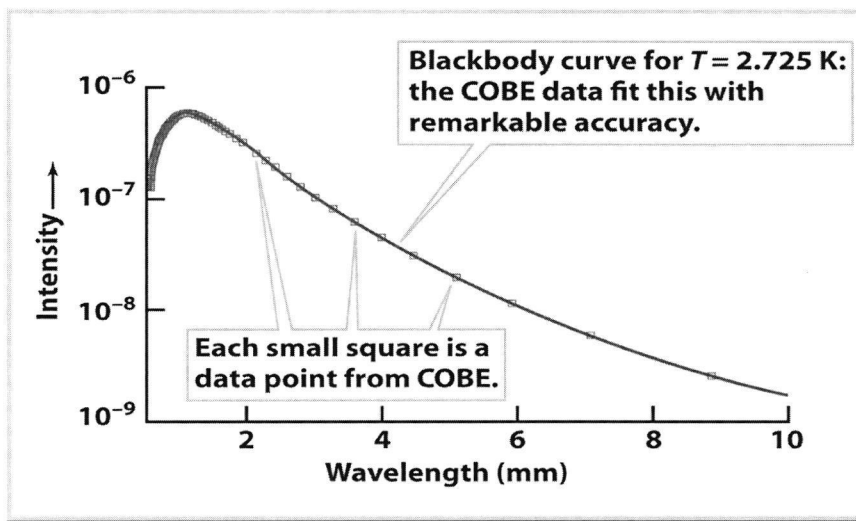
The first high-precision measurement of the CMB came from the Cosmic Background Explorer satellite. Nowadays, three important missions namely COBE [138], WMAP [88], and Planck [117] have been launched to explore the properties of these CMB in order to extract a wealth of information about the conditions of the early universe, in particular, the Hubble parameter H_0 , the baryon density content $\Omega_b h^2$, the cold dark matter density $\Omega_c h^2$, the dark energy density Ω_Λ , the effective number of relativistic species N_{eff} , the primordial helium mass fraction Y_p etc...Hence, the CMB is an important probe of the early universe and evidence of the hot big bang because it represents the oldest electromagnetic radiation from the recombination epoch.

(c) The Primordial Nucleosynthesis:

Big bang nucleosynthesis (BBN) is known to lead only to the formation of the light elements from ^2H up to ^7Li . It indicates a hot big bang through the production of most of the ^4He in the universe. A striking feature of BBN is its dependence on only one parameter the baryon density, which is determined by the Wilkinson Microwave Anisotropy Probe(WMAP) [61] and by the Planck mission as well [117]. Calculations of BBN based on canonical assumptions are successful in producing the abundances of the light elements that match the observations except the case of ^7Li , which seems to be overproduced (see chap.3 for details). This is so-called cosmological lithium problem is a challenging issue in modern astrophysics as we will outline in chap.4. Therefore, although BBN is an important tool that allows us to go back in time 13.7 billion years ago, it seems that something is missing in the physical conditions under which BBN has been operating.

The organization of the present thesis is as follows:

- In chap.2, we describe the observational constraints on the light elements, which will be used to test our calculations. Including any non-standard scenario is not free, rather it should be constrained by observations.
- In chap.3, the basic context of standard big bang nucleosynthesis (briefly SBBN) is reviewed.



The spectrum of the cosmic microwave background

Figure 1.4: The CMB radiation distribution a perfect blackbody of the indicated temperature (a: Courtesy of J. Mather/NASA; b: Courtesy of E. Cheng/NASA COBE Science Team. Taken from "Universe tenth edition" by A. R. Freedman et al., W. H. Freeman and Company).

- In chap.4, a summary of the present status of the lithium problem is presented, where we discuss the astrophysical and nuclear physics aspects of the lithium production. Since such aspects do not help to solve the lithium problem, we focus on the role of non-standard physics during BBN.
- In chap.5, we investigate the effect of varying neutrino number and chemical potentials on the production of light elements, especially on lithium. We also present some analytical calculations that allow us to have a better understanding of BBN.
- In chap.6, non-standard assumptions are introduced such as the role of varying the neutrino temperature and photon cooling through axion dark matter. In addition, we investigated the effect of a unified dark fluid on the production of lithium.
- In chap.7, we will present new constraints on the neutron lifetime from BBN by adopting the most recent primordial helium measurement. This has the potential to affect light element abundances.
- A Summary and outlook are given in chap.8

Chapter 2

Observational constraints on light elements

2.1 Observational constraints

The present work needs to specify the observational abundances of the light elements to use them as constraints for the theoretical treatment. It is not easy to determine observationally the abundances of the primordial light elements due to the scarcity of the objects showing them. In the following, we will describe the observational constraints.

2.1.1 Helium-4

Stellar evolution of this element after the end of BBN could be understood through consecutive star generations. In the stellar population, ${}^4\text{He}$ has increased above its primordial value due to the burning of hydrogen. For this reason the ${}^4\text{He}$ abundance is measured versus metallicity in less evolved systems such as Dwarf Irregular and Blue Compact Galaxies by linear extrapolation to zero metallicity. In other words, the ${}^4\text{He}$ mass fraction is determined by an extrapolation of the Y_p vs O/H and Y_p vs N/H correlations to O/H and N/H equal to zero. Meanwhile, although this method seems reasonable, it could lead to some statistical (stat) and systematic (syst) uncertainties in the evaluation of the primordial ${}^4\text{He}$ abundance. In Table 2.1 and Fig. 2.1, we present many successful attempts to measure the primordial helium abundance. These available data are from 1990 till now where most of the published results are from extragalactic low-metallicity HII regions.

However, independent measurements by WMAP and Planck collaboration show different ranges of the helium abundance with larger uncertainties. These two different values based on the effect of primordial helium on the CMB angular power spectrum. Although some of the data is in good agreement with SBBN calculations, new precise measurements of primordial helium are needed because the

helium abundance is crucial in constraining non-standard physics. In this work we have taken the constraint on ${}^4\text{He}$ from the recent independent measurement by [41] where $Y_p = 0.250_{-0.025}^{+0.033}$ or $0.225 \leq Y_p \leq 0.283$. This new measurement has the potential to constrain non-standard physics during BBN.

Table 2.1: Primordial helium-4 Observations.

| Y_p | Sample | Reference |
|---------------------------|---|-----------|
| 0.228 ± 0.005 | HII galaxies | [111] |
| 0.234 ± 0.002 | low-Z extragalactic H II regions | [109] |
| 0.243 ± 0.003 | H II regions in 23 low-metallicity blue compact galaxies (BCGs) | [67] |
| 0.225 ± 0.013 | eclipsing binaries | [125] |
| 0.2391 ± 0.0020 | 5 low-Z extragalactic HII regions | [94] |
| 0.2421 ± 0.0021 | 82 low-Z extragalactic HII regions | [68] |
| 0.250 ± 0.004 | low-Z extragalactic HII regions | [56] |
| 0.2477 ± 0.0029 | extragalactic HII regions | [113] |
| 0.245 ± 0.012 | NGC 6752 globular cluster blue HB stars | [152] |
| 0.2561 ± 0.0108 | 7 "high quality" extragalactic HII regions | [12] |
| 0.2565 ± 0.0050 | 786 low-Z extragalactic HII regions | [69] |
| 0.2449 ± 0.004 | metal-poor extragalactic HII regions | [13] |
| $0.28_{-0.15}^{+0.14}$ | 7-years WMAP | [88] |
| 0.2446 ± 0.0029 | extragalactic HII regions | [114] |
| $0.262_{-0.037}^{+0.035}$ | Planck collaboration | [117] |
| 0.245 ± 0.007 | extragalactic HII regions | [53] |
| $0.25_{-0.025}^{+0.033}$ | Intergalactic medium | [41] |

2.1.2 Deuterium

The situation of deuterium is reversed since it is the most fragile element and destroyed in stars at temperatures over 10^6K . In other words, it is considered that there are no significant astrophysical sources of deuterium. Rather it is destroyed by stellar processing. Thus, the observations of the deuterium abundance give a lower limit to its primordial abundance. Hydrogen rich-clouds absorbing the light of background QSOs at high redshifts represent the most appropriate environments for the determination of the primordial deuterium abundance. The method of determination requires low metallicity regions to lower astration effects. It requires also a neutral hydrogen column density in the range $17 \leq \log[N(\text{H}_I)/\text{cm}^{-2}] \leq 21$ and a low internal velocity dispersion of the clouds. For these reasons, there are so far only around 18 measurements of the primordial deuterium values. These show a large dispersion in

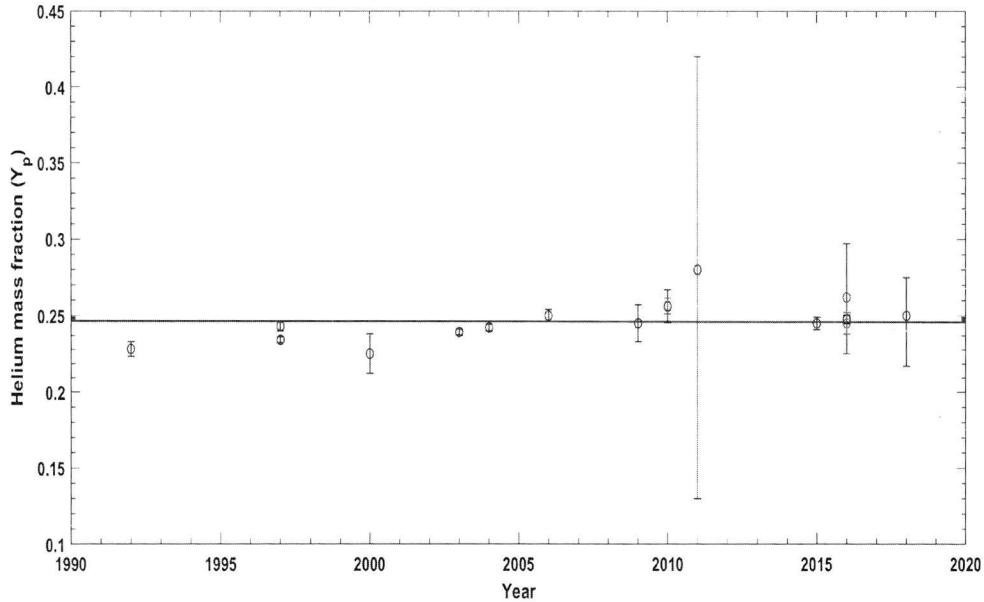


Figure 2.1: The evolution of primordial helium-4 observations from 1990 till 2018. The horizontal line represent the SBBN predictions.

the mean values and the estimated errors making the status of the primordial deuterium abundance puzzling. The non-weighted mean of these 18 measurements is $D/H = (2.53^{+0.16_{stat}+0.09_{syst}}_{-0.16_{stat}-0.08_{syst}}) \times 10^{-5}$. In Table 2.2 we present some of the primordial deuterium measurements where a recent accurate one is given by [42]. However, a following measurement is given by [26] for a system that meets the set of strict criteria by [42]. This system shows a different value for the primordial deuterium abundance. Another low value of deuterium $D/H = (1.2^{+0.5}_{-0.3}) \times 10^{-5}$ is given by [141] who argues therefore that astration factors can vary significantly even at low metallicity. Therefore, a large number of deuterium measurements is needed to understand the dispersion in its abundance. This dispersion is also shown in Fig. 2.2 where the horizontal lines represent SBBN predictions calculated in this work (see chap.3 for more details). It is clear that SBBN predictions are in disagreement with some observations and agreement with others. In addition, we have shown the error bars on each measurement to emphasize that systematic errors should not be underestimated since deuterium is an important tool to constrain the baryon density in the early universe.

The deuterium abundance is an important constraint on non-standard scenarios. Measurements of nuclear cross sections for the reactions with deuterium are essential for the comparison between theoretical predictions and observations. If we adopt the weighted mean of the best available measurements by [42], $\frac{D}{H} = (2.55 \pm 0.03) \times 10^{-5}$, we still find a difference with the calculated value

Table 2.2: Primordial deuterium observations.

| Quasars | Z_{abs} | $(D/H) \times 10^5$ | Reference |
|---------------------|--------------|--|--------------|
| Q1937 – 1009 | 3.572 | 3.3 ± 0.3 | [35] |
| Q1937 – 1009 | 3.256 | $2.45^{+0.3}_{-0.27}$ | [128] |
| Q1009 – 2956 | 2.504 | $4.0^{+0.6}_{-0.7}$ | [36] |
| Q0347 – 3819 | 3.025 | 3.75 ± 0.25 | [91] |
| J 1337+3152 | 3.168 | $1.2^{+0.5}_{-0.3}$ | [141] |
| J 1444+2919 | 2.437 | $1.97^{+0.33}_{-0.28}$ | [26] |
| J 1358+6522 | 3.067 | 2.58 ± 0.07 | [42] |
| J 1358+0349 | 2.853 | 2.62 ± 0.07 | [42] |
| HS 0105+1619 | 2.537 | $2.58^{+0.16}_{-0.15}$ | [42] |
| Q 0913+0715 | 2.618 | $2.53^{+0.11}_{-0.10}$ | [42] |
| J 1419+0829 | 3.050 | 2.51 ± 0.05 | [42] |
| J 1558-0031 | 2.702 | $2.40^{+0.15}_{-0.14}$ | [42] |
| J0407 – 4410 | 2.621 | $2.8^{+0.8}_{-0.6}$ | [106] |
| J1134 + 5742 | 3.411 | $2^{+0.7}_{-0.5}$ | [57] |
| Q1243 + 3047 | 2.526 | $2.42^{+0.35}_{-0.25}$ | [78] |
| Q2206 – 199 | 2.076 | 1.65 ± 0.35 | [119] |
| J1201 + 0116 | 2.988 | 2.50 ± 0.18 | [147] |
| J0744 + 2059 | 2.533 | 2.30 ± 0.08 | [147] |

$\frac{D}{H} = (2.65 \pm 0.07) \times 10^{-5}$ as obtained using the network "PARthENoPE" [124]. Note that the error on the calculated abundance is due to the estimation of the uncertainty in the evaluation of the cross sections for the deuterium reactions while the error on the measured values is due to systematic and statistical errors. Giving this situation, we will adopt in the present work the "conservative range" $2.58 \times 10^{-5} < D/H < 3.75 \times 10^{-5}$. Taking this range is motivated as follows:

- (i) As Fig. 2.2 shows, there is a significant dispersion in the observations.
- (ii) It is reasonable to consider a high value of primordial deuterium since it is easily destroyed in stars [108] or the dispersion in the observations is due to unknown stellar processes [51].

2.1.3 Helium-3 (${}^3\text{He}$)

Helium-3 is sensitive to the baryon to photon ratio of the universe just like deuterium. Although those many environments have been studied to measure the abundance of ${}^3\text{He}$, the determination of its primordial value is a complicated task. For example, terrestrial determinations of ${}^3\text{He}$ show a big dispersion of values. Also, since ${}^3\text{He}$ can not be produced by natural radioactive decay, this confirms that there is no cosmological source for this element, so that most of the terrestrial traces of this element may be due to the testing of nuclear weapons.

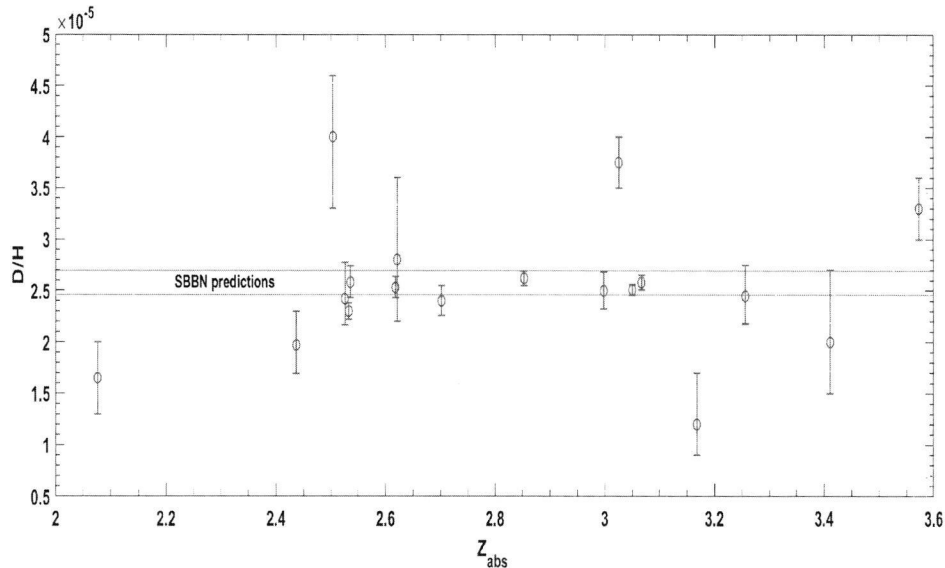


Figure 2.2: Primordial deuterium observations as function of the redshifts of the absorption system. Horizontal lines represent SBBN predictions.

In the solar system, ${}^3\text{He}$ is subjected to stellar processing since D is transformed to ${}^3\text{He}$ in stellar interiors and consequently, low mass stars are net producers of ${}^3\text{He}$. However, ${}^3\text{He}$ is destroyed in hotter regions so that the surviving ${}^3\text{He}$ nuclei from stellar evolution contribute to the chemical composition of the Inter Stellar Medium (ISM). Then it is not easy to find a correlation between ${}^3\text{He}$ and metallicity and consequently, it is difficult to determine the post-BBN value of ${}^3\text{He}$ due to its dependence on galactic evolution models. In such case we will assume a conservative upper limit of the primordial ${}^3\text{He}$ abundance inferred by [25] from the most distant and metal-poor stars such that ${}^3\text{He} \leq (1.1 \pm 0.2) \times 10^{-5}$.

2.1.4 Lithium (${}^7\text{Li}$)

Lithium, with its two isotopes ${}^6\text{Li}$ and ${}^7\text{Li}$, is the focus of the present thesis work because of the large discrepancy between the SBBN predictions and observations. The observations of ${}^7\text{Li}$ in metal-poor halo stars are still a big puzzle for cosmologists and astrophysicists who are trying to explain this discrepancy. The first time one tried to relate the observations of lithium to its primordial abundance was by [140] who argued that the abundance of lithium in metal-poor dwarfs was independent of metallicity within a small dispersion suggesting that this observed value is the one produced by BBN. This behavior was called the "Spite Plateau". However, extending the observations to very low metallicity as seen in Fig. 4.1, there is no plateau anymore. Although metal-poor stars in the halo of the Galaxy represents the best environments to measure the primordial lithium abundance,

lithium could be subject to destruction which makes its behavior very complicated. In Table 2.3 we give a list of the estimates for the ${}^7\text{Li}$ abundances in the last ten years. All of these observed lithium abundances do not agree with SBBN predictions for the range of baryon to photon ratio η deduced from recent CMB observations. In addition, these observations are different from each other, so it is not easy to combine all the observed values of lithium in one single estimate. The non-weighted mean of this data along with the systematic and statistical errors is $Li/H = 1.93^{+0.26_{stat}+0.17_{syst}}_{-0.26_{stat}-0.12_{syst}}$. For this reason, an upper limit on the primordial lithium abundance can be adopted such as $Li/H \leq 2.8 \times 10^{-10}$ since we assume that this reduction is enough and any remaining difference can be explained by stellar processing which seems to be rather complicated.

Table 2.3: Primordial lithium observations.

| $[{}^7\text{Li}] = 12 + \log_{10}({}^7\text{Li})$ | ${}^7\text{Li}/H \times 10^{10}$ | Reference |
|---|----------------------------------|-----------|
| 2.24 ± 0.01 | 1.738 ± 0.040 | [32, 33] |
| $2.09^{+0.19}_{-0.13}$ | $1.230^{+0.675}_{-0.318}$ | [126] |
| 2.34 ± 0.06 | $2.188^{+0.324}_{-0.283}$ | [34] |
| 2.37 ± 0.05 | $2.344^{+0.286}_{-0.255}$ | [100] |
| 2.21 ± 0.09 | $1.622^{+0.373}_{-0.304}$ | [39] |
| 2.095 ± 0.055 | $1.245^{+0.168}_{-0.149}$ | [20] |
| 2.54 ± 0.1 | $3.467^{+0.898}_{-0.713}$ | [83] |
| 2.2 ± 0.086 | $1.58^{+0.35}_{-0.28}$ | [131] |

Chapter 3

The Standard Big Bang Nucleosynthesis

One of the biggest successes in the 20th century is the establishment of the standard model of particle physics and cosmology. This was the cornerstone of the hot big bang model, or simply "Standard Big Bang Nucleosynthesis" (SBBN). The SBBN framework is well understood in the context of the standard model of particle physics. It is a reliable theory to understand the formation of light elements in the universe during the first minutes after the creation. SBBN predicts that the universe is composed of about 75% of hydrogen and 25% of ⁴He and small amounts of D, ³He, ⁷Li and ⁶Li [30]. SBBN is a parameter-free theory since it depends only on the baryon to photon ratio η of the universe, which is well known. These abundances are performed under standard assumptions which include: (i) an isotropic and homogeneous distribution of matter at very high temperature and density, (ii) the expansion of the universe obeys the Hubble law described by Friedmann equations. As a consequence of the expanding and cooling universe, the last photon scattering occurred at 377,000 years after big bang which led to the emerging of the microwave background radiation (CMB).

3.1 Standard big bang nucleosynthesis

3.1.1 Method of calculation

Primordial nucleosynthesis can be viewed as a competition between the expansion time scale of the universe and the lifetime of the reaction rates. In other words, the expansion rate of the universe acts as a "shut-of" for nuclear reactions, so that when it becomes faster than the lifetime of a reaction rate, the corresponding reaction will freeze out. This is the base of the numerical calculations that could be performed using several codes such as NUC123[87] or PArthENoPE [124]. In this work we have used an available public code, the AlterBBN [18] with an up-

dated network of nuclear reactions as shown in Appendix E. Such a code enables us to calculate the abundances of light elements in the standard cosmological model and beyond it to include different non-standard assumptions. Like other BBN codes, in addition to the set of differential equations, AlterBBN requires an input of some cosmological parameters namely: the baryon to photon ratio η which is a key parameter for SBBN, the number of effective relativistic degrees of freedom N_{eff} , the neutron lifetime τ_n and neutrino degeneracy $\beta_{\nu_e, \mu, \tau}$. Varying one of these parameters or including non-standard scenarios is not free, rather the predicted abundances of light elements based on SBBN should be constrained by the observations discussed in chap.2.

Analytical considerations will be rather useful since it is possible to obtain an approximate solutions to the BBN process following basically the approach by [103]. This will help to better clarify the numerical results and deepen our understanding of BBN. Analytical calculations are performed to better interpret the physical processes involved in primordial nucleosynthesis. Special attention is given to three important stages of BBN, namely:(1) the freeze-out of neutrons; (2) the deuterium bottleneck; and (3) the quasi-equilibrium of neutrons and deuterium. These three stages determine the final light-element abundances. That is the analytical treatment not only gives an approximate solution but also allows one to analyze how and why BBN depends upon various cosmological parameters and how light elements are related to each other especially helium, deuterium, and lithium.

3.1.2 How to produce light elements?

Given that $\eta = \frac{n_b - n_{\bar{b}}}{n_\gamma} = (6.14 \pm 0.04) \times 10^{-10}$ the baryon to photon ratio of the universe determined by Planck mission [117] and using a set of differential equations, we can determine light element abundances. This is the simplest scenario which leads to the SBBN predictions.

To summarize the SBBN framework we will start with some definitions. The number density n_i of each species is normalized with respect to the total number density of baryons:

$$Y_i = \frac{n_i}{n_B} \quad i = p, {}^2H, {}^3He, \dots \quad (3.1)$$

The most important nuclei we are interested in are 2H , 3He , 4He and 7Li , so that the abundances of these elements are defined as followings:

$${}^2H/H \equiv Y_{2H}/Y_p, {}^3He/H \equiv Y_{3He}/Y_p, Y_p \equiv 4Y_{4He}, {}^7Li/H \equiv Y_{7Li}/Y_p, \quad (3.2)$$

where all abundances are normalized to hydrogen except 4He is given as mass a fraction.

SBBN is controlled by a set of differential equations as the following:

- Eq.(3.3) is one of the Friedmann equations where H is called the Hubble parameter and it describes the expansion rate of the universe.

$$\frac{\dot{a}}{a} = H = \sqrt{\frac{8\pi G_N}{3}\rho}, \quad (3.3)$$

$a(t)$ denotes the scale factor, the dot represents the derivative with respect to cosmic time and ρ is the total energy density present during BBN. The early universe was radiation-dominated so that relativistic particles dominate the energy content of the universe. Then ρ is given by:

$$\rho = \rho_\gamma + \rho_\nu + \rho_{e^\pm}, \quad (3.4)$$

with

$$\rho_\gamma = \frac{\pi^2}{30}g_\gamma T_\gamma^4, \quad \rho_\nu = \frac{\pi^2}{30}\left(\frac{7g_\nu}{8}\right)T_\nu^4, \quad \rho_{e^\pm} = \frac{\pi^2}{30}\left(\frac{7g_{e^\pm}}{8}\right)T_{e^\pm}^4, \quad (3.5)$$

where $g_\gamma = 2$ is the number of degrees of freedom of photons, $g_\nu = 6$ for neutrinos (3 for neutrinos and 3 for anti-neutrinos) and $g_{e^\pm} = 4$ for electron-positron pairs before they annihilate. $T_\gamma, T_{e^\pm}, T_\nu$ refers to the temperature of photons, electron-positron pairs and neutrinos respectively. These energy densities are obtained by assuming a small chemical potential $|\mu| \ll T$ and mass $m \ll T$. In addition, using a perfect black body distribution and integrating over all frequencies, the number density of photons is

$$n_\gamma = \int_0^\infty n_\gamma(\nu)d\nu \approx \left(\frac{1.202}{\pi^2}\right)g_\gamma T^3 \quad (3.6)$$

where the Boltzmann constant k_B , the reduced Planck constant \hbar and the speed of light c are taken to be equal to one. At a CMB temperature today of $T \approx 2.725K$, the number density is calculated to be $n_\gamma \approx 400cm^{-3}$.

Multiplying the integrand of Eq.(3.6) by $h\nu$ and integrating over all frequencies, we obtain the expression for photon radiation density shown in Eq.(3.5).

Similarly using the number density of fermions given as:

$$n_f \approx 1.202\left(\frac{3}{4\pi^2}\right)g_f T^3 \quad (3.7)$$

we can derive the energy density of fermions when the Fermi-Dirac distribution is used. Note that the index "f" refers to fermions(electrons, positrons and neutrinos).

- The continuity equation or energy conservation equation is given as follows:

$$\dot{\rho} = -3H(\rho + P), \quad (3.8)$$

where P is the total pressure given by:

$$P = P_\gamma + P_e + P_\nu + P_B, \quad (3.9)$$

where P_γ , P_e , P_ν , P_B refer to photon, electron-positron, neutrinos and baryons pressures. The continuity equation is obtained by assuming an adiabatic expansion of the universe. Then the first law of thermodynamics can be written as:

$$d\varepsilon = -PdV \quad (3.10)$$

where ε is the total energy and P is the pressure within an expanding volume V . Given that the volume scales as $V \sim a^3$, we can obtain the continuity equation shown in Eq.(3.8).

- According to the general theory of relativity, the equation of motion or the second Friedmann equation can be written as:

$$\ddot{a} = -\frac{4\pi}{3}G(\rho + 3p)a \quad (3.11)$$

Friedmann equations are used to describe the cosmic expansion during various evolutionary phases. These equations allow us to determine two unknown functions: the scale factor $a(t)$ characterizing the expansion of the universe and $\rho(t)$ the energy density of the universe. Eqs.(3.3, 3.8, 3.11) are not independent, rather we can obtain one of the three equations from the two others. For example, multiplying Eq.(3.11) by \dot{a} and using Eq.(3.8) we can get the first Friedmann equation given by Eq.(3.3). It is shown that these equations lead to:

$$a \sim \sqrt{t} \quad (3.12)$$

while the conservation of stress energy leads to:

$$\rho \sim a^{-4} \quad (3.13)$$

Replacing Eqs. (3.12,3.13) in Eq.(3.3) we can derive the time temperature relation:

$$t_{sec} \simeq \frac{1.39k_{eff}^{-1/2}}{T^2} \quad (3.14)$$

with $k_{eff} = \frac{\pi^2}{30}(g_\gamma + \frac{7g_f}{8})$, the cosmological time in seconds and the temperature in Mev.

Note that the Friedmann equations can be modified when non-standard physics scenarios are adopted, for example by an entropy component or a non-adiabatic accelerated universe [37, 81, 137].

- Since baryons play an important role during BBN, the total baryon number is given as:

$$\frac{\dot{n}_B}{n_B} = -3H \quad (3.15)$$

Nuclear and electromagnetic scatterings keep the non-relativistic baryons in kinetic equilibrium so that their energy density and pressure are given by :

$$\rho_B = [M_u + \sum_i (\Delta M_i + \frac{3}{2}T)Y_i]n_B \quad (3.16)$$

$$P_B = Tn_B \sum_i Y_i, \quad (3.17)$$

with ΔM_i and M_u are the mass excess and the atomic mass unit respectively of nuclide i .

- The density evolution of each species (production and destruction) is given by Boltzmann equations described in Eq.(3.18) where i,j,k,l refer to nuclear species, N_i the number of nuclides of type i entering a given reaction, and Γ denotes the reaction rate.

$$\dot{X}_i = \sum_{j,k,l} N_i (\Gamma_{kl \rightarrow ij} \frac{Y_k^{N_k} Y_l^{N_l}}{N_k! N_l!} - \Gamma_{ij \rightarrow kl} \frac{Y_i^{N_i} Y_j^{N_j}}{N_i! N_j!}) \equiv \Gamma_i \quad (3.18)$$

- The charge neutrality of the universe is given by Eq.(3.19), with ϕ_e is the electron chemical potential and $\hat{L}(\frac{m_e}{T}, \phi_e)$ is the lepton charge density in units of the electron charge.

$$n_B \sum_j Z_j Y_j = n_{e^-} - n_{e^+} \equiv L(\frac{m_e}{T}, \phi_e) \equiv T^3 \hat{L}(\frac{m_e}{T}, \phi_e) \quad (3.19)$$

Finally, the Boltzmann equations for the neutrino species are given by Eq.(3.20) where $f_{\nu_\alpha}(|p|, t)$ denotes neutrino distribution in phase space and $I_{\nu_\alpha}[f_{\nu_e}, f_{\nu_x}]$ represents the collisional integral containing all microscopic processes responsible for creating and destroying ν_α . f_{e^\pm} are the Fermi-Dirac function of electron-positron.

$$(\frac{\partial}{\partial t} - H|p| \frac{\partial}{\partial |p|}) f_{\nu_\alpha}(|p|, t) = I_{\nu_\alpha}[f_{\nu_e}, f_{\bar{\nu}_e}, f_{\nu_x}, f_{\bar{\nu}_x}, f_{e^-}, f_{e^+}], \quad (3.20)$$

To obtain light elements at a given η , it is important to use an updated network of nuclear reactions. The light nuclides intervening in BBN network of nuclear reactions are shown in Fig. 3.1. The network of BBN contains 100 reactions as given in Appendix E, however, we show in Fig. 3.1 the most crucial

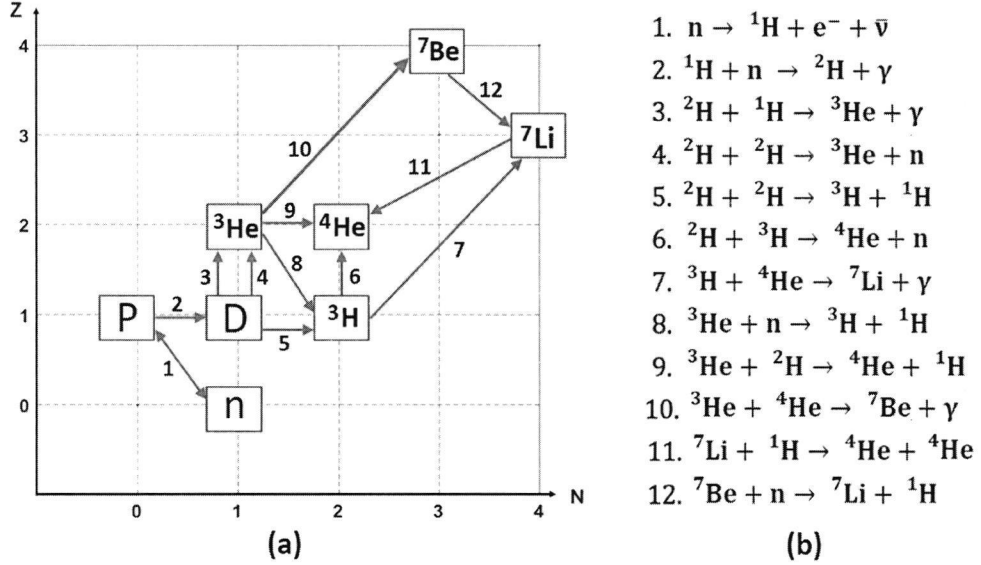


Figure 3.1: Network of the most important nuclear reactions intervening during BBN.

reactions controlling the final element abundances produced by SBBN. The variation of these light elements as a function of temperature is given in Fig. 3.2 that shows the phases where deuterium reaches its maximum value (bottleneck) and when the neutron concentration drops to that of deuterium. These two phases along with the freeze-out of neutrons are crucial for the determination of light elements which will be discussed in detail in chap.5.

Fig. 3.3 shows light element abundances as a function of the baryon density or equivalently the baryon to photon ratio η : ${}^3\text{He}$ and D are sensitive to η in contrast to ${}^4\text{He}$ which depends linearly on η . Deuterium is considered as an excellent baryometer since as shown in Fig. 3.3 it decreases significantly for a small variation of the baryon density. Concerning ${}^7\text{Li}$, its variation as function of baryon density is more complicated. Its production at low baryon density is mainly determined by ${}^3\text{H} + {}^4\text{He} \rightarrow {}^7\text{Li} + \gamma$ while at higher baryon density its production is favoured through ${}^3\text{He} + {}^4\text{He} \rightarrow {}^7\text{Be} + \gamma$ where ${}^7\text{Be}$ will be then transformed to ${}^7\text{Li}$ by radioactive decay via electron capture.

The SBBN predictions obtained in this work are shown in Table 3.1 (the second column). Our calculation shows a good agreement with other works [45, 116] for all elements with minor differences. It is important to mention here that the final lithium abundance obtained in this work is less than the ones obtained in the other works, this is due to the difference in the adopted nuclear rates. We tried

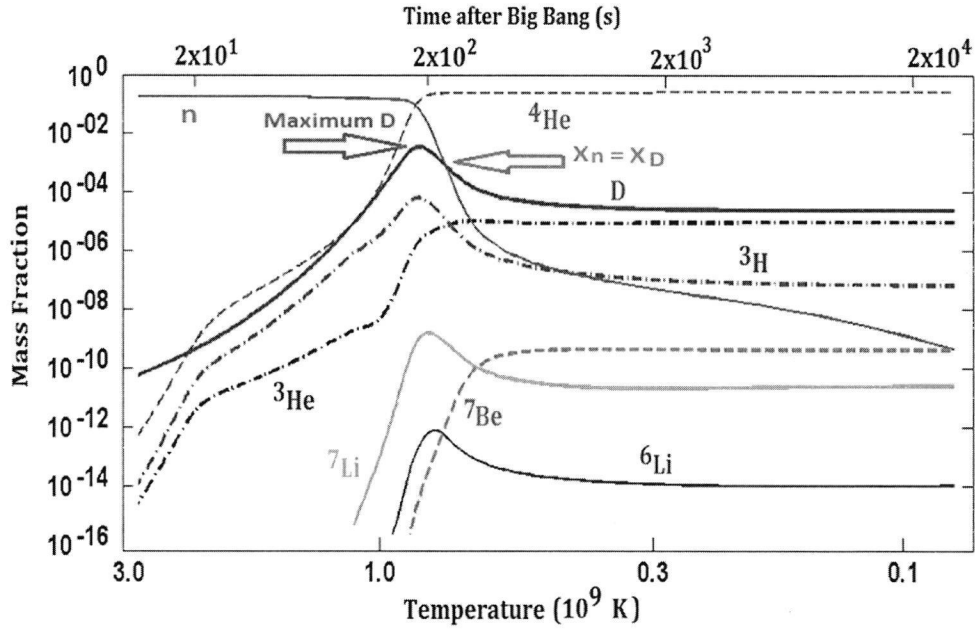


Figure 3.2: Light element abundances as a function of temperature/time and the main reactions leading to these abundances.

to use the most updated nuclear rates that give the lowest lithium abundance to see how much lithium abundance could be reduced by SBBN. However, lithium is still higher than the observations shown in the fifth column of Table 3.1. This discrepancy will be discussed in detail in chap.4.

Table 3.1: Different SBBN predictions compared to observations.

| | This work | Pitrou et al. (2018) [116] | Cyburt et al. (2016) [45] | Observations |
|----------------------------------|-----------------------|-------------------------------|------------------------------|------------------------------|
| Y_p | 0.24610 ± 0.00015 | 0.24709 ± 0.00017 | 0.24709 ± 0.00025 | 0.2449 ± 0.0040 [13] |
| $D/H \times 10^5$ | 2.653 ± 0.123 | 2.459 ± 0.036 | 2.58 ± 0.13 | 2.58 ± 0.07 [42] |
| ${}^3\text{He}/H \times 10^5$ | 1.017 ± 0.0531 | 1.074 ± 0.026 | 1.0039 ± 0.0090 | 1.1 ± 0.2 [25] |
| ${}^7\text{Li}/H \times 10^{10}$ | 4.285 ± 0.378 | 5.623 ± 0.247 | 4.68 ± 0.67 | $1.58^{+0.35}_{-0.28}$ [131] |

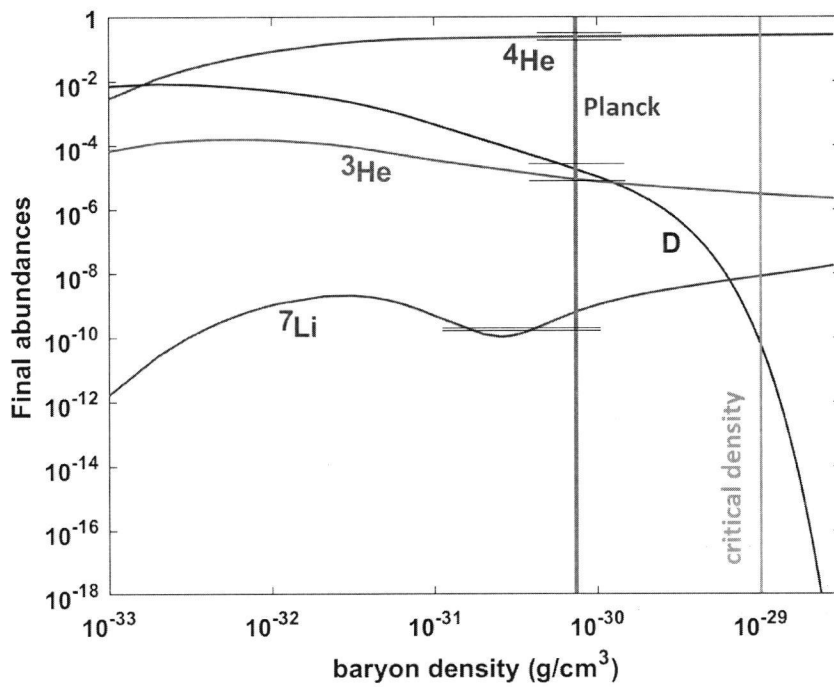


Figure 3.3: Light element abundances as a function of baryon density calculated by taking the relativistic degrees of freedom intervening during BBN to be $N_{eff} = 3$ and the neutron lifetime $\tau_n = 880.2$. The vertical gray band is the Planck determination of baryon density while the orange band represents the critical density of the universe. Horizontal lines represent observations of light elements.

Chapter 4

The present status of the lithium problem

Understanding the production of ${}^7\text{Li}$ in the early universe is currently a challenging problem in modern astrophysics. This is due to the large discrepancy between the SBBN predictions and observations. As we have shown in chap.3 the primordial ${}^7\text{Li}$ abundance does not match the observations. Over the past decades, the observed abundance of ${}^7\text{Li}$ in metal-poor Halo stars was found to be less by a factor of 2-3 than the predicted based on SBBN [43]. Furthermore, the discrepancy has increased to 2.4-4.3 or 4.2σ (from globular cluster stars) and 5.3σ (from Halo field stars) [43]. On the other hand, the so-called "Spite Plateau", that is a constant ${}^7\text{Li}$ abundance down to metallicity $[Fe/H] = -3.0$ was considered to represent the primordial abundance of this element for a long time. This means that ${}^7\text{Li}$ would be independent of metallicity. However, the extended observations below $[Fe/H] = -3.0$ show that the plateau is not obtained [71] as can be seen in Fig.4.1. For a metallicity $[Fe/H] > -3.0$ there is a moderate dispersion in the primordial abundance as shown in the rectangular shape, however, the dispersion becomes more significant for $[Fe/H] < -3.0$ so that the plateau is not obtained. This means that in addition to the discrepancy between SBBN predictions and observations of lithium, there is an additional dispersion in the observations. Thus two problems are encountered:

- Matching the predicted ${}^7\text{Li}$ abundance on the basis of SBBN with observations.
- Understanding the deviation of the ${}^7\text{Li}$ abundance below the plateau at very low metallicity.

A question arises now: are there two separate lithium problems? This makes the lithium puzzle difficult to be explained. This so-called "The Lithium Problem" needs to be resolved, however, resolving this problem seems to be a complex task because no single answer can be extracted. Possible solutions to the lithium problem fall within three categories [55]:

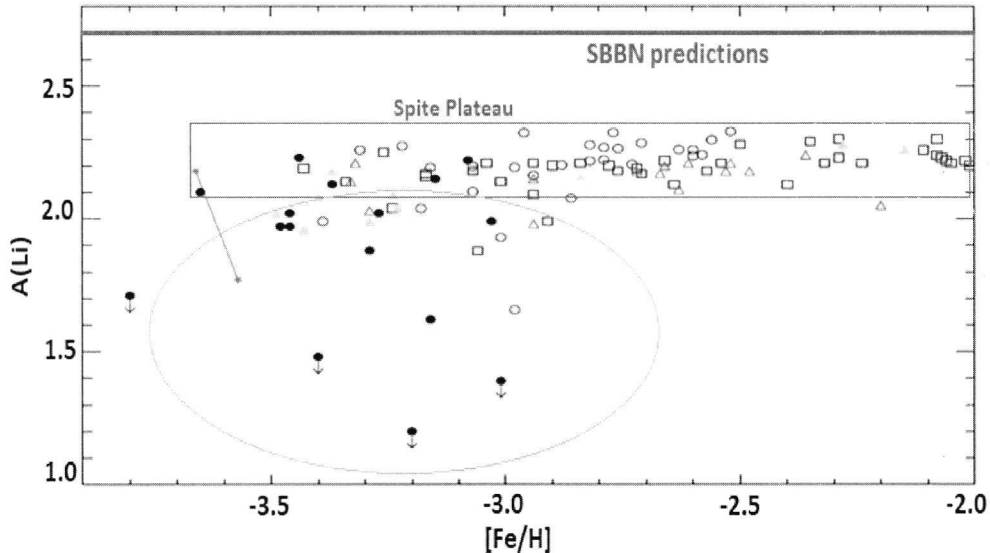


Figure 4.1: Primordial lithium observations as a function of metallicity.

- Astrophysical solutions
- Nuclear physics solutions
- Solutions beyond the standard model of particle physics.

Our attempt in the present work is to get more insight into this complicated task.

4.1 Astrophysical Aspects

It is possible to assume that the observed ${}^7\text{Li}$ abundance in metal-poor stars does not represent the primordial value, because of effective stellar processing. In other words, it is important to figure out how effective is the role of stellar processing. Absorption lines in the atmosphere of metal-poor stars are used to determine the ${}^7\text{Li}$ abundance. These lines are very sensitive to the model atmosphere and the physical conditions under which they are formed. In other words, in order to determine the abundance of lithium, this needs a knowledge of the temperature of the atmosphere which is not trivial since the emergent radiation is not a perfect Planck curve. Then, using different temperature scales and atmosphere models, a dispersion in the lithium abundance was obtained from different groups. In such a case, systematic errors in the determination of lithium could take place so that the difference in the observed lithium seems to lie in the determination of the temperature scale and atmosphere model. However, to explain

the discrepancy between SBBN predictions and observations a shift of 500-600K in temperature is needed, which is not achieved, leaving the lithium problem unresolved [38, 62]. One supposes that there are some physical processes behind the discrepancy between the observed and predicted lithium. This means that if there is a physical process that depletes lithium, it should also explain how lithium exhibits the dispersion at low metallicity and the regular behavior at higher metallicity which is referred to as "Spite Plateau". Reduction of lithium is possible through variations in stellar properties, e.g. rotation, magnetic fields, etc. [123], but the difficulty is to find a stellar mechanism to reduce the plateau level without inducing excessive dispersion in the abundances from star to star. Therefore, a question came out: what is the origin of lithium in the stellar atmospheres? On one hand, one could assume that the observed lithium is not the primordial one since it may be enriched or depleted in stars. On the other hand, it is not easy to find an astrophysical process that could explain the strange behavior of lithium ranging from a metallicity of $[\frac{Fe}{H}] = -4.0$ until $[\frac{Fe}{H}] = -2.0$.

4.2 Nuclear Physics Aspects

An important aspect of understanding the lithium abundance is to have as far as possible reliable cross sections for the involved reactions in the SBBN (see Appendix E). It is emphasized that about 90% of the ${}^7\text{Li}$ is produced through electron capture on ${}^7\text{Be}$. The element ${}^7\text{Be}$ is a bridge to the production of ${}^7\text{Li}$. In particular, several important reactions determining the production of ${}^7\text{Li}$ are: ${}^3\text{He}(\alpha, \gamma){}^7\text{Be}$ and ${}^7\text{Be}(n, p){}^7\text{Li}$. It turns out that if the level of the "Spite Plateau" is to be matched, then the production of ${}^7\text{Be}$ by the ${}^3\text{He}(\alpha, \gamma){}^7\text{Be}$ -reaction should be lower by a factor three to four [55]. If this would be the case, then the ${}^7\text{Be}$ and ${}^8\text{B}$ solar neutrino flux would be reduced by the same factor and this argues against this assumption. Thus, the solar neutrinos constrain that rate. The reaction rate of ${}^7\text{Be}(n, p){}^7\text{Li}$ should be greater by a factor of 2 to lower the ${}^7\text{Li}$ production but this is not achieved yet [29]. In addition, electron screening was also studied and found to have negligible contribution [66].

It should be emphasized that the reactions responsible for the production and destruction of deuterium can also influence indirectly the final abundance of ${}^7\text{Li}$, we come back to this in chap.5.

The following reactions influence the abundance of ${}^3\text{He}$ and D namely ${}^3\text{He}(d, p){}^4\text{He}$, $d(d, n){}^3\text{He}$, and $d(p, \gamma){}^3\text{He}$. For example, if the cross section of $d(d, n){}^3\text{He}$ is reduced by a factor of 2 this will keep the abundance of D higher, and consequently decrease ${}^7\text{Li}$ (see Table 4.1). This is not apparent so far. We show in Table 4.1 the abundances of light elements when multiplying some crucial reaction rates by different factors. This is to see what is the needed increase or decrease in these reaction rates in order to solve the lithium problem. A remaining possibility is the existence of resonances in the reactions ${}^7\text{Be} + d \rightarrow {}^9\text{B}^*$ or via ${}^7\text{Be} + t \rightarrow {}^9\text{B}^*$

Table 4.1: Resultant abundances when reaction rates are multiplied by some factors.

| reaction | factor | Y_p | ${}^3\text{He}/H \times 10^5$ | $D/H \times 10^5$ | ${}^7\text{Li}/H \times 10^{10}$ |
|--|--------|--------|-------------------------------|-------------------|----------------------------------|
| ${}^2\text{H} + p \rightarrow \gamma + {}^3\text{He}$ | 0.25 | 0.2461 | 0.726 | 3.350 | 2.631 |
| ${}^2\text{H} + {}^2\text{H} \rightarrow n + {}^3\text{He}$ | 0.5 | 0.2452 | 0.884 | 3.623 | 2.738 |
| ${}^3\text{He} + {}^2\text{H} \rightarrow p + {}^4\text{He}$ | 3 | 0.2461 | 0.625 | 2.696 | 2.275 |
| ${}^3\text{He} + {}^4\text{He} \rightarrow \gamma + {}^7\text{Be}$ | 0.5 | 0.2461 | 1.017 | 2.653 | 2.219 |
| ${}^7\text{Be} + n \rightarrow p + {}^7\text{Li}$ | 2 | 0.2461 | 1.017 | 2.653 | 2.493 |
| ${}^7\text{Be} + n \rightarrow {}^4\text{He} + {}^4\text{He}$ | 1000 | 0.2461 | 1.017 | 2.653 | 2.392 |

[55].

Although resolving the lithium problem on nuclear physics grounds seems unlikely, some nuclear reaction rates are subject to revision. In particular a new ${}^7\text{Be}(n, \alpha){}^4\text{He}$ rate has been measured [28] the first time for neutron energies down to about 1.0 eV. As we see below this new reaction rate does not significantly affect ${}^7\text{Be}$ production. An increase by a factor of 1000 of this rate would be required to resolve the lithium problem, however the new rate turns out to be less by a factor of 100 leaving the lithium problem unaffected.

4.2.1 The ${}^7\text{Be}(n, \alpha){}^4\text{He}$ rate

The ${}^7\text{Be}(n, \alpha){}^4\text{He}$ reaction leads obviously to the destruction of ${}^7\text{Be}$, thus affecting the final abundance of ${}^7\text{Li}$. Using the new cross section [28] for ${}^7\text{Be}(n, \alpha){}^4\text{He}$ measured over a wide range of neutron energies, we have done a new polynomial fit in an extended range up to 10 GK. In units of $\text{cm}^{-3}\text{s}^{-1}\text{mole}^{-1}$ the Maxwellian average cross section in the following temperature ranges is:

For $0.001 \leq T_9 \leq 2$ ($T_9 = T/10^9\text{K}$) :

$$N_A \langle \sigma v \rangle = 4.844 \times 10^5 + 2.748 \times 10^5 T_9^3 + 3.885 \times 10^5 T_9^2 + 3.544 \times 10^6 \times T_9 \quad (4.1)$$

For $2 \leq T_9 \leq 10$:

$$N_A \langle \sigma v \rangle = 4.353 \times 10^6 - 2.845 \times 10^3 T_9^5 + 9.656 \times 10^4 T_9^4 - 1.219 \times 10^6 T_9^3 + 6.393 \times 10^6 T_9^2 - 5.2 \times 10^6 T_9 \quad (4.2)$$

The comparison among the evaluations of this rate is shown in Fig. 4.2. Our rate as given by Eqs. (4.1, 4.2) is close to that used by [64], but it is more accurate. A clear discrepancy is seen with the older rate used by [153], which is overestimated. This means, ${}^7\text{Be}$ is less destroyed by the new rate.

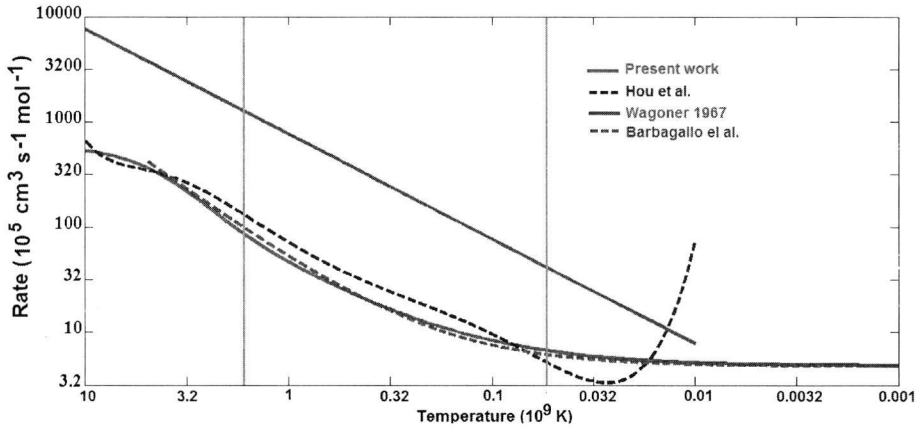


Figure 4.2: Comparison between different calculated rates of ${}^7\text{Be}(n, \alpha){}^4\text{He}$. The vertical yellow bands indicate the BBN temperature range. Note the significant difference between the new rates and that used by Wagoner especially in the BBN range.

4.2.2 $d + {}^7\text{Be}$ rate

A new measurement and evaluations of the $d + {}^7\text{Be}$ rate is given by [127]. The evaluation of this rate by Ref.[47]. The comparison of the two rates shown in Fig. 4.3 indicates a higher new rate in the temperature range relevant to BBN. This means more effective destruction of ${}^7\text{Be}$. However, the effect on ${}^7\text{Li}$ production turns out to be minimal, about 2%. The role of this rate was considered by [55] as a possible solution to the lithium problem, but with an ad hoc assumption by multiplying the rate used by [9] with a factor of 100. Let us do the following test with this rate [127]:

- (i) we multiply it by a factor of 25 and compare the resulting ${}^7\text{Be}$ abundance obtained in both cases. This is shown in Fig. 4.4 indicating clearly the destruction of the ${}^7\text{Be}$ abundance with the increased rate.
- (ii) Using the increased rate as above leads to a decrease of the ${}^7\text{Li}$ abundance down to 2.75×10^{-10} (see the third column of Table. 4.2). Thus, the increased rate by a factor of 25 would solve the lithium problem, but where is the hidden resonance to justify this increase?

In analyzing reaction rates relevant to the production of ${}^7\text{Li}$, we aim to show how they may contribute to the understanding of the lithium problem and to ameliorate its status.

4.2.3 Electron capture of ${}^7\text{Be}$

Another effect to be considered is the electron capture on ${}^7\text{Be}$. This process occurs during the proton-proton chain in solar-like stars and also in the late evo-

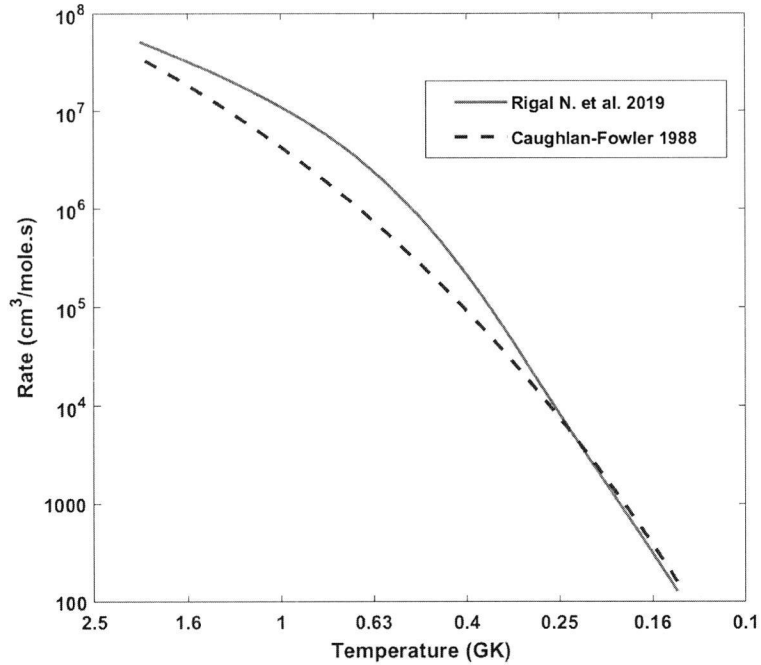


Figure 4.3: Comparison between the new ${}^7\text{Be} + d$ rate and the one by Caughlan-Fowler in the BBN temperature ranges to see the effect on the final abundance of ${}^7\text{Be}$

Table 4.2: Effect of the new ${}^7\text{Be} + d$ rate on the final lithium abundance.

| | Using Caughlan-Fowler 1988 rate | Using the new rate by [127] | Using the new rate by [127] multiplied by a factor of 25 |
|----------------------------------|---------------------------------|-----------------------------|--|
| Y_p | 0.2461 ± 0.0001474 | 0.24709 ± 0.00017 | 0.2461 ± 0.0001474 |
| $D/H \times 10^5$ | 2.653 ± 0.123 | 2.653 ± 0.123 | 2.653 ± 0.124 |
| ${}^3\text{He}/H \times 10^5$ | 1.017 ± 0.053 | 1.017 ± 0.053 | 1.017 ± 0.053 |
| ${}^7\text{Li}/H \times 10^{10}$ | 4.354 ± 0.385 | 4.283 ± 0.378 | 2.754 ± 0.417 |

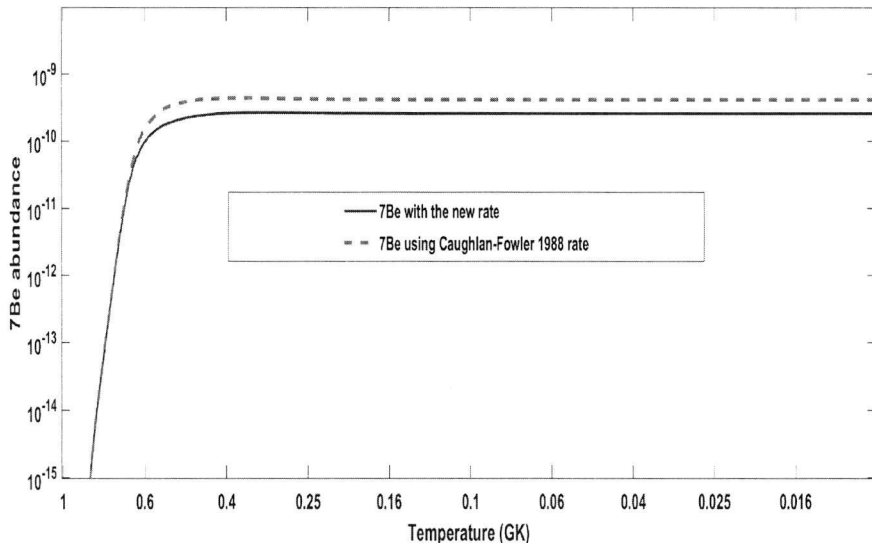


Figure 4.4: ${}^7\text{Be}$ abundance when using the rate by Caughlan-Fowler 1988 (red dashed line) and the new ${}^7\text{Be} + d$ rate multiplied by a factor of 25 (blue solid line).

lutionary phases of stars [144]. However, the physical conditions during the BBN are different, since one deals with a temperature of $T_9 = 0.1 - 1.0$ and an electron density a factor of (100-1000) more abundant than under the conditions of the Sun. In addition, the baryon density during BBN is smaller than in the Sun. In order to account for the electron capture on ${}^7\text{Be}$, for example by adopting the result of [144], extrapolation is needed, which is not done yet. This seems to be a demanding task since relativistic effects should be considered as argued by [102]. It is however emphasized that the electron capture is not important unless its lifetime becomes shorter than the expansion time scale of the universe. In summary, the electron capture on ${}^7\text{Be}$ is not likely to alter the lithium production. Our discussion so far indicates that we may consider some non-standard assumption to get more insight into the lithium production in the early universe. This will be the subject of the following sections.

4.3 Non-standard Physics

4.3.1 Inhomogeneous nucleosynthesis

In contrast to SBBN, intensive studies have been devoted to anisotropic models based upon inhomogeneity in the baryon to photon ratio η [11, 76, 99, 105]. The fluctuations in η are thought to be generated at early epochs of SBBN, perhaps

during the QCD or electroweak transitions. In such case, neutron and proton-rich environments can be created which will promote the production of primordial abundances. In this context, two scenarios are considered: (a) When nucleon diffusion occurs at high temperature before the beginning of nucleosynthesis the final abundance of ${}^4\text{He}$ is reduced. Consequently, the nucleosynthesis time is extended because it will be determined by neutron decay which ultimately leads to an overproduction of D as well as of lithium. (b) If the diffusion occurs during BBN, an overproduction of ${}^4\text{He}$ can take place.

In addition to the above scenarios, when the baryon/antibaryon mass exceeds $10^{-21}M_{\odot}$, an annihilation of antimatter could take place [143]. When the annihilation occurs after the weak freeze-out this leads to a reduction of the ${}^4\text{He}$ abundance. However, if the annihilation occurs after the synthesis of ${}^4\text{He}$ this will lead to overproduction of ${}^3\text{He}$ and D that will contradict observational constraints [27].

Although inhomogeneous nucleosynthesis models represent attractive scenarios for SBBN, these models do not solve the lithium problem because of the observational constraints on other light elements. An overview concerning inhomogeneous nucleosynthesis is given by [98].

4.3.2 Decay of Massive particles during BBN

Even though the identity of dark matter is not well known, some weakly interacting massive particles (WIMPs) could be possible candidates. These are the stable end products of a decay cascade. Dark matter should be of course present during BBN so that these WIMPs will affect light element [75, 46, 79] and could resolve the lithium problem [73, 74].

Including new particles during BBN will modify the energy density or/and the entropy of the early universe and consequently the final abundances of light elements. The decay of some X-particles will affect BBN by inducing hadronic or electromagnetic particles. The effects of these decays depend on the stage of BBN in which the non-thermal decaying particles interact with the background thermal nuclei. The largest contribution of these nonthermal decays is for decays after the weak freeze-out phase[44]. In this context, the effect of the decay of X particles has been studied by [135, 136] in a more general way that may apply to any X particles. This would mean that these decays could be either inert decays which affect only the expansion rate or decays producing entropy which alters the time-temperature relation.

Particle decays during BBN have been the focus of many works where special attention was given to their effect on the lithium problem [129]. We mention here a recent work by [60] where the induced interactions of some X particles with nucleons have led to a significant reduction of lithium without excessive modification of the helium and deuterium abundances. The effect of energetic hadronic decays has also been investigated by [86] where they cause scattering of thermal

nuclei and showers of non-thermal nucleons. Consequently, generated neutrons can react with ${}^7\text{Be}$ and reduce the final lithium abundance. Another attempt to resolve the lithium problem was given by [?, ?] where three components were included, namely photon cooling, the decay of long-lived X particles and fluctuation of a primordial magnetic field. This could lead to an optimum reduction of lithium during BBN. For a detailed analysis of the effects of hadronic and electromagnetic cascades during BBN we refer the reader to detailed reviews by [75, 85].

4.4 Other non-standard BBN modifications

We also mention here a successful attempt with a modification of the Maxwell-Boltzmann distribution of nuclei during BBN [63] to resolve the lithium problem. This has decreased lithium abundance to match observations but at the expense of increasing deuterium. While this attempt seems to be promising, it relies on a specific modification of the distribution which when corrected for momentum conservation is no longer a viable solution.

Anisotropic expansion, including magnetic fields or variations of fundamental constants during BBN, were extensively studied in previous work.

The focus of the present work is to invoke non-standard treatments of the SBBN to find out how lithium production is affected. We attempt to modify the physical conditions of the SBBN by including non-standard scenarios. Our strategy will be to reanalyze the SBBN to find out how non-standard assumptions contribute to resolving the lithium problem. We will adopt $\eta = (6.14 \pm 0.04) \times 10^{-10}$ [118] and a neutron lifetime $\tau_n = 880.2 \pm 1$ [149]. The next section will deal with the role of the neutrino chemical potential in SBBN.

Chapter 5

The role of neutrinos chemical potential in SBBN

5.1 Role of neutrinos in SBBN

The very early universe was dense enough that neutrinos attained thermal equilibrium with a spectrum similar to that of blackbody radiation, namely,

$$B_\lambda(T) = \frac{2hc^2}{\lambda^5(e^{hc/\lambda kT} + 1)} \quad (5.1)$$

The "+1" is due to the fact that neutrinos are described by the Fermi-Dirac statistics. In the SBBN, three types (or flavors) exist (ν_e, ν_τ, ν_μ) and each type has its antineutrino. The total energy density of all three flavors is given by Eq.(3.5). Usually, the temperature T_ν of neutrinos in SBBN is that of the blackbody photons only when $T > 3.5 \times 10^{10}\text{K}$. When $T < 3.5 \times 10^{10}\text{K}$, the expansion of the universe does not enable further interactions of neutrinos with other particles. This leads to neutrino decoupling, so that the neutrinos have expanded and cooled independent of the CMB.

Considering the energy density of relativistic particles, the following is important. The e^\pm pairs annihilation supplies energy to the photons (via $e^+ + e^- \rightarrow \gamma + \gamma$), but not to the neutrinos. It can be shown (see appendix E for derivation) that:

$$T_\nu = (4/11)^{1/3}T, \quad (5.2)$$

where T is the temperature of the CMB photons. The total neutrino energy density is then:

$$\rho_\nu = \frac{\pi^2}{30} \left(\frac{7g_\nu}{8}\right) (4/11)^{1/3} T^4 \quad (5.3)$$

sometimes we write the energy density of relativistic particles as:

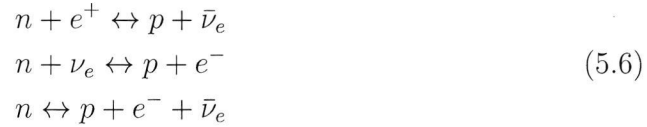
$$\rho = k_{eff} T^4, \quad (5.4)$$

where $k_{eff} = \frac{\pi^2}{30}(g_\gamma + (\frac{7}{8})g_\nu(\frac{4}{11})^{4/3}) = 1.11$ is the effective relativistic degree of freedom for relativistic particles in the SBBN after e^\pm annihilation. The equivalent mass density is

$$\tilde{\rho} = \frac{\rho}{c^2} = k_{eff} \frac{T^4}{c^2} \quad (5.5)$$

Note that the value of k_{eff} is valid back to the end of the e^\pm annihilation (about 1.3 sec). At earlier time (less than 1 sec), k_{eff} will grow, since more relativistic particles are possible (see discussion in chap.6).

Turning the discussion to the BBN itself, a key question should be asked, why about one quarter of the mass of the universe, is in the form of helium? At a $T < 10^{12}\text{K}$ ($t \sim 10^{-4}\text{s}$), the universe was a mixture of photons, electron-positron pairs, and neutrinos. The small number of neutrons and protons were constantly transformed into each other by the reactions:



The constant transformation were easily possible since $(m_n - m_p) = 1.293\text{MeV}$. The Boltzmann equation gives the equilibrium ratio of the number density of neutrons n and protons p as

$$\frac{n}{p} = \frac{g_n}{g_p} \times e^{-(m_p - m_n)/T}, \quad (5.7)$$

where $\frac{g_n}{g_p} = 1$. At $T = 10^{12}\text{K}$, $\frac{n}{p} = 0.986$. As the universe expanded and cooled, the ratio remains as in Eq.(5.7) as the reactions in Eq.(5.6) remained fast enough to sustain equilibrium. However, when T drops below 10^{10}K , the time scale of these reactions exceeded the time scale of the expansion. When T is slightly below 10^{10}K , the weak reaction rates decrease significantly. The reasons are: (i) decreasing of neutrinos energy, (ii) at this stage, the thermal energy of the photons has fallen below 1.022 MeV, the threshold for e^\pm pair creation. Consequently, the e^\pm pair was only annihilated without being replaced. For these reasons, the neutrinos were not able to sustain equilibrium. In other words, this situation is described as "freeze-out" of the rates leading to $\frac{n}{p} = 0.16$ at $T = 10^{10}\text{K}$. Notice that the beta-decay reactions, the forward reaction in Eq.(5.6), continued to operate converting neutrons into protons. However, it was not possible to combine neutrons and protons to deuterium with the reaction $p + n \leftrightarrow {}^2\text{H} + \gamma$, because at a temperature exceeding 10^{10}K , the number density of photons is so high (see Fig. 5.1). This will cause the dissociation of deuterium nuclei. This means the neutrons and protons remain separated until the temperature drops below 10^{10}K . The production of deuterium enables the productions of ${}^4\text{He}$, the most tightly bound nucleus involved in the BBN. The reactions leading to the formation of

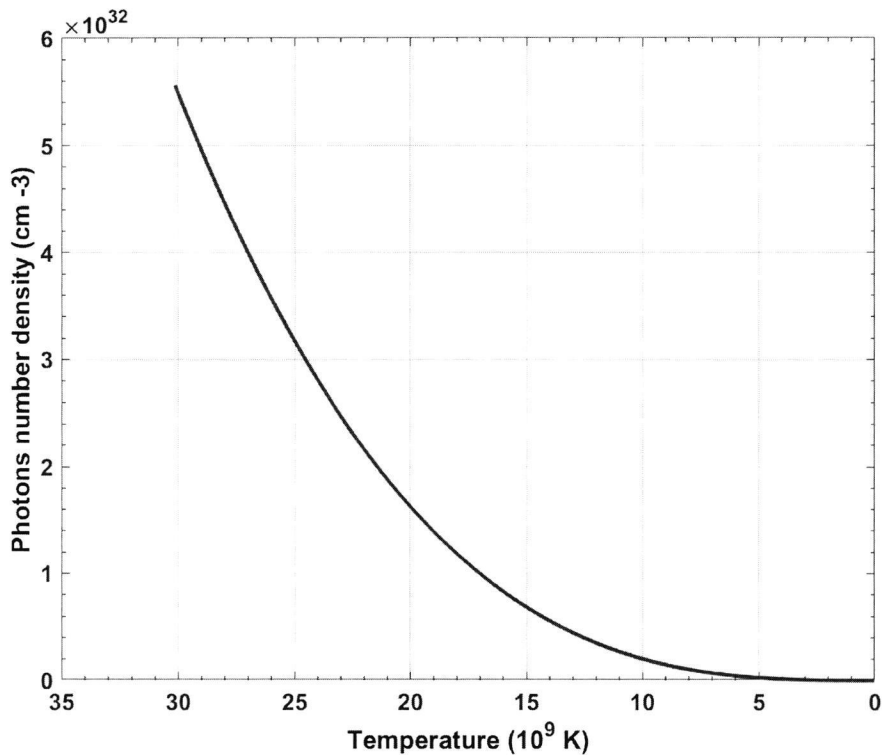


Figure 5.1: Photon number density as function of temperature during BBN.

^4He are described in sec.5.4.

An important point is the following: since most of the available neutrons were used to create the ^4He nuclei, the abundance of ^4He was not sensitive to the baryon density of the universe. The other nuclear species were more sensitive to the baryon density as outlined in sec.3.2.2.

5.2 Neutrino degeneracy and oscillations

The definition of neutrinos degeneracy is related to the asymmetry between the number of neutrinos and antineutrinos. The abundances of the light elements in SBBN are calculated under the assumptions of a homogeneous universe and three families of neutrinos with zero chemical potential and zero mass. Meanwhile, it is established that neutrinos have non-vanishing chemical potentials [65, 90]. Introducing their chemical potential may play an important role in the evolution of the early universe. According to [153], neutrino degeneracy affects element production in two ways:

- It increases the energy density which speeds up the expansion rate of the

universe being related to the scale factor as shown in Eq.(3.3). The energy density of fermions and anti-fermions is given to be [103],

$$\rho_\nu + \rho_{\bar{\nu}} = \left(\frac{7\pi^2}{120}\right)g_f T_\nu^4 \left[1 + \frac{30\beta^2}{7\pi^2} + \frac{15\beta^4}{7\pi^4}\right], \quad (5.8)$$

where $\beta = \frac{\mu}{T}$ is the degeneracy parameter. In the SBBN, $\beta = 0$ and the neutrinos are not considered degenerate. It is then clear from the equation above that adding β will increase the energy density and this is the only way in which muon and tau neutrinos affect the SBBN.

- A second effect is altering the neutron to proton ratio n/p at the temperature of freeze out and this effect is limited to the electron neutrinos owing to their reaction rates (see Eq.(5.14)).

As shown in [77], chemical potentials cannot be constrained based on SBBN because the effect of $\beta_{\nu_{\mu,\tau}}$ can be compensated by a positive β_{ν_e} . To constrain the neutrino chemical potentials one needs additional limits which are obtained from the CMB namely $N_\nu \leq 8$ and $-0.01 \leq \beta_{\nu_e} \leq 0.25$, $|\beta_{\nu_{\mu,\tau}}| \leq 2.9$ and from supernovae a $N_\nu \leq 7$ and $-0.01 \leq \beta_{\nu_e} \leq 0.22$, $|\beta_{\nu_{\mu,\tau}}| \leq 2.6$ [65].

Neutrino oscillation (mixing) is an important phenomenon that has been discovered in the last decades and verified experimentally in 2015 [148]. The existence of neutrino oscillations has revealed new neutrino properties beyond the standard model of particle physics, in particular, a non-vanishing neutrino mass. In other words, neutrino oscillation means that any neutrino species in a well-defined flavor state has a finite probability to be detected in another flavor state. This depends on the distance traveled by the neutrinos, their energy, their mass difference, and the mixing matrix [48]. Many investigations showing this mixing have been studied [10, ?, 3, 4]. The question remains as to whether there is a relation between neutrino degeneracy and oscillations.

Neutrino oscillations (mixing) will lead to equilibration of the lepton asymmetry before the onset of the SBBN. In this case, the equilibration of the chemical potentials will result in a dominant effect from electron neutrinos because of their effect on the freeze-out. This will strongly constrain the abundance of ${}^4\text{He}$, but will not affect the ${}^7\text{Li}$ abundance [132].

On the other hand, in a universe with large lepton asymmetry [65, 93] it is important to allow the neutrino chemical potential to vary independently. This could happen, for example, if there exists hypothetical neutrino-majoron coupling [50], or one neutrino species mixes with a sterile neutrino resulting in a chaotic amplification of the electron neutrino chemical potential [139]. In a paper by [107], different chemical potentials were assumed but for values of the baryon to photon ratio η that are not consistent with the Planck observations. **In the present thesis, the aim of including chemical potentials is to understand the SBBN and to investigate their effect on the lithium abundance.**

5.3 Numerical Results

Degenerate neutrinos during BBN have been extensively studied in previous works [49, 65, 52, 90, 110] where the effects of large lepton asymmetry and additional effective numbers of neutrinos were considered. The present work differs from the previous studies in that we also focus on the range of neutrino chemical potentials that may lead to a significant decrease in the lithium abundance. In this section, we investigate the effects of degenerate neutrinos toward understanding or ameliorating the lithium problem. As mentioned before, equating chemical potentials will not solve the lithium problem, so that we can compensate this effect by increasing the number of neutrinos. Compensating the electron neutrino chemical potentials by increasing the number of neutrinos has been investigated by [52]. However, here we fix the baryon asymmetry to be $\eta = (6.14 \pm 0.04) \times 10^{-10}$ as deduced by Planck. We have done numerical calculations after updating AlterBBN code [18]. Thus we will see that strict ranges on chemical potentials and neutrino number will be obtained. Taking into consideration neutrino oscilla-

Table 5.1: Effect of neutrino chemical potentials ($\beta_{\nu_e} = \beta_{\nu_\mu} = \beta_{\nu_\tau}$) along with varying N_ν on SBBN.

| N_ν | $\beta_{\nu_{e,\mu,\tau}}$ | Y_p | $D/H \times 10^5$ | ${}^7\text{Li}/H \times 10^{10}$ |
|---------|----------------------------|--------|-------------------|----------------------------------|
| 3 | -0.015 | 0.2499 | 2.6613 | 4.4280 |
| 3 | 0 | 0.2461 | 2.6386 | 4.3861 |
| 3.2 | 0.02 | 0.2442 | 2.6827 | 4.2518 |
| 3.3 | 0.04 | 0.2410 | 2.6965 | 4.1526 |

tions, this will lead to the equilibration of chemical potentials before SBBN. In this context we obtained the following:

- The results in Table 5.1 shows that the values of SBBN (see third row in the table) are also closely obtained for the following range of neutrino number and degeneracy parameters:

$$\boxed{3 \leq N_\nu \leq 3.3, -0.015 \leq \beta_{\nu_{\mu,\tau,e}} \leq 0.04} \quad (5.9)$$

- In order to reduce the lithium abundance significantly, the ranges of degeneracy parameters (which we will henceforth simply refer to as "chemical potential") and numbers of neutrinos are shown in Table 5.2 and Eq. (5.10).

$$\boxed{6.7 \leq N_\nu \leq 7.8, 0.175 \leq \beta_{\nu_{\mu,\tau,e}} \leq 0.265} \quad (5.10)$$

It is clear from Eq.(5.10) that the ranges of N_ν are not supported by recent CMB observations (WMAP and Planck missions), which will be discussed in chap.6.

Table 5.2: The ranges of $\beta_{\nu_{e,\mu,\tau}}$ and N_ν that lead to a significant decrease of lithium.

| N_ν | $\beta_{\nu_{e,\mu,\tau}}$ | Y_p | $D/H \times 10^5$ | ${}^7\text{Li}/H \times 10^{10}$ |
|---------|----------------------------|--------|-------------------|----------------------------------|
| 6.7 | 0.23 | 0.2292 | 3.4835 | 2.7978 |
| 6.9 | 0.225 | 0.2317 | 3.5490 | 2.7690 |
| 7.2 | 0.175 | 0.2463 | 3.7520 | 2.7840 |
| 7.4 | 0.245 | 0.2306 | 3.6599 | 2.6415 |
| 7.6 | 0.24 | 0.2331 | 3.7250 | 2.6159 |
| 7.8 | 0.265 | 0.2287 | 3.7398 | 2.5389 |

However, it is possible to assume that the number of neutrinos N_ν during big bang nucleosynthesis (BBN) is not the same as the effective number of relativistic species N_{eff} deduced from CMB. The equivalence between N_{eff} and N_ν is assumed in case of a standard neutrino temperature. However, any variation in the neutrino temperature during or after BBN can be translated into a variation in the effective number of neutrinos obtained from CMB. This case is treated in detail by [59] when neutrino temperature deviates from the standard one after decoupling. Varying neutrino temperature and breaking the degeneracy between BBN and CMB is also extensively studied by [104]. This will be discussed in details in the next chapter.

Table 5.3: The effect of different neutrino chemical potentials showing how ${}^7\text{Li}$ abundance is reduced

| β_{ν_e} | $\beta_{\nu_{\mu,\tau}}$ | Y_p | $D/H \times 10^5$ | ${}^7\text{Li}/H \times 10^{10}$ |
|-----------------|--------------------------|--------|-------------------|----------------------------------|
| 0.19 | 2 | 0.2417 | 3.6797 | 2.7859 |
| 0.2 | 2.05 | 0.2410 | 3.7343 | 2.7226 |
| 0.21 | 1.95 | 0.2352 | 3.5736 | 2.7967 |
| 0.23 | 2 | 0.2322 | 3.6080 | 2.7164 |
| 0.25 | 2.1 | 0.2310 | 3.7173 | 2.5930 |
| 0.26 | 2.1 | 0.2287 | 3.6996 | 2.5761 |

While in Table 5.1 and Table 5.2 the chemical potentials are assumed to be equal, we have done another calculations were the number of neutrinos is fixed to be $N_\nu = 3$ but the chemical potential of electron neutrino β_{ν_e} is different from that of muon and tau neutrinos $\beta_{\nu_{\mu,\tau}}$ (see Table 5.3). In order to achieve a significant reduction of lithium, we derived new limits on the chemical potential given by Eq.(5.11) that substantially reduces the lithium abundance to less than 2.8×10^{-10} .

$$\boxed{N_\nu = 3, 0.19 \leq \beta_{\nu_e} \leq 0.26, 1.95 \leq \beta_{\nu_{\mu,\tau}} \leq 2.1} \quad (5.11)$$

5.4 Analytical calculations

5.4.1 Stages of big bang nucleosynthesis

The final abundances of light elements are sensitive to the physical conditions of the SBBN where the temperature is $T \leq 1$ MeV and the time $t \geq 1$ s. SBBN is based on a competition between the expansion rate and nuclear reaction rates so that when the expansion rate becomes faster than a specific reaction rate, this reaction will freeze-out. Three important stages of BBN will be discussed namely: (1) the freeze-out of neutrons; (2) the deuterium bottleneck; and (3) the quasi-equilibrium of neutrons and deuterium because these three stages determine the final element abundances.

Freeze-out of neutrons

The weak interactions that are given in Eq. (5.6) remain in thermal equilibrium as long as the weak interaction rates $\Gamma_w \sim T^5$ are greater than the expansion rate of $H \sim T^2$. So at lower temperature, Γ_w cannot compete with the expansion rate and the freeze-out of these reactions take place for the following condition [45]:

$$G_F^2 T^5 \sim \Gamma_w(T_F) = H(T_F) \sim G_N^{1/2} T^2 \quad (5.12)$$

where T_F is the freeze-out temperature and G_F is the Fermi constant.

Since the weak interactions determine the neutron to proton ratio an analytical calculation of the weak-reaction freeze-out is given in [103] whereby in SBBN the neutron mass fraction at freeze-out becomes $X_n = \frac{n_n}{n_n + n_p} \approx 0.157$ for which the neutron-to-proton ratio is given in Eq. (5.7). In the SBBN, the freeze-out of neutrons takes place at $T \sim 0.7$ MeV ($\sim 8 \times 10^9$ K). This temperature is not fixed, rather it depends on non-standard scenarios intervening during BBN. For example, if for some reason the expansion rate becomes faster, the weak rates will stop earlier at a higher temperature, and fewer neutrons will be converted into protons leading to a higher neutron to proton ratio and vice-versa. This will mainly increase helium, but also affect deuterium, and consequently lithium abundance. For this reason, **we extended the calculations in [103] to include neutrino chemical potentials**. The equilibrium abundance of neutrons including the degeneracy parameter $\beta_{\nu_e} = \mu_{\nu_e}/T$ can be written as:

$$X_n^{eq} = \frac{1}{1 + e^{\beta_{\nu_e}} e^{Q/T}} \quad (5.13)$$

where $Q = m_n - m_p = 1.293$ MeV. The neutron-to-proton ratio becomes:

$$\frac{n}{p} = e^{-\beta_{\nu_e}} e^{-Q/T}, \quad (5.14)$$

consequently, weak reaction rates will be modified as:

$$\begin{aligned}\lambda_{pe} &= \exp\left(-\frac{Q}{T}\right) \exp(-\beta\nu_e)\lambda_{n\nu} \\ \lambda_{p\bar{\nu}} &= \exp\left(-\frac{Q}{T}\right) \exp(-\beta\nu_e)\lambda_{ne}\end{aligned}\quad (5.15)$$

where $\lambda_{n\nu} \approx \lambda_{ne}$ at $T = T_\nu$.

More explicitly, we find that $\lambda_{n\nu}$ can be well approximated by Eq. (5.16) within the range $-0.5 \leq \beta\nu_e \leq 0.5$,

$$\lambda_{n\nu} \approx 1.63 \exp(+\beta\nu_e) \left(\frac{T_\nu}{Q}\right)^3 \left(\frac{T_\nu}{Q} + 0.25\right)^2 s^{-1}, \quad (5.16)$$

while the other weak rates can be related to Eq. (5.16) using Eq. (5.15).

Eq. (5.16) shows the familiar result that adding a positive chemical potential, $\beta\nu_e$, will exponentially enhance the weak rates. Hence, more neutrons are converted into protons leading to a lower neutron mass fraction at freeze-out. According to Eq. (5.13) this implies that a lower freeze out temperature is obtained. Conversely, more neutrons will be available when adding a negative $\beta\nu_e$ leading to a higher freeze-out temperature. With this modification the standard and non-standard rates can be related:

$$\lambda_{n\nu}^{non-standard} \approx e^{+\beta\nu_e} \lambda_{n\nu}^{standard} \quad (5.17)$$

and the neutron freeze-out mass fraction (see Appendix A for details) is given by:

$$X_n^F = \int_0^\infty \frac{e^{(-5.42e^{\beta\nu_e} k^{-1/2} \int_0^y (x+0.25)^2 (1+e^{-\beta\nu_e} \exp(-\frac{1}{x})) dx) dy}}{2y^2(1 + \cosh(\beta\nu_e + 1/y))} dy. \quad (5.18)$$

Because the freeze out occurs for $T > 0.5$ MeV, the parameter k_{eff} is introduced representing the effective number of freedom for relativistic particles before electron-positron annihilation. Using Eq. (3.5), the effective number of degrees of freedom is written as $k_{eff} = \frac{\pi^2}{30}(g_\gamma + \frac{7}{8}g_f)$ without including chemical potentials. In case chemical potentials are included, and using Eq. (5.8), k_{eff} is modified as follows:

$$k_{eff} = 1.8094 + \left(\frac{\pi^2}{30}\right)\left(\frac{7}{8}N_{\nu,\bar{\nu}}\right) + 0.25\beta_{\nu_e}^2 + \frac{\beta_{\nu_e}^4}{8 * \pi^2} + 2 \times \left(0.25\beta_{\nu_{\mu,\tau}}^2 + \frac{\beta_{\nu_{\mu,\tau}}^4}{8 * \pi^2}\right). \quad (5.19)$$

The effect of $\beta\nu_e$ is directly involved in the weak rates while the effect of $\beta\nu_{\mu,\tau}$ mainly affects the expansion rate or equivalently k_{eff} . It is not easy to obtain an exact expression of the integral in Eq. (5.18) as a function of $\beta\nu_e$ and k_{eff} , so we have made a polynomial fits for a grid of 230 values of $(k_{eff}, \beta\nu_e)$ to obtain the

following expression for X_n^F valid in the ranges of $-0.5 \leq \beta_{\nu_e} \leq 0.5$, $0 \leq \beta_{\nu_{\mu,\tau}} \leq 5$:

$$\begin{aligned} X_n^F = & 0.1279 - 0.1994\beta_{\nu_e} + 0.01015k_{eff} + 0.09137\beta_{\nu_e}^2 - 3.946 \times 10^{-3}\beta_{\nu_e}k_{eff} \\ & - 3.743 \times 10^{-4}k_{eff}^2 + 7.716 \times 10^{-3}\beta_{\nu_e}^3 - 6.744 \times 10^{-4}\beta_{\nu_e}^2 + 7.368 \times 10^{-5}\beta_{\nu_e}k_{eff}^2 \\ & + 5.246 \times 10^{-6}k_{eff}^3. \end{aligned} \quad (5.20)$$

Using this expression in Eq. (5.13) we can obtain the corresponding freeze-out temperature T_F for every $(\beta_{\nu_e}, \beta_{\nu_{\mu,\tau}}, X_n^F)$. Eq. (5.20) illustrates the explicit dependence of the freeze-out of neutron abundance on β_{ν_e} and k_{eff} . Note that Eq. (5.20) is valid also if k_{eff} receives contributions not only from $\beta_{\nu_{\mu,\tau}}$ but also from extra relativistic degrees of freedom or any component that could alter the energy density of the universe.

5.4.2 Deuterium formation epoch

Primordial nuclei are synthesized through chains of nuclear reactions. The first step starts with the formation of deuterium through



However, one can ask why the helium abundance is still negligible at $T \sim 0.3\text{MeV}$ while its binding energy is 28.3 MeV. As long as the temperature remains high, deuterium is easily destroyed by photons with energy in excess of the binding energy of deuterium. Since reactions responsible for converting deuterium into heavier nuclei are dependant on the deuterium concentration, the formation of ${}^3\text{He}$ and ${}^4\text{He}$ is delayed until the nuclear statistical equilibrium (NSE) establishes maximum deuterium abundance. In SBBN this shift in NSE is sometimes referred to the deuterium bottleneck. It occurs at $T_{BN} \approx 0.84 \text{ GK}$ (0.072 MeV) with $D/H \approx 3.665 \times 10^{-3}$, which is obtained by updating reactions of the AlterBBN program [14]. Therefore, before deuterium reaches its bottleneck, the formation of heavier elements is blocked despite their large binding energies (see Fig. 3.2). An analytical expression for the abundance of deuterium at the bottleneck has been derived [103] to be:

$$D/H \approx \frac{1.2 \times 10^{-5}}{X_p(T_{BN}(\text{MeV}) \times \eta_{10})} \quad (5.22)$$

where T_{BN} is the bottleneck temperature, $\eta_{10} = 10^{10} \times \eta$ and $X_p = \frac{n_p}{n_p + n_n}$. However, Eq. (5.22) can be modified by introducing non-standard scenarios which affect the deuterium bottleneck, the final deuterium abundance and the final elements abundances. Extending the analytic derivation of Eq. (5.22) and constraining it with our numerical calculations using the AlterBBN program, we

obtain the following modified expression:

$$\frac{D}{H} = \frac{4 \times 10^{-3}}{X_p(\tilde{k}_{eff}^{-0.5} \times T_{BN}(\text{MeV}) \times \eta_{10} + C(\beta_{\nu_e}, \tilde{k}_{eff}))}, \quad (5.23)$$

with $X_p \approx 1 - X_n^F$. The parameter \tilde{k}_{eff} represents the effective degrees of freedom, but it is now different from k_{eff} given in Eq. (5.19) because e^+e^- annihilation reduces the number of degrees of freedom before deuterium bottleneck is reached. In this case the expression for \tilde{k}_{eff} is:

$$\begin{aligned} \tilde{k}_{eff} = & 0.6579 + \left(\frac{4}{11}\right)^{\frac{4}{3}} \left(\frac{\pi^2}{30}\right) \left(\frac{7}{8} N_{\nu, \bar{\nu}}\right) + \left(\frac{4}{11}\right)^{\frac{4}{3}} \times \left(0.25\beta_{\nu_e}^2 + \frac{\beta_{\nu_e}^4}{8 * \pi^2}\right) \\ & + 2 \times \left(\frac{4}{11}\right)^{\frac{4}{3}} \times \left(0.25\beta_{\nu_{\mu, \tau}}^2 + \frac{\beta_{\nu_{\mu, \tau}}^4}{8 * \pi^2}\right) \end{aligned} \quad (5.24)$$

In Eq. (5.23), T_{BN} and $C(\beta_{\nu_e}, \tilde{k}_{eff})$ are functions of the number of the effective relativistic degrees of freedom \tilde{k}_{eff} and β_{ν_e} . We have found that these dependences can be approximated with the following analytic fits:

$$T_{BN}(\text{MeV}) \approx 0.0745 - 2.1448 \times 10^{-3} \times \tilde{k}_{eff}^{0.3148}, \quad (5.25)$$

or

$$T_{BN}(\text{GK}) \approx 0.8643 - 0.02488 \times \tilde{k}_{eff}^{0.3148}, \quad (5.26)$$

and

$$\begin{aligned} C(\beta_{\nu_e}, \tilde{k}_{eff}) = & 1.181 + 0.6486\beta_{\nu_e} - 0.3511\tilde{k}_{eff} + 0.2937\beta_{\nu_e}^2 - 0.1189\beta_{\nu_e}\tilde{k}_{eff} + 0.06239\tilde{k}_{eff}^2 \\ & - 0.02391\tilde{k}_{eff}\beta_{\nu_e}^2 + 0.00838\tilde{k}_{eff}^2\beta_{\nu_e} - 0.003651\tilde{k}_{eff}^3. \end{aligned} \quad (5.27)$$

Note, that more details concerning the derivation of Eq. (5.23) are given in Appendix B. These analytic relations reveal the following:

1. It is clear from Eqs. (5.25,5.26) that T_{BN} is mainly affected by the expansion rate due to its dependence on the effective degrees of freedom \tilde{k}_{eff} . Furthermore, we will see later that any shift in the bottleneck temperature will affect light elements abundances.
2. Fig. 5.2 shows that the deuterium mass fraction at the bottleneck depends not only on the bottleneck temperature and η_{10} , but also on any non-standard scenarios intervening during BBN. The neutrino chemical potentials affect the deuterium bottleneck, especially β_{ν_e} causes the decrease of the abundance of deuterium at the bottleneck. However, it is a steadily increasing function of $\beta_{\nu_{\mu, \tau}}$ due to the effect on the expansion rate. It is clear

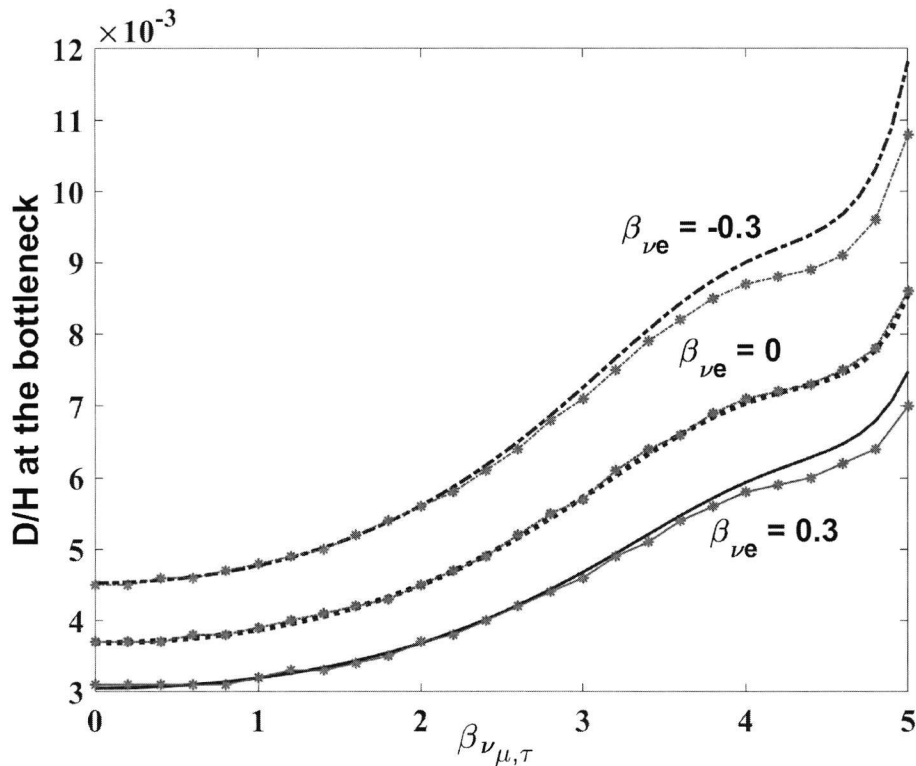
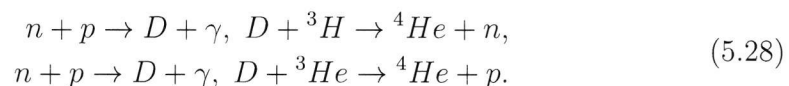


Figure 5.2: Deuterium abundance at the bottleneck temperature as function of the neutrino chemical potentials. The curves with stars are obtained from our analytical calculations while the curves without stars are obtained from numerical ones.

from Fig. 5.2 that our analytical calculations for the deuterium abundance at the bottleneck agree very well with our numerical calculations except for high β' s where there are small differences.

5.4.3 Helium-4

Given that the binding energy of helium is about 28.3 MeV, its abundance is still negligible at a temperature of 0.3 MeV. This is because the rate of deuterium reactions responsible for maintaining the equilibrium of helium with the nucleons is much smaller than the expansion rate at this time. In other words, the nucleosynthesis of ${}^4\text{He}$ occurs after the temperature drops below that of the deuterium bottleneck (see Fig. 3.2). At this point two neutrons are mainly combined with two protons to form ${}^4\text{He}$ via the reaction chains:



Consequently, the abundance of ${}^4\text{He}$ not only depends on the neutron mass fraction, but also on the bottleneck temperature given by Eqs. (5.25,5.26). In order to obtain the primordial helium mass fraction from the above reaction chains we need to also consider the time variation of temperature. According to [103] the helium mass fraction can be estimated by:

$$X_f({}^4\text{He}) \approx 2X_n^F \exp\left(-\frac{t_{BN}}{\tau_n}\right), \quad (5.29)$$

where

$$t_{BN} = 187.0384 \times \frac{\tilde{k}_{eff}^{-0.5}}{T_{BN}(\text{GK})^2}, \quad (5.30)$$

or equivalently $t_{BN} = 1.39 \times \frac{\tilde{k}_{eff}^{-0.5}}{T_{BN}(\text{MeV})^2}$.

Eq. (5.29) was derived for a fixed \tilde{k}_{eff} and for a range of η_{10} . However, a more relevant determination for our purpose is to fix $\eta_{10} = 6.14 \pm 0.04$ by the Planck analysis [117] and include degenerate neutrinos. In this way we have obtained a better estimate of the primordial ${}^4\text{He}$ abundance Y_p that includes the effect of different values of the chemical potentials in the ranges of $-0.5 \leq \beta_{\nu_e} \leq 0.5$ and $0 \leq \beta_{\nu_{\mu,\tau}} \leq 5$. We have chosen such ranges in order to show clearly the effect of the chemical potential on the production of light elements. This leads to:

$$Y_p \approx 1.81X_n^F \exp\left(-1.79\frac{t_{BN}}{\tau_n}\right) + 0.075, \quad (5.31)$$

where $\tau_n \approx 880.2 \pm 1$ seconds is the adopted neutron lifetime [112]. For comparison, the calculation of this mass fraction from [80] is shown in the first column of Table 5.4 where the light element abundances are fitted as a linear function of η_{10} , the expansion rate variation, and β_{ν_e} . In Table 5.4 we take an example in which $\beta_{\nu_e} = 0.1$ and $\beta_{\nu_{\mu,\tau}} = 1$ in order to compare our numerical simulation with the present expressions and those of [80]. The analytic relations derived here provide a better physical picture and relate the light element abundances to the three important stages of BBN. Our treatment is valid for chemical potentials in wider ranges ($-0.5 \leq \beta_{\nu_e} \leq 0.5$, $0 \leq \beta_{\nu_{\mu,\tau}} \leq 5$) and the results are similar to the numerical simulations as demonstrated in Table 5.4.

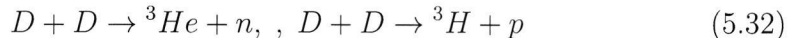
5.4.4 Final deuterium abundance

Let us make a clearer picture of the SBBN. The expansion of the universe controls the freeze-out of light elements. Since the final abundance of ${}^3\text{He}$ and ${}^3\text{H}$ depend on the freeze-out concentration of deuterium, we will derive its approximate abundance by using a system of kinetic equations (see Appendix C for more

Table 5.4: Comparison of light elements abundances for $\beta_{\nu_e} = 0.1$, $\beta_{\nu_{\mu,\tau}} = 1$ between fits presented by (Kneller & Steigman, 2004) and the present work based on our analytical and numerical calculations.

| | (Kneller & Steigman, 2004) | present work (analytical) | present work (numerical simulations) |
|----------------------------------|----------------------------|---------------------------|--------------------------------------|
| Y_p | 0.2368 | 0.2344 | 0.23410 ± 0.00013 |
| $D/H \times 10^5$ | 2.7296 | 2.6969 | 2.8170 ± 0.1344 |
| ${}^3\text{He}/H \times 10^5$ | 1.4211 | 1.0798 | 1.0380 ± 0.0536 |
| ${}^7\text{Li}/H \times 10^{10}$ | 3.9563 | 3.9173 | 3.7880 ± 0.3431 |

details). When deuterium reaches its maximum abundance, the destruction of deuterium will be efficient through



The deuterium abundance begins to decrease because it will be converted into tritium and ${}^3\text{He}$ which will proceed to ${}^4\text{He}$ through



Not all neutrons of the above reactions will add to the helium reservoir. Then, nucleosynthesis is a self-regulating process that leads to steady state solution. In other words, if the abundance of ${}^3\text{He}$ and tritium becomes smaller or greater than the quasi-equilibrium abundance, their concentration will be regulated to return ${}^3\text{He}$ and tritium to their quasi-equilibrium values. If we consider the variation with time of deuterium as indicated by Eq.(C.0.8), the case when $X_D \ll X_n$ leads to a decrease of the deuterium abundance, so that deuterium satisfies the quasi-equilibrium condition ($\frac{dX_D}{dT} \approx 0$) and free neutrons dominate the NSE abundances of all nuclides. However, when the neutron concentration drops to that of deuterium $X_D \sim X_n$, this allows deuterium to regulate the quasi-equilibrium of neutrons and other elements [103]. In this case, the neutron concentrations given by Eq.(C.0.9) satisfy the quasi-equilibrium condition ($\frac{dX_n}{dT} \approx 0$). This self-regulating process leads to steady state solution.

It is important to know the temperature T^* at which the free neutron abundance becomes comparable to that of deuterium because it is one of the parameters affecting the final abundance of deuterium and consequently heavier elements. An estimation of this temperature is approximately $T^* \sim 0.8\text{GK}$ [103].

After the temperature drops below the deuterium bottleneck, its abundance decreases and neutrons start to decay. As explained in Appendix C, we obtained T^* as function of the bottleneck temperature T_{BN} , the mass fraction of protons

and the effective number of relativistic degrees of freedom:

$$T^*(GK) \approx T_{BN}(GK) - \frac{0.232}{\eta_{10} \times X_p \times \tilde{k}_{eff}^{-0.5}}. \quad (5.34)$$

Here, it is seen that increasing \tilde{k}_{eff} will lead to lower T_{BN} , so that the neutron abundance will take more time to decrease to the deuterium concentration. Consequently T^* will be lower. Therefore, the deuterium final abundance can be related to T^* by the following analytic fit :

$$\frac{D}{H} = \frac{1}{X_p \times \eta_{10} \times F(T^*(GK))}, \quad (5.35)$$

with

$$F(T^*(GK)) = 0.36 \times \exp(11.81T^*) + 2.4 \times 10^{-12} \times \exp(44.05T^*) \quad (5.36)$$

Further explanation of this deuterium calculation is given in Appendix C. Eq. (5.35) allows for a better estimate of D/H over the parameter range of chemical potential adopted here. It is clear that if T^* increases, the final deuterium abundance will decrease. This is due to fewer neutrons and/or a lower expansion rate and vice versa.

5.4.5 Helium-3 and tritium

We have derived explicit expressions for the abundances of the elements helium and tritium to analyze how these nuclides depend upon each other and to make a final interpretation concerning the lithium abundance. The expression for the quasi-equilibrium abundance of ${}^3\text{He}$ is given by :

$$\frac{dX_{{}^3\text{He}}}{dt} = \frac{3}{4}\lambda_{DD1}X_D^2 + \frac{3}{2}\lambda_{Dp}X_D X_p - \frac{1}{2}\lambda_{{}^3\text{He}D}X_D X_{{}^3\text{He}} - \lambda_{{}^3\text{He}n}X_{{}^3\text{He}}X_n = 0. \quad (5.37)$$

where X_i refers to the abundance by weight of the corresponding element and λ 's are the reaction rates intervening in the determination of the abundance of a specific element. It follows from the above equation that the final abundance of ${}^3\text{He}$ is:

$$\frac{{}^3\text{He}}{H} \approx \frac{0.074 \times D/H + 4 \times 10^{-6} X_p}{0.46 + 1570 \times D/H}. \quad (5.38)$$

Similarly for the tritium abundance we have :

$$\frac{3}{4}\lambda_{DD2}X_D^2 + \lambda_{{}^3\text{He}n}X_{{}^3\text{He}}X_n \approx \frac{1}{2}\lambda_{D{}^3\text{H}}X_D X_{{}^3\text{H}}$$

So,

$$\frac{{}^3\text{H}}{H} \approx 8.85 \times 10^{-9} - 2.71 \times 10^{-8} X_p + 1.04 \times 10^{-3} \left(\frac{D}{H}\right) + 2.86 \times 10^{-3} \left(\frac{D}{H}\right) X_p + 1.06 \left(\frac{D}{H}\right)^2 \quad (5.39)$$

It is clear from the network shown in Fig. 3.1 that the main production of ${}^3\text{He}$ and tritium comes from the reactions with deuterium. This is also obtained in the analytic calculations of Eqs. (5.38,5.39). Hence, increasing deuterium will lead to an increase in ${}^3\text{He}$ and tritium and vice versa.

5.4.6 Beryllium and lithium

Lithium (${}^7\text{Li}$) is the main focus of the present work. For this reason, it is important to derive analytical expressions of ${}^7\text{Li}$ and ${}^7\text{Be}$ in order to have a better understanding the final abundance of this element. ${}^7\text{Be}$ is directly linked to ${}^7\text{Li}$ production and it is mainly produced and destroyed by the reactions:



The final abundance of ${}^7\text{Be}$ can be obtained similarly to the case of tritium and ${}^3\text{He}$ (using a system of kinetic equations). Then the ${}^7\text{Be}$ abundance is given as :

$$\frac{{}^7\text{Be}}{\text{H}} \approx 9 \times 10^{-14} \times \frac{Y_p \times \frac{{}^3\text{He}}{\text{H}}}{X_p \times \left(\frac{D}{\text{H}}\right)^2}. \quad (5.41)$$

The final abundance of lithium is then determined from the sum of reactions leading to beryllium and lithium. Under standard BBN conditions, one can deduce (using the AlterBBN program) that more than 90% of the lithium comes from beryllium by electron capture after the end of nucleosynthesis. It is important to emphasize that the electron capture rate is irrelevant unless it becomes shorter than the timescale of BBN. Using the network equations with the relevant reactions leading to the production of lithium, we deduced that the final lithium abundance is given by :

$$\frac{{}^7\text{Li}}{\text{H}} \approx 9 \times 10^{-4} \times \frac{Y_p}{X_p} \left(\frac{{}^3\text{H}}{\text{H}} + 2.57 \times 10^{-3} \times \frac{{}^3\text{He}}{\text{H}} \right). \quad (5.42)$$

In the case of a neutrino-degenerate BBN, increasing the expansion rate by adding $\beta_{\nu\mu,\tau}$ will lead to different lithium production than in the SBBN. First, the final abundance of lithium will depend upon the evolution of deuterium which will directly affect beryllium as seen from Eq. (5.41). **For this reason, all solutions leading to lithium destruction are accompanied by an increase in deuterium.** However, as seen in Eqs. (5.41,5.42), deuterium is not the only element affecting lithium production. Both ${}^3\text{He}$ and ${}^4\text{He}$ play an important role when the helium abundance becomes more significant than that of deuterium. Then, Eqs.(5.41, 5.42) show that including any non-standard scenarios to decrease the lithium abundance is constrained by other light elements especially ${}^4\text{He}$ and deuterium which makes the problem more complicated.

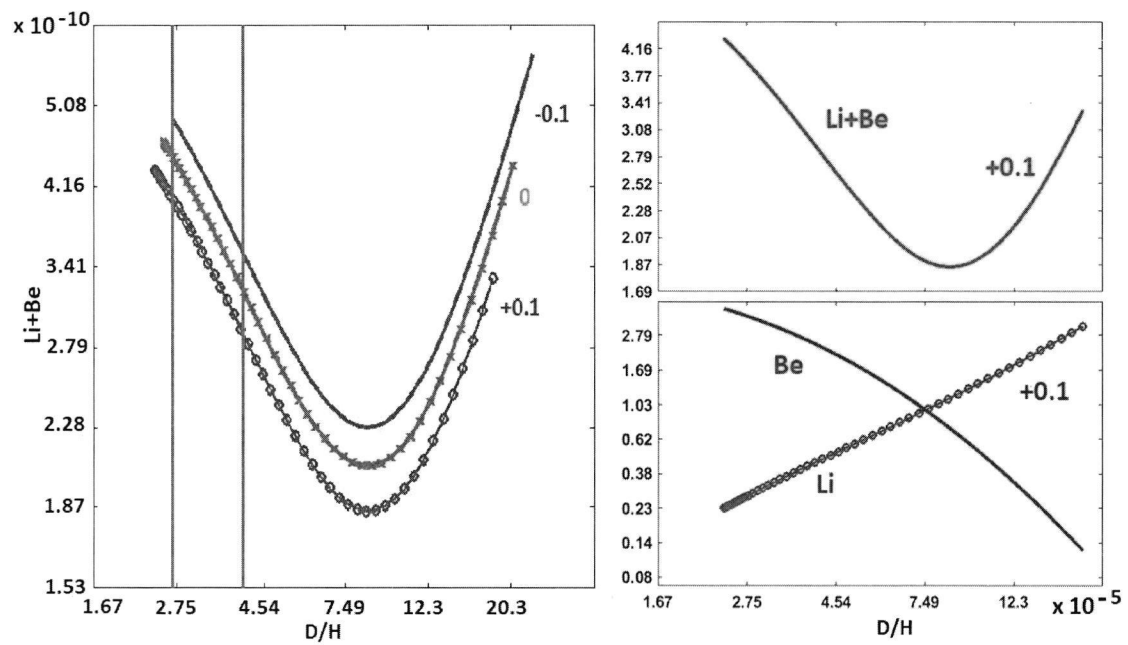


Figure 5.3: Lithium abundance as function of the deuterium abundance for different values of β_{ν_e} as labeled on the curves with the range of $0 \leq \beta_{\nu_{\mu,\tau}} \leq 5$. The vertical lines in the left panel indicate the range of investigation in this work.

To have a clear picture, Fig. 5.3 shows the sum of lithium and beryllium as a function of deuterium. Two regions are found, one is up to the minimum of the curve where the sum is steadily decreasing while the other region shows an increase of the sum. The behavior of the first region is due to the decrease of beryllium which will be transformed into lithium after BBN by electron capture. In this case, beryllium destruction is favored through reaction 12 in Fig. 3.1 (${}^7\text{Be} + n \rightarrow {}^7\text{Li} + p$) where at the same time the production of lithium is not significant and this is shown in the bottom right panel of Fig. 5.3. The increase in the other region is due to the high abundance of lithium produced through reaction 7 in Fig. 3.1 (${}^3\text{H} + {}^4\text{He} \rightarrow {}^7\text{Li} + \gamma$). This means that the role of beryllium is not important in this case. It is emphasized that our range of interest is in the first region as shown by the vertical lines in Fig. 5.3 where the deuterium abundance is still in the ranges of observations.

Chapter 6

Effect of Neutrino temperature and dark components on SBBN

6.1 Neutrinos and the effective degrees of freedom

An extension of the SBBN is to allow the number of neutrinos to be different from three. However, the effective number of relativistic species N_{eff} is not allowed to vary freely due to its effect on the CMB and SBBN predictions. The combination of seven years of WMAP data with baryon Acoustic Oscillations in the distribution of galaxies and the Hubble parameter H_0 leads to $N_{eff} = 4.43^{+0.86}_{-0.88}$ [81]. However, Nine-years WMAP put a more stringent limit on the effective number of relativistic species to be $N_{eff} = 3.84 \pm 0.40$. Another close limit is given by Planck collaboration such as $N_{eff} = 3.15 \pm 0.23$ [117] and $N_{eff} = 2.99 \pm 0.17$ [118].

While limits on N_{eff} from SBBN were intensively investigated [54, 142], limits from astrophysics and cosmology are also important. We mention here the limit given by [89] where constraints on the number of effective relativistic degrees of freedom are deduced from the CMB, CMB lensing, Baryon acoustic oscillations, and galaxy clustering data to be $N_{eff} < 3.8$. Limits on N_{eff} are still a matter of debate and we still need a more accurate determination of N_{eff} . So based on the ranges above, in what follows we will adopt $2 < N_{eff} < 5$ as a constraint when including non-standard scenarios.

6.2 Are neutrinos a candidate for dark matter

While we know several aspects of dark matter such as its energy density and distribution, we don't have much information about its identity and production mechanism. Since baryons are not contributing to dark matter, one can think

of neutrinos or their decay products as possible candidates because neutrinos now have mass. The sterile neutrino, which is a hypothetical new generation of neutrinos other than the three active species, can be produced non-thermally by active-sterile mixing and particle decays [101]. The role of sterile neutrinos in cosmology strongly depends on the magnitude of their mass so that a sterile neutrino with a mass of order 1 keV could be a viable candidate for dark matter [31]. If this would be the case, this will be detectable in the extragalactic X-rays due to its radiative decay channel [49]. Constraints on the properties of a dark matter sterile neutrino (sterile neutrino mass and mixing parameter θ between active and sterile neutrinos) are given in [31] where the Milky Way halo and the halo of dwarf galaxies are the best objects for the search of dark matter with radiative decay channel.

A new investigation for the possibility of detection of sterile neutrinos of mass 50 keV in dark matter searches is given by [121] which are confronted by two problems: the expected event amount of energy to be received by the detector and the expected event rate. Although sterile neutrinos are heavy, they cannot be detected by standard dark matter experiments. For these reasons, electron neutrino scattering is considered by using systems with very small electron binding in order to have a high event rate. In addition, considering the options of nuclear physics (the absorption of an antineutrino on electron capturing nuclear system) and atomic physics (possibility of spin induced excitations) can be useful in detecting sterile neutrino dark matter [121]. Therefore, since explaining dark matter on the basis of the standard model is not likely, many searches with astrophysical and laboratory experiments are used to check the possibility of a sterile neutrino dark matter candidate [6].

6.3 Effect of varying neutrino temperature and chemical potential on the lithium production

During BBN and after the phase of electron-positron annihilation, the ratio of the neutrino temperature to the photon temperature is given by the standard relation [104]:

$$\left(\frac{T_\nu}{T_\gamma}\right)_0^3 = \frac{4}{2g_s - 10.5}, \quad (6.1)$$

where $g_s(T) = \frac{7}{8} \times (g_\nu + g_{e^\pm}) + g_\gamma = 10.75$ is the number of relativistic degrees of freedom contributing to the total entropy, or equivalently, the ratio of the total entropy to the entropy of photons. This determines the effective number of

neutrinos given by:

$$N_{eff}^0 = 3 \left[\frac{11}{4} \left(\frac{T_\nu}{T_\gamma} \right)_0^3 \right]^{4/3} = 3 \left[\frac{11}{2g_s - 10.5} \right]^{4/3}, \quad (6.2)$$

The presence of weakly interacting massive particles (WIMP's) will modify Eq. (6.1) and Eq. (6.2) above. When WIMP's couple to neutrinos or to photons, they change the energy density of relativistic particles and then they speed up the expansion rate of the universe. In addition to the heating of e^\pm , the annihilation of WIMP's can heat the photons. WIMP's can also share some of the entropy with neutrinos which causes the neutrino temperature to be different than that of the SBBN.

Therefore, the neutrino temperature can receive additional contributions in case of adding a dark component namely heating /cooling of photon relative to neutrino temperature which will be discussed in the next section. Here we introduce the neutrino temperature variation by a multiplicative factor α regardless of the source as adopted by Ref. [59].

According to Ref. [59], the total neutrino energy density is proportional to $N_\nu T_\nu^4$, thus a variation in the neutrino temperature can be translated into a variation in the effective number of neutrinos through:

$$N_{eff} T_{\nu SM}^4 = N_\nu T_\nu^4, \quad (6.3)$$

where $T_{\nu SM}$ is the neutrino temperature during the SBBN, N_{eff} is the effective number of neutrinos derived from the Cosmic microwave Background (CMB) and N_ν is the number of neutrinos contributing during SBBN. In SBBN, $N_{eff} = N_\nu$ because $T_{\nu SM} = T_\nu$. However, a deviation from the standard neutrino temperature after neutrino decoupling, leads to a difference between N_{eff} and N_ν . It is clear from Eq. (6.3) that we can vary two parameters while the third one will depend upon the other two. For example, taking $T_\nu = \alpha T_{\nu SM}$ for a fixed N_ν means that N_{eff} will depend on these two parameters. As obtained by Ref. [59], $N_\nu = 5$ is ruled out for any change in T_ν and for $N_{eff} = 3.15 \pm 0.23$. In addition, no ranges for N_ν and T_ν are available that can reduce the lithium abundance significantly. In the present work, in addition of varying the number of neutrinos and their temperature as treated by Ref. [59], we vary also the neutrino chemical potential as shown in Tables 6.1, 6.2. We obtained these results in the following way:

In these tables the neutrino chemical potentials are taken to be equal for the three neutrino species and this is the reason why we increased the number of neutrinos. The factor α represents the modification of neutrino temperature. Using Eq.(5.8), Eq.(6.3) is modified as follows:

$$N_{eff} T_{\nu SM}^4 = N_{\nu 0} \left(1 + \frac{30\beta^2}{7\pi^2} + \frac{15\beta^4}{7\pi^4} \right) T_\nu^4 + \Delta N_\nu T_\nu^4 \quad (6.4)$$

Table 6.1: Light elements abundances with varying neutrino number, chemical potential and temperature.

| $\beta_{\nu_{\mu,\tau,e}}$ | α | N_{eff} | N_ν | Yp | $D/H \times 10^5$ | ${}^7Li/H \times 10^{10}$ |
|----------------------------|----------|-----------|---------|--------|-------------------|---------------------------|
| 0.00 | 1.00 | 3.0000 | 3 | 0.2461 | 2.653 | 4.283 |
| 0.08 | 0.87 | 2.8693 | 5 | 0.2465 | 2.624 | 4.350 |
| 0.19 | 0.73 | 2.8532 | 10 | 0.2460 | 2.614 | 4.356 |
| 0.3 | 0.63 | 3.1691 | 20 | 0.2465 | 2.703 | 4.193 |

Using $T_\nu = \alpha T_{\nu SM}$, the effective number of neutrinos N_{eff} can be written explicitly as :

$$N_{eff} = \alpha^4 \times N_{\nu 0} \left(1 + \frac{30\beta^2}{7\pi^2} + \frac{15\beta^4}{7\pi^4} \right) + \alpha^4 \times \Delta N_\nu \quad (6.5)$$

The equations include the three standard neutrino species ($N_{\nu 0}$) with their chemical potentials while the term $\Delta N_\nu = N_\nu - N_{\nu 0}$ describes the extra massless relativistic species not contributing to the chemical potential. Restricting ourselves to the predicted light element abundances by SBBN within the quoted errors (see Table 3.1) and to the ranges of N_{eff} from Planck [118] $2.48 < N_{eff} < 3.5$, we obtain the following ranges which reproduces the SBBN predictions:

$$\begin{aligned} 3 \leq N_\nu \leq 20, \quad 2.48 \leq N_{eff} \leq 3.5 \\ 0.593 \leq \alpha \leq 1.039, \quad 0 \leq \beta_{\nu_{\mu,\tau,e}} \leq 0.3 \end{aligned} \quad (6.6)$$

The abundances in Table 6.1 show that the predicted values by SBBN can be obtained by this non-standard assumption described above. In other words, the SBBN predictions are not affected by these variation.

In order to obtain a substantial reduction of the lithium abundance, the ranges of Table 6.1 must be extended. To achieve this aim we consider the following ranges:

$$\begin{aligned} 3 \leq N_\nu \leq 20, \quad 6.62 \leq N_{eff} \leq 7.92, \\ 0.76 \leq \alpha \leq 1.27, \quad 0.02 \leq \beta_{\nu_{\mu,\tau,e}} \leq 0.45 \end{aligned} \quad (6.7)$$

Then, if we choose any N_ν , we can achieve a reduction of lithium by a combination of α and $\beta_{\nu_{\mu,\tau,e}}$. This illustrates the importance of these two parameters where we show an example in Table 6.2. We emphasize that the above results are comparable with all successful models that lead to a substantial decrease in lithium at the expense of increasing deuterium to the maximum value allowed by observations as discussed in section 2. The effect of varying $\beta_{\nu_{\mu,\tau,e}}$, N_ν and α can be explained as follows:

1. The effect of varying the number of neutrinos N_ν will lead to an increase in the energy density ρ of the universe and consequently the expansion

Table 6.2: Effect of varying neutrino number, chemical potential and temperature on lithium.

| $\beta_{\nu_{e,\mu,\tau}}$ | α | N_{eff} | N_ν | Y_p | $D/H \times 10^5$ | ${}^7Li/H \times 10^{10}$ |
|----------------------------|----------|-----------|---------|--------|-------------------|---------------------------|
| 0 | 1 | 3 | 3 | 0.2461 | 2.653 | 4.285 |
| 0 | 1 | 6 | 6 | 0.2795 | 3.699 | 3.321 |
| 0.15 | 1 | 6.0293 | 6 | 0.2423 | 3.420 | 3.040 |
| 0.25 | 0.99 | 6.8026 | 7 | 0.2265 | 3.491 | 2.713 |
| 0.25 | 1.02 | 7.5518 | 7 | 0.2272 | 3.697 | 2.526 |
| 0.41 | 0.77 | 7.1083 | 20 | 0.2333 | 3.611 | 2.695 |

rate given by Eq.(3.3). Then, varying the number of neutrinos N_ν will change the relativistic degrees of freedom k_{eff} and consequently light element abundances. As seen from the first two rows of Table 6.2, increasing neutrino number from $N_\nu = 3$ to $N_\nu = 6$ has led to an increase in helium and deuterium abundance but to a decrease in the abundance of lithium. This is due to the dominant effect on deuterium which can be seen from Eq.(5.41).

2. Adding a neutrino chemical potential β will have two effects: the first one is modifying neutrino energy density (see Eq.(5.8)) and then the expansion rate of the universe. The second one is due to the effect of electron-neutrino on the weak rates (see Eq.(5.16)). In other words, adding a positive chemical potential β will enhance the weak rates so that more neutrons are converted into protons which will lead to a decrease in the abundances of 4He , D and 7Li as seen in the third row of Table 6.2. Note that equating all chemical potentials will lead to a dominant effect of electron neutrino chemical potential and consequently a significant effect on 4He due to its sensitivity to the neutron mass fraction at the freeze-out.
3. By multiplying the neutrino temperature by a factor α the effective relativistic degrees of freedom before electron positron annihilation will be modified as follows:

$$k_{eff} = \frac{\pi^2}{30} \left(g_\gamma + \frac{7g_{e^\pm}}{8} + \frac{7g_\nu}{8} \times \alpha^4 \right) \quad (6.8)$$

and after electron-positron annihilation:

$$k_{eff} = \frac{\pi^2}{30} \left(g_\gamma + \frac{7g_\nu}{8} \times \alpha^4 \times \left(\frac{4}{11} \right)^{4/3} \right) \quad (6.9)$$

Then multiplying T_ν by a factor α will alter first the energy density of neutrinos and consequently the expansion rate given by Friedmann equation. Meanwhile, the dominant effect of this temperature variation is on

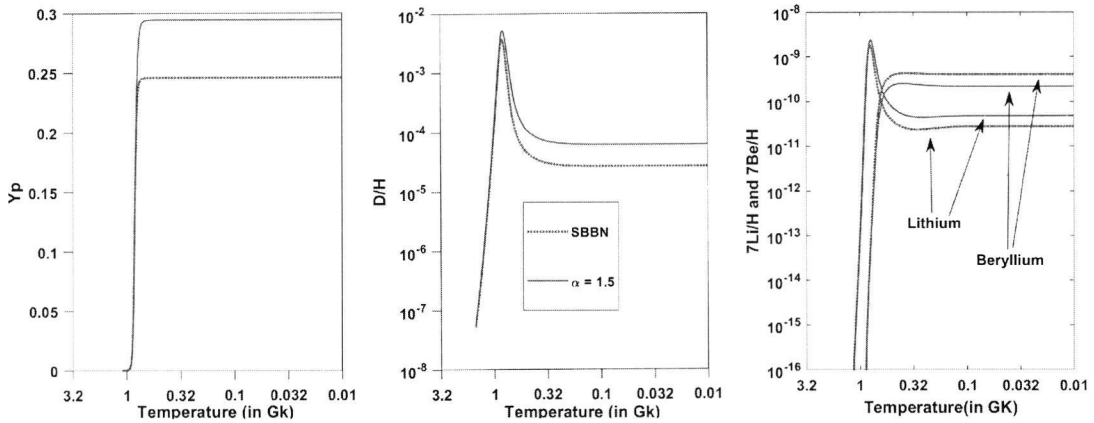


Figure 6.1: Comparison between the SBBN abundances of light elements as function of temperature (red dashed lines) and those obtained when multiplying neutrino temperature by a factor $\alpha = 1.5$ (blue solid lines)

deuterium. As obtained from Fig. 6.1, multiplying neutrino temperature by a factor of 1.5, has affected the abundance of deuterium at the bottleneck and consequently the final deuterium abundance. The deuterium abundance has increased by about 63% while helium has increased by 12%. Since variation of neutrino temperature is taken after neutrino decoupling (after the freeze-out of neutrons) but before deuterium formation epoch, we see that deuterium is more affected than helium (see fourth and fifth rows in Table 6.2). In addition, varying the neutrino temperature will alter the time temperature relation given by Eq.(3.14) due to the change in the effective degrees of freedom k_{eff} .

To understand the effect of these non-standard scenarios on lithium, we go back to the analytical calculations obtained in this work as shown in chap 5. Since more than 90% of beryllium will be converted into lithium by electron capture after BBN epoch, Eq.(5.41) which control the final abundance of lithium shows clearly the connection between beryllium, helium and deuterium. As seen in Fig. 6.1, the increase in deuterium has led to a decrease in the beryllium abundance for $\alpha = 1.5$ due to the anti-correlation relation between these two elements. Meanwhile, if 90% of the final abundance of lithium comes from electron capture on beryllium, the remaining 10% comes from the reactions leading to lithium where the dependence of lithium on helium and tritium is given by Eq.(5.42). For this reason, the increase in helium and tritium have led to an increase in lithium abundance as shown in Fig. 6.1. Thus, the decrease in the final abundance of (${}^7\text{Li}+{}^7\text{Be}$) as shown in the seventh column of Table 6.2 is due to the dominant effect of beryllium.

This result could be promising if the obtained limits on N_{eff} matched the CMB values. However, the obtained ranges on N_{eff} shown in Eq.(6.7) motivated us to extend this scenarios by taking into considerations the effect of dark matter in order to conserve the limits on N_{eff} . The effects of dark matter on lithium will be the focus of the next sections.

6.4 Axion as dark matter

Axions produced during the QCD phase transition could be possible candidate for cold dark matter (CDM)[51] where its density is well determined by WMAP and Planck missions. Such axion dark matter has an average momentum of order of the Hubble expansion rate and satisfies the CDM density if axions would have a mass of order of $10^{-5}ev/c^2$. With this mass range, axions interact weakly through all forces except gravity which make them one of the promising candidates for CDM [51].

An investigation for the interaction of axion-like dark matter with gluons by searching for a time oscillating neutron was performed by [5] as well as the effect of axion-wind spin-precession in order to search for the interaction of axion-like dark matter with nucleons. However, this was not promising for placing limits on such interactions rather this has led to improve upon existing astrophysical limits on the axion-gluon coupling and existing laboratory limits on the axion-nucleon coupling.

A question arises now: what is the effect of axion dark matter on big bang nucleosynthesis? An example of such effect was investigated by [51] where photon cooling through the gravitational field of cold axions after BBN had a significant effect on final element abundances especially on lithium. Photon cooling between the end of BBN and decoupling implies that the baryon-to-photon ratio η_{BBN} during BBN is different from η_{CMB} which is the one measured by Planck and WMAP. More explicitly, the photon cooling implies the energy conservation [51]:

$$\rho_{i,\gamma} = \rho_{f,\gamma} + \rho_{f,a} \quad (6.10)$$

where $\rho_{i,\gamma}$, $\rho_{f,\gamma}$ and $\rho_{f,a}$ are the initial, final energy density of photons and the final energy density of axions respectively. It is assumed that the energy densities of the initial axions and of baryons are negligible, for this reason they do not appear in Eq.(6.10). It follows from Eq.(6.10) that after reaching thermal equilibrium, the initial(T_i) and final (T_f) photon temperature are related through:

$$T_f = (2/3)^{1/4}T_i \quad (6.11)$$

Since the number density of photons is proportional to T^3 it is straightforward to show that:

$$\eta_{BBN} = \left(\frac{2}{3}\right)^{3/4}\eta_{CMB} \quad (6.12)$$

Table 6.3: Light elements abundances calculated by adopting the model of photon cooling with axion dark matter after BBN [51].

| | |
|--|--------|
| $N_\nu = 3$, and $\eta_{BBN} = (4.53 \pm 0.03) \times 10^{-10}$ | |
| Y_p | 0.2431 |
| $D/H \times 10^5$ | 4.27 |
| ${}^3\text{He}/H \times 10^5$ | 1.23 |
| ${}^7\text{Li}/H \times 10^{10}$ | 2.28 |

This model is treated by [51] in order to see if it solves the lithium problem. This implies that $\eta_{BBN} = (4.53 \pm 0.03) \times 10^{-10}$, $N_\nu = 3$ and the effective degrees of freedom from CMB is $N_{eff} = 6.77$ as shown in Table 6.3. The dominant effect of this model is mainly affecting deuterium due to its sensitivity to the baryon to photon ratio and consequently final abundance of lithium. Although this model suppresses the conflict between the BBN predictions and observations of lithium, this have led to an overproduction of deuterium and an increase in N_{eff} that is not allowed by observational constraints (see Table. 6.3).

6.5 Effect of photon cooling along with non-standard neutrino properties

In this section, we add effect of photon cooling with axions to the previous non-standard neutrino properties treated in sec. 6.3 with the aim to decrease the lithium abundance without violating observational constraints on N_{eff} and other light elements.

It is important to emphasize that the baryon to photon ratio as determined by Planck [118] is given to be $\eta = (6.14 \pm 0.04) \times 10^{-10}$, however, photon cooling through axions after BBN implies that $\eta_{BBN} = (4.53 \pm 0.03) \times 10^{-10}$ (see Eq.(6.12)). The energy density of the universe can be written as:

$$\rho_{rad} = \rho_\gamma [1 + N_{eff} \times \frac{7}{8} \times (\frac{4}{11})^{\frac{4}{3}}] \quad (6.13)$$

On the other hand, photon cooling with axions will also modify the effective degrees of freedom where the radiation density after BBN is given to be:

$$\rho_{rad} = \rho_\gamma [1 + \frac{1}{2} + N_\nu \times \frac{7}{8} \times (\frac{4}{11})^{\frac{4}{3}} \times \frac{3}{2}] \quad (6.14)$$

where the factor $3/2$ is due to the photon cooling relative to neutrinos and $1/2$ represents axion degrees of freedom. In this case the relativistic degrees of freedom observed now is given to be

$$N_{eff} = \frac{3}{2}N_\nu + \frac{1}{2} \times \frac{8}{7} \times (\frac{11}{4})^{\frac{4}{3}} \quad (6.15)$$

Table 6.4: Effect of adding photon cooling on lithium along with non-standard neutrino properties.

| $\beta_{\nu_{\mu,\tau,e}}$ | α | N_{eff} | N_ν | Y_p | $D/H \times 10^5$ | ${}^7Li/H \times 10^{10}$ |
|----------------------------|----------|-----------|---------|--------|-------------------|---------------------------|
| 0.05 | 0.82 | 4.2384 | 3 | 0.2313 | 3.469 | 2.779 |
| 0.11 | 0.77 | 4.8464 | 5 | 0.2342 | 3.672 | 2.622 |
| 0.20 | 0.60 | 4.5446 | 12 | 0.2405 | 3.628 | 2.757 |
| 0.33 | 0.50 | 4.0900 | 20 | 0.2266 | 3.387 | 2.792 |

Since photon cooling alone does not help to solve the lithium problem, we vary also the neutrino temperature in order to conserve the constraints on N_{eff} and deuterium. In addition, we vary the chemical potentials to obtain an additional decrease in lithium, but without violating observational constraints on helium. Introducing photon cooling, varying neutrino temperature and chemical potential, we modify the radiation energy density given in Eq.(6.14) as follows:

$$\rho_{rad} = \rho_\gamma [1 + \frac{1}{2} + \frac{7}{8} \times (\frac{4}{11})^{\frac{4}{3}} \times \frac{3}{2} \times \alpha^4 (\Delta N_\nu + N_{\nu 0} (1 + \frac{30\beta^2}{7\pi^2} + \frac{15\beta^4}{7\pi^4}))] \quad (6.16)$$

Then Eq.(6.16) will lead to the new effective degrees of freedom,

$$N_{eff} = \frac{1}{2} \times \frac{8}{7} \times (\frac{11}{4})^{\frac{4}{3}} + \frac{3}{2} \alpha^4 [\Delta N_\nu + N_{\nu 0} (1 + \frac{30\beta^2}{7\pi^2} + \frac{15\beta^4}{7\pi^4})] \quad (6.17)$$

It clear from Eq.(6.17) that multiplying the neutrino temperature with a factor $\alpha < 1$ will decrease the relativistic degrees of freedom to match observations discussed in sec.6.1. In addition, it will decrease deuterium so that the over-abundance observed in Table 6.3 can be reduced. We have performed numerical simulations after updating the code given by Ref. [18] to obtain the ranges shown in Eq.(6.18) and Table 6.4. It is seen from Table 6.4 that N_{eff} is now compatible with recent CMB observations [61, 81] but still higher than the most precise measurement given by Planck. In addition, the lithium decreases significantly at the expenses of increasing deuterium but to a value that is allowed by observations.

$$\begin{aligned} 3 \leq N_\nu \leq 20, \quad 4.08 \leq N_{eff} \leq 5.30 \\ 0.5 \leq \alpha \leq 0.9, \quad 0.01 \leq \beta_{\nu_{\mu,\tau,e}} \leq 0.35 \end{aligned} \quad (6.18)$$

This increase of the deuterium abundance when including non-standard scenarios is discussed recently by [84]. Because of their fragility, deuterons can be destroyed easily if there is a source of non-thermal photons in the early universe, then this could alleviate the increase of deuterium when including non-standard physics during BBN.

A question arises now: how could we explain the increase in the number of neutrinos N_ν during BBN? Could this increase in the number of neutrinos contribute

Table 6.5: Effect of adding photon cooling on lithium along with non-standard neutrino properties for $N_\nu = 3$.

| $\beta_{\nu_{\mu,\tau,e}}$ | α | N_{eff} | N_ν | Yp | $D/H \times 10^5$ | ${}^7\text{Li}/H \times 10^{10}$ |
|----------------------------|----------|-----------|---------|--------|-------------------|----------------------------------|
| 0.07 | 0.81 | 4.143 | 3 | 0.2270 | 3.418 | 2.765 |
| 0.06 | 0.84 | 4.446 | 3 | 0.2292 | 3.525 | 2.689 |
| 0.05 | 0.87 | 4.782 | 3 | 0.2314 | 3.643 | 2.608 |
| 0.05 | 0.90 | 5.157 | 3 | 0.2315 | 3.756 | 2.508 |

to the dark matter in the universe? The possibility that neutrinos are dark matter candidate is extensively investigated [6, 21, 31, 49, 101, 121, ?], however, this issue is not settled yet and it is still a matter of debate. Meanwhile, from particle physics side, the increase in the number of neutrinos N_ν more than three species is not allowed since this increase should be justified by an appropriate model. For this reason, we have shown in Table 6.5 that our results of decreasing lithium abundance could be explained with $N_\nu = 3$. In such case, our calculations are not only based on constraints from cosmology and astrophysics but also from particle physics.

6.6 The effect of a unified dark fluid

We have seen in sec.6.5 that adding axion dark matter was successful to decrease the ${}^7\text{Li}$ abundance with N_{eff} compatible with the recent CMB observations, but still higher than the one determined by the Planck mission. **In order to satisfy the requirements on N_{eff} we found a way by adopting the so-called dark fluid along with non-standard neutrino properties.**

We know that dark matter may be modeled as a system of collision-less particles while dark energy may be described as a scalar field in the context of the quintessence model [15]. However, in this section, a unified fluid [16] is adopted to describe the dark energy and dark matter as two different aspects of the same component. To explore this scenario, a temperature-dependent dark energy density can be added to the radiation density as follows [15]:

$$\rho_D(T) = k_\rho \rho_{rad}(T_0) \left(\frac{T}{T_0} \right)^{n_\rho} \quad (6.19)$$

where $\rho_{rad} = \rho_\gamma + \rho_{e^\pm} + \rho_\nu$, $T_0 = 1.0 \text{ MeV} = 1.16 \times 10^{10} \text{ K}$, k_ρ is the ratio of effective dark fluid density over the total radiation density at T_0 and n_ρ characterizes the adiabatic expansion of the fluid. In the case of $n_\rho = 4$, the dark component mimics a radiation density. The case $n_\rho = 3$ describes a matter density, while $n_\rho = 6$ can describe a scalar field. With these assumptions the Friedmann equation during

BBN should be modified as:

$$\left(\frac{\dot{a}}{a}\right)^2 = H^2 = \frac{8\pi G}{3}(\rho_{rad} + \rho_D) \quad (6.20)$$

In analogy, the temperature-dependent dark entropy can be added as follows:

$$s_D(T) = k_s s_{rad}(T_0) \left(\frac{T}{T_0}\right)^{n_s} \quad (6.21)$$

where

$$s_{rad}(T) = g_s(T) \frac{2\pi^2}{45} T^3 \quad (6.22)$$

and $g_s(T)$ is the effective number of degrees of freedom characterizing the contribution of relativistic particles to the entropy density. This parametrization can be explained on the basis of the first law of thermodynamics where energy and entropy are directly related. As in the case of dark energy density, different values of n_s lead to different behaviors. For example, $n_s = 3$ corresponds to radiation, while other values could be obtained by extra-dimension effect or scalar fields [19]. In addition, to ensure radiation domination during BBN, we should take $k_s \ll 1$. Then, the total entropy becomes:

$$s_{tot}(T) = s_{rad}(T) + s_D(T) \quad (6.23)$$

It is clear from Eqs.(6.19, 6.21) that by including this dark component, four parameters are introduced k_ρ, n_ρ, k_s, n_s . Knowing that the universe was radiation dominated during the time of BBN requires the constraints $n_\rho > 4$ and $k_\rho < 1.0$ [17]. It is important to emphasize that the dominant effect of adding ρ_D is to alter the expansion rate and this clearly seen by Eq.(6.20).

We show in Fig. 6.2 the effect of adding a dark energy density ρ_D for $n_\rho = 6$ (left panel) and for $n_\rho = 7$ (right panel) while varying k_ρ in both cases. This has led to an increase in the abundance of light elements where the dominant effect is on helium (dotted curve). Although deuterium has also increased (solid line), an increase in lithium is also seen, which is due to the dominant effect on helium. A similar effect is obtained when taking $n_\rho = 7$, but for smaller values of k_ρ . We can argue that the effect on final lithium abundance is determined by the variation of helium and deuterium. It is seen in Eqs.(5.40, 5.41)) that the lithium abundance is proportional to the abundance of helium but inversely proportional to that of deuterium. In other words, as seen in the right panel of Fig. 6.2 and for $k_\rho < 0.002$, lithium increases significantly due to the increase in helium. However, for $k_\rho > 0.002$ the increase in lithium is less pronounced since the deuterium abundance increases significantly.

Modifying the entropy content of the universe as given in Eq.(6.23) alters the

time evolution of the temperature described by the energy conservation equation given by Eq.(6.24).

$$\frac{d}{dt}(\rho_{tot}a^3) + P_{tot}\frac{d}{dt}(a^3) - a^3\frac{d\rho_{tot}}{dt}|_{T=cst} - T\frac{d}{dt}(S_D a^3) = 0. \quad (6.24)$$

The effect of dark entropy is clearly shown in Fig. 6.3 where adding s_D has led to

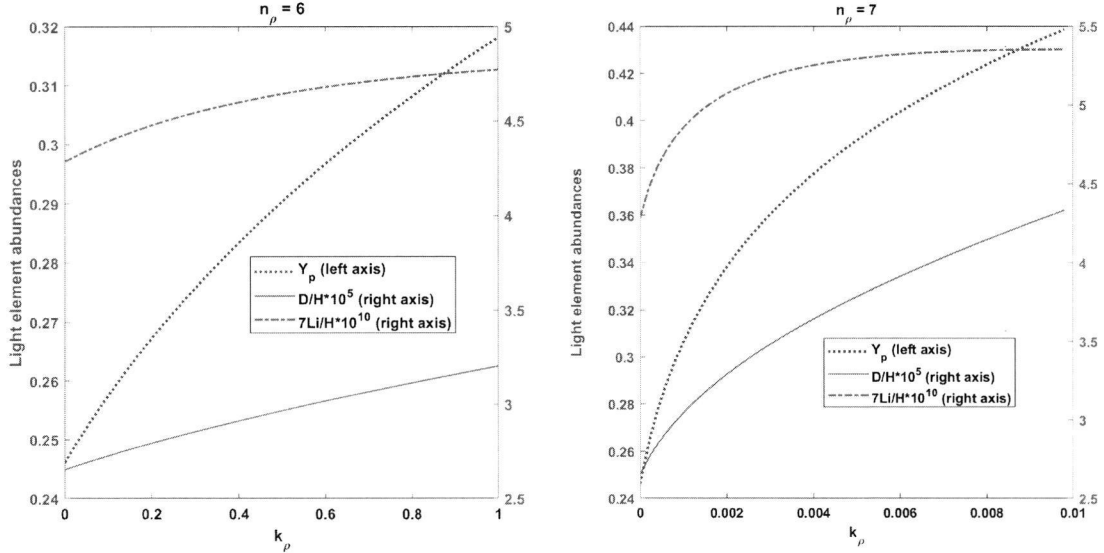


Figure 6.2: Effect of adding dark energy density ρ_D on the abundances of helium (blue dotted line, left axis), deuterium (orange solid line, right axis) and lithium (orange dashed line, right axis).

an increase in deuterium, but to a decrease in the helium and lithium abundances. In this case, the dominant effect of s_D is on deuterium and consequently the final lithium abundance. The dependence of the final lithium abundance on helium and deuterium given by Eqs. (5.41,5.42) is now confirmed by the results shown in Figs.(6.2,6.3). In addition, Fig. 6.4 shows that adding a dark entropy does not only lead to an increase in the deuterium abundance, but to a shift in the temperature of the bottleneck (maximum abundance of deuterium). The shift in the bottleneck temperature alters the abundance of the other light elements since the formation of helium is blocked until deuterium reaches its maximum. For fixed values of k_ρ, n_ρ, k_s, n_s and restricting N_{eff} as measured by the Planck collaboration, the neutrino number and chemical potentials were varied in order to find out how these non-standard scenarios could contribute to the lithium problem. Our calculations summarized in Tables(6.6, 6.7) show the following:

1. Fixing $k_\rho = 0.007$, $n_\rho = 7$, $k_s = 0.00045$ and $n_s = 5$, restricting $2.48 < N_{eff} < 3.5$ in order to be compatible with Planck measurements, and varying the number of neutrinos ($3 \leq N_\nu \leq 20$) along with neutrino chemical

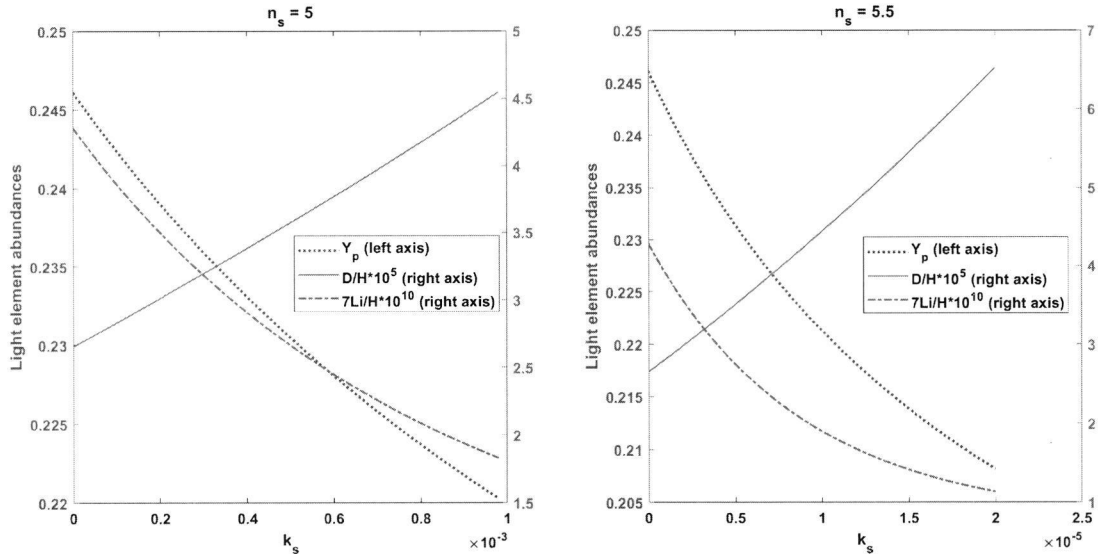


Figure 6.3: Effect of adding dark entropy S_D (see Eq.(6.21)) on the abundances of helium (blue dotted line, left axis), deuterium (orange solid line, right axis) and lithium (orange dashed line, right axis).

potential, we are able to find for every chosen value of N_ν , a combination of α (or N_{eff}) and $\beta_{\nu_{e,\mu,\tau}}$ that reduces lithium abundance. Note that N_{eff} is still given by Eq.(6.5) because the dark component has effect on SBBN predictions due to the power law (see Eqs.(6.19, 6.22)) and negligible contribution after BBN. In other words, although this dark component alters the expansion rate, it has no observational effect on N_{eff} or other cosmological parameters. Eq. (6.25) shows the ranges that lead to a decrease of lithium and we see now with this treatment that N_{eff} is compatible with recent CMB data including Planck and WMAP ones.

$$\begin{aligned}
 k_\rho = 0.007, \quad n_\rho = 7, \quad k_s = 0.00045, \quad n_s = 5, \\
 3 \leq N_\nu \leq 20, \quad 2.48 \leq N_{eff} \leq 3.50 \\
 0.564 \leq \alpha \leq 0.968, \quad 0.83 \leq \beta_{\nu_{\mu,\tau,e}} \leq 0.97
 \end{aligned}
 \tag{6.25}$$

2. Again, on the basis of the standard model of particle physics, it is crucial to show how the lithium problem is resolved with $N_\nu = 3$ since $N_\nu > 3$ is not supported by CERN experiments. This is shown in Table 6.7 in order to emphasize that we do not need to violate particle physics constraints on N_ν .
3. If we have chosen other values of the dark component parameters such as $k_\rho = 0.12$, $n_\rho = 6$, $k_s = 0.0005$ and $n_s = 5$, other ranges can be derived as

Table 6.6: Effect of unified dark fluid on lithium along with non-standard neutrino properties.

| $k_\rho = 0.007, n_\rho = 7, k_s = 0.00045$ and $n_s = 5$ | | | | | | |
|---|----------|-----------|---------|--------|-------------------|---------------------------|
| $\beta_{\nu_{\mu,\tau,e}}$ | α | N_{eff} | N_ν | Yp | $D/H \times 10^5$ | ${}^7Li/H \times 10^{10}$ |
| 0 | 1 | 3. | 3 | 0.4007 | 5.395 | 3.484 |
| 0.88 | 0.86 | 3.3086 | 5 | 0.2301 | 3.696 | 2.535 |
| 0.84 | 0.72 | 2.9432 | 10 | 0.2465 | 3.716 | 2.751 |
| 0.94 | 0.59 | 2.5692 | 20 | 0.2321 | 3.495 | 2.758 |

Table 6.7: Effect of unified dark fluid on lithium along with non-standard neutrino properties with $N_\nu = 3$.

| $k_\rho = 0.007, n_\rho = 7, k_s = 0.00045$ and $n_s = 5$ | | | | | | |
|---|----------|-----------|---------|--------|-------------------|---------------------------|
| $\beta_{\nu_{\mu,\tau,e}}$ | α | N_{eff} | N_ν | Yp | $D/H \times 10^5$ | ${}^7Li/H \times 10^{10}$ |
| 0 | 1 | 3 | 3 | 0.4007 | 5.395 | 3.484 |
| 0.85 | 0.89 | 2.494 | 3 | 0.2301 | 3.460 | 2.762 |
| 0.86 | 0.94 | 3.123 | 3 | 0.2260 | 3.612 | 2.553 |
| 0.84 | 0.97 | 3.500 | 3 | 0.2283 | 3.737 | 2.474 |

shown by Eq.(6.26):

$$\begin{aligned}
 k_\rho &= 0.12, n_\rho = 6, k_s = 0.0005, n_s = 5, \\
 3 &\leq N_\nu \leq 20, 2.48 \leq N_{eff} \leq 3.50, \\
 0.59 &\leq \alpha \leq 1.03, 0 \leq \beta_{\nu_{\mu,\tau,e}} \leq 0.48
 \end{aligned}
 \tag{6.26}$$

Finally, we can choose other values of dark component parameters taking into account that $n_\rho > 4$, $n_s > 3$, $k_\rho < 1$, and $k_s \ll 1$, in order to impose domination of radiation during BBN and to be consistent with CMB observations (the dark component will not dominate after BBN). Then, other ranges of α and $\beta_{\nu_{e,\mu,\tau}}$ can be derived but for simplicity we have fixed the dark component parameters in order to give a better understanding of the physical conditions under which the BBN has been operating and provide many possibilities to ameliorate the lithium problem.

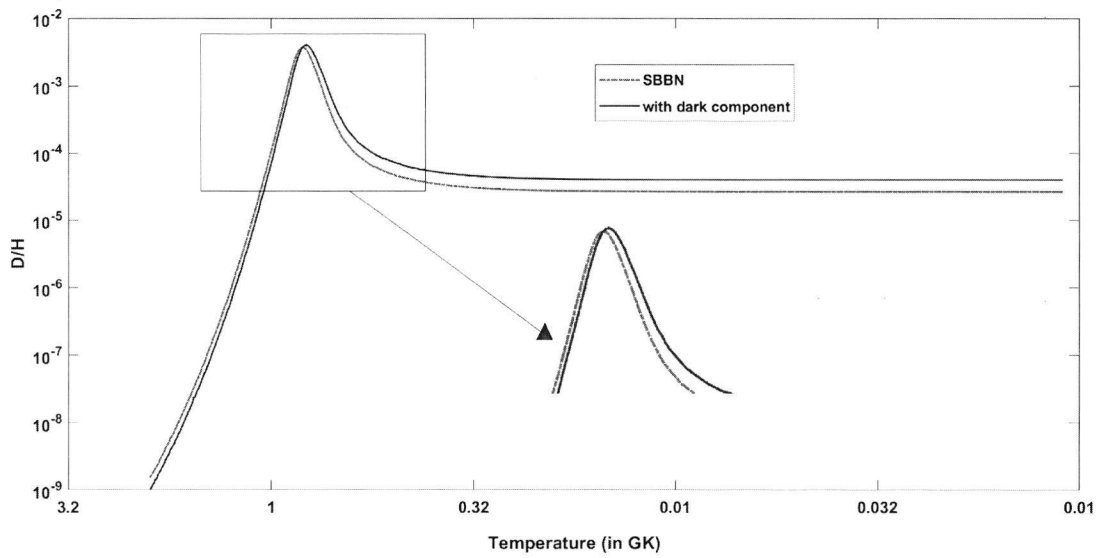


Figure 6.4: Deuterium abundance as function of temperature when adding dark entropy ($k_s = 0.007, n_s = 5$) compared to SBBN

Chapter 7

Constraining the neutron lifetime by SBBN

Neutrons are basic ingredients of ordinary matter where the majority of the mass of the earth is contributed by neutrons. However, when neutrons are not confined in atoms, they are free to undergo β^- decay via the weak nuclear force to a proton, electron, and antineutrino. The decay of neutron is a fundamental process in nuclear and particle physics. The neutron lifetime is a crucial parameter in SBBN, especially in the determination of the final helium abundance. Over the past decades, the value of the neutron lifetime was continuously improved from $\tau_n = 918 \pm 14$ to $\tau_n = 880.2 \pm 1$ [149]. This high precision was the outcome of the cold neutron beam method which uses a Penning trap to capture and count resultant protons, or the ultracold neutrons method which measures the survival of neutrons after storage. These two techniques are called bottle and beam methods. The different measured neutron lifetimes along with the corresponding error bars are shown in Fig. 7.1 where it is clear that the error bars decreased over time. Although we have now a more precise value of neutron lifetime, the two techniques are still in tension in determining the neutron lifetime so that they disagree by about 10s. Is this disagreement a sign of new physics? Two theoretical physicists at the University of California, Benjamin Grinstein, and Bartosz Fornal argued that neutrons could decay into dark matter. If this would be the case, neutrons might disappear faster from bottles than protons appear in beams. Then, neutron decay into a dark matter particle and gamma ray, which could be concrete evidence for experimentalists to look for. Following such hypothesis, the UCNtau experimental team in Los Alamos, and with 99% certainty, reported the absence of gamma ray. Till now, the hypothesis of dark matter is neither completely excluded nor confirmed so that no one has reported the evidence of the discrepancy between beam and bottle methods.

It is obvious that the neutron lifetime plays a crucial role during BBN as discussed in previous chapters. It controls the weak interaction rates at the freeze-out and consequently affects the final abundance of helium as shown in Eq. 5.31.

The following ranges of neutron lifetime are derived:

$$\begin{aligned}
N_{eff} = 2.48, \tau = 937_{-122}^{+186} \text{ or } 815 < \tau_n < 1123s, \\
N_{eff} = 3, \tau = 900_{-117}^{+179} \text{ or } 783 < \tau_n < 1079s, \\
N_{eff} = 3.5, \tau = 868_{-113}^{+173} \text{ or } 755 < \tau_n < 1041s.
\end{aligned}
\tag{7.1}$$

- The above ranges are calculated based on the upper and lower limit of the primordial helium observations. For each range calculated above, we obtain also a different concentration of deuterium and lithium. As shown in the first column of Table 7.3, the lowest lithium abundance is obtained for $N_{eff} = 3.5$ and $\tau_n = 755s$. Then, based on SBBN and with this variation of the neutron lifetime and N_{eff} , the lithium abundance has decreased by about 10% from its SBBN value such that ${}^7\text{Li}/\text{H} = (3.816 \pm 0.336) \times 10^{-10}$. This result is expected because, with $\tau_n = 755s$, fewer neutrons and more protons are available compared to SBBN where $\tau_n = 880.2s$. This has led to a decrease of the helium abundance to its lower limit ($Y_p = 0.225 \pm 0.000149$) and consequently lithium.
- The effects of varying τ_n and N_{eff} on the final element abundances are clearly shown in Fig. 7.2. The dominant effect of varying the neutron lifetime is on helium and this could be clearly explained by the exponential dependence of Y_p on τ_n shown in Eq. 5.31. Increasing the neutron lifetime will lead to an increase in the final helium and deuterium abundance. Since the dominant effect is on helium, this will lead to an increase in the final lithium abundance.
- Although the variation of N_{eff} is not significant (between 2.48 and 3.5), it affects the expansion rate of the universe and consequently the final element abundances. The increase in N_{eff} will lead to an increase in the final abundance of helium and deuterium. Since the dominant effect is on deuterium, the final abundance of lithium will decrease (see Fig. 7.2).
- The ranges of τ_n represented in this analysis are compatible with the recent value of the neutron lifetime $\tau_n = 880.2 \pm 1$ from the particle data group (PDG) [149]. However, our obtained uncertainties are much larger and this is due to the uncertainties on the measured helium abundance.

Table 7.1: light element abundances for $N_{\text{eff}} = 2.48$ and $815 < \tau_n < 1123$.

| | $\tau_n = 815\text{s}$ | $\tau_n = 1123\text{s}$ |
|----------------------------------|------------------------|-------------------------|
| Y_p | 0.225 ± 0.000148 | 0.283 ± 0.000145 |
| $D/H \times 10^5$ | 2.394 ± 0.113 | 2.736 ± 0.128 |
| ${}^3\text{He}/H \times 10^5$ | 0.981 ± 0.052 | 1.029 ± 0.0534 |
| ${}^7\text{Li}/H \times 10^{10}$ | 4.321 ± 0.383 | 4.956 ± 0.438 |

Table 7.2: light element abundances for $N_{\text{eff}} = 3$ and $783 < \tau_n < 1079$.

| | $\tau_n = 783\text{s}$ | $\tau_n = 1079\text{s}$ |
|----------------------------------|------------------------|-------------------------|
| Y_p | 0.225 ± 0.000148 | 0.283 ± 0.000145 |
| $D/H \times 10^5$ | 2.530 ± 0.116 | 2.892 ± 0.132 |
| ${}^3\text{He}/H \times 10^5$ | 1.000 ± 0.052 | 1.049 ± 0.0537 |
| ${}^7\text{Li}/H \times 10^{10}$ | 4.050 ± 0.357 | 4.630 ± 0.418 |

Table 7.3: Light element abundances for $N_{\text{eff}} = 3.5$ and $755 < \tau_n < 1041$.

| | $\tau_n = 755\text{s}$ | $\tau_n = 1041\text{s}$ |
|----------------------------------|------------------------|-------------------------|
| Y_p | 0.225 ± 0.000149 | 0.283 ± 0.000145 |
| $D/H \times 10^5$ | 2.394 ± 0.113 | 2.736 ± 0.128 |
| ${}^3\text{He}/H \times 10^5$ | 1.018 ± 0.053 | 1.069 ± 0.0543 |
| ${}^7\text{Li}/H \times 10^{10}$ | 3.816 ± 0.336 | 4.352 ± 0.390 |

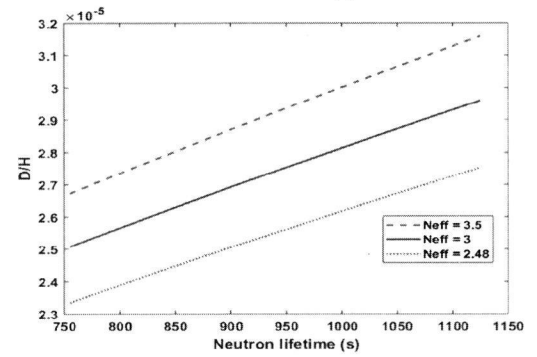
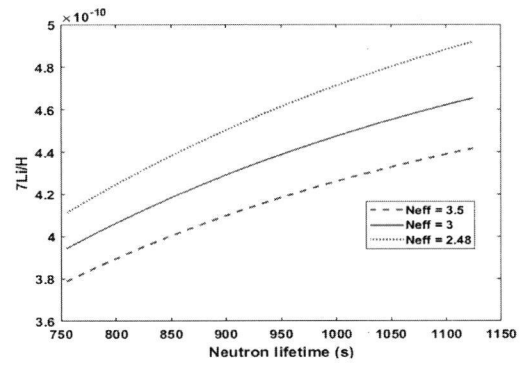
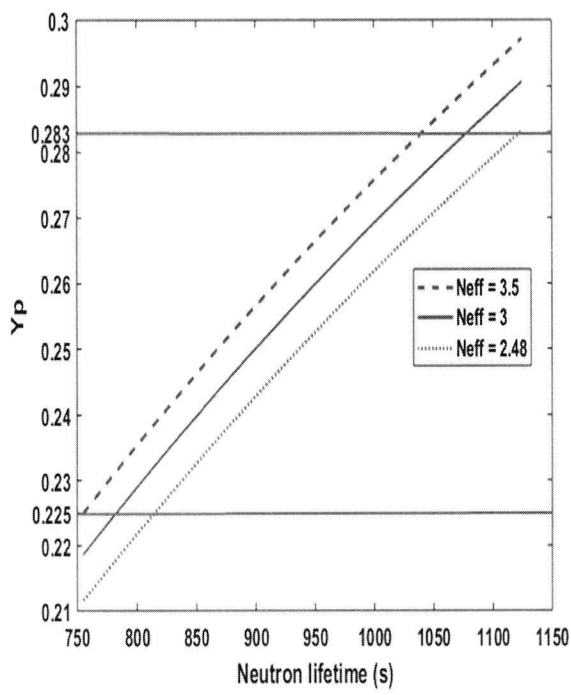


Figure 7.2: light element abundances as function of neutron lifetime for different values of N_{eff} .

Chapter 8

Summary and conclusions

The subject of this work aimed at an understanding the fundamental process leading to the formation of the light elements and their isotopes in the early universe. This fundamental big bang nucleosynthesis (BBN) seems to require some revision in order to understand what is missing in the physical description and to investigate the possibility to resolve the "Lithium Problem" described in this work.

The focus of the present work is to reanalyze the standard big bang nucleosynthesis (SBBN) and to invoke non-standard treatments of BBN motivated by analyzing the lithium problem. It seems that the "Lithium Problem" is difficult to resolve on nuclear and astrophysical grounds, so the present work has the rational to get more insight why this lithium problem exists. For this reason, we have included many non-standard components to the SBBN such as non-standard neutrino properties and dark matter. We have focused on the properties of neutrinos and dark matter due to their importance during BBN. The results of the present work can be summarized as follows:

1. In chap.2, we discussed the constraints on light element abundances which seem to be still a matter of debate, especially for deuterium. Specifying the constraints on light elements is crucial because all BBN predictions, especially when including non-standard scenarios, should be compared to observational constraints.
2. In chap.3, we described the production of light species by the SBBN. We found that all light element abundances agree very well with observations except for lithium. Then, using a network of updated reaction rates (shown in Appendix E), we calculated the abundances of light elements by SBBN. As expected, the lithium problem is evident in this calculation (see Table 3.1). This is to confirm that the so-called lithium problem cannot be resolved by SBBN.
3. The so-called "Spite Plateau" which is a constant behavior of lithium as

a function of metallicity does not exist when observations were extended to very low metallicity. In addition to the discrepancy between SBBN predictions and observations, this introduces another discrepancy besides the well-known lithium problem.

4. As described in chap.4, we attempted to find out how lithium production can be reduced on pure nuclear physics ground. Emphasizing the fact that about 90% of the lithium abundance originates from electron capture of ${}^7\text{Be}$, careful consideration of this weak interaction rate did not lead to the desired solution. Including an additional effect of electron screening was also not successful. We have reviewed a possible solution on astrophysical grounds, due to stellar processing in very metal-poor halo stars. While this is still an open problem not only how to account for lithium depletion in the very-metal poor stars, but also the description of the atmosphere of such stars is a completed task. Since both nuclear physics and astrophysical aspects seem not to resolve the lithium problem, we have introduced non standard ingredients into the SBBN calculations as described in the following.

5. The first modification from SBBN was to investigate the effects of varying the number of neutrinos and their chemical potentials. This modification aims to have a clearer picture of SBBN and to investigate the effect on the production of lithium. We made an effort to obtain analytical approximations to get a better insight into the effects of non-standard assumptions concerning the weak interaction rates and neutron mass fraction at freeze-out (see sec.5.4.1).

We have also obtained analytical expressions to determine the temperature at which the deuterium achieves its maximum abundance (called the bottleneck). Furthermore, we were able to obtain the temperature T^* at which the neutron abundance drops below that of deuterium. This has the advantage to see how the abundances of the light elements are influenced by this epoch of the SBBN (see chap.5 for details). In addition to the analytical work, we have performed numerical calculations using an updated version of the network code (AlterBBN). In our calculations, we were able to obtain limits on the neutrino chemical potential that lead to a significant reduction of lithium abundance. However, this was achieved only with an increase of the deuterium abundance that is still justified by observations.

6. Another ingredient in the non-standard treatment was the scaling of the standard neutrino temperature. As shown in sec.6.3, we were able to reproduce the SBBN results with a suitable choice of the scaling parameter α . This means that our non-standard assumption can be considered as an extension of the SBBN, with the net effect of reducing lithium abundance.
7. Extending the range of variation of neutrino parameters was successful as

a means to reduce the lithium abundance (see Sec.6.3). However, since varying the neutrino temperature has an observational effect on the current relativistic degrees of freedom, the derived range was not compatible with the effective number of relativistic species N_{eff} given by the recent analysis of the CMB as discussed in sec.6.1.

In sec.6.5, photon cooling with axion dark matter after BBN leads to a reduction of the lithium abundance with N_{eff} compatible with recent CMB observations, but it is still in tension with the most precise value deduced by Planck analysis. In sec.6.6, a unified dark fluid combining dark matter and dark energy in one concept is adopted in order to satisfy the requirements on N_{eff} . This approach together with non-standard neutrino properties resulted in a decrease of lithium abundance but for N_{eff} compatible with the recent evaluation of the CMB observation and with the Planck and WMAP conclusions (see sec.6.6 for details).

8. Since including dark component was successful to reduce lithium abundance without violating observational constraints on light elements and on N_{eff} , we emphasize also that this could be achieved without increasing N_ν more than three. This has the potential to account for the constraints from the standard model of particle physics which is verified experimentally.
9. In chap. 8, we described the present status of the measurements concerning the free neutron lifetime. In this chapter, we tried to constrain the neutron lifetime through the helium abundance and the range of N_{eff} .
10. As a conclusion, our diverse attempts to reduce the lithium abundance from the value predicted by the SBBN was possible only when non-standard assumptions were included as outlined above. It is amazing and striking that such a reduction goes along with a maximum abundance of deuterium, which luckily maybe allowed by observations [26]. To avoid a maximum of deuterium, new particles or interactions are suggested by [60], [130]. This is announced as a future perspective.

A final remark is at a place. The big bang theory occupies a fundamental place in the understanding of the early phase of the universe. It touches the imagination in basic scientific research in cosmology. The big bang nucleosynthesis is a striking tool to relate our imagination to observations. It seems some more physics is missing to understand the lithium problem. The present work was a step toward a better understanding of this cosmological problem.

Appendix A

Freeze-out of neutrons

The balance equation for the neutrons mass fraction X_n is given by:

$$\frac{dX_n}{dt} = -\lambda_{n \rightarrow p} X_n + \lambda_{p \rightarrow n} X_p = -\lambda_{n \rightarrow p} (1 + e^{-\frac{Q}{T}}) (X_n - X_n^{eq}) \quad (\text{A.0.1})$$

where $\lambda_{n \rightarrow p} = \lambda_{ne} + \lambda_{n\nu}$ and $\lambda_{p \rightarrow n} = \lambda_{pe} + \lambda_{p\bar{\nu}}$ which are the total rates of direct and inverse reactions respectively where:

$$X_n^{eq} = \frac{1}{1 + \exp(\beta_{\nu_e}) \exp(Q/T)}, \quad (\text{A.0.2})$$

t is the time in seconds and T is the temperature in MeV. The solution of equation (A.0.1) is given by as the following[103]:

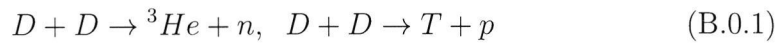
$$X_n(t) = X_n^{eq}(t) - \int_0^t \exp\left(-\int_{\tilde{t}}^t \lambda_{n \rightarrow p}(\tilde{t}) \left(1 + e^{-\frac{Q}{\tilde{T}}}\right) d\tilde{t}\right) \dot{X}_n^{eq}(\tilde{t}) d\tilde{t} \quad (\text{A.0.3})$$

with the initial condition $X_n \rightarrow X_n^{eq}$ as $t \rightarrow 0$. The dot denotes the derivative with respect to time. To have an estimation for the freeze out concentration, it is assumed that $X_n^{eq} \rightarrow 0$ as $T \rightarrow 0$ and $\lambda_{n \rightarrow p} \approx 2\lambda_{n\nu}$ because the main contribution of the integral comes from $T > m_e$. Therefore by replacing the integration variable t by $y = T/Q$ using Eq. (3.14) we obtain the expression for the freeze-out concentration given by Eq. (5.18). This is different from the one given by [103] because we included the neutrino chemical potential.

Appendix B

Deuterium bottleneck

The Deuterium bottleneck takes place when the main reactions converting Deuterium into Tritium and Helium-3 become effective:



The mass fraction X_D of Deuterium can be written as :

$$\Delta X_D = -\frac{1}{2}\lambda_{DD}X_D^2\Delta t \quad (\text{B.0.2})$$

where $\lambda_{DD} = \lambda_{DD1} + \lambda_{DD2}$ are the rates of reactions given in Eq. (B.0.1) when a substantial amount of available Deuterium is converted into ${}^3\text{He}$ within a cosmological time t , it is assumed that $\Delta X_D \approx X_D$. This assumption leads to Eq. (B.0.2)[103]. However, we extended the calculation of Deuterium bottleneck to include neutrinos chemical potential by integrating Eq. (B.0.2) so that:

$$\frac{D}{H} \approx \frac{4 \times 10^{-3}}{X_p(k_{eff}^{-0.5} \times T_{BN}(\text{Mev}) \times \eta_{10} + C)} \quad (\text{B.0.3})$$

where C is a constant which is time independent but it is function of neutrinos chemical potential. Therefore, Eq. (5.23) is obtained by constraining C with our numerical calculations.

Appendix C

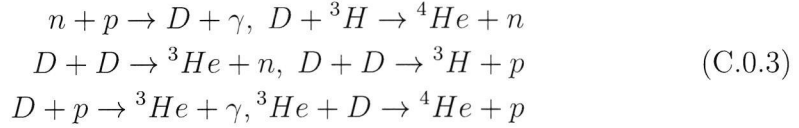
Final deuterium abundance

To calculate elements abundance we must deal with a system of kinetic equations [103]. For a reaction $AB \rightarrow CD$:

$$\dot{X}_A = -A_B^{-1} \lambda_{AB} X_A X_B \quad (\text{C.0.1})$$

$$\dot{X}_c = A_c A_A^{-1} A_B^{-1} \lambda_{AB} X_A X_B \quad (\text{C.0.2})$$

Here $X_A = \frac{A_A n_A}{n_N}$ is the concentration by weight of the corresponding element (${}^4\text{He}$, n , D , ...), n_N is the total number of nucleons (baryons) and A is their mass number. For example, for the production and destruction of deuterium we consider the following reactions :



and then the concentration of deuterium as function of time is given by:

$$\frac{dX_D}{dt} = 2\lambda_{pn} X_p X_n - \frac{1}{2} \lambda_{DD} X_D^2 - \lambda_{Dp} X_D X_p - \frac{1}{3} \lambda_{D^3\text{H}} X_D X_{^3\text{H}} - \frac{1}{3} \lambda_{^3\text{He}D} X_D X_{^3\text{He}} \quad (\text{C.0.4})$$

where λ 's are the reaction rates of different reactions. Similarly kinetic equations for X_n , $X_{^3\text{H}}$, and $X_{^3\text{He}}$ can be obtained by taking into consideration all reactions producing and destroying n , ${}^3\text{H}$, and ${}^3\text{He}$:

$$\frac{dX_n}{dt} = -\lambda_{pn} X_p X_n - \frac{1}{3} \lambda_{^3\text{He}n} X_{^3\text{He}} X_n + \frac{1}{4} \lambda_{DD1} X_D^2 + \frac{1}{6} \lambda_{D^3\text{H}} X_D X_{^3\text{H}} \quad (\text{C.0.5})$$

$$\frac{dX_{^3\text{H}}}{dt} = \frac{3}{4} \lambda_{DD2} X_D^2 + \lambda_{^3\text{He}n} X_{^3\text{He}} X_n - \frac{1}{2} \lambda_{D^3\text{H}} X_D X_{^3\text{H}} \quad (\text{C.0.6})$$

$$\frac{dX_{^3\text{He}}}{dt} = \frac{3}{4} \lambda_{DD1} X_D^2 + \frac{3}{2} \lambda_{Dp} X_D X_p - \lambda_{^3\text{He}n} X_n X_{^3\text{He}} - \frac{1}{2} \lambda_{^3\text{He}D} X_D X_{^3\text{He}} \quad (\text{C.0.7})$$

Assuming the quasi-equilibrium condition for ${}^3\text{He}$ and ${}^3\text{H}$, $\frac{dX_{3\text{H}}}{dt} \approx 0$ and $\frac{dX_{3\text{He}}}{dt} \approx 0$, and using the time temperature relation of Eq. (3.14), Eqs. (C.0.4,C.0.5) can be written as:

$$\frac{dX_D}{dT} = 4\alpha\eta_{10}(X_D^2 + R_2X_D - \frac{1}{2}R_1X_n) \quad (\text{C.0.8})$$

$$\frac{dX_n}{dT} = \alpha\eta_{10}(R_1X_n - X_D^2) \quad (\text{C.0.9})$$

where:

$$\eta_{10} = \eta \times 10^{10} \quad (\text{C.0.10})$$

$$R_1 \equiv 4X_p \frac{\lambda_{pn}}{\lambda_{DD}} \approx (3 - 8) \times 10^{-3} \quad (\text{C.0.11})$$

$$R_2 \equiv 2X_p \frac{\lambda_{pD}}{\lambda_{DD}} \approx (2.3 - 2.5) \times 10^{-5} \quad (\text{C.0.12})$$

$$\alpha \equiv \alpha(T) = 0.86 \times 10^5 K(T) \quad (\text{C.0.13})$$

Here the experimental values of the ratio of the corresponding reactions rates are used. $K(T)$ describes the temperature dependence of $\langle\sigma v\rangle_{DD}$. Its value changes from 1 to 0.5 when the temperature drops from 0.09 Mev to 0.04 Mev. To calculate the deuterium abundance, two cases should be treated: the stage of nucleosynthesis when $X_D \ll X_n$ and the stage when neutron concentration becomes of order of Deuterium concentration [103].

1. When $X_D \ll X_n$ so deuterium will satisfy the quasi-equilibrium condition $\frac{dX_D}{dT} \approx 0$. Since $R_2 \ll R_1$, the term R_2X_D will be small compared to R_1X_n and it follows from Eq. (C.0.8) and Eq. (C.0.9) the following solution:

$$X_D = \sqrt{\frac{R_1X_n}{2}} \left[1 + O\left(\frac{X_D}{X_n}\right) \right] \quad (\text{C.0.14})$$

This solution is valid after deuterium concentration reaches its maximal value of order 10^{-3} but not valid after neutrons concentration drops to deuterium ones.

2. The second case is after neutron concentration becomes of order the deuterium concentration $X_D \sim X_n \sim R_1$:

$$\frac{dX_n}{dT} = \frac{1}{2}\alpha\eta_{10}R_1X_1 \quad (\text{C.0.15})$$

At the beginning of nucleosynthesis at $T = T_{BN}$, most of the neutrons are still free so that the solution of Eq. (C.0.15) is given by :

$$X_n(T) \approx 0.12 \times \exp\left(\frac{1}{2}\alpha\eta_{10}R_1(T - T_{BN})\right) \quad (\text{C.0.16})$$

when neutron concentration drops to that of deuterium, using Eq. (C.0.16) we derived an approximate expression of T^* as given in Eq. (5.34) different from the one given in [103] because we included neutrinos chemical potential. After T^* is reached, the neutron concentration satisfies the quasi-equilibrium condition:

$$\frac{dX_n}{dT} \approx 0 \rightarrow X_n = \frac{1}{R_1} X_D^2 \left[1 + O\left(\frac{X_n}{X_D}\right) \right] \quad (\text{C.0.17})$$

and Eq. (C.0.8) becomes:

$$\frac{dX_D}{dT} = 2\alpha\eta_{10}(X_D^2 + 2R_2X_D) \quad (\text{C.0.18})$$

To find the final abundance of deuterium we must integrate Eq. (C.0.18) between T and T^* , therefore we can assume the general expression of D/H as given in Eq. (5.35) where $F(T^*)$ can be constrained with our numerical calculations.

Appendix D

Entropy conservation

All three neutrino species decouple from the radiation and electron-positron plasma before the electron-positron pairs begin to annihilate at $T \sim m_e \approx 0.5\text{Mev}$. The resulting energy from electron-positron annihilation heats the photon, then the temperature of radiation will be higher than the temperature of neutrinos. Let us now derive the ratio of neutrino-radiation temperature during SBBN. The ratio of the entropy of electron-positron pairs to the entropy of neutrinos remains conserved [103] such as:

$$\frac{s_\gamma + s_{e^\pm}}{s_\nu} = C, \quad (\text{D.0.1})$$

where s_γ , s_{e^\pm} , s_ν represent the entropy of radiation, electron-positron and neutrinos. C is a constant.

Knowing that the entropy $s_\nu \propto T_\nu^3$ and $s_\gamma \propto T_\gamma^3$ (see Eq.(6.22)) we can write:

$$\left(\frac{T_\gamma}{T_\nu}\right)^3 \left(1 + \frac{s_{e^\pm}}{s_\gamma}\right) = C \quad (\text{D.0.2})$$

It is clear that after neutrino decoupling but before e^\pm annihilation, $T_\nu = T_\gamma$ and $\frac{s_{e^\pm}}{s_\gamma} = 7/4$. This condition will give $C = 11/4$ and Eq.(D.0.2) becomes:

$$\frac{T_\gamma}{T_\nu} = \left(\frac{11}{4}\right)^{1/3} \left(1 + \frac{s_{e^\pm}}{s_\gamma}\right)^{-1/3} \quad (\text{D.0.3})$$

When the electron-positron pairs begin to annihilate, their entropy starts to decrease until it becomes zero. Note that the annihilation is not instantaneous. Then from here we obtain the ratio of the temperature of neutrino to the temperature of photon as follows:

$$\left(\frac{T_\gamma}{T_\nu}\right) = \left(\frac{11}{4}\right)^{1/3} = 1.401 \quad (\text{D.0.4})$$

Appendix E

Used nuclear rates

Table E.1: Nuclear rates

| nb | reaction | ref | nb | reaction | ref |
|----|--|-------|----|---|-------|
| 0 | $n \leftrightarrow p$ | [145] | 50 | ${}^7\text{Be} + \alpha \rightarrow \gamma + {}^{11}\text{C}$ | [8] |
| 1 | ${}^3\text{H} \rightarrow e^- + \nu + {}^3\text{He}$ | [151] | 51 | ${}^8\text{B} + \alpha \rightarrow p + {}^{11}\text{C}$ | [154] |
| 2 | ${}^8\text{Li} \rightarrow e^- + \nu + 2 {}^4\text{He}$ | [22] | 52 | ${}^8\text{Li} + \alpha \rightarrow n + {}^{11}\text{B}$ | [97] |
| 3 | ${}^{12}\text{B} \rightarrow e^- + \nu + {}^{12}\text{C}$ | [23] | 53 | ${}^9\text{Be} + \alpha \rightarrow n + {}^{12}\text{C}$ | [47] |
| 4 | ${}^{14}\text{C} \rightarrow e^- + \nu + {}^{14}\text{N}$ | [24] | 54 | ${}^9\text{Be} + D \rightarrow n + {}^{10}\text{B}$ | [87] |
| 5 | ${}^8\text{B} \rightarrow e^+ + \nu + 2 {}^4\text{He}$ | [22] | 55 | ${}^{10}\text{B} + D \rightarrow p + {}^{11}\text{B}$ | [87] |
| 6 | ${}^{11}\text{C} \rightarrow e^+ + \nu + {}^{11}\text{B}$ | [23] | 56 | ${}^{11}\text{B} + D \rightarrow n + {}^{12}\text{C}$ | [87] |
| 7 | ${}^{12}\text{N} \rightarrow e^+ + \nu + {}^{12}\text{C}$ | [23] | 57 | ${}^4\text{He} + \alpha + n \rightarrow \gamma + {}^9\text{Be}$ | [47] |
| 8 | ${}^{13}\text{N} \rightarrow e^+ + \nu + {}^{13}\text{C}$ | [24] | 58 | ${}^4\text{He} + 2\alpha \rightarrow \gamma + {}^{12}\text{C}$ | [47] |
| 9 | ${}^{14}\text{O} \rightarrow e^+ + \nu + {}^{14}\text{N}$ | [24] | 59 | ${}^8\text{Li} + p \rightarrow n + \alpha + {}^4\text{He}$ | [87] |
| 10 | ${}^{15}\text{O} \rightarrow e^+ + \nu + {}^{15}\text{N}$ | [24] | 60 | ${}^8\text{B} + n \rightarrow p + \alpha + {}^4\text{He}$ | [87] |
| 11 | $H + n \rightarrow \gamma + {}^2\text{H}$ | [1] | 61 | ${}^9\text{Be} + p \rightarrow d + \alpha + {}^4\text{He}$ | [47] |
| 12 | ${}^2\text{H} + n \rightarrow \gamma + {}^3\text{H}$ | [154] | 62 | ${}^{11}\text{B} + p \rightarrow 2\alpha + {}^4\text{He}$ | [47] |
| 13 | ${}^3\text{He} + n \rightarrow \gamma + {}^4\text{He}$ | [154] | 63 | ${}^{11}\text{C} + n \rightarrow 2\alpha + {}^4\text{He}$ | [154] |
| 14 | ${}^6\text{Li} + n \rightarrow \gamma + {}^7\text{Li}$ | [98] | 64 | ${}^{12}\text{C} + n \rightarrow \gamma + {}^{13}\text{C}$ | [154] |
| 15 | ${}^3\text{He} + n \rightarrow p + {}^3\text{H}$ | [134] | 65 | ${}^{13}\text{C} + n \rightarrow \gamma + {}^{14}\text{C}$ | [154] |
| 16 | ${}^7\text{Be} + n \rightarrow p + {}^4\text{He}$ | [134] | 66 | ${}^{14}\text{N} + n \rightarrow \gamma + {}^{15}\text{N}$ | [154] |
| 17 | ${}^6\text{Li} + n \rightarrow \alpha + {}^3\text{H}$ | [47] | 67 | ${}^{13}\text{N} + n \rightarrow p + {}^{13}\text{C}$ | [8] |
| 18 | ${}^7\text{Be} + n \rightarrow \alpha + {}^4\text{He}$ | [28] | 68 | ${}^{14}\text{N} + n \rightarrow p + {}^{14}\text{C}$ | [8] |
| 19 | ${}^2\text{H} + p \rightarrow \gamma + {}^3\text{He}$ | [7] | 69 | ${}^{15}\text{O} + n \rightarrow p + {}^{15}\text{N}$ | [8] |
| 20 | ${}^3\text{H} + p \rightarrow \gamma + {}^4\text{He}$ | [47] | 70 | ${}^{15}\text{O} + n \rightarrow \alpha + {}^{12}\text{C}$ | [47] |
| 21 | ${}^6\text{Li} + p \rightarrow \gamma + {}^7\text{Be}$ | [8] | 71 | ${}^{12}\text{C} + p \rightarrow \gamma + {}^{13}\text{N}$ | [8] |
| 22 | ${}^6\text{Li} + p \rightarrow \alpha + {}^3\text{He}$ | [134] | 72 | ${}^{13}\text{C} + p \rightarrow \gamma + {}^{14}\text{N}$ | [8] |
| 23 | ${}^7\text{Li} + p \rightarrow \alpha + {}^4\text{He}$ | [134] | 73 | ${}^{14}\text{C} + p \rightarrow \gamma + {}^{15}\text{N}$ | [47] |
| 24 | ${}^2\text{H} + \alpha \rightarrow \gamma + {}^6\text{Li}$ | [8] | 74 | ${}^{13}\text{N} + p \rightarrow \gamma + {}^{14}\text{O}$ | [47] |
| 25 | ${}^3\text{H} + \alpha \rightarrow \gamma + {}^7\text{Li}$ | [134] | 75 | ${}^{14}\text{N} + p \rightarrow \gamma + {}^{15}\text{O}$ | [47] |

| | | | | | |
|----|--|-------|----|---|-------|
| 26 | ${}^3\text{He} + \alpha \rightarrow \gamma + {}^7\text{Be}$ | [145] | 76 | ${}^{15}\text{N} + p \rightarrow \gamma + {}^{16}\text{O}$ | [47] |
| 27 | ${}^2\text{H} + D \rightarrow n + {}^3\text{He}$ | [120] | 77 | ${}^{15}\text{N} + p \rightarrow \alpha + {}^{12}\text{C}$ | [8] |
| 28 | ${}^2\text{H} + D \rightarrow p + {}^3\text{H}$ | [120] | 78 | ${}^{12}\text{C} + \alpha \rightarrow \gamma + {}^{16}\text{O}$ | [47] |
| 29 | ${}^3\text{H} + D \rightarrow n + {}^4\text{He}$ | [134] | 79 | ${}^{10}\text{B} + \alpha \rightarrow p + {}^{13}\text{C}$ | [154] |
| 30 | ${}^3\text{He} + D \rightarrow p + {}^4\text{He}$ | [134] | 80 | ${}^{11}\text{B} + \alpha \rightarrow p + {}^{14}\text{C}$ | [47] |
| 31 | ${}^3\text{He} + {}^3\text{He} \rightarrow 2p + {}^4\text{He}$ | [8] | 81 | ${}^{11}\text{C} + \alpha \rightarrow p + {}^{14}\text{N}$ | [47] |
| 32 | ${}^7\text{Li} + D \rightarrow n + \alpha + {}^4\text{He}$ | [134] | 82 | ${}^{12}\text{N} + \alpha \rightarrow p + {}^{15}\text{O}$ | [47] |
| 33 | ${}^7\text{Be} + D \rightarrow p + \alpha + {}^4\text{He}$ | [127] | 83 | ${}^{13}\text{N} + \alpha \rightarrow p + {}^{16}\text{O}$ | [47] |
| 34 | ${}^7\text{Li} + n \rightarrow \gamma + {}^8\text{Li}$ | [154] | 84 | ${}^{10}\text{B} + \alpha \rightarrow n + {}^{13}\text{N}$ | [47] |
| 35 | ${}^{10}\text{B} + n \rightarrow \gamma + {}^{11}\text{B}$ | [154] | 85 | ${}^{11}\text{B} + \alpha \rightarrow n + {}^{14}\text{N}$ | [47] |
| 36 | ${}^{11}\text{B} + n \rightarrow \gamma + {}^{12}\text{B}$ | [97] | 86 | ${}^{12}\text{B} + \alpha \rightarrow n + {}^{15}\text{N}$ | [154] |
| 37 | ${}^{11}\text{C} + n \rightarrow p + {}^{11}\text{B}$ | [47] | 87 | ${}^{13}\text{C} + \alpha \rightarrow n + {}^{16}\text{O}$ | [8] |
| 38 | ${}^{10}\text{B} + n \rightarrow \alpha + {}^7\text{Li}$ | [8] | 88 | ${}^3\text{He} + {}^3\text{H} \rightarrow \gamma + {}^6\text{Li}$ | [58] |
| 39 | ${}^7\text{Be} + p \rightarrow \gamma + {}^8\text{B}$ | [8] | 89 | ${}^6\text{Li} + D \rightarrow n + {}^7\text{Be}$ | [97] |
| 40 | ${}^9\text{Be} + p \rightarrow \gamma + {}^{10}\text{B}$ | [47] | 90 | ${}^6\text{Li} + D \rightarrow p + {}^7\text{Li}$ | [97] |
| 41 | ${}^{10}\text{B} + p \rightarrow \gamma + {}^{11}\text{C}$ | [8] | 91 | ${}^3\text{He} + {}^3\text{H} \rightarrow D + {}^4\text{He}$ | [47] |
| 42 | ${}^{11}\text{B} + p \rightarrow \gamma + {}^{12}\text{C}$ | [8] | 92 | ${}^3\text{H} + {}^3\text{H} \rightarrow 2n + {}^4\text{He}$ | [47] |
| 43 | ${}^{11}\text{C} + p \rightarrow \gamma + {}^{12}\text{N}$ | [47] | 93 | ${}^3\text{He} + {}^3\text{H} \rightarrow n + p + {}^4\text{He}$ | [47] |
| 44 | ${}^{12}\text{B} + p \rightarrow n + {}^{12}\text{C}$ | [154] | 94 | ${}^7\text{Li} + {}^3\text{H} \rightarrow n + {}^9\text{Be}$ | [150] |
| 45 | ${}^9\text{Be} + p \rightarrow \alpha + {}^6\text{Li}$ | [8] | 95 | ${}^7\text{Be} + {}^3\text{H} \rightarrow p + {}^9\text{Be}$ | [134] |
| 46 | ${}^{10}\text{B} + p \rightarrow \alpha + {}^7\text{Be}$ | [8] | 96 | ${}^7\text{Li} + {}^3\text{He} \rightarrow p + {}^9\text{Be}$ | [134] |
| 47 | ${}^{12}\text{B} + p \rightarrow \alpha + {}^9\text{Be}$ | [154] | 97 | ${}^{11}\text{B} + D \rightarrow p + {}^{12}\text{B}$ | [70] |
| 48 | ${}^6\text{Li} + \alpha \rightarrow \gamma + {}^{10}\text{B}$ | [47] | 98 | ${}^{12}\text{C} + d \rightarrow p + {}^{13}\text{C}$ | [70] |
| 49 | ${}^7\text{Li} + \alpha \rightarrow \gamma + {}^{11}\text{B}$ | [8] | 99 | ${}^{13}\text{C} + d \rightarrow p + {}^{14}\text{C}$ | [70] |

Appendix F

Abbreviations

| | |
|--------|--------------------------------------|
| BBN | Big Bang Nucleosynthesis |
| CMB | Cosmic Microwave Background |
| SBBN | Standard Big Bang Neucleosynthesis |
| WMAP | Wilkinson Microwave Anisotropy Probe |
| WIMP's | Weakly interacting massive particles |

Bibliography

- [1] Ando S. et al., *Phys. Rev. C* 74, 025809 (2006).
- [2] Abazajian K. et al., *Phys. Rev. D* 64, 023501 (2001).
- [3] Abe S. et al. (KamLAND Collaboration), *Phys.Rev.Lett.* 100, 221803 (2008).
- [4] Abe Y. et al. (Double Chooz Collaboration), *Phys.Rev. D* 86, 052008 (2012).
- [5] Abel C. et al., *Phys. Rev. X* 7, 041034 (2017).
- [6] Adhikari R. et al., *JCAP* 01, 025 (2017).
- [7] Adelberger E. G. et al., *Rev. Mod. Phys.* 83, 195 (2011).
- [8] Angulo C., *AIP Conference Proceedings* 495, 1 (1999).
- [9] Angulo C. et al., *Astrophys.J.* 630, 2 (2005).
- [10] Aharmim B. et al. (SNO Collaboration), *Phys.Rev. C* 88, 025501 (2013).
- [11] Applegate J. H. et al., *Phys. Rev. D* 35, 1151 (1987).
- [12] Aver E. et al., *JCAP* 1005, 003 (2010).
- [13] Aver E. et al., arXiv: 1503:08146 (2015).
- [14] Arbey A. et al., arXiv:1806.11095 (2018).
- [15] Arbey A., *AIP Conf.Proc.* 1241, 700-707 (2009).
- [16] Arbey A., arXiv:astro-ph/0506732.
- [17] Arbey A. and Mahmoudi F., *Phys. Lett. B* 669, 46-51 (2008).
- [18] Arbey A., *Computer Physics Communications* 183, 1822-1831 (2012).
- [19] Arbey A. and Mahmoudi M., *JHEP* 2010, 51 (2010).
- [20] Asplund M. et al., *ApJ.* 644, 229(2006).

- [21] Abazajian K., Fuller G. M., and Patel M., *Phys.Rev. D* 64, 023501 (2001).
- [22] Ajzenberg-Selove F., *Nucl. Phys. A* 490, 1-225 (1988).
- [23] Ajzenberg-Selove F., *Nucl. Phys. A* 506, 1-158 (1990).
- [24] Ajzenberg-Selove F., *Nucl. Phys. A* 449, 1-155 (1986).
- [25] Bania T. M. et al., *Nature* 415, 54 (2002).
- [26] Balashev S. A. et al., *MNRAS* 458, 2 (2016).
- [27] Balestra F. et al., *Nuovo Cim.* 100A, 323 (1988).
- [28] Barbagallo M. et al., *Phys. Rev. Lett.* 117, 152701 (2016).
- [29] Barbagallo M. et al., *EPJ Web of Conferences* 146, 01012 (2017).
- [30] Bertulani C. A. et al., arXiv:1802.03469v1, (2018).
- [31] Boyarsky A. et al., *PRL* 97, 261302 (2006).
- [32] Bonifacio P. and Molar P., *MNRAS* 285, 847 (1997).
- [33] Bonifacio P., Molaro P., and Pasquini L., *MNRAS* 292, L1 (1997).
- [34] Bonifacio P. et al., *Astronom. Astroph.* 390, 91 (2002).
- [35] Burles S. & Tytler D., *ApJ* 499, 699 (1998a).
- [36] Burles S. & Tytler D., *ApJ* 507, 732 (1998b).
- [37] Cai R. et al., *JHEP* 08, 090 (2008).
- [38] Casagrande L. et al., *Astron. Astrophys.* 512, A54 (2010); arXiv:1001.3142.
- [39] Charbonnel C. and Primas, F., *ApJ* 442, 961 (2005).
- [40] Caughlan G. R. and Fowler W.A., *Atomic data and nuclear data tables* 40, 291 (1988).
- [41] Cook R. and Fumagalli M., *Nature Astronomy* 2, 957961 (2018).
- [42] Cooke R. J. et al., *ApJ* 781, 31 (2014); Cooke R. J. et al., *ApJ* 830, 148 (2016).
- [43] Cyburt R. H., Fields B. D., and Olive K. A., *JCAP* 0811, 012 (2008).
- [44] Cyburt R. H. et al., *JCAP* 0910, 021 (2009).

- [45] Cyburt R. H., Fields B. D., and Olive K. A., *Rev. Mod. Phys.* 88, 015004 (2016).
- [46] Cyburt R. H., Ellis J., Fields B. D., Olive K. A., *Phys. Rev. D* 67, 103521 (2003); arXiv:astro-ph/0211258.
- [47] Caughlan G. R. and Fowler W.A., *Atomic data and nuclear data tables* 40, 291 (1988).
- [48] De Gouvea A. et al., arXiv:1310.4340 (2013).
- [49] Dolgov A. D. and Hansen S. H., *Astropart. Phys.* 16, 339 (2002).
- [50] Dolgov A.D. and Takahshi F., *Nucl.Phys. B* 688, 189-213 (2004).
- [51] Erken O. et al., *Phys. Rev. Lett.* 108, 061304 (2012).
- [52] Esposito S. et al., *JHEP* 09, 038 (2000).
- [53] Fernndez V. et al., arXiv:1804.10701 (2016).
- [54] Fields B. and Olive K., *Nuclear Physics A* 777, 208225 (2006).
- [55] Fields B. D., *Annual Review of Nuclear and Particle Physics* 61, 47-68 (2011).
- [56] Fukugita M. and Kawasaki M., *ApJ* 646, 691-695 (2006).
- [57] Fumagalli M. et al., *Science* 334, 1245 (2011).
- [58] Fukugita M. and Kajino T., *Phys. Rev. D* 42, 4251 (1990).
- [59] Galvez R. and Scherrer R., *Phys. Rev. D* 95, 063507 (2017).
- [60] Goudelis A. et al., *Phys. Rev. Lett.* 116, 211303 (2016).
- [61] Hinshaw G. et al., arXiv:1212.5226 (2013).
- [62] Hosford A. et al., *Astron. Astrophys.* 511, A47 (2010); arXiv:1004.0863 (2010).
- [63] Hou S. Q. et al., *ApJ* 834, 165 (2017).
- [64] Hou S. Q. et al., *Phys. Rev. C* 91, 055802 (2015).
- [65] Hansen S. et al. , *Phys. Rev. D* 65, 023511 (2001).
- [66] Itoh N. et al., *ApJ* 488, 507-514 (1997).
- [67] Izotov Y. I. et al., *Astrophys.J.Suppl.* 108, 1 (1997).

- [68] Izotov Y. I. and Thuan T. X., *ApJ* 602, 200-230 (2004).
- [69] Izotov Y. I. and Thuan T. X., *Astrophys. J. Lett.* 710, L67-L71 (2010).
- [70] Iocco F. et al., *Phys. Rev. D* 75, 7304 (2007).
- [71] Iocco F., *Mem.S.A.It.Suppl.* 22, 19 (2012).
- [72] Iocco F. et al., *Phys.Rept.* 472, 1-76, (2009).
- [73] Jedamzik K., *Phys. Rev. D* 70, 083510 (2004); arXiv:astro-ph/0405583.
- [74] Jedamzik K., *Phys. Rev. D* 70, 063524 (2004); arXiv:astro-ph/0402344.
- [75] Jedamzik K., *Phys. Rev.D* 74, 103509 (2006).
- [76] Jedamzik K. et al., *ApJ* 423, 50 (1994).
- [77] Kang H. and Steigman G., *Nucl. Phys. B* 372, 494 (1992).
- [78] Kirkman D. et al., *ApJ* 149, 1 (2003).
- [79] Kawasaki M., Kohri K., and Moroi T., *Phys. Rev. D* 71, 083502 (2005); arXiv:astro-ph/0408426.
- [80] Kneller, J. P. and Steigman G., *New J. Phys.* 6, 117 (2004).
- [81] Komatsu E. et al., *Astrophys.J.Suppl.* 192, 18 (2011).
- [82] Komatsu N. and Kimura S., *Phys. Rev. D* 87, 043531 (2013).
- [83] Korn A.J. et al., *Nature* 442, 657 (2006).
- [84] Kusakabe, Motohiko et al. *Phys.Rev. D* 99, 043505 (2019).
- [85] Kusakabe M. et al., *Int. J. Mod. Phys. E* 26, 1741004 (2017).
- [86] Kusakabe M. et al., *Phys. Rev. D* 90, 045009 (2014).
- [87] Kawano L., *FERMILAB-PUB-92-004-A* (1992).
- [88] Larson D. et al., *Astrophys.J.Suppl.* 192, 16 (2011).
- [89] Leistedt B. et al., *Phys. Rev. Lett.* 113 (2014) 041301.
- [90] Lesgourgues J. and Pastor S. , *Advance in High Energy Physics* 2012, 608515 (2012).
- [91] Levshakov S. A. et al., *ApJ* 565, 696 (2002).
- [92] Lind K. et al., *A&A* 554, A96 (2013)

- [93] Lunardini C. and Smirnov A. Yu., *Phys.Rev.D* 64, 073006 (2001).
- [94] Luridiana V. et al., *ApJ* 592, 2 (2003).
- [95] Mathews G. et al., *Phys.Rev. D* 71, 021302 (2005).
- [96] Makki T. R., El Eid M. F. and Mathews G. J., *MPLA* 33, 1950194 (2019).
- [97] Malaney R. A. and Fowler W. A., *ApJ* 345, L5-L8 (1989).
- [98] Malaney R. and Mathews G., *Phys. Rept.* 229, 145 (1993).
- [99] Mathews G. J. et al., *ApJ* 358, 36 (1990).
- [100] Melendez J. et al. *ApJ.* 615, L33 (2004).
- [101] Merle A., arXiv:1702.08430.
- [102] Morresi T. et al., *Advanced Theory and Simulations* 1, 1800086 (2018).
- [103] Mukhanov V., *Physical Foundations of Cosmology* (Cambridge University Press, New York, 2005) 421.
- [104] Nollett K. M. and Steigman G., *Phys. Rev. D* 91, 083505 (2015).
- [105] Nakamura R. et al., *Int.J.Mod.Phys. E* 26, 8, 1741003 (2017).
- [106] Noterdaeme P. et al., *A&A* 542, L33 (2012).
- [107] Olive K. A. et al., *Phys. Lett. B* 265, 239-244, (1991).
- [108] Olive K. et al., *MNRAS* 426, 2 (2012).
- [109] Olive K. et al., *ApJ* 483, 2 (1997).
- [110] Orito M. et al., arXiv:astro-ph/0005446 (2001).
- [111] Pagel B. E. J. et al., *MNRAS* 225, 2 (1992).
- [112] Patrignani C. et al. (Particle Data Group), *Chin. Phys. C* 40, 100001 (2016) and 2017 update.
- [113] Peimbert M. et al., *ApJ.* 666, 636-646 (2007).
- [114] Peimbert, A. et al., arXiv:1608.02062 (2016).
- [115] Pisanti O. et al., *Comput. Phys. Commun.* 178, 956-971 (2008).
- [116] Pitrou C. et al., *Phys. Rept.* 04, 005 (2018).
- [117] P. A. R. Ade et al., *A&A* 594, A13 (2016).

- [118] Planck Collaboration, arXiv:1807.06209 (2018).
- [119] Pettini M. and Bowen D. V., *ApJ* 560, 41 (2001).
- [120] Pizzone R. G. et al., *ApJ* 786, 2 (2014).
- [121] Paraskevi C. and John D. Vergados, *Advances in High Energy Physics* 2018, 1479313 (2018).
- [122] Perlmutter S. et al., *Bull.Am.Astron.Soc.* 29, 1351 (1997).
- [123] Pinsonneault M. H. et al., *ApJ* 574,1 (2002).
- [124] Pisanti O. et al., *Comput. Phys. Commun.* 178, 956 (2008); arXiv:0705.0290.
- [125] Ribas I. et al., *MNRAS* 313, 1 (2000).
- [126] Ryan S.G. et al., *ApJ* 523, 654 (1999).
- [127] Rigal N. et al., *Phys. Rev. Lett.* 122, 182701 (2019).
- [128] Riemer-Sørensen S. et al., *MNRAS* 447, 2925 (2015).
- [129] Sato J. et al., *Int.J.Mod.Phys. E* 26, 8, 1741005 (2017).
- [130] Salvati L. et al., *JCAP* 8, 022 (2016).
- [131] Sbordone L. et al., *A&A* 522, A26 (2010).
- [132] Schwarz D. J. and Stuke M., *New J. Phys.* 15, 033021 (2013).
- [133] Schindt B. et al., *ApJ* 507, 46-63 (1998).
- [134] Serpico D. et al., *JCAP* 0412, 010 (2004).
- [135] Scherrer R. J. and Turner M. S., *ApJ*. 331, 33-37 (1988).
- [136] Scherrer R. J. and Turner M. S., *ApJ*. 331, 19-32 (1988).
- [137] Sefiedgar A.S., *Advances in High Energy Physics* 2014, 727245 (2014).
- [138] Smoot G. F. et al., *ApJ* 396, L1 (1992).
- [139] Shi X., *Phys. Rev. D* 54, 2753 (1996).
- [140] Spite M. and Spite F., *Nature* 297, 483 (1982).
- [141] Srianand R. et al., *MNRAS* 405, 1888 (2010).
- [142] Steigman G., *Advances in High Energy Physics* 2012, 268321 (2012).

- [143] Steigman G., *Ann. Rev. Astron. Astrophys.* 14, 339 (1976).
- [144] Simonucci S. et al., *ApJ* 764, 118 (2013).
- [145] Smith M. S., Kawano L. H. and Malaney R. A., *Astrophys. J. Suppl.* 85, 219 (1993).
- [146] Salpeter E. E., *Aust. J. Phys.* 7, 373 (1954); Salpeter E. E. and Van Horn H. M., *Astrophys. J.* 155, 183 (1969).
- [147] Scott Matthew Gustafson, UNIVERSITY OF CALIFORNIA, SAN DIEGO, thesis dissertation, "Measurements of Primordial Deuterium and Lyman-Alpha Forest Evolution with High-Resolution Quasar Spectroscopy" (2016).
- [148] Takaaki Kajita, *Experimental Studies of Neutrino Oscillations*, World Scientific (2016).
- [149] Tanabashi M. et al. (Particle Data Group), *Phys. Rev. D* 98, 030001 (2018).
- [150] Thomas D. et al., *ApJ* 406, 569 (1993).
- [151] Tilly D. R., Weller H. R., and Hasan H. H., *Nucl. Phys.* A474, 1 (1987).
- [152] Villonava S. et al., *A&A* 499, 3 (2009).
- [153] Wagoner V. et al. , *Astrophysical J.* 148, 3W (1967).
- [154] Wagoner V., *Astrophys. J. Suppl.* 18, 247 (1969).

Publications during the Ph.D

A critical analysis of the Big Bang Nucleosynthesis

Tahani R. Makki* and Mounib F. El Eid†

Department of Physics, American University of Beirut, Lebanon

**trm03@mail.aub.edu*

†*meid@aub.edu.lb*

Grant J. Mathews‡

Department of Physics, Center for Astrophysics, University of Notre Dame, USA

gmathews@nd.edu

Received 19 October 2018

Revised 12 February 2019

Accepted 9 April 2019

Published 14 June 2019

Standard Big Bang Nucleosynthesis (SBBN) represents one of the basic tools to understand the early evolution of the universe. In this paper, we reanalyze this process to focus on the so-called lithium problem. ${}^7\text{Li}$ is overproduced during SBBN compared to its primordial abundance as obtained from observations. For this reason, we extend the scenarios of SBBN in two directions: (i) equating all neutrino chemical potentials and including more neutrino families, (ii) varying neutrino chemical potentials independently. Since the so-called cosmological lithium problem is not resolved on nuclear/astrophysical ground, we argue that this problem should be examined by invoking nonstandard assumptions.

Keywords: Nucleosynthesis in the early universe; the lithium problem; neutrinos; non-standard physics.

1. Introduction

Being based on a well-determined Standard Model of particle physics and cosmology, Standard Big Bang Nucleosynthesis (SBBN) allows for an understanding of the formation of light elements in the early universe.^{22,34,75} Only the light elements, ${}^3\text{He}$, ${}^4\text{He}$, D and ${}^7\text{Li}$, are synthesized due to the rapid expansion of the universe. The calculation of their abundances is performed assuming a homogeneous universe and vanishing neutrino chemical potentials and masses. Meanwhile, the effects of dark matter, massive decaying particles or extra neutrino families are not taken into account in the SBBN. However, it has been established that neutrinos

†,‡Corresponding authors.

have nonvanishing chemical potentials and they have mass as verified by neutrino oscillations.^{43,58} In addition, the existence of dark matter is well established and its cosmic abundance has been accurately determined.^{57,72} The SBBN is introduced in Sec. 2. The resulting abundances by SBBN are in good agreement with observations except for ⁷Li. This so-called ‘‘Lithium Problem’’ will be discussed in Sec. 3. In Sec. 4, attempts are made to include nonstandard Big Bang Nucleosynthesis (BBN) scenarios in order to find out if the lithium problem can be resolved. The constraints on the abundances from observations are discussed in Sec. 5. Our numerical results for neutrino degenerate BBN and its effect on the lithium problem are given in Sec. 6. Some analytical considerations are described in Sec. 7. Finally, a summary and conclusions are given in Sec. 8.

2. SBBN

The SBBN model is based on three striking facts: (i) the Hubble expansion of the universe described by the Friedmann equations, (ii) the Cosmic Microwave background (CMB), and (iii) the formation of the light elements, in particular, the production of the element helium needs high temperature, so that the Big Bang was hot indeed.

2.1. *Friedmann equations and thermodynamics of the early universe*

According to the general theory of relativity, Friedmann equations are used to describe the cosmic expansion during various evolutionary phases. These equations allow us to determine two unknown functions: $a(t)$ the scale factor characterizing the expansion of the universe and $\rho(t)$ the energy density of the universe. Assuming an adiabatic expansion of the universe, the first law of thermodynamics can be written as

$$d\varepsilon = -p dV, \quad (1)$$

where ε is the total energy and p is the pressure within an expanding volume V . Given that the volume scales as $V \sim a^3$, the continuity equation is

$$\dot{\rho} = -3H(\rho + p), \quad (2)$$

where H is the Hubble parameter defined by $H = \frac{\dot{a}}{a}$.

On the other hand, according to General Relativity, the equation of motion or the first Friedmann equation can be written as

$$\ddot{a} = -\frac{4\pi}{3}G(\rho + 3p)a. \quad (3)$$

Multiplying Eq. (3) by \dot{a} and using Eq. (2) we will obtain the second Friedman, as

$$H^2 + \frac{k}{a^2} = \frac{8\pi G}{3}\rho, \quad (4)$$

where G is Newton's gravitational constant and k corresponds to the spacial curvature of the universe ($k = 0$ in case of a flat universe, $k = 1$ for positive curvature and $k = -1$ for negative curvature). Equations (2)–(4) are not independent, we can take any two equations and derive the third one. It can be shown that these equations lead to

$$a \sim \sqrt{t} \quad (5)$$

and the conservation of stress–energy leads to

$$\rho \sim a^{-4}. \quad (6)$$

Note that the Friedmann equations can be modified when nonstandard physics scenarios are adopted for example by an entropy component or non-adiabatic accelerated universe.^{23,53,88}

It is emphasized that the early universe was radiation-dominated, in other words, relativistic particles dominate the energy content of the universe. Using a perfect black body distribution and integrating over all frequencies, the number density of photons is

$$N_\gamma = \int_0^\infty n_\gamma(\nu) d\nu \approx \left(\frac{1.202}{\pi^2} \right) g_\gamma \left(\frac{k_B T}{c\hbar} \right)^3, \quad (7)$$

where $g_\gamma = 2$ refers to photon degrees of freedom, k_B is the Boltzmann constant and \hbar is the reduced Planck constant. At a CMB temperature today of $T \approx 2.725$ K the number density is calculated to be $n_\gamma \approx 400 \text{ cm}^{-3}$.

Multiplying the integrand Eq. (7) by $h\nu$ and integrating over all frequencies, the expression for radiation density is

$$\rho_\gamma = \left(\frac{\pi^2}{30} \right) g_\gamma \left(\frac{k_B^4 T^4}{\hbar^3 c^3} \right). \quad (8)$$

Similarly the number and energy density of fermions are given when the Fermi–Dirac distribution is used:

$$n_f \approx 1.202 \left(\frac{3}{4\pi^2} \right) g_f \left(\frac{k_B T}{c\hbar} \right)^3, \quad (9)$$

$$\rho_f = \frac{7}{8} \left(\frac{\pi^2}{30} \right) g_f \left(\frac{k_B^4 T^4}{\hbar^3 c^3} \right), \quad (10)$$

where $g_f = 6$ for neutrinos (3 for neutrinos and 3 for antineutrinos) and $g_f = 4$ for electron–positron pairs before they annihilate. By assuming a small chemical potential $|\mu| \ll k_B T$ and mass $m \ll k_B T/c^2$, Eqs. (7)–(10) are derived in physical units. Then the total radiation energy density present during SBBN is

$$\rho_r = \rho_\gamma + \rho_f = \frac{\pi^2}{30} \left(g_\gamma + \frac{7g_f}{8} \right) \left(\frac{k_B^4 T^4}{\hbar^3 c^3} \right). \quad (11)$$

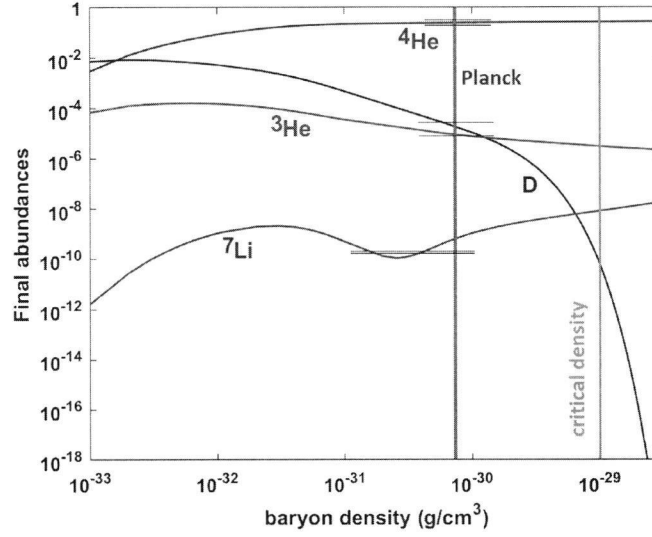


Fig. 1. Light element abundances as a function of baryon density. Vertical band is Planck determination of baryon density. Horizontal lines represent observations.

Comparing Eq. (11) to Eqs. (5) and (6) we can derive the time temperature relation:

$$t_{\text{sec}} \simeq \frac{1.39k_{\text{eff}}^{-1/2}}{T^2}, \quad (12)$$

with $k_{\text{eff}} = \frac{\pi^2}{30}(g_\gamma + \frac{7g_l}{8})$, where the cosmological time in seconds and the temperature in MeV.

2.2. Role of the CMB in probing the early universe

The ‘‘Cosmic Microwave Background’’ (CMB) resembling a perfect black body of about 2.75 Kelvin was scattered when the hot universe was 380,000 years into Big Bang. Three important missions namely COBE,⁸⁹ WMAP^{40,57} and Planck⁷² have been launched to explore the properties of these CMB in order to extract a wealth of information about the conditions of the early universe, in particular, the Hubble parameter H , the baryon density content $\Omega_b h^2$, the cold dark matter density $\Omega_c h^2$, the dark energy density Ω_Λ , the effective number of relativistic species N_{eff} , the primordial helium mass fraction $Y_{4\text{He}}$, etc. Hence, the CMB is an important probe of the early universe because it represents the oldest electromagnetic radiation from the recombination epoch.

2.3. How to produce light elements?

The SBBN predicts that the universe is composed of about 75% Hydrogen, 25% ^4He and small amounts of D , ^3He , ^7Li and ^6Li . Knowing the baryon to photon ratio of the universe $\eta = \frac{n_b - n_{\bar{b}}}{n_\gamma} = (6.11 \pm 0.06) \times 10^{-10}$ as determined by Planck mission⁷² leads to the determination of light element abundances because it is a key parameter of SBBN. Figure 1 shows light element abundances as a function

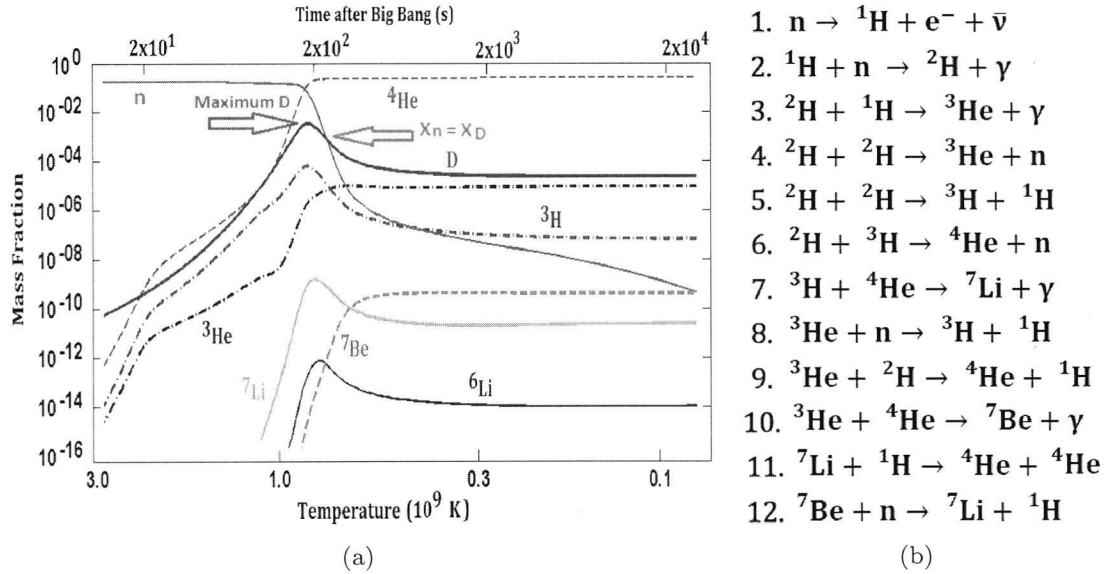


Fig. 2. Light element abundances as a function of temperature/time and the main reactions leading to these abundances.

Table 1. Comparison between different SBBN predictions.

| | This work | Pitrou <i>et al.</i> ⁷¹ | Cyburt <i>et al.</i> ²⁸ | Observations |
|----------------------------------|-----------------------|------------------------------------|------------------------------------|--------------------------|
| Y_p | 0.24610 ± 0.00015 | 0.24709 ± 0.00017 | 0.24709 ± 0.00025 | 0.2449 ± 0.0040^7 |
| $D/H \times 10^5$ | 2.6386 ± 0.1222 | 2.459 ± 0.036 | 2.58 ± 0.13 | 2.58 ± 0.07^{25} |
| ${}^3\text{He}/H \times 10^5$ | 1.0151 ± 0.0529 | 1.074 ± 0.026 | 1.0039 ± 0.0090 | 1.1 ± 0.2^{11} |
| ${}^7\text{Li}/H \times 10^{10}$ | 4.3861 ± 0.3875 | 5.623 ± 0.247 | 4.68 ± 0.67 | $1.58_{-0.28}^{+0.3584}$ |

of η : ${}^3\text{He}$ and D are sensitive to η in contrast to ${}^4\text{He}$ which depend linearly on η . Concerning ${}^7\text{Li}$, its production at low η is mainly determined by $T + {}^4\text{He} \rightarrow {}^7\text{Li}$ while at high η its production is favored through ${}^3\text{He} + {}^4\text{He} \rightarrow {}^7\text{Be}(e^+\nu)$.

To obtain light elements at a given η , it is important to use an updated network of nuclear reactions. We have done this calculation with results shown in Fig. 2 and Table 1. We have used the updated reaction rates that lead to the lowest standard lithium abundance as compared with other works. This illustrates how the lithium abundance can be reduced due to nuclear reactions. However, the result is still significantly higher than observations.

3. The Lithium Problem

Over the past decades, the observed abundance of ${}^7\text{Li}$ in metal-poor Halo stars was found to be less by a factor of 2–3 than the value predicted on the basis of SBBN.²⁶ However, this discrepancy has increased to 2.4–4.3 or 4.2σ (from globular cluster stars) and 5.3σ (from Halo field stars).²⁶ For a long time, the observed abundance of ${}^7\text{Li}$ in metal-poor halo stars was thought to be independent of metallicity down

to a metallicity of $[\text{Fe}/H] = -3.0$.⁹¹ This was considered to represent the primordial abundance of this element. However, extended observations below $[\text{Fe}/H] = -3.0$ show a dependence of metallicity.⁴⁷ This other ‘‘Lithium problem’’ also needs to be resolved. In other words two problems are encountered:

- Matching the predicted ${}^7\text{Li}$ abundance on the basis of the SBBN with observations (see Table 1).
- Understanding the deviation of the ${}^7\text{Li}$ abundance at very low metallicity (see Fig. 1 from Ref. 47).

Is it possible to explain the lithium problem by a specific astrophysical or nuclear physics process? Or do we need nonstandard physics? Resolving these ‘‘Lithium problems’’ seems to be complex task because no single answer is apparent.

In the following we summarize some proposed solutions to the lithium problem.³⁵

3.1. Astrophysical aspects

It is possible that the evaluations of the lithium abundance are not accurate enough, so that they do not confirm the prediction by the SBBN. Absorption lines in the atmosphere of metal-poor stars are used to determine the lithium abundance. These lines are very sensitive to the model atmosphere and the physical conditions under which they are formed. It should be emphasized that a mechanism which leads to a depletion of ${}^7\text{Li}$ in very metal-poor halo stars should not affect the plateau at relatively high metallicity. In other words, if the lithium was processed by stars, then one must find a stellar mechanism that can explain simultaneously the regular behavior at high metallicity and low dispersion at low metallicity. In addition, stellar properties, e.g. rotation, magnetic fields, etc.⁸⁰ may play a role.

It was thought at one time that ${}^6\text{Li}$ was constraining any stellar processing of ${}^7\text{Li}$ because the high temperature needed to reduce ${}^7\text{Li}$ would eventually destroy the observed plateau¹⁰ of ${}^6\text{Li}$ that is three orders of magnitude higher than SBBN predictions. However, this is no longer a problem because there is no ${}^6\text{Li}$ plateau⁶⁰ due to line asymmetries which were neglected in previous determinations.

3.2. Nuclear physics aspects

Concerning the reaction rates of SBBN, most of them are updated and uncertainties are revised,³⁶ however, there are two important reactions that may be subject to revision. These are ${}^3\text{He}(\alpha, \gamma){}^7\text{Be}$ and ${}^7\text{Be}(n, p){}^7\text{Li}$. To match the observed abundance of ${}^7\text{Li}$, the first reaction should be lower by a factor of 3–4.³⁵ Taking this at face value would mean that ${}^7\text{Be}$ and ${}^8\text{B}$ solar neutrinos flux would be reduced by the same factor which argues against this assumption. It is interesting that solar neutrinos constraint this rate. The destruction reaction rate ${}^7\text{Be}(n, p){}^7\text{Li}$ should be greater by factor of 2 to reduce the ${}^7\text{Li}$ production but this has not been constrained by measurements.¹⁵

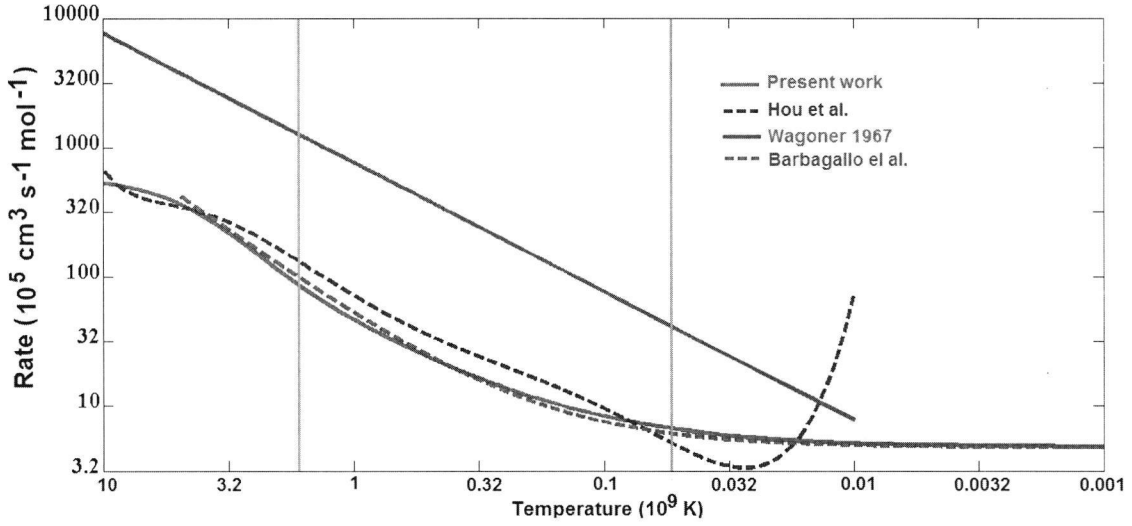


Fig. 3. (Color online) Comparison between different calculated rates of ${}^7\text{Be}(n, \alpha){}^4\text{He}$. The vertical yellow bands indicate the BBN temperature range. Note the significant difference between the new rates and that used by Wagoner especially in the BBN range.

3.2.1. The ${}^7\text{Be}(n, \alpha){}^4\text{He}$ rate

The ${}^7\text{Be}(n, \alpha){}^4\text{He}$ reaction is a possible means for the destruction of ${}^7\text{Be}$ which is the precursor of primordial lithium. Using the new cross-section¹⁴ for ${}^7\text{Be}(n, \alpha){}^4\text{He}$ measured over a wide range of neutron energies, we have done a new fit in an extended range up to 10 GK. In units of $\text{cm}^{-3} \text{s}^{-1} \text{mole}^{-1}$ the Maxwellian average cross-section in the following temperature ranges is

For $0.001 \leq T_9 \leq 2$:

$$N_A \langle \sigma v \rangle = 4.844 \times 10^5 + 2.748 \times 10^5 T_9^3 + 3.885 \times 10^5 T_9^2 + 3.544 \times 10^6 \times T_9. \quad (13)$$

For $2 \leq T_9 \leq 10$:

$$N_A \langle \sigma v \rangle = 4.353 \times 10^6 - 2.845 \times 10^3 T_9^5 + 9.656 \times 10^4 T_9^4 - 1.219 \times 10^6 T_9^3 + 6.393 \times 10^6 T_9^2 - 5.2 \times 10^6 T_9, \quad (14)$$

where T_9 is the temperature in units of 10^9 K. The comparison among the evaluation of this rate is shown in Fig. 3. It is seen that this rate as above and also the one given by Ref. 42 are significantly different from the one that has been employed for a long time¹⁰¹ especially in the range of BBN temperatures (shown in vertical lines in Fig. 3). We mention that the new rate is more accurate than the one given by Ref. 42.

In summary, and as our calculation shows, updating all nuclear reaction rates and using the newest versions of BBN codes by Refs. 8 and 70, the lithium problem is not resolved on nuclear physics ground. Therefore, in the following, we focus on the aspects of nonstandard BBN.

4. Nonstandard Physics

4.1. *Inhomogeneous nucleosynthesis*

In contrast to SBBN, intensive studies have been devoted to anisotropic models based upon inhomogeneity in baryon to photon ratio η .^{5,49,63,74} The fluctuations in η is thought to be generated at early epochs of SBBN, perhaps during the QCD or electroweak transitions. In such case, neutron and proton rich environments can be created which will promote the production of primordial abundances. In this context, two scenarios are considered: (a) When nucleon diffusion occurs at high temperature before the beginning of nucleosynthesis the final abundance of ${}^4\text{He}$ is reduced, consequently, the nucleosynthesis time is extended because it will be determined by neutron decay which ultimately leads to an overproduction of D as well as of lithium. However, (b) if the diffusion occurs during BBN, an overproduction of ${}^4\text{He}$ can take place.

In addition to the above scenarios, when the baryon/antibaryon mass exceeds $10^{-21} M_{\odot}$, an annihilation of antimatter could take place.⁹⁴ When the annihilation occurs after the weak freeze-out this leads to a reduction of the ${}^4\text{He}$ abundance. However, if the annihilation occurs after the synthesis of ${}^4\text{He}$ this will lead to overproduction of ${}^3\text{He}$ and D that will contradict observational constraints.¹³

Although inhomogeneous nucleosynthesis models represent attractive scenarios for SBBN, these models do not solve the lithium problem because of the observational constraints on other light elements. An overview concerning inhomogeneous nucleosynthesis can be found in Ref. 73.

4.2. *Decay of massive particles during BBN*

Including new particles during BBN will modify the energy density or/and the entropy of the early universe and consequently the final abundances of light elements. The stable end products of the decay of some X -particles will affect BBN by inducing hadronic or electromagnetic particles. The effects of these decays depend on the stage of BBN in which the non-thermal decaying particles interact with the background thermal nuclei. The largest contribution of these non-thermal decays is for decays after the weak freeze-out phase.²⁷ In this context, the effect of the decay of X -particles has been studied by Refs. 86 and 87 in a more general way that may apply to any X -particles. This would mean that these decays could be either inert decays which affect only the expansion rate or decays producing entropy which alter the time temperature relation.

Particle decays during BBN have been the focus of many works where special attention was given to their effect on the lithium problem.⁸³ We mention here a recent work by Ref. 39 where the induced interactions of some X -particles with nucleons have led to significant reduction of lithium without excessive modification of the helium and deuterium abundances. The effect of energetic hadronic decays has also been investigated by Ref. 55 where they cause scattering of thermal nuclei and showers of non-thermal nucleons. Consequently, generated neutrons can

react with ${}^7\text{Be}$ and reduce the final lithium abundance. Another attempt to resolve the lithium problem was given by Refs. 97 and 98 where three components were included, namely photon cooling, the decay of long-lived X -particles and a primordial magnetic field. This could lead to an optimum reduction of lithium during BBN. For a detailed analysis of the effects of hadronic and electromagnetic cascades during BBN we refer the reader to detailed reviews by Refs. 48 and 56.

In the aim to resolve the lithium problem, we mention here a successful attempt dealing with a modification of Maxwell–Boltzmann distribution of nuclei during BBN.⁴¹ This has decreased the lithium abundance to match observations but at the expenses of increasing deuterium. While this attempt seems to be promising, it relies on a specific modification to the distribution which when corrected for momentum conservation is no longer a viable solution. In the following, we focus on Neutrino properties and how they contribute to the lithium Problem.

4.3. Primordial neutrinos

Neutrinos are everywhere, some reach us from natural sources (Sun or cosmic rays) while others come from artificial sources (nuclear reactors). Primordial neutrinos or relic neutrinos are the remnant from the early universe where the density of neutrinos and antineutrinos for each flavor is calculated to be $n_{\nu_i 0} = n_{\bar{\nu}_i 0} \approx 53 \text{ cm}^{-3}$ using Eq. (9). Although neutrinos are much less than 1% of the present critical density, they play a crucial role in the early evolution of the universe. For example, since it is recently verified that neutrinos have masses, sterile or active neutrinos may be candidates for dark matter.^{1,16,99} In addition, they have important effects on SBBN and the CMB because these epochs are each sensitive to neutrino properties (number, chemical potential, temperature, etc.). This will be discussed in more detail in Secs. 6 and 7.

4.3.1. Role of neutrinos in SBBN

The cosmological effect of Neutrinos during BBN is well established.⁹³ In particular, they contribute to the total energy density and regulate the expansion rate of the universe. During the early evolution of the universe, the expansion rate as measured by the Hubble parameter H can be written explicitly in terms of the energy density of massless and relativistic particles as

$$\begin{aligned} H^2 &= \frac{8\pi G}{3}(\rho_\gamma + \rho_{e^\pm} + \rho_{\nu,\bar{\nu}}) \\ &= \left(\frac{8\pi G}{3}\right) \left(\frac{\pi^2}{30}\right) \left(\frac{7g_{e^\pm}}{8} + \frac{7g_{\nu,\bar{\nu}}}{8} + g_\gamma\right) \left(\frac{k^4}{h^3 c^3}\right) T^4. \end{aligned} \quad (15)$$

The standard neutrino species remain in kinetic equilibrium as long as the leptons scattering processes are effective:

$$\begin{aligned} \nu_l + l^\pm &\leftrightarrow \nu_l + l^\pm, \\ \nu_{\bar{l}} + l^\pm &\leftrightarrow \nu_{\bar{l}} + l^\pm, \end{aligned} \quad (16)$$

where l refers to lepton. In addition, the chemical equilibrium is also achieved by the creation and annihilation processes given by

$$\begin{aligned}\nu_l + \nu_{\bar{l}} &\leftrightarrow l + \bar{l}, \\ \nu_l + l' &\leftrightarrow \nu_{l'} + l.\end{aligned}\tag{17}$$

When the rates of these reactions drop below the expansion rate of the universe, neutrinos decouple from the background radiation. This happens at $T \sim 1$ MeV for electron neutrinos due to their weak interactions given by Eq. (18). After decoupling they propagate without suffering further scattering, preserving the Planckian spectrum.

$$\begin{aligned}n + e^+ &\leftrightarrow p + \bar{\nu}_e, \\ n + \nu_e &\leftrightarrow p + e^-, \\ n &\leftrightarrow p + e^- + \bar{\nu}_e.\end{aligned}\tag{18}$$

Prior to e^\pm annihilation the plasma has common temperature. However, when the temperature drops below the electron mass $T < m_e \sim 0.5$ MeV, the electron-positron begin to annihilate without being replaced (the annihilation process is not instantaneous). The released energy heats the photons relative to the neutrinos. It can be shown on the basis of entropy conservation within a comoving volume $sa^3 = \text{const.}$ that

$$\frac{T_\nu}{T_\gamma} = (4/11)^{1/3},\tag{19}$$

where the entropy density s is defined,⁷⁹

$$s = g_{\text{eff}} \frac{2\pi^2}{45} \left(\frac{k^4}{\hbar^3 c^3} \right) T^3\tag{20}$$

with g_{eff} represents the relativistic degrees of freedom contributing to the total entropy density,

$$g_{\text{eff}} = \sum_{i=\text{bosons}} g_i \left(\frac{T_i}{T} \right)^3 + \frac{7}{8} \sum_{i=\text{fermions}} g_i \left(\frac{T_i}{T} \right)^3,\tag{21}$$

where $g_{\text{eff}} = \frac{7}{8}g_f + g_b = \frac{7}{8} \times (6 + 4) + 2 = 10.75$ before e^+e^- annihilation and $g_{\text{eff}} = 5.25 \times \left(\frac{T_\nu}{T_\gamma} \right)^3 + 2 = 3.91$ after e^+e^- annihilation. On the basis of this discussion, it becomes clear now that any modification in neutrino properties such as energy, number density or temperature will affect light element abundances.

4.3.2. Neutrino degeneracy and oscillations

Degeneracy of neutrinos is related to the asymmetry between the number of neutrinos and antineutrinos. The abundances of the light elements in SBBN are calculated under the assumptions of a homogeneous universe and three families of neutrinos with zero chemical potential and mass. Meanwhile, it is established that neutrinos have nonvanishing chemical potentials.^{43,58} Introducing their chemical potential

may play an important role in the evolution of the universe. According to Ref. 101, neutrino degeneracy affects element production in two ways.

- (a) It increases the energy density which speeds up the expansion rate of the universe which is related to the scale factor as shown in Eq. (4). The energy density of fermions and anti-fermions is given to be⁷⁷

$$\rho_\nu + \rho_{\bar{\nu}} = \left(\frac{7\pi^2}{120} \right) g_f T_\nu^4 \left[1 + \frac{30\beta^2}{7\pi^2} + \frac{15\beta^4}{7\pi^4} \right], \quad (22)$$

where $\beta = \frac{\mu}{T}$ is the degeneracy parameter. In the SBBN, $\beta = 0$ and the neutrinos are not considered degenerate. It is then clear from the equation above that adding β will increase the energy density and this is the only way in which muon and tau neutrinos affect the SBBN.

- (b) A second effect is altering the neutron to proton ratio n/p at the temperature of freeze-out and this effect is limited to the electron neutrinos owing to their reaction rates (see Eq. (30)).

As shown in Ref. 50, chemical potentials cannot be constrained on the basis of the SBBN because the effect of $\beta_{\nu_{\mu,\tau}}$ can be compensated by a positive β_{ν_e} . To constraint the neutrino chemical potentials, one needs additional limits which are obtained from the CMB, namely, $N_\nu \leq 8$ and $-0.01 \leq \beta_{\nu_e} \leq 0.25$, $|\beta_{\nu_{\mu,\tau}}| \leq 2.9$ and from supernovae a $N_\nu \leq 7$ and $-0.01 \leq \beta_{\nu_e} \leq 0.22$, $|\beta_{\nu_{\mu,\tau}}| \leq 2.6$.⁴³ Neutrino oscillation (mixing) is an important phenomenon that has been discovered in the last decades and verified experimentally in 2015.⁹⁵ The existence of neutrino oscillations have revealed new neutrino properties beyond the Standard Model of particle physics in particular a nonvanishing neutrino mass. In other words, neutrino oscillation mean that any neutrino species in a well-defined flavor state has a finite probability to be detected in another flavor state. This depends on the distance traveled by the neutrinos, their energy, their mass difference and the mixing matrix.²⁹ Many investigations showing this mixing have been studied.^{2-4,102} The question remains as to whether there is a relation between neutrino degeneracy and oscillations.

Neutrino oscillations (mixing) will lead to an equilibration of the lepton asymmetry before the onset of the SBBN. In this case the equilibration of the chemical potentials will result in a dominant effect of electron neutrino because of their effect on the freeze-out. This will strongly constrain the abundance of ^4He , but will not affect ^7Li abundance.⁸⁵

On the other hand, in a universe with large lepton asymmetry^{43,61} it is important to allow the neutrino chemical potential to vary. This could happen, for example if there exists hypothetical neutrino–majoron coupling³¹ or one neutrino species mixes with a sterile neutrino resulting in a chaotic amplification of the electron neutrino chemical potential.⁹⁰ In a paper by Ref. 64, different chemical potentials were assumed but for values of η that are not consistent with the Planck observations. In the present work, the aim of including chemical potentials is to understand the SBBN and to investigate their effect on lithium abundance.

Table 2. Primordial helium-4 observations.

| Y_p | Sample | Reference |
|---------------------------|--|-----------|
| 0.228 ± 0.005 | HII galaxies | 66 |
| 0.234 ± 0.002 | low-Z extragalactic HII regions | 78 |
| 0.243 ± 0.003 | HII regions in 23 low-metallicity blue compact galaxies (BCGs) | 44 |
| 0.225 ± 0.013 | eclipsing binaries | 81 |
| 0.2391 ± 0.0020 | 5 low-Z extragalactic HII regions | 62 |
| 0.2421 ± 0.0021 | 82 low-Z extragalactic HII regions | 45 |
| 0.250 ± 0.004 | low-Z extragalactic HII regions | 37 |
| 0.2477 ± 0.0029 | extragalactic HII regions | 68 |
| 0.245 ± 0.012 | NGC 6752 globular cluster blue HB stars | 100 |
| 0.2561 ± 0.0108 | 7 “high quality” extragalactic HII regions | 6 |
| 0.2565 ± 0.0050 | 786 low-Z extragalactic HII regions | 46 |
| 0.2449 ± 0.0040 | metal-poor extragalactic HII regions | 7 |
| $0.28^{+0.14}_{-0.15}$ | 7 years WMAP | 57 |
| 0.2446 ± 0.0029 | extragalactic HII regions | 69 |
| $0.262^{+0.035}_{-0.037}$ | Planck collaboration | 72 |
| 0.245 ± 0.007 | extragalactic HII regions | 33 |

5. Constraints

In order to investigate the effects of nonstandard scenarios, observational constraints on the abundances of the light elements should be specified. These are described for light elements as follows.

5.1. Helium-4 (^4He)

Any nonstandard scenario could be constrained by the primordial ^4He abundance. However, some uncertainties remain in the extrapolation of the primordial value to very low metallicity. In Table 2, we present some of the available data from 1990 till now where most of the published results are from extragalactic low-metallicity HII regions. However, independent measurements by WMAP and the Planck collaboration show different ranges of the helium abundance with larger uncertainties. These two different values are based on the effect of primordial helium on the CMB angular power spectrum. Although some of the data is in good agreement with SBBN calculations, new precise measurements of primordial helium are needed because the helium abundance is crucial in constraining nonstandard physics. In this work, a conservative limit on the primordial helium abundance of $0.228 \leq Y_p \leq 0.260$ will be adopted in the investigation of nonstandard scenarios described before.

5.2. Deuterium

It is the most fragile element and destroyed in stars at temperatures in excess of 10^6 K so that its observed value gives a lower limit on the primordial abundance. So far, there are 15 measurements of the primordial deuterium values that show a large

Table 3. Primordial deuterium observations.

| Quasar | Z_{abs} | $(D/H) \times 10^5$ | Reference |
|--------------|------------------|------------------------|-----------|
| Q1937 – 1009 | 3.572 | 3.3 ± 0.3 | 20 |
| Q1009 – 2956 | 2.504 | $4.0^{+0.6}_{-0.7}$ | 21 |
| Q0347 – 3819 | 3.025 | 3.75 ± 0.25 | 59 |
| J1337 + 3152 | 3.168 | $1.2^{+0.5}_{-0.3}$ | 92 |
| J1358 + 6522 | 3.067 | 2.58 ± 0.07 | 25 |
| J1444 + 2919 | 2.437 | $1.97^{+0.33}_{-0.28}$ | 12 |

dispersion in the mean values and in the estimated errors. The unweighted mean of these 15 measurements is $D/H = (2.55 \pm 0.19) \times 10^{-5}$. In Table 3, we present some of primordial deuterium measurements where a recent accurate one is given by Ref. 25. However, a following measurement is given by Ref. 12 for a system that meets the set of strict criteria by Ref. 25 shows a different value for the primordial deuterium abundance. Another low value of deuterium $D/H = (1.2^{+0.5}_{-0.3}) \times 10^{-5}$ is given by Ref. 92 who argue therefore that astration factors can vary significantly even at low metallicity. In addition, it has been argued by Ref. 65 that higher values near the upper limit of the observed deuterium may be more representative of the true primordial abundance compared with systems where the deuterium abundance would have been subject to destruction. Therefore, a large number of deuterium measurements is needed in order to understand the dispersion in its abundance (see Ref. 12 for more detailed discussion). In this work we will adopt the conservative range of $2.58 \times 10^{-5} < D/H < 3.75 \times 10^{-5}$.

5.3. Helium-3 (^3He)

The determination of primordial ^3He is a complicated task. The reason is due to the stellar processing of this element since D is transformed to ^3He and consequently the low mass stars are net producers of ^3He . However it is not easy to determine the output of ^3He into the interstellar medium (ISM). Then, we will mention the value of ^3He inferred¹¹ from the most distant and metal-poor stars $^3\text{He} \leq (1.1 \pm 0.2) \times 10^{-5}$.

5.4. Lithium (^7Li)

This element is the focus of the present work because of the large discrepancy between the SBBN predictions and observations. Observations from metal-poor halo stars are still a big puzzle for cosmologists and astrophysicists who are trying to explain this discrepancy. In Table 4, we give a list of the estimates for the ^7Li abundances in the last ten years. It is clear that all observed lithium abundances do not agree with SBBN predictions. For this reason an upper limit on the primordial lithium abundance can be adopted such as $\text{Li}/H \leq 2.8 \times 10^{-10}$ since achieving this limits by nonstandard assumptions would be sufficient to match the observations because the difference can be explained by some stellar processing.

Table 4. Primordial lithium observations.

| $[\text{}^7\text{Li}] = 12 + \log_{10}(\text{}^7\text{Li})$ | $\text{}^7\text{Li}/H \times 10^{10}$ | Reference |
|---|---------------------------------------|-----------|
| 2.24 ± 0.01 | 1.738 ± 0.040 | 17, 18 |
| $2.09^{+0.19}_{-0.13}$ | $1.230^{+0.675}_{-0.318}$ | 82 |
| 2.34 ± 0.06 | $2.188^{+0.324}_{-0.283}$ | 19 |
| 2.37 ± 0.05 | $2.344^{+0.286}_{-0.255}$ | 76 |
| 2.21 ± 0.09 | $1.622^{+0.373}_{-0.304}$ | 24 |
| 2.095 ± 0.055 | $1.245^{+0.168}_{-0.149}$ | 10 |
| 2.54 ± 0.1 | $3.467^{+0.898}_{-0.713}$ | 54 |
| 2.2 ± 0.086 | $1.58^{+0.35}_{-0.28}$ | 84 |

6. Numerical Results

Degenerate neutrinos during BBN have been extensively studied in previous works^{30,32,43,58,79} where the effects of large lepton and additional effective numbers of neutrinos were considered. The present work differs from the previous studies in that we also focus on the range of neutrino chemical potentials that may lead to a significant decrease in the lithium abundance. In this section, we investigate the effects of degenerate neutrinos toward understanding or ameliorating the lithium problem. As mentioned before, equating chemical potentials will not solve the lithium problem, so that we can compensate this effect by increasing the number of neutrinos. Compensating the electron neutrino chemical potentials by increasing the number of neutrinos has been investigated by Ref. 32. However, here we fix the baryon asymmetry to be $\eta = (6.11 \pm 0.06) \times 10^{-10}$ as deduced by Planck. We will see that strict ranges on chemical potentials and neutrino number will be given.

Taking into consideration neutrino oscillations, this will lead to the equilibration of chemical potentials before SBBN. In this context we obtained the following.

- The results in Table 5 shows that the values of SBBN (see third row in the table) are also closely obtained for the following range of neutrino number and chemical potentials:

$$3 \leq N_\nu \leq 3.3, \quad -0.015 \leq \beta_{\nu_{\mu,\tau,e}} \leq 0.04. \quad (23)$$

- In order to reduce the lithium abundance significantly, the ranges of chemical potentials and numbers of neutrinos are shown in Table 6 and Eq. (24).

$$6.7 \leq N_\nu \leq 7.8, \quad 0.175 \leq \beta_{\nu_{\mu,\tau,e}} \leq 0.265. \quad (24)$$

It is clear from Eq. (24) that the ranges of N_ν are not supported by recent CMB observations (WMAP and Planck missions). However, it is not necessarily that the number of neutrinos N_ν during BBN is the same as the effective number of relativistic species N_{eff} deduced from CMB. The equivalence between N_{eff} and N_ν is assumed in case of a standard neutrino temperature $T_{\nu\text{SM}}$. However, any variation in the neutrino temperature during or after BBN can be translated into

Table 5. Effect of neutrino chemical potentials ($\beta_{\nu_e} = \beta_{\nu_\mu} = \beta_{\nu_\tau}$) along with varying N_ν on SBBN.

| N_ν | β_{ν_e} | $\beta_{\nu_{\mu,\tau}}$ | Y_p | $D/H \times 10^5$ | ${}^7\text{Li}/H \times 10^{10}$ |
|---------|-----------------|--------------------------|--------|-------------------|----------------------------------|
| 3 | -0.015 | -0.015 | 0.2499 | 2.6613 | 4.4280 |
| 3 | 0 | 0 | 0.2461 | 2.6386 | 4.3861 |
| 3.2 | 0.02 | 0.02 | 0.2442 | 2.6827 | 4.2518 |
| 3.3 | 0.04 | 0.04 | 0.2410 | 2.6965 | 4.1526 |

Table 6. The ranges of $\beta_{\nu_{e,\mu,\tau}}$ and N_ν that lead to a significant decrease of lithium.

| N_ν | β_{ν_e} | $\beta_{\nu_{\mu,\tau}}$ | Y_p | $D/H \times 10^5$ | ${}^7\text{Li}/H \times 10^{10}$ |
|---------|-----------------|--------------------------|--------|-------------------|----------------------------------|
| 6.7 | 0.23 | 0.23 | 0.2292 | 3.4835 | 2.7978 |
| 6.9 | 0.225 | 0.225 | 0.2317 | 3.5490 | 2.7690 |
| 7.2 | 0.175 | 0.175 | 0.2463 | 3.7520 | 2.7840 |
| 7.4 | 0.245 | 0.245 | 0.2306 | 3.6599 | 2.6415 |
| 7.6 | 0.24 | 0.24 | 0.2331 | 3.7250 | 2.6159 |
| 7.8 | 0.265 | 0.265 | 0.2287 | 3.7398 | 2.5389 |

a variation in the effective number of neutrinos obtained by CMB observations through:

$$N_{\text{eff}} T_{\nu\text{SM}}^4 = N_\nu T_\nu^4. \tag{25}$$

This case is treated in details by Ref. 38 when neutrino temperature deviate from the standard one after decoupling. Varying neutrino temperature and breaking the degeneracy between BBN and CMB is also extensively studied by Ref. 52. We also investigated the effect of varying neutrino temperature along with dark matter in a recent work by Ref. 96 where we focused on the effect on lithium without violating CMB constraints. The remaining unanswered question is then whether this increase in the number of neutrino species may contribute to the dark matter or not.

While in Tables 5 and 6 the chemical potentials are assumed to be equal, we have done another calculations where the number of neutrinos is fixed to be $N_\nu = 3$ but the chemical potentials are different (see Table 7). So to achieve a significant

Table 7. The effect of different neutrino chemical potentials on lithium.

| β_{ν_e} | $\beta_{\nu_{\mu,\tau}}$ | Y_p | $D/H \times 10^5$ | ${}^7\text{Li}/H \times 10^{10}$ |
|-----------------|--------------------------|--------|-------------------|----------------------------------|
| 0.19 | 2 | 0.2417 | 3.6797 | 2.7859 |
| 0.2 | 2.05 | 0.2410 | 3.7343 | 2.7226 |
| 0.21 | 1.95 | 0.2352 | 3.5736 | 2.7967 |
| 0.23 | 2 | 0.2322 | 3.6080 | 2.7164 |
| 0.25 | 2.1 | 0.2310 | 3.7173 | 2.5930 |
| 0.26 | 2.1 | 0.2287 | 3.6996 | 2.5761 |

reduction of lithium, we derived new limits on the chemical potential given by Eq. (26) that substantially reduces the lithium abundance to less than 2.8×10^{-10} .

$$N_\nu = 3, \quad 0.19 \leq \beta_{\nu_e} \leq 0.26, \quad 1.95 \leq \beta_{\nu_{\mu,\tau}} \leq 2.1. \quad (26)$$

7. Analytical Calculations

7.1. Stages of BBN

The final abundances of light elements are sensitive to the physical conditions of the SBBN where the temperature is $T \leq 1$ MeV and the time $t \geq 1$ s. SBBN is based on a competition between the expansion rate and nuclear reaction rates so that when the expansion rate becomes faster than a specific reaction rate, this reaction will freeze-out. Three important stages of BBN will be discussed namely: (1) the freeze-out of neutrons; (2) the deuterium bottleneck; and (3) the quasi-equilibrium of neutrons and deuterium because these three stages determine the final element abundances.

7.1.1. Freeze-out of neutrons

The weak interactions given in Eq. (18) remain in thermal equilibrium as long as the weak interaction rates $\Gamma_{\text{weak rates}} \sim T^5$ are greater than the expansion rate $H \sim T^2$. So at lower temperature, $\Gamma_{\text{weak rates}}$ cannot compete with the expansion rate and the freeze-out of these reactions take place for the following condition²⁸:

$$G_F^2 T^5 \sim \Gamma_{\text{weak rates}}(T_F) = H(T_F) \sim G_N^{1/2} T^2, \quad (27)$$

where T_F is the freeze-out temperature.

Since the weak interactions determine the neutron to proton ratio an analytical calculation of the weak-reaction freeze-out is given in Ref. 77 whereby in SBBN the neutron mass fraction at freeze-out becomes $X_n = \frac{n_n}{n_n + n_p} \approx 0.157$ for which the neutron-to-proton ratio is

$$\frac{n}{p} = e^{-Q/T_F}, \quad (28)$$

where $Q = m_n - m_p = 1.293$ MeV.

In the SBBN the freeze-out of neutrons takes place at $T \sim 0.7$ MeV. This temperature is not fixed, rather it depends on nonstandard scenarios intervening during BBN. For example if for some reason the expansion rate becomes faster, the weak rates will stop earlier (at higher temperature), less neutrons will be converted into protons leading to a higher neutron to proton ratio and vice versa. This will mainly increase helium, but also affect deuterium, and consequently lithium abundance. For this reason, we extended the calculations in Ref. 77 to include neutrino chemical potentials. The equilibrium abundance of neutrons including the chemical potential $\beta_{\nu_e} = \mu_{\nu_e}/T$ can be written as

$$X_n^{\text{eq}} = \frac{1}{1 + e^{\beta_{\nu_e}} e^{Q/T}} \quad (29)$$

for which the neutron-to-proton ratio becomes

$$\frac{n}{p} = e^{-\beta\nu_e} e^{-Q/T}, \quad (30)$$

consequently, weak reaction rates will be modified as

$$\begin{aligned} \lambda_{pe} &= \exp\left(-\frac{Q}{T}\right) \exp(-\beta\nu_e) \lambda_{n\nu}, \\ \lambda_{p\bar{\nu}} &= \exp\left(-\frac{Q}{T}\right) \exp(-\beta\nu_e) \lambda_{ne}, \end{aligned} \quad (31)$$

where $\lambda_{n\nu} \approx \lambda_{ne}$ at $T = T_\nu$.

More explicitly, we find that $\lambda_{n\nu}$ can be well approximated by Eq. (32) within the range $-0.5 \leq \beta\nu_e \leq 0.5$,

$$\lambda_{n\nu} \approx 1.63 \exp(+\beta\nu_e) \left(\frac{T_\nu}{Q}\right)^3 \left(\frac{T_\nu}{Q} + 0.25\right)^2 \text{ s}^{-1}, \quad (32)$$

while the other weak rates can be related to Eq. (32) using Eq. (31).

Equation (32) shows the familiar result that adding a positive chemical potential, $\beta\nu_e$, will exponentially enhance the weak rates. Hence, more neutrons are converted into protons leading to a lower neutron mass fraction at freeze-out. According to Eq. (29) this implies that a lower freeze-out temperature is obtained. Conversely, more neutrons will be available when adding a negative $\beta\nu_e$ leading to a higher freeze-out temperature. With this modification the standard and non-standard rates can be related:

$$\lambda_{n\nu}^{\text{nonstandard}} \approx e^{+\beta\nu_e} \lambda_{n\nu}^{\text{standard}}, \quad (33)$$

and the neutron freeze-out mass fraction is given by

$$X_n^F = \int_0^\infty \frac{e^{(-5.42e^{\beta\nu_e} k^{-1/2} \int_0^y (x+0.25)^2 (1+e^{-\beta\nu_e} \exp(-\frac{1}{x})) dx)} dy}{2y^2 (1 + \cosh(\beta\nu_e + 1/y))}. \quad (34)$$

More explanation concerning the derivation of Eq. (34) is given in Appendix A.

Because the freeze-out occurs for $T > 0.5$ MeV, the parameter k_{eff} represents the effective number of relativistic degrees of freedom before electron-positron annihilation

$$\begin{aligned} k_{\text{eff}} &= 1.8094 + \left(\frac{\pi^2}{30}\right) \left(\frac{7}{8} N_{\nu, \bar{\nu}}\right) + 0.25\beta_{\nu_e}^2 + \frac{\beta_{\nu_e}^4}{8 \times \pi^2} \\ &+ 2 \times \left(0.25\beta_{\nu_{\mu, \tau}}^2 + \frac{\beta_{\nu_{\mu, \tau}}^4}{8 \times \pi^2}\right). \end{aligned} \quad (35)$$

Note that g is also a common notation for the number of relativistic degrees of freedom. In this paper we use $k_{\text{eff}} = \frac{\pi^2}{30} (g_\gamma + \frac{7}{8} g_f)$. The effect of $\beta\nu_e$ is directly involved in the weak rates while the effect of $\beta\nu_{\mu, \tau}$ mainly affects the expansion

rate or equivalently k_{eff} . It is not easy to obtain an exact expression of the integral in Eq. (34) as a function of β_{ν_e} and k_{eff} , so we have made a polynomial fits for a grid of 230 values of $(k_{\text{eff}}, \beta_{\nu_e})$ to obtain the following expression for X_n^F valid in the ranges of $-0.5 \leq \beta_{\nu_e} \leq 0.5$, $0 \leq \beta_{\nu_{\mu,\tau}} \leq 5$:

$$\begin{aligned} X_n^F = & 0.1279 - 0.1994\beta_{\nu_e} + 0.01015k_{\text{eff}} + 0.09137\beta_{\nu_e}^2 - 3.946 \times 10^{-3}\beta_{\nu_e}k_{\text{eff}} \\ & - 3.743 \times 10^{-4}k_{\text{eff}}^2 + 7.716 \times 10^{-3}\beta_{\nu_e}^3 - 6.744 \times 10^{-4}\beta_{\nu_e}^2 \\ & + 7.368 \times 10^{-5}\beta_{\nu_e}k_{\text{eff}}^2 + 5.246 \times 10^{-6}k_{\text{eff}}^3. \end{aligned} \quad (36)$$

Using this expression in Eq. (29) we can obtain the corresponding freeze-out temperature T_F for every $(\beta_{\nu_e}, \beta_{\nu_{\mu,\tau}}, X_n^F)$. Equation (36) illustrates the explicit dependence of the neutron freeze-out abundance on β_{ν_e} and k_{eff} . Note that Eq. (36) is valid also if k_{eff} receives contributions not only from $\beta_{\nu_{\mu,\tau}}$ but also from extra relativistic degrees of freedom or any component that could alter the energy density of the universe.

7.2. Deuterium formation epoch

Complex nuclei are synthesized through nuclear interactions. The first step starts with the formation of deuterium through



However, one can ask why the helium abundance is still negligible at $T \sim 0.3$ MeV while its binding energy is 28.3 MeV. As long as the temperature remains high, deuterium is easily destroyed by photons with energy in excess of the binding energy of deuterium. Since reactions responsible for converting deuterium into heavier nuclei are dependent on the deuterium concentration, the formation of ${}^3\text{He}$ and ${}^4\text{He}$ is delayed until the nuclear statistical equilibrium (NSE) shifts from a completely dissociated nucleon gas into a gas in which deuterium can survive. In SBBN this shift in NSE is sometimes referred to the deuterium bottleneck. It occurs at $T_{\text{BN}} \approx 0.84$ GK (0.072 MeV) with $D/H \approx 3.665 \times 10^{-3}$ which is obtained by updating reactions of the AlterBBN program.⁸ Therefore, before deuterium reaches its bottleneck, the formation of heavier elements is blocked despite their large binding energies (see Fig. 2).

An analytical expression for the deuterium bottleneck has been derived⁷⁷ to be

$$\frac{D}{H} \approx \frac{1.2 \times 10^{-5}}{X_p(T_{\text{BN}}(\text{MeV}) \times \eta_{10})}, \quad (38)$$

where T_{BN} is the Bottleneck temperature, $\eta_{10} = 10^{10} \times \eta$ and $X_p = \frac{n_p}{n_p + n_n}$. However, Eq. (38) can be modified by introducing nonstandard scenarios which affect the deuterium bottleneck, the final deuterium abundance and the final elements abundances. Extending the analytic derivation of Eq. (38) and constraining it with

our numerical calculations using the AlterBBN program, we obtain the following modified expression:

$$\frac{D}{H} = \frac{4 \times 10^{-3}}{X_p(k_{\text{eff}}^{-0.5} \times T_{\text{BN}}(\text{MeV}) \times \eta_{10} + C(\beta_{\nu_e}, k_{\text{eff}}))}, \quad (39)$$

with $X_p \approx 1 - X_n^F$. In Eq. (39), T_{BN} and $C(\beta_{\nu_e}, k_{\text{eff}})$ are functions of the number of the effective relativistic degrees of freedom k_{eff} and β_{ν_e} . We have found that these dependences can be approximated with the following analytic fits:

$$T_{\text{BN}}(\text{MeV}) \approx 0.0745 - 2.1448 \times 10^{-3} \times k_{\text{eff}}^{0.3148} \quad (40)$$

or

$$T_{\text{BN}}(\text{GK}) \approx 0.8643 - 0.02488 \times k_{\text{eff}}^{0.3148}, \quad (41)$$

and

$$\begin{aligned} C(\beta_{\nu_e}, k_{\text{eff}}) = & 1.181 + 0.6486\beta_{\nu_e} - 0.3511k_{\text{eff}} + 0.2937\beta_{\nu_e}^2 \\ & - 0.1189\beta_{\nu_e}k_{\text{eff}} + 0.06239k_{\text{eff}}^2 - 0.02391k_{\text{eff}}\beta_{\nu_e}^2 \\ & + 0.00838k_{\text{eff}}^2\beta_{\nu_e} - 0.003651k_{\text{eff}}^3. \end{aligned} \quad (42)$$

The parameter k_{eff} in the above equation, is now different from the one given in Eq. (35) because e^+e^- annihilation reduces the number of degrees of freedom before the deuterium bottleneck is reached. In this case the expression for k_{eff} is

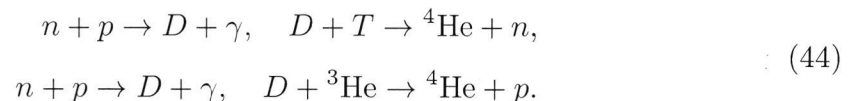
$$\begin{aligned} k_{\text{eff}} = & 0.6579 + \left(\frac{4}{11}\right)^{\frac{4}{3}} \left(\frac{\pi^2}{30}\right) \left(\frac{7}{8}N_{\nu,\bar{\nu}}\right) + \left(\frac{4}{11}\right)^{\frac{4}{3}} \times \left(0.25\beta_{\nu_e}^2 + \frac{\beta_{\nu_e}^4}{8 \times \pi^2}\right) \\ & + 2 \times \left(\frac{4}{11}\right)^{\frac{4}{3}} \times \left(0.25\beta_{\nu_{\mu,\tau}}^2 + \frac{\beta_{\nu_{\mu,\tau}}^4}{8 \times \pi^2}\right). \end{aligned} \quad (43)$$

Note that more details concerning the derivation of Eq. (39) are given in Appendix B. These analytic relations reveal the following.

- (1) It is clear from Eqs. (40) and (41) that T_{BN} is mainly affected by the expansion rate. Furthermore, we will see later that any shift in the bottleneck temperature will affect light elements abundances.
- (2) Figure 4 shows that the deuterium mass fraction at the bottleneck depends not only on the bottleneck temperature and η_{10} , but also on the expansion rate and β_{ν_e} . It is a steadily increasing function $\beta_{\nu_{\mu,\tau}}$ but depends mainly on β_{ν_e} .

7.3. Helium-4

The nucleosynthesis of ${}^4\text{He}$ occurs after the temperature drops below that of deuterium bottleneck. At this point two neutrons are mainly combined with two protons to form ${}^4\text{He}$ via the reaction chains:



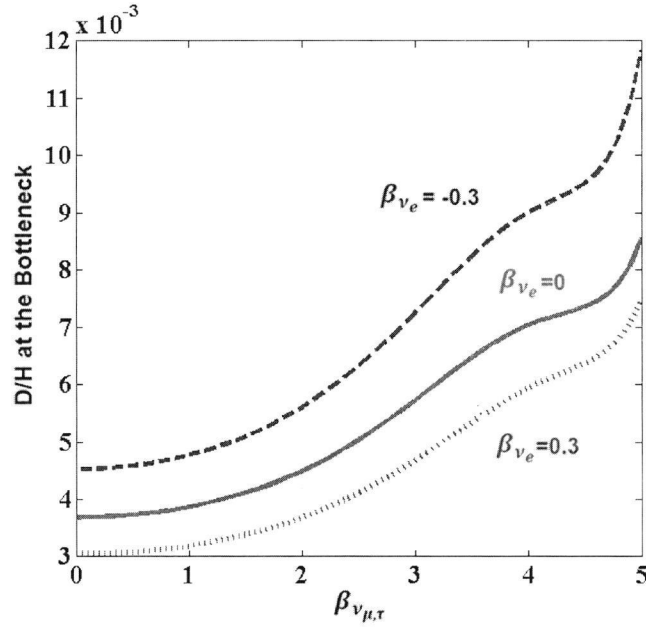


Fig. 4. Deuterium abundance at the bottleneck as function of the neutrino chemical potentials.

Consequently, the abundance of ${}^4\text{He}$ not only depends on the neutron mass fraction, but also on the bottleneck temperature given by Eqs. (40) and (41). In order to obtain the primordial helium mass fraction from the above reaction chains, we need to also consider the time variation of temperature. According to Ref. 77 the helium mass fraction can be estimated by

$$X_f({}^4\text{He}) \approx 2X_n^F \exp\left(-\frac{t_{\text{BN}}}{\tau_n}\right), \quad (45)$$

where

$$t_{\text{BN}} = 187.0384 \times \frac{k_{\text{eff}}^{-0.5}}{T_{\text{BN}}(\text{GK})^2} \quad (46)$$

$$\text{or equivalently } t_{\text{BN}} = 1.39 \times \frac{k_{\text{eff}}^{-0.5}}{T_{\text{BN}}(\text{MeV})^2}.$$

Equation (45)⁷⁷ was derived for a fixed k_{eff} and for a range of η_{10} . However, a more relevant determination for our purpose is to fix $\eta_{10} = 6.11 \pm 0.06$ by the Planck analysis⁷² and include degenerate neutrinos. In this way, we have obtained a better estimate of the primordial ${}^4\text{He}$ abundance Y_p that includes the effect of different values of the chemical potentials in the ranges of $-0.5 \leq \beta_{\nu_e} \leq 0.50 \leq \beta_{\nu_{\mu,\tau}} \leq 5$. This leads to:

$$Y_p \approx 1.81X_n^F \exp\left(-1.79\frac{t_{\text{BN}}}{\tau_n}\right) + 0.075, \quad (47)$$

where $\tau_n \approx 880.2 \pm 1$ sec is the adopted neutron lifetime.⁶⁷ For comparison, the calculation of this mass fraction from Ref. 51 is shown in the first column of Table 8

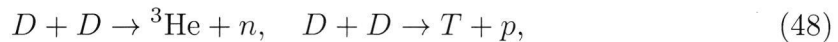
Table 8. Comparison of light elements abundances for $\beta_{\nu_e} = 0.1$, $\beta_{\nu_{\mu,\tau}} = 1$ between fits presented by Kneller and Steigman⁵¹ and the present work.

| | Kneller and Steigman ⁵¹ | Present work | Numerical simulations |
|----------------------------------|------------------------------------|--------------|-----------------------|
| Y_p | 0.2368 | 0.2344 | 0.23410 ± 0.00013 |
| $D/H \times 10^5$ | 2.7296 | 2.6969 | 2.8170 ± 0.1344 |
| ${}^3\text{He}/H \times 10^5$ | 1.4211 | 1.0798 | 1.0380 ± 0.0536 |
| ${}^7\text{Li}/H \times 10^{10}$ | 3.9563 | 3.9173 | 3.7880 ± 0.3431 |

where the light element abundances are fit as a linear function of η_{10} , the expansion rate variation, and β_{ν_e} . In Table 8, we take an example in which $\beta_{\nu_e} = 0.1$ and $\beta_{\nu_{\mu,\tau}} = 1$ in order to compare our numerical simulation with the present expressions and those of Ref. 51. The analytic relations derived here provide a better physical picture and relate the light element abundances to the three important stages of BBN. Our treatment is valid for chemical potentials in wider ranges ($-0.5 \leq \beta_{\nu_e} \leq 0.5$, $0 \leq \beta_{\nu_{\mu,\tau}} \leq 5$) and the results are similar to the numerical simulations as demonstrated in Table 8.

7.4. Final deuterium abundance

Let us make a clearer picture of the SBBN. When deuterium reaches its maximum abundance, the destruction of deuterium will be efficient through



so that the deuterium abundance begins to decrease because it will be converted into tritium and ${}^3\text{He}$ which will proceed to ${}^4\text{He}$ through



Nucleosynthesis is a self-regulating process, in other words, if the abundance of ${}^3\text{He}$ and tritium becomes smaller or greater than the quasi-equilibrium abundance, their concentration will be regulated to return ${}^3\text{He}$ and tritium to their quasi-equilibrium values. In this context, two stages of quasi-equilibrium should be considered: the first one is when $X_D \ll X_n$ so that deuterium satisfies the quasi-equilibrium condition ($\frac{dX_D}{dT} \approx 0$) and free neutrons dominate the NSE abundances of all nuclides. The second one is after neutron abundance drops to that of deuterium $X_D \sim X_n$, in this case the neutrons satisfy the quasi-equilibrium condition ($\frac{dX_n}{dT} \approx 0$) and deuterium regulates the quasi-equilibrium of neutrons and other elements.⁷⁷ It is important to know the temperature T^* at which the free neutron abundance becomes comparable to that of deuterium because it is one of the parameters affecting the final abundance of deuterium and consequently heavier elements. An estimation of this temperature is approximately $T^* \sim 0.07$ MeV.⁷⁷

After the temperature drops below the deuterium bottleneck, its abundance decreases and neutrons start to decay. As explained in Appendix C, we obtained

T^* as function of the bottleneck temperature T_{BN} , the mass fraction of protons and the effective number of relativistic degrees of freedom:

$$T^*(\text{GK}) \approx T_{\text{BN}}(\text{GK}) - \frac{0.232}{\eta_{10} \times X_p \times k_{\text{eff}}^{-0.5}}. \quad (50)$$

Here, it is seen that increasing k_{eff} will lead to lower T_{BN} , so that the neutron abundance will take more time to decrease to the deuterium concentration. Consequently T^* will be lower. Therefore, the deuterium final abundance can be related to T^* by the following an analytic fit:

$$\frac{D}{H} = \frac{1}{X_p \times \eta_{10} \times F(T^*(\text{GK}))}, \quad (51)$$

with

$$F(T^*(\text{GK})) = 0.36 \times \exp(11.81T^*) + 2.4 \times 10^{-12} \times \exp(44.05T^*). \quad (52)$$

Further explanation of this deuterium calculation is given in Appendix C. Equation (51) allows for a better estimate of D/H over the parameter range of chemical potential adopted here. It is clear that if T^* increases, the final deuterium abundance will decrease. This is due to fewer neutrons and/or a lower expansion rate and vice versa.

7.5. Helium-3 and tritium

We have derived explicit expressions for the abundances of helium and tritium to analyze how these nuclides depend upon each other and to make a final interpretation concerning the lithium abundance. The expression for the quasi-equilibrium abundance of ^3He is given by

$$\begin{aligned} \frac{dX_{^3\text{He}}}{dt} &= \frac{3}{4}\lambda_{DD1}X_D^2 + \frac{3}{2}\lambda_{Dp}X_DX_p - \frac{1}{2}\lambda_{^3\text{He}D}X_DX_{^3\text{He}} \\ &\quad - \lambda_{^3\text{He}n}X_{^3\text{He}}X_n = 0, \end{aligned} \quad (53)$$

where X refers to the abundance by weight of a given element and λ 's are the experimentally measured rates of the used reactions.

It follows that the final abundance of ^3He is

$$\frac{^3\text{He}}{H} \approx \frac{0.074 \times D/H + 4 \times 10^{-6} X_p}{0.46 + 1570 \times D/H}. \quad (54)$$

Similarly for the tritium abundance we have

$$\frac{3}{4}\lambda_{DD2}X_D^2 + \lambda_{^3\text{He}n}X_{^3\text{He}}X_n \approx \frac{1}{2}\lambda_{DT}X_DX_T.$$

So,

$$\begin{aligned} \frac{T}{H} &\approx 8.85 \times 10^{-9} - 2.71 \times 10^{-8} X_p + 1.04 \times 10^{-3} \left(\frac{D}{H}\right) \\ &\quad + 2.86 \times 10^{-3} \left(\frac{D}{H}\right) X_p + 1.06 \left(\frac{D}{H}\right)^2. \end{aligned} \quad (55)$$

It is clear from the network shown in Fig. 2 that the main production of ^3He and tritium comes from the reactions of deuterium. This is also obtained in the analytic formulation of Eqs. (54) and (55). Hence, increasing deuterium will lead to an increase in ^3He and tritium and vice versa.

7.6. *Beryllium and lithium*

Beryllium is mainly produced and destroyed by the reactions:



We give the final abundance of ^7Be is then given by

$$\frac{^7\text{Be}}{H} \approx 9 \times 10^{-14} \times \frac{Y_p \times \frac{^3\text{He}}{H}}{X_p \times \left(\frac{D}{H}\right)^2}. \tag{57}$$

The final abundance of lithium is then determined from the sum of reactions leading to beryllium and lithium. Under standard BBN conditions, one can deduce (using the AlterBBN program) that more than 90% of lithium comes from beryllium by electron capture after the epoch of nucleosynthesis. It is important to mention that the electron capture rate is irrelevant unless it becomes shorter than the timescale of BBN. Using the network equations with the relevant reactions leading to the production of lithium, we deduced that the final lithium abundance is given by

$$\frac{^7\text{Li}}{H} \approx 9 \times 10^{-4} \times \frac{Y_p}{X_p} \left(\frac{T}{H} + 2.57 \times 10^{-3} \times \frac{^3\text{He}}{H} \right). \tag{58}$$

In the case of neutrino degenerate BBN, increasing the expansion rate by adding $\beta_{\nu_{\mu,\tau}}$ will lead to different lithium production than in the SBBN. First, the final abundance of lithium will depend upon the evolution of deuterium which will directly affect beryllium as seen from Eq. (57). For this reason all solutions leading to lithium destruction are accompanied by an increase in deuterium. However, as seen in Eqs. (57) and (58), deuterium is not the only element affecting lithium production. Both helium isotopes ^3He and ^4He play an important role when the helium abundance becomes more significant than that of deuterium.

To have a clear picture, Fig. 5 shows the sum of lithium and beryllium as function of deuterium. Two regions are found, one is up to the minimum of the curve where the sum is steadily decreasing while the other region shows an increase of the sum. The behavior of the first region is due to the decrease of beryllium (which will be transformed into lithium after the SBBN), at the same time the production of lithium is not significant and this is shown in the bottom right panel of Fig. 5. The increase in the other region is due to the high abundance of lithium produced through reaction 7 in Fig. 2(b). This means that the role of beryllium is not important in this case. It is emphasized that our range of interest is in the first region as shown by the vertical lines in Fig. 5.

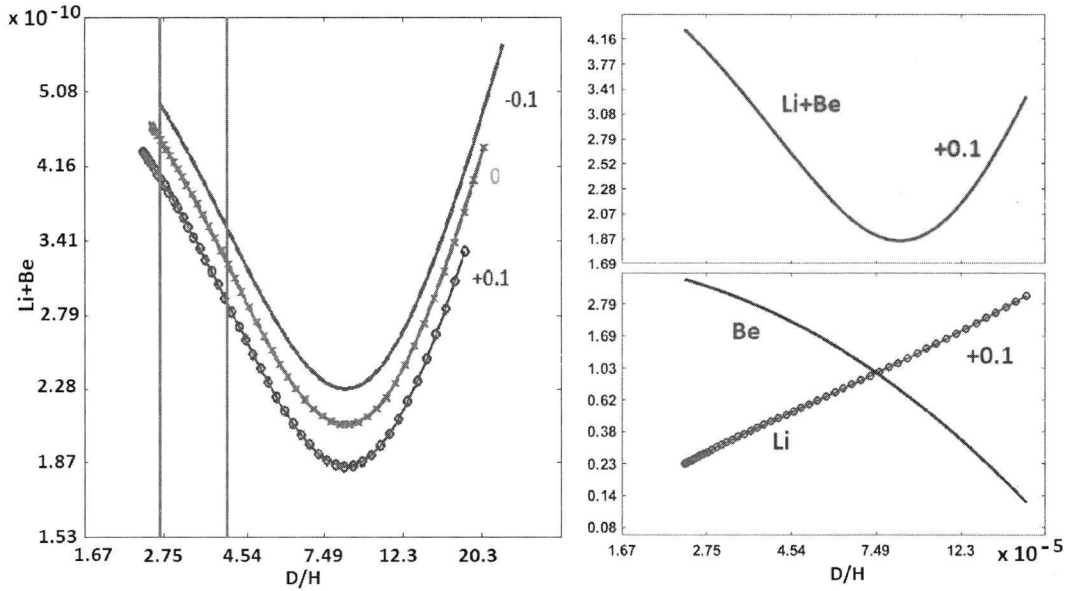


Fig. 5. Lithium abundance as function of the deuterium abundance for different values of β_{ν_e} as labeled on the curves with the range of $0 \leq \beta_{\nu_{\mu,\tau}} \leq 5$.

8. Conclusions

The widely studied BBN seems to require certain revisions motivated by the lithium problem described above. This seems to indicate that nonstandard assumptions are to be introduced which means that some physical conditions are still missing to describe the SBBN. In the present work, we gave an overview of the physics of the early universe where we described the present status of the lithium problem. We have focused on the properties of neutrinos due to their importance during BBN. The results of the present work can be summarized as follows.

- As outlined in Sec. 3.1, the depletion of lithium obtained from SBBN to match observations is not successful on the basis of an astrophysical solution due to stellar processes. In addition, resolving the lithium problem is not likely on purely nuclear physics ground (see Sec. 3.2). Therefore, we have introduced some nonstandard assumptions which seem to be a useful ingredient to ameliorate the lithium problem.
- Our efforts to use analytical expressions whenever suitable has the advantage to get better insight into the effect of nonstandard scenarios on the weak rates and the neutron mass fraction at the freeze-out. This allows us to better understand the dependence of light elements on different cosmological parameters and on each others, and to see the effect of the neutrino chemical potentials on the production of light elements.
- Another important stage of BBN is when the deuterium bottleneck (or maximum deuterium abundance) is reached. We have obtained explicit expressions of the temperature at which this bottleneck occurs, in addition we were able to find the temperature T^* when the neutron abundance decreases to that of deuterium.

This allows one to easily see how deuterium and all other light elements are related to these important stages of BBN.

- Beyond the analytical considerations, we have done numerical calculations to obtain limits on the neutrino chemical potentials that lead to a significant reduction of lithium. However, the desired reduction of lithium is achieved only if the deuterium increases to the maximum allowed value by observations.
- In a forthcoming paper,⁹⁶ the present analysis is extended by including the effect of additional nonstandard neutrino properties and a dark matter component.⁹ This also has the possibility to reduce the lithium abundance significantly.

Appendix A. Freeze-Out of Neutrons

The balance equation for the neutrons mass fraction X_n is given by

$$\frac{dX_n}{dt} = -\lambda_{n \rightarrow p} X_n + \lambda_{p \rightarrow n} X_p = -\lambda_{n \rightarrow p} (1 + e^{-\frac{Q}{T}}) (X_n - X_n^{\text{eq}}), \quad (\text{A.1})$$

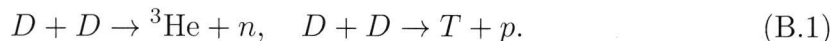
where $\lambda_{n \rightarrow p} = \lambda_{ne} + \lambda_{n\nu}$ and $\lambda_{p \rightarrow n} = \lambda_{pe} + \lambda_{p\bar{\nu}}$ which are the total rates of direct and inverse reactions respectively, $X_n^{\text{eq}} = \frac{1}{1 + \exp(\beta\nu_e) \exp(Q/T)}$, t is the time in seconds and T is the temperature in MeV. The solution of Eq. (A.1) is given as follows⁷⁷:

$$X_n(t) = X_n^{\text{eq}}(t) - \int_0^t \exp\left(-\int_{\tilde{t}}^t \lambda_{n \rightarrow p}(\tilde{t})(1 + e^{-\frac{Q}{\tilde{T}}}) d\tilde{t}\right) \dot{X}_n^{\text{eq}}(\tilde{t}) d\tilde{t} \quad (\text{A.2})$$

with the initial condition $X_n \rightarrow X_n^{\text{eq}}$ as $t \rightarrow 0$. The “dot” denotes the derivative with respect to time. To have an estimation for the freeze-out concentration, it is assumed that $X_n^{\text{eq}} \rightarrow 0$ as $T \rightarrow 0$ and $\lambda_{n \rightarrow p} \approx 2\lambda_{n\nu}$ because the main contribution of the integral comes from $T > m_e$. Therefore by replacing the integration variable t by $y = T/Q$ using Eq. (12) we obtain the expression for the freeze-out concentration given by Eq. (34). This is different from the one given by Ref. 77 because we included the neutrino chemical potential.

Appendix B. Deuterium Bottleneck

The deuterium bottleneck takes place when the main reactions converting deuterium into tritium and helium-3 become effective:



The mass fraction X_D of deuterium can be written as

$$\Delta X_D = -\frac{1}{2} \lambda_{DD} X_D^2 \Delta t, \quad (\text{B.2})$$

where $\lambda_{DD} = \lambda_{DD1} + \lambda_{DD2}$ are the rates of reactions given in Eq. (B.1) when a substantial amount of available deuterium is converted into ${}^3\text{He}$ within a cosmological time t , it is assumed that $\Delta X_D \approx X_D$. This assumption leads to Eq. (B.2).⁷⁷

However, we extended the calculation of deuterium bottleneck to include neutrinos chemical potential by integrating Eq. (B.2) so that

$$\frac{D}{H} \approx \frac{4 \times 10^{-3}}{X_p(k_{\text{eff}}^{-0.5} \times T_{\text{BN}}(\text{MeV}) \times \eta_{10} + C)}, \quad (\text{B.3})$$

where C is a constant which is time independent but it is function of neutrinos chemical potential. Therefore, Eq. (39) is obtained by constraining C with our numerical calculations.

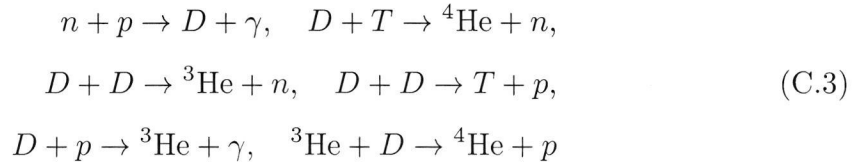
Appendix C. Final Deuterium Abundance

To calculate elements abundance we must deal with a system of kinetic equations.⁷⁷ For a reaction $AB \rightarrow CD$:

$$\dot{X}_A = -A_B^{-1} \lambda_{AB} X_A X_B, \quad (\text{C.1})$$

$$\dot{X}_c = A_c A_A^{-1} A_B^{-1} \lambda_{AB} X_A X_B. \quad (\text{C.2})$$

Here, $X_A = \frac{A_A n_A}{n_N}$ is the concentration by weight of the corresponding element (${}^4\text{He}, n, D \dots$), n_N is the total number of nucleons (baryons) and A is their mass number. For example, for the production and destruction of deuterium, we consider the following reactions:



and then the concentration of deuterium as function of time is given by

$$\begin{aligned} \frac{dX_D}{dt} &= 2\lambda_{pn} X_p X_n - \frac{1}{2} \lambda_{DD} X_D^2 - \lambda_{Dp} X_D X_p - \frac{1}{3} \lambda_{DT} X_D X_T \\ &\quad - \frac{1}{3} \lambda_{{}^3\text{He}D} X_D X_{{}^3\text{He}}, \end{aligned} \quad (\text{C.4})$$

where λ 's are the reaction rates of different reactions. Similarly kinetic equations for X_n , X_T , and $X_{{}^3\text{He}}$ can be obtained by taking into consideration all reactions producing and destroying n , T and ${}^3\text{He}$:

$$\frac{dX_n}{dt} = -\lambda_{pn} X_p X_n - \frac{1}{3} \lambda_{{}^3\text{He}n} X_{{}^3\text{He}} X_n + \frac{1}{4} \lambda_{DD1} X_D^2 + \frac{1}{6} \lambda_{DT} X_D X_T, \quad (\text{C.5})$$

$$\frac{dX_T}{dt} = \frac{3}{4} \lambda_{DD2} X_D^2 + \lambda_{{}^3\text{He}n} X_{{}^3\text{He}} X_n - \frac{1}{2} \lambda_{DT} X_D X_T, \quad (\text{C.6})$$

$$\frac{dX_{{}^3\text{He}}}{dt} = \frac{3}{4} \lambda_{DD1} X_D^2 + \frac{3}{2} \lambda_{Dp} X_D X_p - \lambda_{{}^3\text{He}n} X_n X_{{}^3\text{He}} - \frac{1}{2} \lambda_{{}^3\text{He}D} X_D X_{{}^3\text{He}}. \quad (\text{C.7})$$

Assuming the quasi-equilibrium condition for ${}^3\text{He}$ and T , $\frac{dX_T}{dt} \approx 0$ and $\frac{dX_{{}^3\text{He}}}{dt} \approx 0$, and using the time temperature relation of Eq. (12), Eqs. (C.4) and (C.5) can be written as

$$\frac{dX_D}{dT} = 4\alpha\eta_{10} \left(X_D^2 + R_2 X_D - \frac{1}{2} R_1 X_n \right), \quad (\text{C.8})$$

$$\frac{dX_n}{dT} = \alpha\eta_{10} (R_1 X_n - X_D^2), \quad (\text{C.9})$$

where

$$\eta_{10} = \eta \times 10^{10}, \quad (\text{C.10})$$

$$R_1 \equiv 4X_p \frac{\lambda_{pn}}{\lambda_{DD}} \approx (3 - 8) \times 10^{-3}, \quad (\text{C.11})$$

$$R_2 \equiv 2X_p \frac{\lambda_{pD}}{\lambda_{DD}} \approx (2.3 - 2.5) \times 10^{-5}, \quad (\text{C.12})$$

$$\alpha \equiv \alpha(T) = 0.86 \times 10^5 K(T). \quad (\text{C.13})$$

Here the experimental values of the ratio of the corresponding reaction rates are used. $K(T)$ describes the temperature dependence of $\langle\sigma v\rangle_{DD}$. Its value changes from 1 to 0.5 when the temperature drops from 0.09 MeV to 0.04 MeV. To calculate the deuterium abundance, two cases should be treated: the stage of nucleosynthesis when $X_D \ll X_n$ and the stage when neutron concentration becomes of order of deuterium concentration.⁷⁷

- (1) When $X_D \ll X_n$ so deuterium will satisfy the quasi-equilibrium condition $\frac{dX_D}{dT} \approx 0$. Since $R_2 \ll R_1$, the term $R_2 X_D$ will be small compared to $R_1 X_n$ and it follows from Eqs. (C.8) and (C.9) the following solution:

$$X_D = \sqrt{\frac{R_1 X_n}{2}} \left[1 + O\left(\frac{X_D}{X_n}\right) \right]. \quad (\text{C.14})$$

This solution is valid after deuterium concentration reaches its maximal value of order 10^{-3} but not valid after neutrons concentration drops to deuterium ones.

- (2) The second case is after neutron concentration becomes of order the deuterium concentration $X_D \sim X_n \sim R_1$:

$$\frac{dX_n}{dT} = \frac{1}{2} \alpha \eta_{10} R_1 X_1. \quad (\text{C.15})$$

At the beginning of nucleosynthesis at $T = T_{\text{BN}}$, most of the neutrons are still free so that the solution of Eq. (C.15) is given by

$$X_n(T) \approx 0.12 \times \exp\left(\frac{1}{2} \alpha \eta_{10} R_1 (T - T_{\text{BN}})\right) \quad (\text{C.16})$$

when neutron concentration drops to that of deuterium, using Eq. (C.16) we derived an approximate expression of T^* as given in Eq. (50) different from the one given in Ref. 77 because we included neutrinos chemical potential. After T^* is reached, the neutron concentration satisfies the quasi-equilibrium condition:

$$\frac{dX_n}{dT} \approx 0 \rightarrow X_n = \frac{1}{R_1} X_D^2 \left[1 + O\left(\frac{X_n}{X_D}\right) \right] \quad (\text{C.17})$$

and Eq. (C.8) becomes

$$\frac{dX_D}{dT} = 2\alpha\eta_{10}(X_D^2 + 2R_2X_D). \quad (\text{C.18})$$

To find the final abundance of deuterium we must integrate Eq. (C.18) between T and T^* , therefore we can assume the general expression of D/H as given in Eq. (51) where $F(T^*)$ can be constrained with our numerical calculations.

Acknowledgments

The authors thank the anonymous referee for the valuable comments. They would also thank Prof. Maurizio Busso and Prof. Massimo Barbagallo for the discussion about the nuclear reactions. Tahani Makki thanks the National Council for Scientific Research (CNRS) for supporting this research and the dean's office of the faculty of arts and sciences at the American university of Beirut for supporting travel to international meetings.

References

1. K. Abazajian *et al.*, *Phys. Rev. D* **64**, 023501 (2001).
2. KamLAND Collab. (S. Abe *et al.*), *Phys. Rev. Lett.* **100**, 221803 (2008).
3. Double Chooz Collab. (Y. Abe *et al.*), *Phys. Rev. D* **86**, 052008 (2012).
4. SNO Collab. (B. Aharmim *et al.*), *Phys. Rev. C* **88**, 025501 (2013).
5. J. H. Applegate *et al.*, *Phys. Rev. D* **35**, 1151 (1987).
6. E. Aver *et al.*, *J. Cosmol. Astropart. Phys.* **2010**(05), 003 (2010).
7. E. Aver *et al.*, arXiv:1503:08146.
8. A. Arbey *et al.*, arXiv:1806.11095.
9. A. Arbey, *AIP Conf. Proc.* **1241**, 700 (2009).
10. M. Asplund *et al.*, *Astrophys. J.* **644**, 229 (2006).
11. T. M. Bania *et al.*, *Nature* **415**, 54 (2002).
12. S. A. Balashev *et al.*, *Mon. Not. R. Astron. Soc.* **458**, 2188 (2016).
13. F. Balestra *et al.*, *Nuovo Cimento A* **100**, 323 (1988).
14. M. Barbagallo *et al.*, *Phys. Rev. Lett.* **117**, 152701 (2016).
15. M. Barbagallo *et al.*, *EPJ Web Conf.* **146**, 01012 (2017).
16. A. Boyarsky *et al.*, *Phys. Rev. Lett.* **97**, 261302 (2006).
17. P. Bonifacio and P. Molar, *Mon. Not. R. Astron. Soc.* **285**, 847 (1997).
18. P. Bonifacio, P. Molaro and L. Pasquini, *Mon. Not. R. Astron. Soc.* **292**, L1 (1997).
19. P. Bonifacio *et al.*, *Astron. Astrophys.* **390**, 91 (2002).
20. S. Burles and D. Tytler, *Astrophys. J.* **499**, 699 (1998).
21. S. Burles and D. Tytler, *Astrophys. J.* **507**, 732 (1998).
22. A. Coc and E. Vangioni, *Int. J. Mod. Phys. E* **26**, 1741002 (2017).

23. R. Cai *et al.*, *JHEP* **2008**(08), 090 (2008).
24. C. Charbonnel and F. Primas, *Astrophys. J.* **442**, 961 (2005).
25. R. J. Cooke *et al.*, *Astrophys. J.* **781**, 31 (2014).
26. R. H. Cyburt, B. D. Fields and K. A. Olive, *J. Cosmol. Astropart. Phys.* **2008**(11), 012 (2008).
27. R. H. Cyburt *et al.*, *J. Cosmol. Astropart. Phys.* **2009**(10), 021 (2009).
28. R. H. Cyburt, B. D. Fields and K. A. Olive, *Rev. Mod. Phys.* **88**, 015004 (2016).
29. A. De Gouvea *et al.*, arXiv:1310.4340.
30. A. D. Dolgov and S. H. Hansen, *Astropart. Phys.* **16**, 339 (2002).
31. A. D. Dolgov and F. Takahshi, *Nucl. Phys. B* **688**, 189 (2004).
32. S. Esposito *et al.*, *JHEP* **2000**(09), 038 (2000).
33. V. Fernandez *et al.*, arXiv:1804.10701.
34. B. Fields and K. Olive, *Nucl. Phys. A* **777**, 208225 (2006).
35. B. D. Fields, *Annu. Rev. Nucl. Part. Phys.* **61**, 47 (2011).
36. M. Foley *et al.*, *Int. J. Mod. Phys. E* **26**, 1741008 (2017).
37. M. Fukugita and M. Kawasaki, *Astrophys. J.* **646**, 691 (2006).
38. R. Galvez and R. Sherrer, *Phys. Rev. D* **95**, 063507 (2017).
39. A. Goudelis *et al.*, *Phys. Rev. Lett.* **116**, 211303 (2016).
40. G. Hinshaw *et al.*, arXiv:1212.5226.
41. S. Q. Hou *et al.*, *Astrophys. J.* **834**, 165 (2017).
42. S. Q. Hou *et al.*, *Phys. Rev. C* **91**, 055802 (2015).
43. S. Hansen *et al.*, *Phys. Rev. D* **65**, 023511 (2001).
44. Y. I. Izotov *et al.*, *Astrophys. J. Suppl. Ser.* **108**, 1 (1997).
45. Y. I. Izotov and T. X. Thuan, *Astrophys. J.* **602**, 200 (2004).
46. Y. I. Izotov and T. X. Thuan, *Astrophys. J. Lett.* **710**, L67 (2010).
47. F. Iocco, *Mem. S. A. It. Suppl.* **22**, 19 (2012).
48. K. Jedamzik, *Phys. Rev. D* **74**, 103509 (2006).
49. K. Jedamzik *et al.*, *Astrophys. J.* **423**, 50 (1994).
50. H. Kang and G. Steigman, *Nucl. Phys. B* **372**, 494 (1992).
51. J. P. Kneller and G. Steigman, *New J. Phys.* **6**, 117 (2004).
52. K. M. Nollett and G. Steigman, *Phys. Rev. D* **91**, 083505 (2015).
53. N. Komatsu and S. Kimura, *Phys. Rev. D* **87**, 043531 (2013).
54. A. J. Korn *et al.*, *Nature* **442**, 657 (2006).
55. M. Kusakabe *et al.*, *Phys. Rev. D* **90**, 045009 (2014).
56. M. Kusakabe *et al.*, *Int. J. Mod. Phys. E* **26**, 1741004 (2017).
57. D. Larson *et al.*, *Astrophys. J. Suppl.* **192**, 16 (2011).
58. J. Lesgourgues and S. Pastor, *Adv. High Energy Phys.* **2012**, 608515 (2012).
59. S. A. Levshakov *et al.*, *Astrophys. J.* **565**, 696 (2002).
60. K. Lind *et al.*, *Astron. Astrophys.* **554**, A96 (2013).
61. C. Lunardini and A. Yu. Smirnov, *Phys. Rev. D* **64**, 073006 (2001).
62. V. Luridiana *et al.*, *Astrophys. J.* **592**, 2 (2003).
63. R. Nakamura *et al.*, *Int. J. Mod. Phys. E* **26**, 1741003 (2017).
64. K. A. Olive *et al.*, *Phys. Lett. B* **265**, 239 (1991).
65. K. Olive *et al.*, *Mon. Not. R. Astron. Soc.* **426**, 1427 (2012).
66. B. E. J. Pagel *et al.*, *Mon. Not. R. Astron. Soc.* **255**, 325 (1992).
67. Particle Data Group (C. Patrignani *et al.*), *Chinese Phys. C* **40**, 100001 (2016); Particle Data Group (M. Tanabashi *et al.*), *Phys. Rev. D* **98**, 030001 (2018).
68. M. Peimbert *et al.*, *Astrophys. J.* **666**, 636 (2007).
69. A. Peimbert *et al.*, arXiv:1608.02062.
70. O. Pisanti *et al.*, *Comput. Phys. Commun.* **178**, 956 (2008).

71. C. Pitrou *et al.*, *Phys. Rep.* **754**, 1 (2018).
72. P. A. R. Ade *et al.*, *Astron. Astrophys.* **594**, A13 (2016).
73. R. Malaney and G. Mathews, *Phys. Rep.* **229**, 145 (1993).
74. G. J. Mathews *et al.*, *Astrophys. J.* **358**, 36 (1990).
75. G. J. Mathews *et al.*, *Int. J. Mod. Phys. E* **26**, 1741001 (2017).
76. J. Melendez *et al.*, *Astrophys. J.* **615**, L33 (2004).
77. V. Mukhanov, The hot universe in *Physical Foundations of Cosmology* (Cambridge Univ. Press, 2005), Chap. 3, pp. 69–130.
78. K. Olive *et al.*, *Astrophys. J.* **483**, 788 (1997).
79. M. Orito *et al.*, arXiv:astro-ph/0005446.
80. M. H. Pinsonneault *et al.*, *Astrophys. J.* **574**, 398 (2002).
81. I. Ribas *et al.*, *Mon. Not. R. Astron. Soc.* **313**, 99 (2000).
82. S. G. Ryan *et al.*, *Astrophys. J.* **523**, 654 (1999).
83. J. Sato *et al.*, *Int. J. Mod. Phys. E* **26**, 1741005 (2017).
84. L. Sbordone *et al.*, *Astron. Astrophys.* **522**, A26 (2010).
85. D. J. Schwarz and M. Stuke, *New J. Phys.* **15**, 033021 (2013).
86. R. J. Scherrer and M. S. Turner, *Astrophys. J.* **331**, 33 (1988).
87. R. J. Scherrer and M. S. Turner, *Astrophys. J.* **331**, 19 (1988).
88. A. S. Sefiedgar, *Adv. High Energy Phys.* **2014**, 727245 (2014).
89. G. F. Smoot *et al.*, *Astrophys. J.* **396**, L1 (1992).
90. X. Shi, *Phys. Rev. D* **54**, 2753 (1996).
91. M. Spite and F. Spite, *Nature* **297**, 483 (1982).
92. R. Srikanand *et al.*, *Mon. Not. R. Astron. Soc.* **405**, 1888 (2010).
93. G. Steigman, *Adv. High Energy Phys.* **2012**, 268321 (2012).
94. G. Steigman, *Annu. Rev. Astron. Astrophys.* **14**, 339 (1976).
95. T. Kajita, *Experimental Studies of Neutrino Oscillations* (World Scientific, 2016).
96. T. R. Makki, M. F. El Eid and G. J. Mathews, arXiv:1901.03726.
97. D. G. Yamazaki *et al.*, *Phys. Rev. D* **90**, 023001 (2014).
98. D. G. Yamazaki *et al.*, *Int. J. Mod. Phys. E* **26**, 1741006 (2017).
99. S. Yoshida *et al.*, *Phys. Rev. Lett.* **81**, 5505 (1998).
100. S. Villonava *et al.*, *Astron. Astrophys.* **499**, 755 (2009).
101. V. Wagoner *et al.*, *Astrophys. J.* **148**, 3 (1967).
102. Super-Kamiokande Collab. (R. Wendell *et al.*), *Phys. Rev. D* **81**, 092004 (2010).

Accepted for publication

International Journal of Modern Physics E
© World Scientific Publishing Company

Impact of Neutrino Properties and Dark Matter on the Primordial Lithium Production

Tahani R. Makki

Department of Physics, American University of Beirut, Lebanon
trm03@mail.aub.edu

Mounib F. El Eid

Department of Physics, American University of Beirut, Lebanon
meid@aub.edu.lb

Grant J. Mathews

Department of Physics, Center for Astrophysics, University of Notre Dame, USA
gmathews@nd.edu

Received Day Month Year

Revised Day Month Year

The light elements and their isotopes were produced during standard big bang nucleosynthesis (SBBN) during the first minutes after the creation of the universe. Comparing the calculated abundances of these light species with observed abundances, it appears that all species match very well except for lithium (${}^7\text{Li}$) which is overproduced by the SBBN. This discrepancy is rather challenging for several reasons to be considered on astrophysical and on nuclear physics ground, or by invoking non-standard assumptions which are the focus of the present paper. In particular, we consider a variation of the chemical potentials of the neutrinos and their temperature. In addition, we investigated the effect of dark matter on ${}^7\text{Li}$ production. We argue that including non-standard assumptions can lead to a significant reduction of ${}^7\text{Li}$ abundance compared to that of SBBN. This aspect of lithium production in the early universe may help to resolve the outstanding cosmological lithium problem.

Keywords: Big Bang Nucleosynthesis; Lithium Problem; Non-Standard Physics.

PACS numbers:

1. Introduction

Big bang nucleosynthesis (BBN) can accurately account for inferred primordial abundances of light elements except for the isotope ${}^7\text{Li}$. Once the baryon-to-photon ratio η fixed by analysis² of the cosmic microwave background (CMB), the primordial abundance of ${}^7\text{Li}$ deduced from Li surface absorption lines observed on the surface of metal-poor halo stars⁵ is about a factor of three below that predicted by BBN. This is called the "Lithium Problem".⁶ The lithium problem is difficult

2 Authors' Names

to resolve. The reason is that not only the nuclear physics involved in its production should be considered, but also astrophysical and non-standard cosmological aspects. The main concern of this work is to investigate the effect of neutrinos and dark matter on the production of light elements during big bang nucleosynthesis (BBN), especially on lithium. It is emphasized that these non-standard scenarios require observational constraints on light elements and updated parameters from the analysis of the cosmic microwave background (CMB). These are based upon a calculation for the specified values of the effective number of relativistic species, N_{eff} , the neutron lifetime τ_n , and the baryon to photon ratio η_{BBN} during BBN. This paper is outlined as follows: in section 2, we discuss observational constraints on light elements that should be adopted when including non-standard scenarios. The limits on N_{eff} from cosmology and astrophysics are discussed in section 3. This will be an important parameter in constraining non-standard scenarios. In sections 4 we investigate whether neutrinos are possible candidates for dark matter. In section 5 we give a fast overview of varying neutrino temperature as treated in more detail in Ref. 1. Since this model alone does not help to reduce the lithium abundance, we extend this calculation by including neutrino chemical potentials. This is presented in section 6 where the results have led to a decrease of lithium at the expense of a large N_{eff} which is not supported by recent CMB observations. In section 7, we review the model of photon cooling with axion dark matter after BBN.³³ This model is extended in section 8 by including also the effect of non-standard neutrino properties where we have achieved a reduction of lithium with a value of N_{eff} compatible with recent CMB observations, but it is still higher than that inferred from the Planck analysis.² To satisfy the requirements on N_{eff} as predicted by Planck, we have treated the effect of a dark fluid³ which is presented in section 9. Concluding remarks are given in section 10.

2. Observational constraints on light elements

The predicted light element abundances by SBBN are shown in Table 1. They are in agreement with the observed values except for ${}^7\text{Li}$ as inferred from the observations of metal-poor halo stars. In addition, the extension of observations to very low metallicity below $[Fe/H] = -3$ are inconsistent with the expected "Spite Plateau"⁴ requiring a constant abundance of lithium as metallicity decreases. Up to now, resolving this problem has not been achieved on purely astrophysical or nuclear physics grounds. Therefore, it is worthwhile to focus on non-standard scenarios including non-standard neutrino properties along with dark matter effects. The goal of these non-standard scenarios is to decrease the abundance of lithium below that predicted by SBBN while taking into account the observational constraints on other light elements. These conservative constraints are adopted from many observations as follows:

- The constraints on ${}^4\text{He}$ are usually taken from direct measurements of extragalactic low-metallicity HII regions. However, in this work, we will

| | |
|---|------------------------|
| $N_\nu = 3, \tau_n = 880.2s$ and $\eta_{BBN} = (6.14 \pm 0.04) \times 10^{-10}$ | |
| Y_p | 0.2461 ± 0.0001474 |
| $D/H \times 10^5$ | 2.653 ± 0.123 |
| ${}^3\text{He}/H \times 10^5$ | 1.017 ± 0.053 |
| ${}^7\text{Li}/H \times 10^{10}$ | 4.283 ± 0.378 |

Table 1. Light element abundances predicted by SBBN after updating the AlterBBN code.³⁹

take the recent independent measurement by Ref. 7 where $Y_p = 0.250_{-0.025}^{+0.033}$ or $0.225 \leq Y_p \leq 0.283$. This expanded range allows for an investigation of non-standard physics during BBN.

- There are 15 measurements of the primordial deuterium that show a large dispersion in the mean values and the estimated errors. Hence, it is too early to talk about deuterium plateau. The most precise measurement is given by Ref. 8 who obtained $D/H = (2.53 \pm 0.04) \times 10^{-5}$. However, a following measurement¹⁹ for a system that meets the set of strict criteria by Ref. 8 shows a different value for the primordial deuterium abundance where $D/H = (1.97_{-0.28}^{+0.33}) \times 10^{-5}$. It has been argued²⁰ that higher values near the upper limit of the observed deuterium may be more representative of the true primordial abundance compared with systems where the deuterium abundance would have been subject to destruction. In addition, because of their fragility, deuterons can be destroyed easily if there is a source of non-thermal photons in the early universe.²² Therefore in this work we adopt the conservative range of deuterium of $2.58 \times 10^{-5} \leq D/H \leq 3.75 \times 10^{-5}$.
- While the true primordial abundance of lithium is not understood yet, primordial lithium abundance is recently taken to be ${}^7\text{Li}/H = (1.6 \pm 0.3) \times 10^{-10}$.²³ However, in this work, we will adopt a higher upper limit of lithium of ${}^7\text{Li}/H \leq 2.8 \times 10^{-10}$ assuming that achieving this limit by non-standard treatment is sufficient and any remaining difference can be explained by stellar processing.

3. Neutrinos and the effective degrees of freedom

One possible extension of the SBBN is to allow the number of neutrinos to be different from three. However, the effective number of relativistic degrees of freedom N_{eff} is not allowed to vary freely due to its effect on both the CMB and SBBN predictions. The combination of seven-year WMAP data with Baryon Acoustic Oscillations in the distribution of galaxies and the Hubble parameter H_0 leads to $N_{eff} = 4.43_{-0.88}^{+0.86}$.²⁴ However, the nine-year WMAP³⁶ put more stringent limits on N_{eff} to be $N_{eff} = 3.84 \pm 0.40$. While limits on N_{eff} from SBBN have been intensively investigated,^{25,26} limits from astrophysics and cosmology are also important. We mention here the limit given in Ref. 27 where $N_{eff} < 3.8$ was deduced from the

4 *Authors' Names*

CMB lensing, baryon acoustic oscillations, and galaxy clustering data. Limits on N_{eff} are still a matter of debate and we still need a more accurate determination of N_{eff} . In what follows we will adopt the more stringent range of N_{eff} from the more recent analysis of Planck² to which $2.48 < N_{eff} < 3.5$ (3σ).

4. Neutrinos as a candidate for dark matter

While we know several aspects of dark matter such as its present energy density and distribution, we don't have much information about its identity and production mechanism. Since baryons do not contribute to dark matter, one can think of neutrinos or their decay products as possible candidates³⁰ since neutrinos are now known to have mass. The role of massive and unstable neutrinos in the formation of structure in the early universe is also discussed in Ref. 15. Also, CP violating effects in neutrino oscillations generating an (anti)neutrino excess have been considered.^{11,14} Here we consider a sterile neutrino, which is a hypothetical new generation of neutrinos other than the three active species, can be produced non-thermally by active-sterile mixing and particle decays.²⁸ The role of sterile neutrinos in cosmology strongly depends on the magnitude of their mass, so that a sterile neutrino with a mass the order of keV could be a viable candidate for dark matter.²⁹ If this would be the case, such dark matter could be detectable in the extragalactic x-rays due to its radiative decay channel.³⁰ Constraints on the properties of a dark matter sterile neutrino (sterile neutrino mass and mixing parameter θ between active and sterile neutrinos) are given in Ref. 29 where the Milky Way halo and halo of dwarf galaxies are the best objects for the search of dark matter with a radiative decay channel.

A new investigation into the possibility of detection of sterile neutrinos of mass 50 keV in dark matter searches is given by Ref. 31. However, these searches are confronted by two problems: the expected event amount of energy to be received by the detector and the expected event rate. Although sterile neutrinos are heavy, they cannot be detected by standard dark matter experiments. For these reasons, electron neutrino scattering is considered by using systems with very small electron binding in order to have a high event rate. In addition, nuclear physics options (the absorption of an antineutrino on electron capturing nuclear system) and atomic physics (possibility of spin induced excitations) may be useful in detecting sterile neutrino dark matter.³¹ Therefore, since explaining dark matter on the basis of the standard model is not likely, many searches with astrophysical and laboratory experiments are being used to check the possibility of a sterile neutrino dark matter candidate.³²

5. Variation of neutrino temperature

During BBN and after the phase of electron-positron annihilation, the ratio of the neutrino temperature to the photon temperature is given by the standard relation:³⁵

$$\left(\frac{T_\nu}{T_\gamma}\right)_0^3 = \frac{4}{2g_s(T_{\nu d}) - 10.5}, \quad (1)$$

where $T_{\nu d}$ is the neutrino decoupling temperature and g_s is the number of relativistic degrees of freedom contributing to the total entropy, or equivalently, the ratio of the total entropy to the entropy of photons. This determines the effective number of neutrinos given by:

$$N_{eff}^0 = 3 \left[\frac{11}{4} \left(\frac{T_\nu}{T_\gamma}\right)_0^3 \right]^{4/3} = 3 \left[\frac{11}{2g_s(T_{\nu d}) - 10.5} \right]^{4/3} \quad (2)$$

These degrees of freedom contribute to the total entropy so that $g_s = \frac{7}{8} \times (g_\nu + g_{e^\pm}) + g_\gamma = 10.75$ where $g_\nu = 6$, $g_{e^\pm} = 4$ and $g_\gamma = 2$ are the degrees of freedom of neutrinos, electrons-positrons, and photons respectively.

The effect on BBN from the presence of heavy particles^{16,17} and or decay of unstable particles or primordial black holes^{12,13} have been discussed extensively in the literature.^{10,18} Here, we note that the presence of a massive particle, such as weakly interacting massive particles (WIMP's) will modify Eq. (1) and Eq. (2) above. When a WIMP couples to neutrinos or to photons, they speed up the expansion rate because they can alter the energy density of relativistic particles. In addition to the heating of e^\pm , the annihilation of WIMP's can heat the photons. WIMP's can also share some of the entropy with neutrinos which causes the neutrino temperature to be different than that of the SBBN.

Therefore, the neutrino temperature can receive different contributions either directly by WIMP interactions or by adding a dark component namely heating /cooling of photon relative to neutrino temperature which will be discussed in sections 7 and 8. In what follows, we represent the variation of neutrino temperature by a multiplicative factor α regardless of the source as treated by Ref. 1.

6. Effect of varying neutrino temperature and chemical potential on the lithium production

As noted in Ref. 1, since the total neutrino energy density is proportional to $N_\nu T_\nu^4$, a variation in the neutrino temperature can be translated into a variation in the effective number of neutrinos through:

$$N_{eff} T_{\nu SM}^4 = N_\nu T_\nu^4, \quad (3)$$

where $T_{\nu SM}$ is the standard neutrino temperature, N_{eff} is the effective number of neutrinos derived from the cosmic microwave background (CMB) and N_ν is the number of neutrinos present during SBBN. In SBBN, $N_{eff} = N_\nu$ because

$T_{\nu SM} = T_\nu$ in Eq. (3). However, if we deviate from SBBN, this leads to a difference between N_{eff} and N_ν after neutrino decoupling. It is clear from Eq. (3) that we can vary two parameters while the third will depend upon the other two. For example, if the neutrino temperature is modified by a factor alpha, $T_\nu = \alpha T_{\nu SM}$ for a fixed N_ν , then N_{eff} will depend on these two parameters. As obtained by Ref. 1, $N_\nu = 5$ is ruled out for any change in T_ν and $N_{eff} = 3.15 \pm 0.23$. In addition, no ranges for N_ν and T_ν are available that can reduce the lithium abundance significantly. However, the range of N_{eff} is model dependent, and if one relaxes the BBN constraint, one can allow for a broader range based upon the Planck constraint. In the present work, in addition of varying the number of neutrinos and their temperature as treated by Ref. 1, we also vary the ratio of chemical potential to temperature $\beta_{\nu\mu,\tau,e}$, which we will henceforth simply refer to as the "chemical potential". In other words, we vary the number of neutrinos contributing to BBN between 3 and 20 ($3 \leq N_\nu \leq 20$) and we derive ranges of N_{eff} (or equivalently α) and $\beta_{\nu\mu,\tau,e}$ that reproduce the SBBN predictions or reduce lithium abundance significantly.

In this context, Tables 2 and 3 are obtained as follows:

The neutrino temperature is modified by a factor α where neutrino chemical potentials $\beta_{\nu\mu,\tau,e}$ are taken to be equal. Since the total neutrino energy density is given by:

$$\rho_\nu + \rho_{\bar{\nu}} = \frac{7\pi^2}{240} g_\nu \left[1 + \frac{30\beta^2}{7\pi^2} + \frac{15\beta^4}{7\pi^4} \right] T_\nu^4, \quad (4)$$

then Eq.(3) is modified as follows:

$$N_{eff} T_{\nu SM}^4 = N_{\nu 0} \left(1 + \frac{30\beta^2}{7\pi^2} + \frac{15\beta^4}{7\pi^4} \right) T_\nu^4 + \Delta N_\nu T_\nu^4 \quad (5)$$

Consequently, the effective number of neutrinos N_{eff} can be written explicitly as:

$$N_{eff} = \alpha^4 \times N_{\nu 0} \left(1 + \frac{30\beta^2}{7\pi^2} + \frac{15\beta^4}{7\pi^4} \right) + \alpha^4 \times \Delta N_\nu \quad (6)$$

Eqs.(5, 6) include the three standard neutrino species $N_{\nu 0}$ with their chemical potentials while ΔN_ν is for extra relativistic species not contributing to the chemical potential with $\Delta N_\nu = N_\nu - N_{\nu 0}$. Restricting ourselves to the predicted light element abundances by SBBN (see Table 1) and to the ranges of N_{eff} from Planck² $2.48 < N_{eff} < 3.5$ (3σ), we obtain the following ranges which reproduce the SBBN predictions within the quoted errors (see Table 2):

$$\begin{aligned} 3 \leq N_\nu \leq 20, \quad 2.48 \leq N_{eff} \leq 3.5 \\ 0.593 \leq \alpha \leq 1.039, \quad 0 \leq \beta_{\nu\mu,\tau,e} \leq 0.3 \end{aligned} \quad (7)$$

The effect of varying $\beta_{\nu\mu,\tau,e}$, N_ν and α on the abundances of light elements can be explained as follows:

- (1) The effect of varying the number of neutrinos N_ν :

The increase in the number of neutrinos N_ν will lead to an increase in the

Instructions for typing manuscripts (paper's title) 7

energy density ρ of the universe and consequently the expansion rate given by Eq.(8).

$$H^2 = \frac{8\pi G}{3}\rho \quad (8)$$

with,

$$\rho = \rho_\gamma + \rho_f = k_{eff}T^4, \quad (9)$$

where ρ_γ and ρ_f represent the energy density of photons and fermions respectively. Before electron-positron annihilation k_{eff} is given by:

$$k_{eff} = \frac{\pi^2}{30}(g_\gamma + \frac{7g_{e^\pm}}{8} + \frac{7}{8}\alpha^4 \times g_\nu), \quad (10)$$

while after electron-positron annihilation,

$$k_{eff} = \frac{\pi^2}{30}(g_\gamma + \frac{7}{8}\alpha^4 \times g_\nu \times (\frac{4}{11})^{4/3}), \quad (11)$$

with $g_\gamma = 2$, $g_{e^\pm} = 4$ and $g_\nu = 6$ refer to degrees of freedom of photon, electron-positron pairs, and three standard neutrino species respectively.

Varying the number of neutrinos N_ν will change the relativistic degrees of

| $\beta_{\nu,\mu,\tau,e}$ | α | N_{eff} | N_ν | Yp | $D/H \times 10^5$ | ${}^7Li/H \times 10^{10}$ |
|--------------------------|----------|-----------|---------|--------|-------------------|---------------------------|
| 0.00 | 1.00 | 3.0000 | 3 | 0.2461 | 2.653 | 4.283 |
| 0.08 | 0.87 | 2.8693 | 5 | 0.2465 | 2.624 | 4.350 |
| 0.19 | 0.73 | 2.8532 | 10 | 0.2460 | 2.614 | 4.356 |
| 0.3 | 0.63 | 3.1691 | 20 | 0.2465 | 2.703 | 4.193 |

Table 2. Effect of varying neutrino number, chemical potential, and temperature on SBBN predictions.

| $\beta_{\nu,\mu,\tau,e}$ | α | N_{eff} | N_ν | Yp | $D/H \times 10^5$ | ${}^7Li/H \times 10^{10}$ |
|--------------------------|----------|-----------|---------|--------|-------------------|---------------------------|
| 0 | 1 | 3 | 3 | 0.2461 | 2.653 | 4.285 |
| 0 | 1 | 6 | 6 | 0.2795 | 3.699 | 3.321 |
| 0.15 | 1 | 6.0293 | 6 | 0.2423 | 3.420 | 3.040 |
| 0.25 | 0.99 | 6.8026 | 7 | 0.2265 | 3.491 | 2.713 |
| 0.25 | 1.02 | 7.5518 | 7 | 0.2272 | 3.697 | 2.526 |
| 0.41 | 0.77 | 7.1083 | 20 | 0.2333 | 3.611 | 2.695 |

Table 3. Effect of varying neutrino number, chemical potential and temperature on lithium.

freedom, then the time temperature relation given by Eq.(12). This affects final element abundances.

$$t_{sec} \simeq \frac{1.39k_{eff}^{-1/2}}{T^2} \quad (12)$$

8 *Authors' Names*

The cosmological time is given in seconds and the temperature in Mev.

The first two rows of Table 3 show that increasing neutrino number from $N_\nu = 3$ to $N_\nu = 6$ leads to an increase in the helium and deuterium abundances but to a decrease in the abundance of lithium.

- (2) The effect of a neutrino chemical potential:

Adding a neutrino chemical potential $\beta_{\nu_{\mu,\tau,e}}$ will have two effects: the first is modifying the neutrino energy density (see Eq.(4) and hence, the expansion rate of the universe. The second is due to the effect of the electron-neutrino on the weak rates given by Eq.(13).³⁸ Adding a positive chemical potential $\beta_{\nu_{\mu,\tau,e}}$ will enhance the weak rates so that more neutrons are converted into protons. This will lead to a decrease in the abundances of ^4He , D and ^7Li as seen in the third row of Table 3. Note that equating all chemical potentials will lead to a large effect of the electron neutrino chemical potential and consequently a significant effect on ^4He due to its sensitivity to the neutron mass fraction at the freeze-out.

$$\lambda_{n\nu} \approx 1.63 \exp(+\beta_{\nu_e}) \left(\frac{T_\nu}{Q}\right)^3 \left(\frac{T_\nu}{Q} + 0.25\right)^2 s^{-1}, \quad (13)$$

- (3) The effect of varying the neutrino temperature by a factor α :

Multiplying the neutrino temperature by a factor α , will modify k_{eff} as shown in Eqs.(10, 11) and consequently the expansion rate and the time temperature relation given by Eq.(12). This temperature variation mainly affects deuterium. We also note that changing the effective neutrino temperatures also can alter the weak rates (see Eq.(13)) and thus affect the neutron to proton ratio n/p . This would affect the primordial helium abundance.

As shown in Fig. 1, multiplying neutrino temperature by a factor of 1.5 affects the abundance of deuterium at the bottleneck and consequently the final deuterium abundance. For $\alpha = 1.5$, deuterium abundance increases by about 63% while helium increases by 12%. In this case, the weak rates and the expansion rate of the universe are both enhanced, and since the variation of the neutrino temperature is taken after decoupling of neutrinos but before the deuterium formation epoch, we see that deuterium is more affected than helium (see fourth and fifth rows in Table 3).

- (4) To understand the effect of these non-standard scenarios on lithium, we have derived some analytic calculations following the ones given by Ref. 37 (see Ref. 38 for a detailed discussion). Those analytic expressions allow us to understand the dependence of light elements during three stages of BBN namely, the freeze-out of neutrons, the deuterium bottleneck and when the neutron concentration drops to that of deuterium. Eq.(14) gives an approximate estimation of the abundance of beryllium as a function of other light elements. Since more than 90% of beryllium will be converted into lithium by electron capture after the BBN epoch, Eq.(14) controls the final abundance of lithium and it shows clearly the connection between beryllium, helium, and deuterium. As seen in

Fig. 1, the increase in deuterium leads to a decrease in the beryllium abundance due to the anti-correlation relation between these two elements. Meanwhile, if 90% of the final abundance of lithium comes from the electron capture of beryllium, the remaining 10% comes from the reactions leading to lithium where the dependence of lithium on helium and tritium is given by Eq.(15). For this reason, the increase in helium and tritium have led to an increase in the lithium abundance as shown in Fig. 1. We are interested in the final abundance of lithium (${}^7\text{Li}+{}^7\text{Be}$), then the decrease in the final abundance of lithium as shown in the seventh column of Table 3 is due to the dominant effect on beryllium.

$$\frac{{}^7\text{Be}}{\text{H}} \approx 9 \times 10^{-14} \times \frac{Y_p \times \frac{{}^3\text{He}}{\text{H}}}{X_p \times \left(\frac{D}{\text{H}}\right)^2}. \quad (14)$$

$$\frac{{}^7\text{Li}}{\text{H}} \approx 9 \times 10^{-4} \times \frac{Y_p}{X_p} \left(\frac{{}^3\text{H}}{\text{H}} + 2.57 \times 10^{-3} \times \frac{{}^3\text{He}}{\text{H}} \right), \quad (15)$$

where X_p is the proton mass fraction.

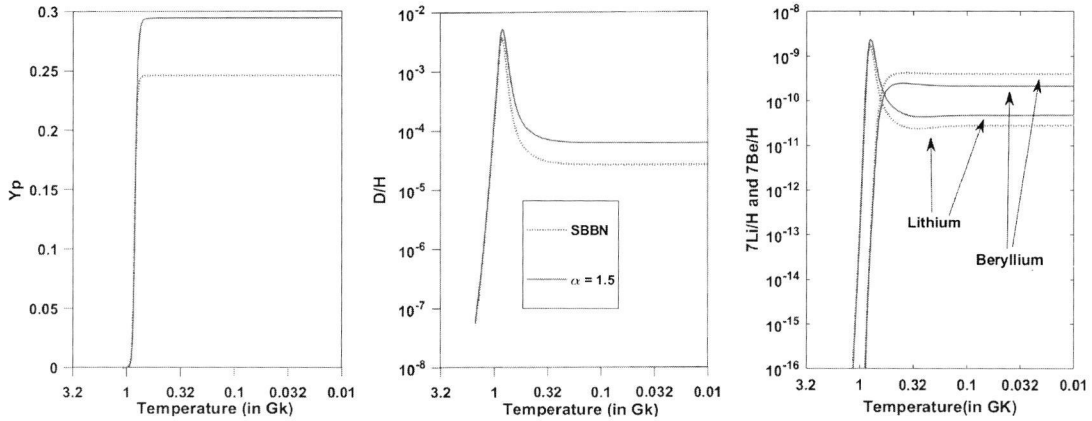


Fig. 1. light element abundances as a function of temperature for $\alpha = 1.5$ (blue solid lines) compared to SBBN abundances (red dashed lines).

An inspection of Table 2 shows that the abundances predicted by SBBN can be obtained by the non-standard assumption described above. In other words, despite these variations of neutrino temperature and chemical potentials, the abundances predicted by SBBN are not affected. However, in order to obtain a substantial reduction of the lithium abundance, the ranges of Table 2 must be extended. This

is achieved if the following ranges are adopted:

$$\begin{aligned} 3 \leq N_\nu \leq 20, \quad 6.62 \leq N_{eff} \leq 7.92, \\ 0.76 \leq \alpha \leq 1.27, \quad 0.02 \leq \beta_{\nu_{\mu,\tau,e}} \leq 0.45 \end{aligned} \quad (16)$$

Then, if we choose any N_ν , we can achieve a reduction of lithium by a combination of α and $\beta_{\nu_{\mu,\tau,e}}$. Some of these combinations are shown in Table 3 in order to illustrate the importance of these parameters on SBBN. We emphasize that the above results are compatible with all successful models that lead to a substantial decrease in lithium at the expense of increasing deuterium to the maximum value allowed by observations as discussed in section 2. This result could be promising if the obtained limits on N_{eff} matched the CMB limits. However, the obtained ranges on N_{eff} shown in Eq.(16) motivated us to extend this scenario by taking into consideration the effect of dark matter to conserve the limits on N_{eff} . Possible effects of dark matter on lithium will be the focus of the next sections.

7. Axion dark matter

Axions produced during the QCD phase transition could be a possible candidate for cold dark matter (CDM) where its density is well determined by the WMAP and Planck missions. This axion dark matter will have an average momentum of order the Hubble expansion rate and they satisfy the CDM density if they would have a mass of the order of $10^{-5} \text{eV}/c^2$. With this mass range, axions interact weakly through all forces except gravity which makes them a promising candidate for CDM.³³

An investigation into the interaction of axion-like dark matter with gluons by searching for a time oscillating neutron has been performed by Ref. 34. They also investigated the effect of axion-wind spin-precession to search for the interaction of axion-like dark matter with nucleons. This led to improvements upon existing astrophysical limits on the axion-gluon coupling and existing laboratory limits on the axion-nucleon coupling.

The question arises about the effect of axion dark matter on BBN. An example of such an effect was investigated in Ref. 33 where photon cooling through the gravitational field of cold axions after BBN had a significant effect on final element abundances especially on lithium. Photon cooling between the end of BBN and decoupling implies that the baryon to photon ratio η_{BBN} during BBN is different from η_{CMB} which is the one measured by Planck: $\eta_{CMB} = 6.14 \pm 0.04$. More explicitly, the photon cooling is accounted for the energy conservation³³ by:

$$\rho_{i,\gamma} = \rho_{f,\gamma} + \rho_{f,a} \quad (17)$$

where $\rho_{i,\gamma}, \rho_{f,\gamma}$ are the initial/final energy density of photons and $\rho_{f,a}$ is the final energy density of axions respectively assuming that the energy densities of the initial axions and baryons are negligible. It follows from Eq.(17) that after reaching the thermal equilibrium, the initial and final photon temperatures are related through:

$$T_f = (2/3)^{1/4} T_i \quad (18)$$

| | |
|--|--------|
| $\eta_{BBN} = (4.53 \pm 0.03) \times 10^{-10}$ | |
| Y_p | 0.2431 |
| $D/H \times 10^5$ | 4.28 |
| ${}^3\text{He}/H \times 10^5$ | 1.23 |
| ${}^7\text{Li}/H \times 10^{10}$ | 2.25 |

Table 4. The effect of photon cooling on light element abundances as obtained by updating AlterBBN code.³⁹

Since the number density of photons is proportional to T^3 , it is straightforward to show that the baryon-to-photon ratio during BBN will be modified as follows:

$$\eta_{BBN} = \left(\frac{2}{3}\right)^{3/4} \eta_{CMB} \quad (19)$$

This model was considered in Ref. 33 as a means to resolve the lithium problem. Although this model suppresses the conflict between BBN predictions and observations of lithium, this leads to an overproduction of deuterium (see Table 4) and an increase in N_{eff} ($N_{eff} = 6.7$) that is excluded by observational constraints.

8. Combined effect of photon cooling and non-standard neutrino properties

Because of the difficulty of accounting for the lithium problem. Authors have considered combined effects (e.g. Ref. 21). In this section, we add the effect of photon cooling with axions to the previous variations done before as a means to decrease the lithium abundance without violating observational constraints on N_{eff} and other light elements. The baryon to photon ratio as determined by Planck² is given to be $\eta = (6.14 \pm 0.04) \times 10^{-10}$, however, photon cooling through axions after BBN implies that $\eta_{BBN} = (4.53 \pm 0.03) \times 10^{-10}$ (see Eq. (19)). Photon cooling with axions will also modify the effective degrees of freedom. The energy density of the universe can be written as:

$$\rho_{rad} = \rho_\gamma \left[1 + N_{eff} \times \frac{7}{8} \times \left(\frac{4}{11}\right)^{\frac{4}{3}} \right]. \quad (20)$$

On the other hand, due to photon cooling through axion dark matter, the radiation density after BBN is given to be:

$$\rho_{rad} = \rho_\gamma \left[1 + \frac{1}{2} + N_\nu \times \frac{7}{8} \times \left(\frac{4}{11}\right)^{\frac{4}{3}} \times \frac{3}{2} \right], \quad (21)$$

where the factor $3/2$ is due to the photon cooling relative to neutrinos and $1/2$ represents the axion degrees of freedom. In this case, the relativistic degrees of freedom observed now becomes:

$$N_{eff} = \frac{3}{2} N_\nu + \frac{1}{2} \times \frac{8}{7} \times \left(\frac{11}{4}\right)^{\frac{4}{3}} \quad (22)$$

| $\beta_{\nu_{\mu,\tau,e}}$ | α | N_{eff} | N_ν | Y_p | $D/H \times 10^5$ | ${}^7Li/H \times 10^{10}$ |
|----------------------------|----------|-----------|---------|--------|-------------------|---------------------------|
| 0.05 | 0.82 | 4.2384 | 3 | 0.2313 | 3.469 | 2.779 |
| 0.11 | 0.77 | 4.8464 | 5 | 0.2342 | 3.672 | 2.622 |
| 0.20 | 0.60 | 4.5446 | 12 | 0.2405 | 3.628 | 2.757 |
| 0.33 | 0.50 | 4.0900 | 20 | 0.2266 | 3.387 | 2.792 |

Table 5. Effect of adding photon cooling on lithium along with non-standard neutrino properties.

Since taking into account only the effect of photon cooling does not help to solve the lithium problem (see Table 4), we vary also the neutrino temperature in order to conserve the constraints on N_{eff} and deuterium. In addition, we vary the chemical potential to obtain an additional decrease in lithium without violating observational constraints on helium. Introducing photon cooling, varying the neutrino temperature and chemical potential, we modify the radiation energy density given in Eq.(21) as follows:

$$\rho_{rad} = \rho_\gamma \left[1 + \frac{1}{2} + \frac{7}{8} \times \left(\frac{4}{11} \right)^{\frac{4}{3}} \times \frac{3}{2} \times \alpha^4 (\Delta N_\nu + N_{\nu 0} (1 + \frac{30\beta^2}{7\pi^2} + \frac{15\beta^4}{7\pi^4})) \right] \quad (23)$$

Then Eq.(23) will lead to new effective degrees of freedom,

$$N_{eff} = \frac{1}{2} \times \frac{8}{7} \times \left(\frac{11}{4} \right)^{\frac{4}{3}} + \frac{3}{2} \alpha^4 [\Delta N_\nu + N_{\nu 0} (1 + \frac{30\beta^2}{7\pi^2} + \frac{15\beta^4}{7\pi^4})] \quad (24)$$

It clear from Eq.(24) that multiplying the neutrino temperature with a factor $\alpha < 1$ will decrease the effective number of relativistic degrees of freedom to match observations as discussed in section 3. In addition, it will decrease deuterium so that the overabundance observed in Table 4 can be reduced. We have performed numerical simulations to obtain the ranges shown in Eq.(25) that lead to a substantial decrease in lithium abundance.

$$\begin{aligned} 3 \leq N_\nu \leq 20, \quad 4.08 \leq N_{eff} \leq 5.30 \\ 0.5 \leq \alpha \leq 0.9, \quad 0.01 \leq \beta_{\nu_{\mu,\tau,e}} \leq 0.35 \end{aligned} \quad (25)$$

Some of the results are shown in Table 5 where N_{eff} is now compatible with the recent CMB observations,^{24,36} but it is still higher than the most precise measurement given by Planck mission. In addition, lithium decreases significantly at the expense of increasing deuterium but to a value that is allowed by observations.

9. The effect of a unified dark fluid

We have seen in section 8 that adding axion dark matter could decrease the 7Li abundance while keeping N_{eff} compatible with the recent CMB observations. However, N_{eff} is still higher than the value determined by Planck analysis. To satisfy the requirements on N_{eff} we found a way by adopting the so-called dark fluid along with non-standard neutrino properties. We know that dark matter may be modeled as a system of collision-less particles while dark energy may be described as a scalar

field in the context of a quintessence model.⁴⁴ However, in this section, a unified fluid⁴³ is adopted to describe the dark energy and dark matter as two different aspects of the same component. To explore this scenario, a temperature-dependent dark energy density can be added to the radiation density as follows:^{3,44}

$$\rho_D(T) = k_\rho \rho_{rad}(T_0) \left(\frac{T}{T_0} \right)^{n_\rho} \quad (26)$$

where $\rho_{rad} = \rho_\gamma + \rho_{e^\pm} + \rho_\nu$, $T_0 = 1.0 \text{ MeV} = 1.16 \times 10^{10} \text{ K}$, k_ρ is the ratio of the effective dark fluid density to the total radiation density at T_0 and n_ρ characterizes the adiabatic expansion of the fluid. In the case of $n_\rho = 4$, the dark component mimics a radiation density. The case $n_\rho = 3$ describes a non-relativistic matter density, while $n_\rho = 6$ can describe a scalar field. With these assumptions, the Friedmann equation during BBN is modified to:

$$\left(\frac{\dot{a}}{a} \right)^2 = H^2 = \frac{8\pi G}{3} (\rho_{rad} + \rho_D). \quad (27)$$

In analogy, the temperature-dependent dark entropy can be added as follows:³⁹

$$s_D(T) = k_s s_{rad}(T_0) \left(\frac{T}{T_0} \right)^{n_s}, \quad (28)$$

where

$$s_{rad}(T) = g_s(T) \frac{2\pi^2}{45} T^3, \quad (29)$$

and $g_s(T)$ is the number of degrees of freedom characterizing the contribution of relativistic particles to the entropy density. Then, the total entropy becomes:

$$s_{tot}(T) = s_{rad}(T) + s_D(T) \quad (30)$$

It is clear from Eqs. (26, 28) that by including this dark component, four parameters are introduced k_ρ, n_ρ, k_s, n_s . Knowing that the universe was radiation dominated during the time of BBN requires the constraints $n_\rho \geq 4$ and $k_\rho < 1$.³ It is important to emphasize that the dominant effect of adding ρ_D is to alter the expansion rate and this is clearly seen in Eq. (27). To have a clear understanding of this dark component on BBN, we show in Fig. 2 the effect of adding a dark energy density ρ_D for $n_\rho = 6$ (left panel) and for $n_\rho = 7$ (right panel) while varying k_ρ in both cases. This has led to an increase in the abundance of light elements where the dominant effect is on helium (dotted blue curve). Although deuterium increases (solid orange line), lithium also increases and this is due to the dominant effect on helium. A similar effect is obtained when taking $n_\rho = 7$, but for smaller values of k_ρ . We can say that the effect on the final lithium abundance can be seen as a competition between the helium, and deuterium abundance. Lithium is directly proportional to helium and inversely proportional to deuterium (see Eqs. (14,15)). In other words, as seen in the right panel of Fig. 2 and for $k_\rho < 0.002$, lithium increases significantly due to the dominant effect of helium. However, for $k_\rho > 0.002$ the lithium abundance

increases slowly since deuterium starts to control the final lithium abundance. Meanwhile, modifying the entropy content of the universe as given by Eq.(28) alters the time evolution of the temperature described by the energy conservation equation shown in Eq.(31).³⁹

$$\frac{d}{dt}(\rho_{tot}a^3) + P_{tot}\frac{d}{dt}(a^3) - a^3\frac{d\rho_{tot}}{dt}|_{T=cst} - T\frac{d}{dt}(s_D a^3) = 0, \quad (31)$$

where $\rho_{tot} = \rho_{rad} + \rho_D$ and P_{tot} is the corresponding pressure. The effect of dark entropy is clearly shown in Fig. 3 where adding s_D has led to an increase in deuterium, but to a decrease in the helium and lithium abundances. In this case, the dominant effect of s_D is on deuterium and consequently the final lithium abundance. The dependence of the final lithium abundance on helium and deuterium is given by Eqs.(14,15). This confirms the results shown in Figs.(2,3). In addition, Fig. 4 shows that adding a dark entropy does not only lead to an increase in the deuterium abundance, but to a shift in the temperature of the bottleneck (maximum abundance of deuterium). The shift in the bottleneck temperature alters the abundances of other light elements since the formation of helium is blocked until deuterium reaches its maximum.

Then, for fixed values of k_ρ, n_ρ, k_s, n_s and restricting N_{eff} as measured by Planck,

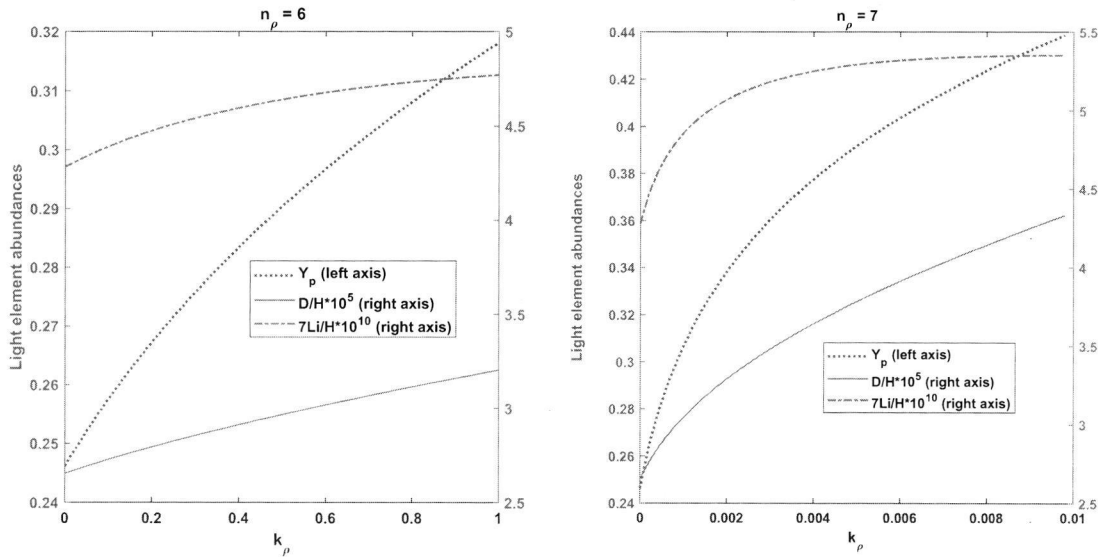


Fig. 2. Effect of adding dark energy density ρ_D on the abundances of helium (blue dotted line, left axis), deuterium (orange solid line, right axis) and lithium (orange dashed line, right axis).

we can vary the neutrino number and chemical potentials in order to see how these non-standard scenarios could contribute to the lithium problem. Our calculations

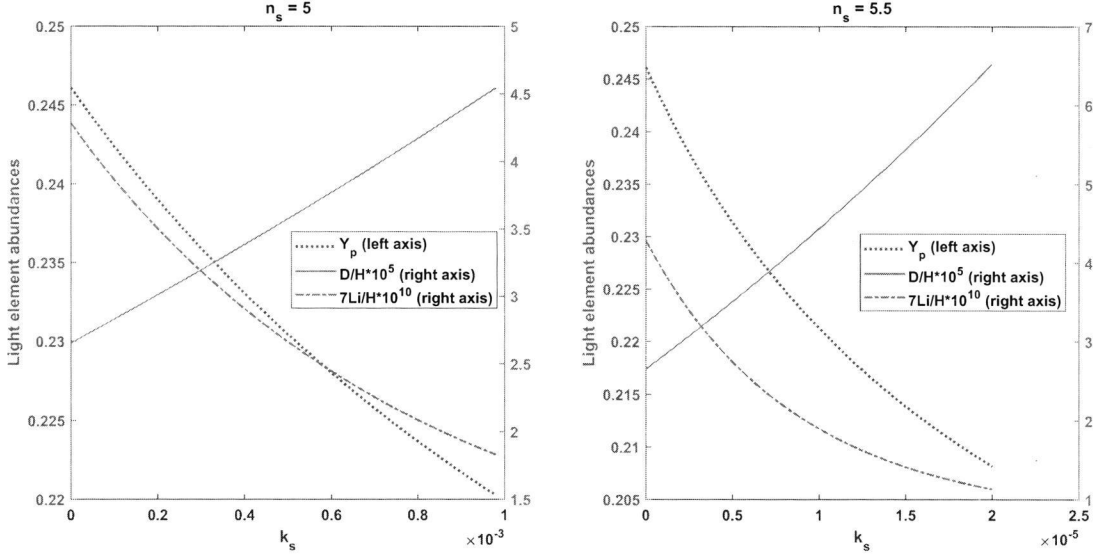


Fig. 3. Effect of adding dark entropy S_D on the abundances of helium (blue dotted line, left axis), deuterium (orange solid line, right axis) and lithium (orange dashed line, right axis).

summarized in Table 6 show the following:

Fixing $k_\rho = 0.007$, $n_\rho = 7$, $k_s = 0.00045$ and $n_s = 5$, restricting the range of $2.48 < N_{eff} < 3.5$ in order to be compatible with Planck measurements, and varying the number of neutrinos ($3 \leq N_\nu \leq 20$) along with neutrino chemical potential, we are able to find for every chosen value of N_ν , a combination of α (or N_{eff}) and $\beta_{\nu_{e,\mu,\tau}}$ that reduces the lithium abundance. The ranges that lead to a decrease of lithium are shown in Eq.(32). Note that N_{eff} is still given by Eq.(6) because the dark component has an effect on BBN predictions due to the power law (see Eqs.(26, 28)) and a negligible contribution after BBN. In other words, although this dark component alters the expansion rate, it has no observational effect on N_{eff} or other cosmological parameters.

$$\begin{aligned} k_\rho = 0.007, n_\rho = 7, k_s = 0.00045, n_s = 5, \\ 3 \leq N_\nu \leq 20, 2.48 \leq N_{eff} \leq 3.50, \\ 0.564 \leq \alpha \leq 0.968, 0.83 \leq \beta_{\nu_{\mu,\tau,e}} \leq 0.97. \end{aligned} \quad (32)$$

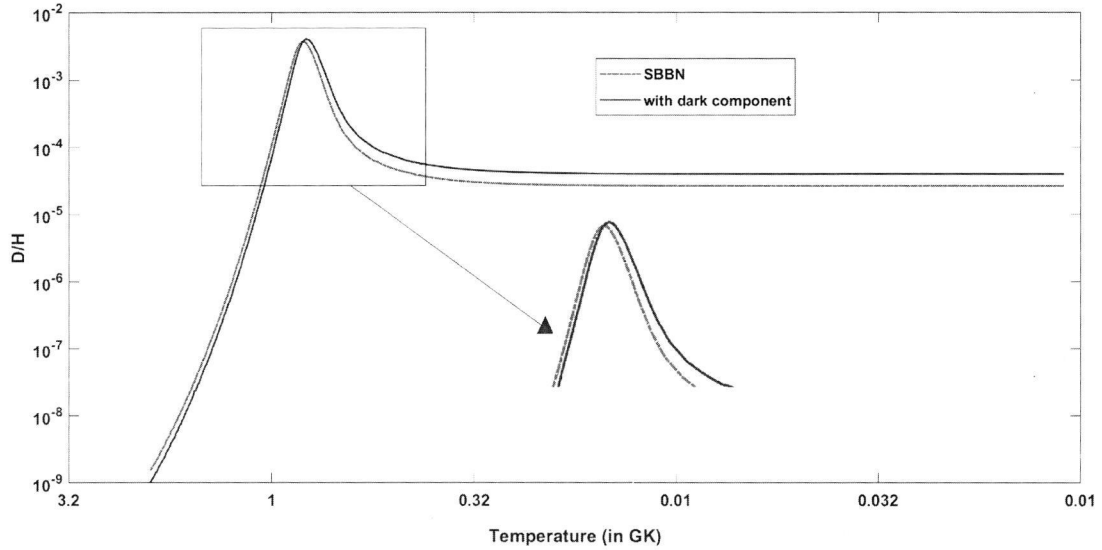
If we choose other values of dark component parameters such as $k_\rho = 0.12$, $n_\rho = 6$, $k_s = 0.0005$ and $n_s = 5$, other ranges will be derived as shown by Eq.(33):

$$\begin{aligned} k_\rho = 0.12, n_\rho = 6, k_s = 0.0005, n_s = 5, \\ 3 \leq N_\nu \leq 20, 2.48 \leq N_{eff} \leq 3.50, \\ 0.59 \leq \alpha \leq 1.03, 0 \leq \beta_{\nu_{\mu,\tau,e}} \leq 0.48 \end{aligned} \quad (33)$$

| $k_\rho = 0.007, n_\rho = 7, k_s = 0.00045$ and $n_s = 5$ | | | | | | |
|---|----------|-----------|---------|--------|-------------------|----------------------------------|
| $\beta_{\nu_{\mu,\tau,e}}$ | α | N_{eff} | N_ν | Y_p | $D/H \times 10^5$ | ${}^7\text{Li}/H \times 10^{10}$ |
| 0 | 1 | 3 | 3 | 0.4007 | 5.395 | 3.484 |
| 0.88 | 0.86 | 3.3086 | 5 | 0.2301 | 3.696 | 2.535 |
| 0.84 | 0.72 | 2.9432 | 10 | 0.2465 | 3.716 | 2.751 |
| 0.94 | 0.59 | 2.5692 | 20 | 0.2321 | 3.495 | 2.758 |

Table 6. Effect of unified dark fluid on lithium along with non-standard neutrino properties.

Finally, we can choose other values of dark component parameters so other ranges of α and $\beta_{\nu_{\mu,\tau,e}}$ can be derived, but for simplicity we have fixed the dark component parameters in order to give a better understanding of the physical conditions under which the BBN has been operating and provide examples to ameliorate the lithium problem.

Fig. 4. Deuterium abundance as function of temperature when adding dark entropy ($k_s = 0.007, n_s = 5$) compared to SBBN.

10. Conclusion

In order to reduce the primordial ${}^7\text{Li}$ abundance by Standard Big Bang Nucleosynthesis (SBBN), we investigated the effect of many non-standard assumptions. We first considered the effects of a variation of the neutrino number, chemical potential,

and temperature. Second, it was necessary to add the effect of dark components. Our results may be summarized as follows:

- It was possible to reproduce the SBBN predictions for a certain range of neutrino temperature, number, and chemical potential (see section 6 and Table 2). This finding motivated a non-standard treatment that may lead to a reduction of the lithium abundance.
- Extending the range of variation of the above parameters was successful to reduce the lithium abundance, but with N_{eff} not compatible with the recent analysis of the CMB. One way out was to add photon cooling with axion dark matter after BBN as described in section 8. This led to a reduction of the lithium abundance with N_{eff} compatible with recent CMB observations as discussed in section 3. However, this range of N_{eff} is still in tension with the most precise value deduced by Planck mission.
- Taking into consideration a unified dark fluid along with non-standard neutrino properties leads to a decrease in lithium for ranges of N_{eff} that satisfies recent CMB observations including the well known Planck and WMAP.
- As a final remark, we think that decreasing the primordial lithium abundance below the predictions of the SBBN is achieved only with a maximum deuterium abundance which is still marginally consistent with observations (see Ref. 19). However, it is worth investigating the possibility of reducing lithium abundance while avoiding the increase of deuterium by including new particles or interactions.^{45,46} This will be the focus of future work.

References

1. Galvez R. and Scherrer R., *Phys. Rev. D* **95** (2017) 063507.
2. Planck Collaboration, arXiv:1807.06209 (2018).
3. Arbey A. and Mahmoudi F., *Phys. Lett. B* **669** (2008) 46-51.
4. Spite F. and Spite M., *A&A* **115** (1982) 357–366.
5. Sbordone L. et al., *A&A* **522** (2010) A26.
6. Fields B. D., *Annual Review of Nuclear and Particle Physics* **61** (2011) 47-68.
7. Cook R. and Fumagalli M., *Nature Astronomy* **2** (2018) 957961.
8. Cooke R. J. et al., *ApJ* **781** (2014) 31.
9. Dolgov A. D., *Phys. Rept.* **370** (2002) 333-535.
10. Khlopov M. Yu., Barrau A. and Grain J., *Classical and Quantum Gravity* **23** (2006) 6.
11. Khlopov M. Yu., Petcov S. T., *Phys. Lett.* **99B** (1980) 2.
12. Chechetkin V. M., Khlopov M. Yu., and Sapozhnikov M. G., *Riv. Nuovo Cimento* **5**(1982) 10.
13. Zeldovich I. B., Starobinskii A. A., Khlopov M. I., and Chechetkin V. M., *Soviet Astronomy Letters* **3** (1977) 110-112.
14. Petcov S. T. and Zhou Ye-Ling, *Phys. Lett. B* **785** (2018) 95-104.
15. Doroshkevich A. G., Khlopov M. Yu., *MNRAS* **211** (1984) 277-282.
16. Polnarev A. G. and Khlopov, M. Y., *Soviet Astronomy* **26** (1982) 9-12.
17. M. Khlopov, *Int. J. Mod. Phys. A* **28** (2013) 1330042.

18 *Authors' Names*

18. Dimopoulos S., Esmailzadeh R., Hall L. J., and Starkman G. D., *Astrophys. J.* **330** (1988) 545.
19. Balashev S. A. et al., *MNRAS* **458** (2016) 2.
20. Olive K. et al., *MNRAS* **426**(2012) 2.
21. Yamazaki D. G. et al., *Phys. Rev. D* **90** (2014) 023001.
22. Kusakabe M. et al., *Phys. Rev. D* **99** (2019) 043505.
23. Cyburt R. H., Fields B. D., and Olive K. A., *Rev. Mod. Phys.* **88** (2016) 015004.
24. Komatsu E. et al., *Astrophys.J.Suppl.* **192** (2011) 18.
25. Fields B. and Olive K., *Nuclear Physics A* **777** (2006) 208-225.
26. Steigman G., *Advances in High Energy Physics* **2012** (2012) 268321.
27. Leistedt B. et al., *Phys. Rev. Lett.* **113** (2014) 041301.
28. Merle A., *arXiv:1702.08430*.
29. Boyarsky A. et al., *Phys. Rev. Lett.* **97** (2006) 261302.
30. Dolgov A. D. and Hansen S. H., *Astropart. Phys.* **16** (2002) 339.
31. Paraskevi C. and John D. Vergados, *Advances in High Energy Physics* **2018** (2018) 1479313.
32. Adhikari R. et al., *JCAP* **01** (2017) 025.
33. Erken O. et al., *Phys. Rev. Lett.* **108** (2012) 061304.
34. Abel C. et al., *Phys. Rev. X* **7** (2017) 041034.
35. Nollet K. M. and Steigman G., *Phys.Rev.D.* **91** (2015) 083505.
36. Hinshaw G. et al., *ApJ.* **208** (2013) 2.
37. Mukhanov V., *Physical Foundations of Cosmology*, New York: Cambridge University Press, 2005.
38. Makki T. R., El Eid M. F. and Mathews G. J., *MPLA* **33** (2019) 1950194.
39. Arbey A., *Comput. Phys. Communications* **183** (2012) 1822-1831.
40. Valentino E. Di et al., *Phys. Rev. D* **90** (2014) 023543.
41. Olive K. et al., *MNRAS* **426** (2012)1427–1435.
42. Kusakabe, Motohiko et al., *Phys.Rev. D* **99** (2019) 043505.
43. Arbey A., *arXiv:astro-ph/0506732*.
44. Arbey A., *AIP Conf.Proc.* **1241** (2010) 700-707.
45. Salvati L. et al., *JCAP* **08** (2016) 022.
46. Goudelis A. et al., *Phys. Rev. Lett.* **116** (2016) 211303.

Acknowledgements

Tahani Makki would thank the dean's office of the faculty of arts and sciences at the American University of Beirut(AUB) and the graduate council for supporting this research, for their tremendous help, guidance, and facilities throughout her Ph.D thesis. She would also thank the National Council for Scientific Research (CNRS) for their partial support of this research.

PAPER • OPEN ACCESS

The lithium problem: new insight in the big bang nucleosynthesis (BBN) beyond the standard model

To cite this article: T R Makki and M F El Eid 2017 *J. Phys.: Conf. Ser.* **869** 012091

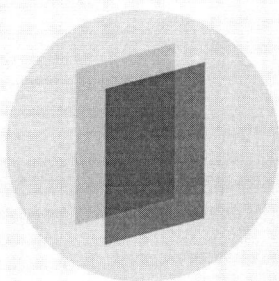
View the [article online](#) for updates and enhancements.

Related content

- [Gravitino dark matter and the lithium primordial abundance within a pre-BBN modified expansion](#)
Sean Bailly
- [SUSY-catalyzed big bang nucleosynthesis as a solution of lithium problems](#)
Motohiko Kusakabe, Toshitaka Kajino and Grant J Mathews
- [Observations of Li in metal-poor stars](#)
Norbert Christlieb

Recent citations

- [Nucleosynthesis in relation to cosmology](#)
Mounib F El Eid



IOP | ebooks™

Bringing you innovative digital publishing with leading voices to create your essential collection of books in STEM research.

Start exploring the collection - download the first chapter of every title for free.

The lithium problem: new insight in the big bang nucleosynthesis (BBN) beyond the standard model

T R Makki and M F El Eid

Department of Physics, American University of Beirut, Lebanon.

E-mail: trm03@mail.aub.edu

Abstract. The production of the light elements in the framework of the standard Big Bang nucleosynthesis model (SBBN) matches the observed abundances except in case of ${}^7\text{Li}$, where observations lie a factor 2.4-4.3 below SBBN+WMAP (*Wilkinson Microwave Anisotropy Probe*) predictions. This so-called “Lithium problem” needs to be resolved beyond the SBBN. In this contribution we focus on the effect of degenerate neutrinos and the addition of dark component, including dark energy density and dark entropy. We find that the effect of the degeneracy parameter is significant if chemical potentials of neutrino families are different. Concerning the dark component, the major effect comes from adding dark entropy.

1. Introduction

The standard Big Bang nucleosynthesis model (SBBN) represents one cornerstone of the Big Bang theory. It leads to the synthesis of light elements (${}^2\text{D}$, ${}^3\text{He}$, ${}^4\text{He}$, ${}^6\text{Li}$, ${}^7\text{Li}$ and ${}^7\text{Be}$) during the first three minutes after Big Bang. The SBBN is a parameter-free theory, since it depends only on the baryon to photon ratio η which is meanwhile well determined by the WMAP. It is found that $\eta = (6.23 \pm 0.17) \times 10^{-10}$ [1, 2]. The observed abundances of ${}^4\text{He}$, ${}^3\text{He}$ and ${}^2\text{D}$ are in good agreement with SBBN+WMAP predictions but not in case of ${}^7\text{Li}$. The observation of ${}^7\text{Li}$ in old Halo stars [3], yields ${}^7\text{Li}/\text{H} = (1.23_{-0.32}^{+0.68}) \times 10^{-10}$ where the SBBN prediction [4] ${}^7\text{Li}/\text{H} = (4.681 \pm 0.335) \times 10^{-10}$.

Some dispersion is found for deuterium: according to [5] $\text{D}/\text{H} = 2.8_{-0.6}^{+0.8} \times 10^{-5}$, while recent observations by [6] shows $\text{D}/\text{H} = (2.53 \pm 0.04) \times 10^{-5}$. The element ${}^4\text{He}$ is strongly constrained primordial value of $X({}^4\text{He}) = 0.228 \pm 0.005$ as obtained from seven metal-poor galaxies [7]. Other investigation by [8] indicate a range $0.232 < X({}^4\text{He}) < 0.258$. Not only the difference is between observations and predictions but observing ${}^7\text{Li}$ in very metal poor stars does not confirm the known plateau [9]. This constitutes presently “the Lithium problem”. The overproduction of ${}^7\text{Li}$ seems not to be resolved by the SBBN, for example on astrophysical or nuclear physics grounds, a non-standard scenario of the SBBN seems to be needed to resolve the ${}^7\text{Li}$ problem. In particular, modifying neutrinos properties (neutrinos degeneracy, oscillations, non-vanishing mass...) and adding the effect of a dark component [10-12].

2. Non-standard BBN

2.1. Non-vanishing neutrinos chemical potential

According to [13], neutrinos degeneracy affects elements production in two ways:

(i) It increases the energy density leading to speed up the expansion rate of the universe as appears in the Friedmann equation. The Hubble parameter is then given by:



$$\left(\frac{\dot{a}}{a}\right)^2 = H^2 = \frac{8\pi G}{3}\rho_{rad} = kT^4, \quad k = \frac{\pi^2}{30}\left(g_b + \frac{7}{8} \times g_f\right), \quad (1)$$

where g 's are the relativistic degrees of freedom, a is the scale parameter and ρ is the total energy density. The energy density of fermions and anti-fermions is given by [14]:

$$\rho_f + \rho_{\bar{f}} = \frac{7\pi^2}{120}gT^4 \left[1 + \frac{30\beta^2}{7\pi^2} + \frac{15\beta^4}{7\pi^4}\right], \quad (2)$$

where $\beta = \frac{\mu_f}{T}$ is the degeneracy parameter. In the SBBN, $\beta = 0$ (non-degenerate neutrinos). Clearly including β increases the energy density (or k) and this is the only way in which ν_μ and ν_τ modify the SBBN. As a consequence of a larger expansion rate, freeze-out temperature will be higher leading to higher neutrons mass fraction. This will result in increasing D and ${}^4\text{He}$ but ${}^7\text{Li}$ will decrease as shown in table 2.

(ii) A second effect concerns the electron neutrinos, which are involved in the weak interactions rates:

$$n + \nu_e \leftrightarrow p + e^-, \quad n + e^+ \leftrightarrow p + \bar{\nu}_e, \quad n \leftrightarrow p + e^+ + \bar{\nu}_e \quad (3)$$

A new equilibrium ratio is obtained (see [14]):

$$\frac{n}{p} = \exp[-(\beta_{\nu_e} + Q/T)] \quad (4)$$

Where $Q = m_n - m_p = 1.29$ MeV, T in MeV, and β_{ν_e} is the electron neutrino degeneracy parameter.

The rate of the first reaction can be written as [14]:

$$\lambda_{n\nu} \approx 1.63 \left(\frac{T_\nu}{Q}\right)^3 \left(\frac{T_\nu}{Q} + 0.25\right)^2 s^{-1} \quad (5)$$

The other rates are related to it.

Taking $-0.5 < \beta_{\nu_e} < 0.5$, equation (5) becomes:

$$\lambda_{n\nu} \approx 1.63 \times \exp(+\beta_{\nu_e}) \left(\frac{T_\nu}{Q}\right)^3 \left(\frac{T_\nu}{Q} + 0.25\right)^2 s^{-1} \quad (6)$$

It is seen that the rate is enhanced exponentially when $\beta_{\nu_e} > 0$, thus it becomes faster and more neutrons are converted into protons, so that the freeze-out temperature is delayed (see table 1). As table 1 shows the effect on ${}^7\text{Li}/H$ is significant. Using equation (6) we calculate the mass fraction of neutrons at freeze-out:

$$X_n^* = \int_0^\infty e^{(-5.42k^{-1/2}e^{\beta_{\nu_e}} \int_0^y (x+0.25)^2 (1+e^{-\beta_{\nu_e}} \exp(-\frac{1}{x})) dx)} \frac{dy}{2y^2(1+\cosh(\beta_{\nu_e}+1/y))} \quad (7)$$

And to get the freeze-out temperature T^* we use the modified $X_n^{eq} = \frac{1}{1+\exp(\beta_{\nu_e})\exp(Q/T^*)}$. (8)

The integral in equation (7) does not allow an explicit dependence of X_n^* on β 's. For this reason we took different values of $-0.5 < \beta_{\nu_e} < 0.5$ and $0 < \beta_{\nu_\mu}, \beta_{\nu_\tau} < 2.5$ (or and $3.53 < k < 8.6$) and we evaluated this integral in the above ranges, where some results are given in tables 1 and 2.

Table 1. Effect of adding (β_{ν_e}) on freeze-out temperature and light elements (numbers in brackets are power of ten in all tables and figures).

| β_{ν_e} | X_n^* | T^* | X(${}^4\text{He}$) | D/H | ${}^7\text{Li}/H$ |
|-----------------|---------|--------|----------------------|-----------|-------------------|
| -0.2 | 0.1987 | 0.8110 | 2.987(-1) | 2.832(-5) | 5.224(-10) |
| 0 or (SBBN) | 0.1571 | 0.7695 | 2.464(-1) | 2.509(-5) | 4.681(-10) |
| 0.2 | 0.1217 | 0.7279 | 2.030(-1) | 2.291(-5) | 4.073(-10) |

Table 2. Effect of adding ($\beta_{\nu_\mu} = \beta_{\nu_\tau}$) on freeze-out temperature and light elements.

| $\beta_{\nu_\mu} = \beta_{\nu_\tau}$ | K | X_n^* | T^* | X(${}^4\text{He}$) | D/H | ${}^7\text{Li}/H$ |
|--------------------------------------|--------|---------|--------|----------------------|-----------|-------------------|
| 2.5 | 7.6511 | 0.1864 | 0.8773 | 3.133(-1) | 4.882(-5) | 2.710(-10) |
| 1.0 | 4.0690 | 0.1624 | 0.7881 | 2.592(-1) | 2.826(-5) | 4.317(-10) |
| SBBN | 3.53 | 0.1571 | 0.7695 | 2.464(-1) | 2.509(-5) | 4.681(-10) |

Table 3. Effect of adding $\beta_{\nu_e} = 0.28$ and $\beta_{\nu_\mu} = \beta_{\nu_\tau} = 2$ together on light elements.

| X(^4He) | D/H | $^3\text{He}/\text{H}$ | $^7\text{Li}/\text{H}$ |
|--------------------|-----------|------------------------|------------------------|
| 2.219(-1) | 3.361(-5) | 1.127(-5) | 2.814(-10) |

Adding β_{ν_e} or $\beta_{\nu_\mu}, \beta_{\nu_\tau}$ independently will have effect on ^7Li but it will violate observational constraints on D and ^4He . Therefore, adding $\beta_{\nu_e} = 0.28$ along with $\beta_{\nu_\mu} = \beta_{\nu_\tau} = 2$ together will lead to ^7Li depletion without violating observational constraints (see table 3).

2.2. Adding dark energy density

It is known that dark matter and dark energy play a decisive role in the evolution of the universe. Due to the fact that the identity of dark matter is not well known a unified adiabatically expanded fluid is adopted so that the dark energy and dark matter can be considered as two different aspects of the same component. To illustrate this model, temperature-dependent dark energy density is added to radiation density as follows [10,11]:

$$\rho_D(T) = \rho_D(T_0) \left(\frac{T}{T_0}\right)^{n_\rho}, \quad (9)$$

where $T_0 = 1.0 \text{ Mev} = 1.16 \times 10^{10} \text{ K}$, and n_ρ is a constant characterizing the power law. In case of $n_\rho = 4$, the dark component mimics a radiation density. The case $n_\rho = 3$ describes a matter density behavior, while $n_\rho = 6$ describes a scalar field. With these assumptions the Friedmann equation

$$\left(\frac{\dot{a}}{a}\right)^2 = H^2 = \frac{8\pi G}{3}(\rho_{rad} + \rho_D), \quad (10)$$

Where $\rho_{rad}(T)$ is as in equation (1). Including $\rho_D(T)$, two parameters will be introduced :

$n_\rho = 3(w_D + 1)$, describing the behavior of the dark fluid ($w_D = \frac{P_D}{\rho_D}$ and P is the pressure of the dark component) and $k_\rho = \frac{\rho_D(T_0)}{\rho_{rad}(T_0)}$, which is the ratio of effective dark fluid density over the total radiation density at BBN time (taken to be $T_0 = 1 \text{ Mev}$).

$$\text{Then equation (9) becomes: } \rho_D(T) = k_\rho \rho_{rad}(T_0) \left(\frac{T}{T_0}\right)^{n_\rho}. \quad (11)$$

Knowing that the universe was radiation dominated during the time of BBN requires the constraints $n_\rho \geq 4.0$ and $K_\rho < 1.0$ [10]. Adding dark density alone will not be sufficient to resolve the Lithium problem. The point is that the dark energy density being temperature dependent will increase the expansion rate leading higher ^4He abundance and to higher production of ^7Li (see table 4). This is contrary to the case when adding β_{ν_μ} and β_{ν_τ} as described above where the abundance of ^7Li decreases because of higher abundance of Deuterium. These two different outcomes have different effects on the expansion rate and the freeze-out temperature and this illustrate how sensitive the Lithium production to these assumptions.

Table 4. Effect of adding $\rho_D(T)$ with $k_\rho = 0.5$ and $n_\rho = 6$.

| X(^4He) | D/H | $^3\text{He}/\text{H}$ | $^7\text{Li}/\text{H}$ |
|--------------------|-----------|------------------------|------------------------|
| 2.920(-1) | 2.816(-5) | 1.016(-5) | 5.082(-10) |

2.3. Adding Dark entropy

In analogy to the dark energy component, a dark entropy component can be added as well. This is described by [4] and [12] as:

$$s_D(T) = k_s s_{rad}(T_0) \left(\frac{T}{T_0}\right)^{n_s}, \text{ where } s_{rad}(T) = h_{eff}(T) \frac{2\pi^2}{45} T^3, \quad (12)$$

and $h_{eff}(T)$ are the effective degrees of freedom characterizing the contribution of particles to the entropy density. Then, the total entropy becomes:

$$s_{tot}(T) = s_{rad}(T) + s_D(T) \quad (13)$$

The direct effect of adding dark entropy is altering the time-temperature relation and clearly the light elements abundances. In this case the energy conservation equation will read:

$$\frac{ds_{tot}}{dt} = -3Hs_{tot} \quad \text{or} \quad \frac{d}{dt}(\rho_{tot}a^3) + P_{tot} \frac{d}{dt}(a^3) + T \frac{d}{dt}(s_D a^3) = 0, \quad (14)$$

where the third term corresponds to the dark entropy. The effect of adding dark entropy is increasing the temperature of the universe, altering the freeze-out of neutrons and the time when it takes place. Deuterium bottleneck (the highest D abundance where $D/H \sim 10^{-3}$ at $T \approx 0.07 \text{ MeV}$) is shifted which leads to higher final D abundance. In addition, ${}^7\text{Li}$ abundance decreases to match the observational range which is shown in table 5 and figure 1 without violating observational constraints.

Table 5. Effect of adding $s_D(T)$ with $k_s = 5.5 \times 10^{-4}$ and $n_s = 5$.

| X(${}^4\text{He}$) | D/H | ${}^3\text{He}/\text{H}$ | ${}^7\text{Li}/\text{H}$ |
|----------------------|-----------|--------------------------|--------------------------|
| 2.306(-1) | 3.489(-5) | 1.154(-5) | 2.781(-10) |

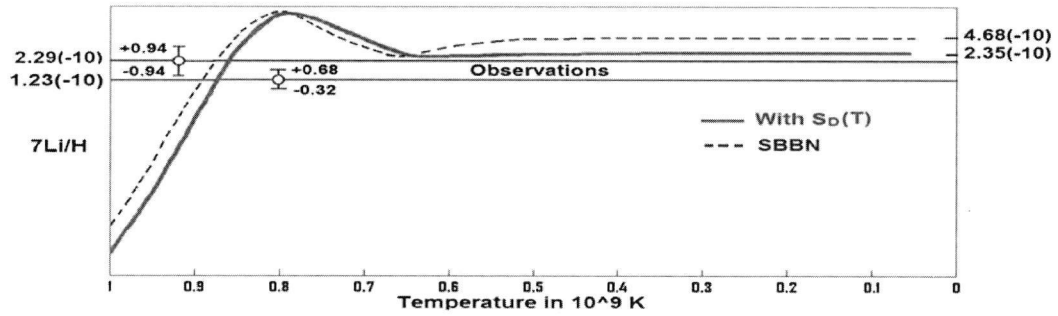


Figure 1. ${}^7\text{Li}$ as function of temperature in SBBN and when adding dark entropy ($k_s = 0.00075$, $n_s = 5$). Notice that ${}^7\text{Li}$ decreases to match the range of observations.

References

- [1] Cyburt R H *et al* 2009 *JCAP* **21** 0910
- [2] Dunkley J *et al* 2009 *Astrophys. J. Suppl.* **180** 306
- [3] Ryan S G *et al* 2000 *ApJ Lett.* **530** L57.
- [4] Arbey A 2012 *Computer Physics Communications* 2012 **183** 1822.
- [5] Noterdaeme P *et al* 2012 *A&A* **542** L33.
- [6] Cooke R *et al* 2014 *ApJ* **781** 31.
- [7] Songaila A *et al* 1994 *Nature* **368** 599.
- [8] Fields D B and Olive K 2006 *Nuclear physics* **777** 208
- [9] Spite F and Spite M 1982 *Astron. Astroph.* **115** 382.
- [10] Arbey A and Mahmoudi F 2008 *Phys. Lett. B* **669** 46.
- [11] Arbey A 2009 *AIP Conf. Proc.* **1241** 700
- [12] Arbey A and Mahmoudi F 2010 *JHEP* **1005** 051
- [13] Wagoner V *et al* 1967 *ApJ* **148** 3W.
- [14] Mukhanov V 2005 *Physical foundations of cosmology*, Cambridge university press,

Big Bang Nucleosynthesis (BBN) and Non-Standard Physics

Tahani Makki^{1,*} and Mounib El Eid¹

¹Department of Physics, American University of Beirut, Lebanon

Abstract. A brief overview on standard big bang nucleosynthesis (shortly, SBBN) is presented. First, we describe the outcome of the SBBN concerning the abundances of the light elements up to ${}^7\text{Li}$. A comparison with observations reveals a Lithium overproduction, which is not understood yet and is termed as “Cosmological Lithium Problem”. Resolving that problem is not easy, since many aspects are involved which nuclear, astrophysical and even a non-standard scenario may be invoked. These items are described in some details owing to the limited available space.

1 Introduction

The standard big bang nucleosynthesis (SBBN) is well understood in the context of the standard model of particle physics. It predicts that the universe is composed of about 75% of Hydrogen and 25% of ${}^4\text{He}$ and small amounts of D, ${}^3\text{He}$, ${}^7\text{Li}$ and ${}^6\text{Li}$ [4]. The most important nuclear reactions intervening in SBBN are given in Fig.1, while a comparison between SBBN calculations and observations is given in Table 1. It is clear that all abundances agree with observations except for Lithium which is higher by a factor of 3 than observations. This discrepancy constitute now one of the most intriguing problems in cosmology. In addition, Lithium was shown to have a constant behavior as function of metallicity, so called "Spite Plateau"[17]. Such a behavior is now in conflict with recent observations at very low metallicity which makes the Lithium problem more complicated. Solving the Lithium problem by taking into considerations accurate measurements of nuclear cross sections seems not possible [4]. In addition, the possibility of an astrophysical solution is also unlikely [13] because it will be constrained by the plateau at high metallicity.

2 Non-Standard Big Bang Nucleosynthesis

Including new particles/physics and changing fundamental constants were extensively studied to see the effect of these scenarios on SBBN or to constrain them by SBBN predictions. In addition, some non-standard scenarios were included for the aim to decrease the Lithium abundance. We mention a promising attempt by [7] where modifying the velocity distributions of nuclei during BBN have led to a decrease in Lithium to match observations.

In the following we give an example of non-standard scenario by adding extra dimension like dark component [1] and introducing a variable number of neutrinos and their chemical potential (β). Increasing the number of neutrinos and/or adding β will increase the standard radiation density ρ_{rad}

*e-mail: trm03@mail.aub.edu

- | | |
|--|--|
| 1. $n \rightarrow {}^1\text{H} + e^- + \bar{\nu}$ | 7. ${}^3\text{H} + {}^4\text{He} \rightarrow {}^7\text{Li} + \gamma$ |
| 2. ${}^1\text{H} + n \rightarrow {}^2\text{H} + \gamma$ | 8. ${}^3\text{He} + n \rightarrow {}^3\text{H} + {}^1\text{H}$ |
| 3. ${}^2\text{H} + {}^1\text{H} \rightarrow {}^3\text{He} + \gamma$ | 9. ${}^3\text{He} + {}^2\text{H} \rightarrow {}^4\text{He} + {}^1\text{H}$ |
| 4. ${}^2\text{H} + {}^2\text{H} \rightarrow {}^3\text{He} + n$ | 10. ${}^3\text{He} + {}^4\text{He} \rightarrow {}^7\text{Be} + \gamma$ |
| 5. ${}^2\text{H} + {}^2\text{H} \rightarrow {}^3\text{H} + {}^1\text{H}$ | 11. ${}^7\text{Li} + {}^1\text{H} \rightarrow {}^4\text{He} + {}^4\text{He}$ |
| 6. ${}^2\text{H} + {}^3\text{H} \rightarrow {}^4\text{He} + n$ | 12. ${}^7\text{Be} + n \rightarrow {}^7\text{Li} + {}^1\text{H}$ |

Figure 1. The most important nuclear reactions for big bang nucleosynthesis.**Table 1.** Comparison between SBBN predictions and observations.

| | Predictions | Observations |
|----------------------------------|-------------|-----------------------------|
| Y_p | 0.2457 | 0.2449 ± 0.0040 [2] |
| $D/H \times 10^5$ | 2.6719 | $2.8^{+0.8}_{-0.6}$ [10] |
| ${}^3\text{He}/H \times 10^5$ | 1.0193 | 1.1 ± 0.2 [3] |
| ${}^7\text{Li}/H \times 10^{10}$ | 4.3003 | $1.58^{+0.35}_{-0.28}$ [14] |

shown in Eq.1. A second effect of β is altering the neutron to proton ratio at the freeze out temperature and this effect is limited to the electron neutrino owing to the involved weak interaction rates. The dark component will modify the expansion rate by additional effective dark fluid ρ_D (Eq.1). The expansion rate is related to the Hubble constant (H) via a modified Friedmann equation [1]:

$$\left(\frac{\dot{a}}{a}\right)^2 = H^2 = \frac{8\pi G}{3} (\rho_{rad} + \rho_D) \quad (1)$$

with ρ_D given by:

$$\rho_D(T) = k_\rho \rho_{rad}(T_0) \left(\frac{T}{T_0}\right)^{n_\rho} \quad (2)$$

where T_0 is chosen to be $1 \text{ MeV} = 1.16 \times 10^{10} \text{ K}$, k_ρ is the ratio of effective dark fluid density over the total radiation density at T_0 and n_ρ characterizes the adiabatic expansion of the fluid. Modifying the energy density of the universe which is radiation dominated will alter the standard-time temperature relation, $t(s) = 1.39 \times \frac{k^{-0.5}}{(T(\text{MeV}))^2}$ [9], and consequently light element abundances. Note that k is the effective number of relativistic degrees of freedom due to photon, neutrino, electron and positron degrees of freedom. In Table 2 (second and third columns) we present the effect of dark component along with neutrino chemical potentials β (assumed to be equal for all species) where the calculated abundances agrees with observations. This is to confirm that SBBN is a rich ground for many non-standard physics.

On the other hand, it could happen that non-equality between chemical potential still exist. For example, hypothetical neutrino-majoron coupling can reopen the window of allowing large muon/tau neutrino asymmetry together with a small electronic asymmetry ([5]). In addition, one can assume one neutrino species mixes with a sterile neutrino resulting in chaotic amplification of electron neutrino chemical potential ([15]) or assuming just a non-vanishing electron neutrino chemical potential ([16]) in a Linearly Coasting Cosmology. In a universe preferring large lepton asymmetry([6], [8]), it is important to allow neutrino chemical potential to be different in the aim to understand the SBBN

Table 2. Effect of including non-standard neutrino properties and dark component.

| | $n_\rho = 6.3, k_\rho = 0.1$ | | $n_\rho = 0, k_\rho = 0$ |
|----------------------------------|------------------------------|---------------------------|--|
| | $N_\nu = 3, \beta = 0.2$ | $N_\nu = 4, \beta = 0.25$ | $\beta_{\nu_e} = 0.23, \beta_{\nu_{\mu,\tau}} = 2$ |
| Y_p | 0.2515 | 0.2471 | 0.2319 |
| $D/H \times 10^5$ | 2.7029 | 2.9517 | 3.6530 |
| ${}^3\text{He}/H \times 10^5$ | 1.0243 | 1.0569 | 1.1430 |
| ${}^7\text{Li}/H \times 10^{10}$ | 4.3602 | 3.8121 | 2.6550 |

and to investigate their effect on Lithium abundance. In this way we obtain constraints on these chemical potentials shown in Eq. 3 which lead to significant reduction of Lithium as shown in the fourth column of Table 2.

$$0.18 \leq \beta_{\nu_e} \leq 0.3, \quad 2 \leq \beta_{\nu_{\mu,\tau}} \leq 2.3 \quad (3)$$

As in most successful attempts to resolve the Lithium problem beyond the SBBN, in the present work the decrease in Lithium abundance is achieved at the expenses of increasing Deuterium. A remaining open scheme that is worth to investigate is the possibility of reducing Lithium abundance without much increase in Deuterium by including for example new particles/interactions. More detailed analysis of these non-standard physics will be presented in an upcoming paper by [18].

Acknowledgement

Tahani Makki would thank the organizing committee of the Ninth European Summer School on Experimental Nuclear Astrophysics for their support, especially she would thank prof. Rosario Gianluca Pizzone and Prof. Livio Lamia for their tremendous help.

References

- [1] Arbey A. and Mahmoudi F., Phys. Lett. B 669, 46-51 (2008).
- [2] Aver E., Olive K.A., and Skillman E.D., arXiv: 1503:08146 (2015).
- [3] Bania T.M. et al., Nature 415, 54 (2002).
- [4] Bertulani C.A. et al., arXiv:1802.03469v1, (2018).
- [5] Dolgov A.D. and Takahshi F., Nucl. Phys. B, 688, 189-213 (2004).
- [6] Hansen S. et al., Phys. Rev. D 65, 023511 (2001).
- [7] Hou S.Q. et al., ApJ 834, 165 (2017).
- [8] Lunardini C. and Smirnov A.Yu., Phys. Rev. D 64, 073006 (2001).
- [9] Mukhanov V., Physical Foundations of Cosmology (Cambridge University Press, New York, 2005) 421.
- [10] Noterdaeme P. et al., A & A 542, L33 (2012).
- [11] P.A.R. Ade et al., A & A 594, A13 (2016).
- [12] Pizzone R.G., et al., ApJ 786, 112 (2014).
- [13] Prantzos N., A&A 542, A67 (2012).
- [14] Sbordone L. et al., A&A 522, A26 (2010).
- [15] Shi X., Phys. Rev. D 54, 2753 (1996).
- [16] Singh P., JCAP 05, 061 (2015).
- [17] Spite M. and Spite F., Nature 297, 483 (1982).
- [18] T.R. Makki, M.F. El Eid, and G.J. Mathews, submitted to MNRAS (2018).

Cosmological Solutions to the Lithium Problem

G. J. Mathews¹, A. Kedia¹, N. Sasankan¹, M. Kusakabe², Y. Luo^{3,4}, T. Kajino^{2,3,4}, D. Yamazaki^{3,5}, T. Makki⁶, and M. El Eid⁶

¹*Department of Physics, Center for Astrophysics, University of Notre Dame, Notre Dame, IN 46556 USA*

²*IRCBB, School of Physics, Beihang University, Beijing 100083 China*

³*National Astronomical Observatory of Japan Tokyo, 181-8588, Japan*

⁴*Graduate School of Science, The University of Tokyo, Tokyo, 113-0033, Japan*

⁵*University Education Center, Ibaraki University, 2-1-1, Bunkyo, Mito, 310-8512, Japan*

⁶*Department of Physics, American University of Beirut, Lebanon*

E-mail: gmathews@nd.edu

(Received August 26, 2019)

The abundance of primordial lithium is derived from the observed spectroscopy of metal-poor stars in the galactic halo. However, the observationally inferred abundance remains at about a factor of three below the abundance predicted by standard big bang nucleosynthesis (BBN). The resolution of this dilemma can be either astrophysical (stars destroy lithium after BBN), nuclear (reactions destroy lithium during BBN), or cosmological, i.e. new physics beyond the standard BBN is responsible for destroying lithium. Here, we overview a variety of possible cosmological solutions, and their shortcomings. On the one hand, we examine the possibility of physical processes that modify the velocity distribution of particles from the usually assumed Maxwell-Boltzmann statistics. A physical justification for this is an inhomogeneous spatial distribution of domains of primordial magnetic field strength as a means to reduce the primordial lithium abundance. Another possibility is that scattering with the mildly relativistic electrons in the background plasma alters the baryon distribution to one resembling a Fermi-Dirac distribution. We show that neither of these possibilities can adequately resolve the lithium problem. A number of alternate hybrid models are discussed including a mix of neutrino degeneracy, unified dark matter, axion cooling, and the presence of decaying and/or charged supersymmetric particles.

KEYWORDS: Big Bang Nucleosynthesis, Cosmology, Stars and Stellar Evolution

1. Introduction

The yield of light elements from big bang nucleosynthesis (BBN) is the only direct probe of the radiation dominated epoch during the early universe. BBN occurs as the universe cools from about 10^{10} to 10^8 K spanning times of about 1 to 10^4 sec into the big bang. The only other probe is the spectrum of temperature fluctuations in the CMB [1] which contains information of the first quantum fluctuations in the universe, and the details of the distribution and evolution of dark matter, baryonic matter, photons and electrons near the time of the surface of photon last scattering (about 3.8×10^5 yr into the big bang).

One of the most powerful aspects of standard BBN is the simplicity [2–7] of the equations. Because the contributions to the total mass-energy from non-relativistic matter, curvature, and dark energy are negligible, the Friedmann equation to describe the cosmic expansion is just:

$$\left(\frac{\dot{a}}{a}\right) = \sqrt{\frac{8}{3}\pi G\rho_{\text{rad}}} = 0.677T_{\text{MeV}}^2 \text{ sec}^{-1} , \quad (1)$$

where ρ_{rad} is the mass energy density in relativistic particles, H_0 is the present value of the Hubble parameter, and T_{MeV} is the temperature in MeV.

Also, at the time of BBN the timescale for Compton scattering is short. Hence, the number density of particles of type i with momenta between p and $p + dp$ is simply given by Fermi-Dirac or Bose-Einstein distributions,

$$n_i(p)dp = \frac{g_i}{2\pi^2} p^2 \left[\exp\left(\frac{E_i(p) - \mu_i}{kT}\right) \pm 1 \right]^{-1} dp \quad (2)$$

where $E_i(p)$ is the energy of the particle, the \pm sign is negative for bosons and positive for fermions, while g_i is the number of degenerate spin states of the particle (e.g. $g = 1$ for neutral massless leptons, and $g_i = 2$ for charged leptons and photons).

The nuclear reactions, however, must be followed in detail as they fall out of equilibrium. For nuclide i undergoing reactions of the type $i + j \leftrightarrow l + k$ one can write [2]:

$$\frac{dY_i}{dt} = \sum_{i,j,k} N_i \left(\frac{Y_l^{N_l} Y_k^{N_k}}{N_l! N_k!} n_k \langle \sigma_{lk} v \rangle - \frac{Y_i^{N_i} Y_j^{N_j}}{N_i! N_j!} n_j \langle \sigma_{ij} v \rangle \right) \quad (3)$$

where $Y_i = X_i/A_i$ is the abundance fraction, N_i is the number of reacting identical particles, n_i is the number density of nucleus i and $\langle \sigma_{ij} v \rangle$ denoted the maxwellian averaged reaction cross section,

$$\langle \sigma_{ij} v \rangle = \sqrt{\frac{8}{\pi \mu_{ij}}} (T)^{-\frac{3}{2}} \int_0^\infty \sigma_{ij}(E) \exp[-E/T] E dE, \quad (4)$$

where $\mu_{ij} = m_i m_j / (m_i + m_j)$ is the reduced mass of the reacting system.

Once the forward reaction rate is known, the reverse reaction rate can be deduced from an application (cf. Ref. [8]) of the principle of detailed balance. The reaction rates relevant to BBN have been conveniently tabularized in analytic form in several sources [9–11]. These rates are a crucial ingredient to BBN calculations. In all there are only 16 reactions of significance during BBN. [5, 6, 12]. Ideally, one would like to know these relevant nuclear reaction rates to very high precision ($\sim 1\%$). Fortunately, unlike in stars, the energies at which these reactions occur in the early universe are for the most part directly accessible in laboratory experiments. Although considerable progress has been made [6, 12–16] toward quantifying and reducing uncertainties in the relevant rates, improved reaction rates are still desired for the neutron life time [17, 18], along with the ${}^2\text{H}(p, \gamma){}^3\text{He}$, ${}^2\text{H}(d, n){}^3\text{He}$, ${}^3\text{He}(d, p){}^4\text{He}$, ${}^3\text{He}(\alpha, \gamma){}^7\text{Be}$, and ${}^7\text{Be}(n, \alpha){}^4\text{He}$ reactions (see [20]).

One of the powers of standard-homogeneous BBN is that once the reaction rates are known, all of the light-element abundances are determined in terms of the single parameter, the baryon-to-photon ratio, η . The crucial test of the standard BBN is, therefore, whether the independently determined value of η from fits to the CMB reproduces all of the observed primordial abundances. Most of the best available abundance constraints have been summarized recently in [6]. Of most relevance to this work is the primordial abundance of ${}^7\text{Li}$.

The good news, is that once the value of η was fixed by measurements of the CMB [1] to be $\eta \equiv n_b/n_\gamma \approx 2.738 \times 10^{-8} \Omega_b h^2 = (6.11 \pm 0.04) \times 10^{-10}$, there appears to be good agreement between the predictions of BBN for most light elements (i.e. D, ${}^3\text{He}$, ${}^4\text{He}$) and the primordial abundances as inferred from observations. In particular, the uncertainties in the ${}^4\text{He}$ abundance deduced from line-strength observations of H II regions in low-metallicity irregular galaxies is now better understood [21] and agrees with BBN. Also, the D/H abundance seems very well determined from narrow-line absorption features along the line of sight to distant quasars [22] and agrees surprisingly well with BBN.

2. Lithium Abundance

Unlike the other light elements, the primordial abundance of ${}^7\text{Li}$ is best determined from old metal-poor halo stars with masses from about $0.75 M_{\odot}$ to $0.95 M_{\odot}$ and temperatures of about 6,000 K to 6,700 K corresponding to the Spite plateau (see Refs. [5,6,13] and Refs. therein). There is, however, an uncertainty in this determination due to the fact that the surface lithium in these stars may have experienced gradual depletion over the stellar lifetime due to mixing with the higher temperature stellar interiors where ${}^7\text{Li}$ would be destroyed. The best current limit as summarized in Ref. [6] is: ${}^7\text{Li}/\text{H} = (1.58 \pm 0.35) \times 10^{-10}$.

There is, however, one glaring problem that remains in BBN. The calculated and observed ${}^7\text{Li}/\text{H}$ ratios differ by about a factor of 3. This is known as "the lithium problem." A number of recent papers have addressed this problem [6,13,14,23–29]. At present it is not yet known if this discrepancy derives from a destruction of lithium on the old stars used to deduce the primordial lithium abundance, or if it requires exotic new physics in the early universe [13, 14, 23, 24, 26], or even a modification of the particle statistics in BBN itself [27, 28]. In this paper, we summarize some recent work and their prospects for solving the lithium problem.

3. Solutions to the Lithium Problem?

3.1 Nuclear Solution

One possible solution is in nuclear physics, such as we heard at this workshop [19, 20]. During the big bang, most of the lithium is formed as ${}^7\text{Be}$. Hence, a means to destroy lithium might be a strong resonance in the ${}^7\text{Be}(n, p){}^7\text{Li}$ reaction followed by the destruction of more fragile ${}^7\text{Li}$, and/or resonances in the ${}^7\text{Be}(n, \alpha){}^4\text{He}$ reaction. However, it is already clear [19, 20] that these resonances help but do not solve the problem.

3.2 Astrophysical Solution

The first author of this manuscript suspects that the most likely solution is from stellar astrophysics. It has been suggested for years, however, that the lack of a dispersion in the abundances of different stars in the Spite plateau argues against stellar destruction. This is because the star-to-star variations of stellar parameters such as rotation, meridional mixing, magnetic fields, turbulence, etc. among stars could lead to dispersions in the observed surface abundances. Nevertheless, the apparent metallicity dependence in the Li abundance [30] suggests that at least some processing of lithium on the surface of these stars has occurred. Indeed, there are at least two recent works [31, 32] demonstrating that a narrow dispersion can result even after destroying lithium by a factor of 3 by turbulent diffusion [31] or convective over-shoot [32] for a broad range of stellar parameters.

3.3 Cosmological Solutions

Nevertheless, a number of works have looked at possible interesting cosmological solutions that involve modifications to the fundamental assumptions of the big bang itself. Here, we will discuss a few possibilities that we have considered. These illustrate the difficulty in resolving the lithium problem this way.

3.3.1 Modified Statistics

Although a simple Maxwell-Boltzmann (MB) distribution for the baryons is a long-standing assumption during BBN, there have been a number of recent papers in which this assumption is relaxed. For example, it is known [33] that the MB distribution is not a unique solution to the Boltzmann equa-

tion. Hou et al. [28] considered a distribution function of the form:

$$f_q(\mathbf{v}_i) = B_q(m_i c^2/kT) \left(\frac{m_i}{2\pi kT} \right)^{3/2} \left[1 - (q-1) \frac{m_i v_i^2}{2kT} \right]^{1/(q-1)}, \quad (5)$$

where $B_q(m_i c^2/kT)$ is a normalization constant determined from the requirement $\int f_q(\mathbf{v}_i) d\mathbf{v}_i = 1$, and q is a free parameter. In the limit $q \rightarrow 1$ the MB distribution is recovered. However, by directly inserting this form into the reaction rate formula [4] it was shown in [28] that the lithium abundance could be reduced enough to resolve the lithium problem. The reason this works is that for slightly positive q the high-energy tail of the distribution is suppressed relative to MB statistics. Since the formation of ${}^7\text{Be}$ via the ${}^3\text{He}(\alpha, \gamma){}^7\text{Be}$ reaction has the highest Coulomb barrier during BBN, it is the most sensitive to the high-energy tail of the distribution. Hence ${}^7\text{Be}$ production is diminished.

However, this occurred at the expense of increasing the D/H value above that consistent with observations. Moreover, in subsequent work [34] it has been shown that the assumption that the relative velocity distribution of nuclear reactions is a Tsallis distribution for individual nuclei that also obey a Tsallis distribution leads to a breakdown in momentum conservation. When this is corrected, the lithium problem cannot be resolved in this way.

3.3.2 Primordial Magnetic Field

One of the problems with imposing a Tsallis distribution, is that it requires a physical mechanism to force the statistics to deviate from MB. In [35, 36], however, it was demonstrated that by imposing isocurvature sub-horizon fluctuations in a primordial magnetic field (PMF), the averaging over the domains after nucleosynthesis leads to an effective distribution similar to a Tsallis distribution but for which momentum conservation is implicit. However, just as in [28] the destruction of lithium is always at the cost of increasing the D/H abundance, and hence, a PMF is not a viable solution to the lithium problem.

3.3.3 Relativistic Electron Scattering in the BBN Plasma

Although the thermodynamics of a relativistic or nonrelativistic single-component gas have been known for many decades [37], the solution of the multi-component relativistic Boltzmann equation has only recently been attempted [38, 39] and transport coefficients have only been deduced for the case of equal or nearly identical-mass particles. Moreover, there has been recent interest in the possibility of a modification of the baryon distribution function from that of Maxwell Boltzmann (MB) statistics, either in the form of Tsallis statistics [27, 28], primordial magnetic fields [35], or as a result of scattering from a background of relativistic electrons [40] which obey Fermi Dirac (FD), rather than MB statistics (see however [41]), or small relativistic corrections to Boltzmann equation derivation of the distribution function along with effects of nuclear kinetic drag. [42].

In the work of Ref. [42] the starting point was the FD distribution for baryons from which corrections were deduced. However, in Ref. [40] it was noted based upon a Langevin approximation in kinetic-energy equipartition and a Monte Carlo simulation that the momentum distribution of nuclei more closely resembled the electron momentum distribution and therefore modified statistics when the electrons were relativistic. In [41], however, a derivation has been made of the exact solution to the relativistic Boltzmann equation without an *a priori* assumption of what the baryon distribution should be. We showed that the problem can be approximated as an ideal two component system of baryons immersed in a bath of relativistic electrons, for which the collision term is completely dominated by elastic scattering from relativistic electrons. We showed that in the condition of relativistic pressure equilibrium (rather than kinetic-energy equipartition) the resultant baryon distribution does indeed follow MB statistics independently of the electron distribution function. This was verified by an evaluation of the relativistic Boltzmann equation and by revised numerical Monte-Carlo simulations [43]. In [40] the sampling of electrons for collision with baryons was done from the distribution

function $f(v)$ where v is the relative velocity in the cosmological frame. However, this did not take into account the effect of the instantaneous viscosity (i.e electrons moving opposite to the direction of motion of a baryon collide more frequently with the baryon). This was corrected by sampling from $vf(v)$, where v is the relative velocity in the frame of baryon. When that correction was made, the resultant distribution obeys MB statistics even for highly relativistic electrons.

3.3.4 Exotica

There have been numerous other attempts to resolve the lithium problem [7]. For example, in [23,44] we showed that a next-to-lightest supersymmetric X^- particle (most likely the *selectron*) could revise the BBN reaction network. In particular, a resonant ${}^7\text{Be}_X(p, \gamma){}^8\text{B}_X$ reaction and ${}^7\text{Be}_X \rightarrow {}^7\text{Li} + X^0$ decay could lead to a depletion of ${}^7\text{Li}$ in the final BBN abundances. However, this scenario can only work for an exceedingly narrow range of lifetimes and abundances for the X^- particle, without overproducing ${}^6\text{Li}$ or deuterium.

In another work [45, 46] it was shown that a time-dependent quark mass could lead to a depletion of lithium. In particular, it was shown [45] that resonance energies and widths of ${}^8\text{Be}^*$ states relevant to the ${}^7\text{Be}(n, p){}^7\text{Li}$ could be changed thereby enhancing the destruction of BBN lithium. Unfortunately, this is accompanied by an enhanced D/H abundance which precludes the possibility of solving the lithium problem.

3.3.5 Hybrid Models

In view of the difficulty of consistently overproducing D/H in models that attempt to reduce the ${}^7\text{Li}$ production, there have been some attempts [26, 29] to apply hybrid models involving multiple simultaneous extensions of the standard BBN model. The essence of this approach is to use one extension to deplete ${}^7\text{Li}$ and another to restore D/H to the observed value. For example, in [25, 26] it was shown that the simultaneous imposition of photon cooling after BBN, plus X -particle decay, plus a primordial magnetic field could satisfy the D/H and ${}^7\text{Li}$ constraints, but at the cost of overproducing ${}^6\text{Li}$. Alternatively in [29] the right combinations of varying: the neutrino temperatures; neutrino chemical potentials; number of neutrino species; plus photon cooling; and/or a form of unified dark matter, could help to alleviate (but not completely resolve) the lithium problem.

4. Conclusion

In summary, it is the firm opinion of the first author of this manuscript that there is no obvious cosmological solution to the lithium problem. One inevitably encounters excess deuterium or violates other abundance constraints. Although, one might argue that the D/H constraint might be relaxed, the first author is convinced that the solution must be the destruction of lithium on the surfaces of metal poor halo stars. To quote the lines of King Lear, that were published in the first lines of the foundational paper of nuclear astrophysics by Burbidge, Burbidge, Fowler and Hoyle [47], "*It is the stars, The stars above us, govern our condition*". Although it has been fun to work on the cosmological approaches, the first author is convinced that the lithium problem is an astrophysics issue.

5. Acknowledgments

Work at the University of Notre Dame supported by the U.S. Department of Energy under Nuclear Theory Grant DE-FG02-95-ER40934. One of the authors (M.K.) acknowledges support from the Japan Society for the Promotion of Science.

References

- [1] P. A. R. Ade et al., Planck XIII Collaboration, *Astron. Astrophys.* **594**, A13 (2016)
- [2] R.V. Wagoner, *ApJ.* **179**, 343 (1973)
- [3] J. Yang, M.S. Turner, G. Steigman, D.N. Schramm, and K.A. Olive, *ApJ.* **281**, 493 (1984)
- [4] R. A. Malaney and G. J. Mathews, G. J., *Phys. Rep.* **229**, 145 (1993)
- [5] F. Iocco et al., *Phys. Rep.*, **47**, 1 (2009)
- [6] R. H. Cyburt, B. D. Fields and K. A. Olive, T.-H. Yeh, *Rev. Mod. Phys.* **88** 015004 (2016)
- [7] G. J. Mathews, M. Kusakabe and T. Kajino, *Int. J. Mod. Phys. E* **26**, 1741001 (2017)
- [8] G. J. Mathews, Y. Pehlivan, T. Kajino, A. B. Balantekin and M. Kusakabe, *Astrophys. J.* **727** 10 (2011).
- [9] R. H. Cyburt et al., *Astrophys. J. Suppl.* **189**, 240 (2010)
- [10] G. R. Caughlan and W. A. Fowler, *At. Data Nucl. Data Tables* **40**, 283 (1988)
- [11] C. Angulo et al., *Nucl. Phys. A* **656**, 656 (1999)
- [12] M. Foley, N. Sasankan, M. Kusakabe and G. J. Mathews, *Int. J. Mod. Phys. E* **26**, 1741008 (2017)
- [13] A. Coc and E. Vangioni, *Int. J. Mod. Phys. E* **26**, 1741002 (2017).
- [14] R. Nakamura, M.-A. Hashimoto, R. Ichimasa and K. Arai, *Int. J. Mod. Phys. E* **26**, 1741003 (2017)
- [15] P. Descouvemont et al., *ADNDT*, **88**, 203 (2004)
- [16] C. Pitrou et al., *Phys. Rep.* *Submitted* (2018)
- [17] A. P. Serebrov and A. K. Fomin, *Phys. Rev. C* **82**, 035501 (2010).
- [18] G. J. Mathews T. Kajino, and T. Shima, *Phys. Rev. D* **71**, 021302 (2005)
- [19] S. Hayakawa, et al. (this conference proceedings) (2019).
- [20] S. Ishikawa, et al. (this conference proceedings) (2019).
- [21] E. Aver, K. A. Olive, and E. D. Skillman, *JCAP* **05**, 003 (2010), *JCAP* **11**, 017 (2013); arXiv:1503:08146.
- [22] R. Cooke et al., *Astrophys. J.* **781** 31 (2014); R. Cooke et al., *Astrophys. J.* **830**, 148 (2016)
- [23] M. Kusakabe, G. J. Mathews, T. Kajino and M.-K. Cheoun, *Int. J. Mod. Phys. E* **26**, 1741004 (2017)
- [24] J. Sato, T. Shimomura and M. Yamanaka, *Int. J. Mod. Phys. E* **26**, 1741005 (2017)
- [25] D. G. Yamazaki, M. Kusakabe, T. Kajino, G. J. Mathews and M.-K. Cheoun, *Phys. Rev. D* **90**, 023001 (2014)
- [26] D. Yamazaki, M. Kusakabe, T. Kajino, G. J. Mathews and M.-K. Cheoun, *Int. J. Mod. Phys. E* **26**, 1741006 (2017)
- [27] C. A. Bertulani, J. Fuqua, J., and M. S. Hussein, *ApJ*, 767, 67 (2013).
- [28] S. Q. Hou, J. J. He, J. J. A. Parikh, D. Kahl, D. C. A. Bertulani, T. Kajino, G. J. Mathews, and G. Zhao, *Astrophys. J.*, 834, 165-170 (2017)
- [29] T. Makki, M. El Eid, Mounib, and G. J. Mathews, *Math. Phys. Lett A* in press (2019), arXiv:1901.03726
- [30] J. Meléndez, J. et al., *A&A*, 515, L3 (2010).
- [31] O. Richard, G. Michaud, and J. Richer, *Astrophys. J.*, 619, 538 (2005).
- [32] X. Fu, A. Bressan, P. Molaro, and P. Marigo, *MNRAS*, 452, 3256 (2015).
- [33] Tsallis, C. 1988, *JSP*, 52, 479
- [34] M. Kusakabe, T. Kajino, G. J. Mathews, and Y. Luo, *Phys. Rev. D* **99**, 043505 (2019).
- [35] Y. Luo, T. Kajino, M. Kusakabe and G. J. Mathews, *ApJ*, 872, 172, (2019).
- [36] Y. Luo, this conference proceedings (2019).
- [37] F. Jüttner, *Z. Phys.*, **47**, 5342 (1928)
- [38] G. M. Kremer, arXiv:1207.3977
- [39] G. M. Kremer and W. Marques, *Phys. Fluids*, **25** 017102 (2013).
- [40] N. Sasankan, A. Kedia, M. Kusakabe, and G. J. Mathews, arXiv:1810.05976
- [41] N. Sasankan, A. Kedia, M. Kusakabe, and G. J. Mathews, in preparation.
- [42] S. D. McDermott and M. S. Turner, arXiv:1811.04932.
- [43] A. Kedia, N. Sasankan, M. Kusakabe, and G. J. Mathews, in preparation.
- [44] M. Kusakabe, K. Kim, M.-K. Cheoun, T. Kajino, Y. Kino and G. J. Mathews, *Astrophys. J. Suppl.* **214**, 5 (2014)
- [45] K. Mori and M. Kusakabe, *Phys. Rev.*, **D99**, 083013 (2019); K. Mori, this conference proceedings.
- [46] M.-K. Cheoun, T. Kajino M. Kusakabe and G. J. Mathews, *Phys. Rev.* **D84**, 043001 (2011).
- [47] E. M. Burbidge, G. R. Burbidge, W. A. Fowler, and F. Hoyle, *Rev. Mod. Phys.*, **29**, 547 (1957).